

Polyelectrolyte Complexes and their Therapeutic Potential

Dissertation

zur Erlangung des akademischen Grades eines
Doktors der Naturwissenschaften (Dr. rer. nat.)
an der Bayreuther Graduiertenschule für Mathematik und
Naturwissenschaften der Universität Bayreuth

vorgelegt von

Christopher Volker Synatschke

geboren in Lemgo

Bayreuth, 2013

Die vorliegende Arbeit wurde in der Zeit von September 2009 bis Februar 2013 am Lehrstuhl für Makromolekulare Chemie II der Universität Bayreuth unter Betreuung durch Herrn Prof. Dr. Axel H. E. Müller angefertigt.

Vollständiger Abdruck der von der Bayreuther Graduiertenschule für Mathematik und Naturwissenschaften der Universität Bayreuth genehmigten Dissertation zur Erlangung des akademischen Grades eines Doktors der Naturwissenschaften (Dr. rer. nat.).

Dissertation eingereicht am:	12. April 2013
Zulassung durch die Prüfungskommission:	16. April 2013
Wissenschaftliches Kolloquium:	10. Juni 2013
Korrigierte Version der Dissertation:	13. Januar 2014

Prüfungsausschuss:

Prof. Dr. Axel H. E. Müller (Erstgutachter)

Prof. Dr. Ruth Freitag (Zweitgutachterin)

Prof. Dr. Patrick Theato (Drittgutachter)

Prof. Dr. Stephan Förster

Prof. Dr. Andreas Fery (Vorsitz)

**“If you live each day as if it was your last,
someday you'll most certainly be right.”**

— *Unknown*

“Why do you go away?

**So that you can come back. So that you can see the place
you came from with new eyes and extra colors. And the
people there see you differently, too.**

**Coming back to where you started is not the same as never
leaving.”**

— *Terry Pratchett, A Hat Full of Sky*

Für meine Mutter Elisabeth

Table of Contents

Summary	1
Zusammenfassung	5
Glossary	9
Chapter 1 – Introduction	13
1. Polymer-Aided Drug Delivery	13
1.1. <i>Polymer-Drug Conjugates</i>	13
1.2 <i>Important Concepts in Drug Delivery: Stealth Effect and EPR</i>	14
1.3 <i>Polymer Micelles and Vesicles</i>	16
1.4 <i>Photodynamic Therapy</i>	19
1.5 <i>Complex Drug Delivery Systems: Multicompartment Micelles</i>	20
2. Delivery of Genes	23
2.1 <i>Viral Vectors</i>	24
2.2 <i>Non-Viral Vectors</i>	24
2.3 <i>Barriers to a Successful Delivery of Genes</i>	25
2.4 <i>Polymeric Vectors</i>	28
3. Aim of this Thesis	32
4. References	33
Chapter 2 - Overview over the Thesis	39
1. Influence of Polymer Architecture and Molecular Weight of Poly(2-(Dimethylamino)ethyl Methacrylate) Polycations on Transfection Efficiency and Cell Viability in Gene Delivery	40
2. Nano-Particulate Non-Viral Agent for the Effective Delivery of pDNA and siRNA to Differentiated Cells and Primary Human T Lymphocytes	43
3. Double-Layered Micellar Interpolyelectrolyte Complexes – How Many Shells to a Core?	46
4. Micellar Interpolyelectrolyte Complexes With a Compartmentalized Shell	48
5. Multicompartment Micelles with Adjustable Poly(ethylene glycol) Shell for Efficient <i>in Vivo</i> Photodynamic Therapy	50
6. Individual Contributions to Joint Publications	55
7. References	59

Chapter 3

Influence of Polymer Architecture and Molecular Weight of Poly(2-(Dimethylamino)ethyl Methacrylate) Polycations on Transfection Efficiency and Cell Viability in Gene Delivery61

Chapter 4

Nano-Particulate Non-Viral Agent for the Effective Delivery of pDNA and siRNA to Differentiated Cells and Primary Human T Lymphocytes91

Chapter 5

Double-Layered Micellar Interpolyelectrolyte Complexes – How Many Shells to a Core?..137

Chapter 6

Micellar Interpolyelectrolyte Complexes with a Compartmentalized Shell173

Chapter 7

Multicompartment Micelles with Adjustable Poly(ethylene glycol) Shell for Efficient *in Vivo* Photodynamic Therapy205

List of Publications243

Publications243

Patent Applications244

Acknowledgements245

Erklärung251

Summary

This thesis describes the preparation of polyelectrolyte nanostructures, the characterization of interpolyelectrolyte complexes (IPECs) made from these structures and their use in a therapeutic context. The therapeutic use of such IPECs connects the two major topics of this work: First, the delivery of genes into eukaryotic cells *in vitro* (cell culture) by means of new star-shaped polycations was explored. Second, the structure of ionic multicompartiment micelles (MCMs) when complexed with polyions was studied and the performance of these nanostructures as delivery agents of anti-cancer drugs both *in vitro* and *in vivo* (in mice) was tested.

To better understand structure-property relationships of polycations relevant for gene delivery, a library of poly(2-(dimethylamino)ethyl methacrylate) (PDMAEMA) homopolymers was synthesized *via* atom radical transfer polymerization (ATRP). Star-shaped polymers with a different number of arms (linear, 3-, 5- and 20-arm stars) and molecular weights (arm lengths) were created by using sugar-based or inorganic nanoparticles as core molecules with varying number of initiation sites. The cytotoxicity as well as transfection performance of polyplexes from these polymers and plasmid DNA was determined for different PDMAEMA-nitrogen/DNA phosphate (N/P) ratios in Chinese Hamster Ovary (CHO-K1) cells. Generally, for each polymer maximal transfection efficiency was found at an N/P ratio between 5 and 10, where good transfection performance was coupled with good viability. A decrease of the cytotoxicity of polymers with a given molecular weight was observed with increasing degree of branching, *i.e.*, with increased arm-number. To reach significant transfection efficiency, a minimum molecular weight of approximately 20 kDa was found to be necessary. Star-shaped PDMAEMA with roughly 20 arms from a silsesquioxane nanoparticle initiator (Si-PDMAEMA) showed exceptionally high transfection efficiency, surpassing that of poly(ethylene imine) in the CHO-K1 cell line. The superior transfection behavior of this specific polymer was demonstrated in a variety of different cell lines, including non-dividing or differentiated (C2C12 and human T lymphocytes) ones, which are notoriously difficult to transfect. Additionally, polymeric micelles were produced from a polybutadiene-*block*-PDMAEMA (PB-*b*-PDMAEMA) diblock copolymer in aqueous

solution and subsequently used for gene transfection. Their transfection efficiency was in the same range as that of Si-PDMAEMA, hinting towards a general design principle for highly effective gene vectors. This consists of a star-shaped architecture of PDMAEMA chains emanating from a common center, where the material of the core seems to be of minor importance. Apart from plasmid DNA delivery, both PB-*b*-PDMAEMA micelles and Si-PDMAEMA successfully transported siRNA into eukaryotic cells, showing a significantly enhanced knockdown of the targeted genes in the respective cell line.

The second major part of this thesis deals with the structure of ionic MCMs complexed with diverse polycations as well as the drug delivery capabilities of some of these complex micellar structures. MCMs from polybutadiene-*block*-poly(1-methyl-2-vinyl pyridinium)-*block*-poly(methacrylic acid) (PB-*b*-P2VPq-*b*-PMAA; BVqMAA) triblock terpolymers were used as the basis for further structural modifications. These micelles exhibit a core-shell-corona morphology, where PB forms the core of the micelles, a discontinuous (patchy) shell consisting of an IPEC between P2VPq and PMAA is present and finally a corona of excess PMAA stabilizes the micelles in aqueous solution. At sufficiently high pH a portion of the corona carries negative charges, which were then used to form further IPECs with either cationic homopolymers or double-hydrophilic block copolymers featuring one positively charged block. If polycations other than poly(2-vinyl pyridine) such as quaternized PDMAEMA (PDMAEMAq) were used for the complexation, a new and distinguishable IPEC compartment was formed on top of the already existing P2VPq/PMAA IPEC. In the case of MCMs with a short to moderate block length of the corona, *i.e.*, the degree of polymerization (DP) of PMAA was between 345 to 550 units, a layered arrangement of the newly formed IPEC compartment was found. Stable colloidal particles were observed at all mixing ratios if the double hydrophilic diblock copolymers with one water-soluble but uncharged block were used for complexation with the micelles. However, in the case of homopolycation addition macroscopic aggregation and sedimentation occurred above critical mixing ratios.

For BVqMAA micelles with a long PMAA corona (DP of PMAA = 1350) complexed with different quaternized homopolymers, a patchy arrangement of the newly formed IPEC compartment instead of a layered one was found. The formation of this new structure is due to an interfacial energy minimization between the new IPEC and the

compartmentalized core of the micelles that became possible due to the exceptionally long PMAA corona of the precursor micelles.

Finally, MCMs from BVqMAA were tested for their capacity to deliver a hydrophobic anti-cancer drug for photodynamic therapy (PDT) to lung cancer cells (A549) *in vitro* and *in vivo*. The influence of the corona composition on the biological properties of the micellar carriers was studied by forming complexes with a double-hydrophilic diblock copolymer, poly(L-lysine)-*block*-poly(ethylene glycol) (PLL-*b*-PEG). A new cylinder-on-sphere morphology was observed in electron microscopy for BVqMAA/PLL-*b*-PEG complex micelles at high complexation ratios between lysine and MAA units. The corona composition strongly influenced the *in vitro* cytotoxicity after photo-activation of the drug carrying micelles and this correlated well with the uptake behavior. Highest cytotoxicity and uptake were found for pure BVqMAA micelles, both decreasing with increasing amount of PLL-*b*-PEG attached to the micelles. In mice, a prolonged blood circulation time in the range of several hours was exclusively observed when fully PEGylated micelles were injected, but not for partially or non-PEGylated carriers. Further, the former micelles were the only ones showing an enhanced accumulation in a subcutaneous tumor model 24 h after intravenous injection. The amount of drug delivered to the tumor tissue by the micelles was sufficient to suppress tumor growth for up to 21 days after a single dose injection and photoirradiation step. The potential of complex micelles on the basis of BVqMAA MCMs could thus be proven.

Zusammenfassung

Diese Dissertation behandelt die Herstellung von polymeren Nanostrukturen unter Verwendung von Polyelektrolyten, sowie die Erzeugung und Charakterisierung von Interpolyelektrolytkomplexen (IPEK) und deren Verwendung in medizinischen bzw. therapeutischen Fragestellungen. Der therapeutische Nutzen solcher Strukturen verbindet die zwei Teilgebiete dieser Arbeit. Im ersten Teil wird die nichtvirale Transfektion von Kulturzellen (*in vitro*) mit Hilfe von neuen verzweigten Polykationen, insbesondere von sternförmigen Polymerarchitekturen, auf Basis von Poly(2-(dimethylamino)ethyl methacrylat) (PDMAEMA) untersucht. Der zweite Themenkomplex behandelt die Struktur von kompartimentierten Polymermizellen, die sich durch Selbstanordnung von geladenen Triblock-Terpolymeren ausbilden. Dabei wurde vorrangig die Komplexbildung mit entgegengesetzt geladenen Polyionen untersucht. Schließlich wurde die Fähigkeit solcher komplexen mizellaren Strukturen zum Wirkstofftransport in der Krebstherapie sowohl an Kulturzellen als auch an Tiermodellen getestet.

Zum Verständnis von Struktur-Wirkungsbeziehungen wurde eine Materialbibliothek aus sternförmigen DMAEMA-Polymeren unter Verwendung der kontrollierten Polymerisationsmethode „atom transfer radical polymerization“, ausgehend von verschiedenen Initiatormolekülen, hergestellt. Es konnten lineare sowie sternförmige Polymere mit verschiedener Armzahl (3-, 5- und 20-Arm-Sterne) erzeugt werden. Für jede Klasse von Polymeren wurden mehrere Proben mit verschiedenen Molekulargewichten (= Armlängen) synthetisiert. Alle DMAEMA-Polymere wurden dann für die Komplexbildung mit Plasmid-DNA in verschiedenen Mischungsverhältnissen von PDMAEMA-Stickstoff zu DNA-Phosphat (N/P Verhältnis) verwendet und die resultierenden Polyplexe auf ihre Transfektionseigenschaften hin untersucht. Für die Bestimmung der jeweiligen Zytotoxizität und des Anteils an erfolgreich transfizierten Zellen (definiert als Transfektionseffizienz) wurden Ovarienzellen aus chinesischen Hamstern (CHO-K1) verwendet. Es zeigte sich, dass in der Regel ein N/P Verhältnis zwischen 5 und 10 für eine erfolgreiche Transfektion bei gleichzeitig geringer Zytotoxizität erforderlich war. Des Weiteren wurde der Trend einer Verringerung der durch die Polymere verursachten Zytotoxizität mit steigendem

Verzweigungsgrad bei vergleichbaren Molekulargewichten gefunden. Polykationen unterhalb eines kritischen Molekulargewichts von ca. 20 kDa zeigten keine relevante Transfektionseffizienz unabhängig vom N/P Verhältnis. Die PDMAEMA-Sterne mit etwa 20 Armen (Si-PDMAEMA), ausgehend von einem Silsesquioxan-Nanopartikel als Initiator-molekül, zeigten eine überragende Transfektionseffizienz in CHO-K1 Zellen, gekoppelt mit einer geringen Zytotoxizität. Diese verbesserten Transfektionseigenschaften konnten auch in anderen Zelllinien bestätigt werden, obwohl diese als sehr viel schwieriger zu transfizieren gelten. Darunter befanden sich unter anderem konfluente, nicht-teilende C2C12 Zellen sowie ausdifferenzierte humane T-Lymphozyten. Außerdem konnten die guten Transfektionsergebnisse von Si-PDMAEMA ebenfalls mit Mizellen aus einem amphiphilen Diblockcopolymer erreicht werden. Die Mizellen bestanden aus Polybutadien-*block*-PDMAEMA (PB-*b*-PDMAEMA), wobei die Kern-Schale-Struktur der Mizellen in Lösung der von sternförmigen Polymeren ähnelt. Dies wird als Hinweis auf ein generelles Design-Prinzip gedeutet: PDMAEMA Strukturen, die viele Arme ausgehend von einem gemeinsamen zentralen Punkt haben, sind bei der nicht-viralen Gentransfektion besonders effektiv. Beide Polymere (Si-PDMAEMA und PB-*b*-PDMAEMA Mizellen) zeigten außerdem eine hohe Effizienz bei der RNA Interferenz-Therapie, da siRNA ebenfalls effektiv in verschiedene Zelllinien transportiert werden konnte.

Der zweite Themenkomplex dieser Dissertation behandelt die Struktur ionischer kompartimentierter Mizellen, nachdem diese mit entgegengesetzt geladenen Polyelektrolyten komplexiert wurden. Abschließend wurde die Fähigkeit solcher Strukturen zum Wirkstofftransport in therapeutischen Anwendungen untersucht. Als Basis für diese Untersuchungen dienten kompartimentierte Mizellen, die aus dem amphiphilen und amphoteren Triblockterpolymer Polybutadien-*block*-poly(1-methyl-2-vinyl pyridinium)-*block*-polymethacrylsäure (PB-*b*-P2VPq-*b*-PMAA; BVqMAA) durch Selbstassemblierung in wässrigen Lösungen eine Kern-Schale-Korona Struktur ausbilden. Der Kern dieser Mizellen besteht aus PB, während sich die diskontinuierliche Schale aus einem IPEK aus P2VPq und PMAA zusammensetzt. Nach außen hin werden die Mizellen durch eine dichte Korona aus überschüssigem, nicht an der Komplexbildung mit P2VPq beteiligtem, PMAA stabilisiert. Da die Korona Ketten bei ausreichend hohem pH Wert negativ geladen sind, konnten sie für die Komplexbildung mit diversen Polykationen

sowie doppelt hydrophilen Diblockcopolymeren mit einem kationischen Block verwendet werden. Sofern sich das für die Komplexierung verwendete Polykation von dem bereits vorhandenen P2VPq unterschied, wie zum Beispiel im Falle von quaternisiertem PDMAEMA (PDMAEMAq), bildete sich ein neues Kompartiment auf dem ursprünglichen Kern (PB und P2VPq/PMAA IPEK) der Mizellen aus. Dieses Kompartiment bestand aus dem IPEK zwischen PMAA und zugegebenem Polykation und ließ sich von der ersten Schale in elektronenmikroskopischen Aufnahmen deutlich unterscheiden. Es hatte die Form einer durchgängigen Schale, wenn die BVqMAA Mizellen eine kurze bis mittlere Korona-Länge hatten (345 – 550 MAA Einheiten pro BVqMAA Kette). Wurde für die Komplexbildung anstelle eines Homopolymers ein amphiphiles Diblockcopolymer mit einem positiven und einem wasserlöslichen aber ungeladenen Block verwendet, so konnte eine kollektive Stabilität der erzeugten komplexen Mizellen über den gesamten Mischbereich zwischen Mizellen und Polykationen erreicht werden. Oberhalb einer kritischen Menge an zugegebenem Homopolykation war dagegen eine Aggregation und makroskopische Phasenseparation der Mizellen zu beobachten.

Bei BVqMAA Mizellen mit einer besonders langen PMAA Korona (1350 Einheiten) wurde eine unregelmäßige Verteilung des neu gebildeten IPEK anstelle einer durchgängigen Schale bei der Zugabe von Polykation-Homopolymeren um den Kern gefunden. Als Ursache für diese neuen Strukturen wird eine Grenzflächenminimierung zwischen ursprünglichem Kern und neu gebildetem Kompartiment vermutet. Die Minimierung wird ermöglicht, da die besonders lange Korona das neue Kompartiment effektiv gegen eine Wechselwirkung mit dem wässrigen Medium abschirmen kann und so die Lösungs-Stabilität der gesamten Mizelle nicht negativ beeinflusst wird.

Abschließend wurden die Mizellen aus BVqMAA auf ihre Effizienz im Transport von hydrophoben Wirkstoffmolekülen für eine photodynamische Krebstherapie (PDT) sowohl in Zellkultur als auch in Mäusen mit Tumormodellen getestet. Durch die Komplexbildung der Mizellen mit dem doppelt hydrophilen Diblockcopolymer Poly(L-lysin)-block-poly(ethylenglykol) (PLL-*b*-PEG) konnte die Zusammensetzung der Mizell-Korona von reinem PMAA kontinuierlich zu einer PEG-Korona verändert werden. Der Einfluss der Korona auf die biologischen Eigenschaften der Mizellen in Abhängigkeit ihrer Zusammensetzung konnte so untersucht werden. Bei einem hohen Anteil an zugegebenem PLL-*b*-PEG wurde eine stabile, neue Mizellstruktur gefunden, wobei sich

das neu gebildete IPEK-Kompartiment in Zylinderform senkrecht auf dem Mizellkern stehend ausgebildet. Bei Untersuchungen der durch die Wirkstoff-tragenden Mizellen verursachten Zytotoxizität konnte ein deutlicher Einfluss der Korona-Zusammensetzung gefunden werden. BVqMAA Mizellen ohne PLL-*b*-PEG zeigten die höchste Zytotoxizität gegenüber humanen Lungenkrebszellen (A549). Diese Zytotoxizität wurde mit steigendem Anteil an PLL-*b*-PEG in der Mizellkorona stetig geringer, wobei der Trend gut mit der in die Zellen aufgenommenen Menge an Wirkstoff korrelierte. Vollständig PEGylierte Mizellen zeigten die geringste Menge an zellulär aufgenommenem Wirkstoff und die geringste Zytotoxizität. In Mäusen wurde eine verlängerte Blutzirkulation im Bereich mehrerer Stunden nach intravenöser Injektion lediglich für vollständig PEGylierte Mizellen beobachtet, während teilweise oder nicht PEGylierte Mizellen innerhalb kurzer Zeit nicht mehr im Blutkreislauf nachweisbar waren. Auch eine signifikante Akkumulation in subkutanen A549-Tumoren 24 h nach der Mizell-Verabreichung wurde nur für vollständig PEGylierte Mizellen gefunden. Die Menge an Wirkstoff, welche durch die Mizellen in den Tumor transportiert wurde, war ausreichend, um nach einmaliger Injektion der Mizellen und einer einzigen Laser-Bestrahlung eine effiziente Wachstumsunterdrückung des Tumors über einen Zeitraum von 21 Tagen zu erreichen. Somit konnte das Potential der BVqMAA Mizellen für einen Wirkstofftransport *in vitro* und *in vivo* erfolgreich nachgewiesen werden.

Glossary

AIBN	-	azobisisobutyro nitrile
ANOVA	-	analysis of variance
ATRP	-	atom transfer radical polymerization
BHT	-	butylated hydroxytoluene
b-PEI	-	branched polyethyleneimine
BVqMAA	-	polybutadiene- <i>block</i> -poly(1-methyl-2-vinyl pyridinium)- <i>block</i> -poly(methacrylic acid)
BVT	-	polybutadiene- <i>block</i> -poly(vinyl pyridine)- <i>block</i> -poly(<i>tert</i> -butyl methacrylate)
CD-spectroscopy	-	circular dichroism spectroscopy
cmc	-	critical micelle concentration
CPDB	-	2-(2-cyanopropyl)dithio benzoate
cryo-TEM	-	cryogenic transmission electron microscopy
CTA	-	chain transfer agent
DAMA	-	2-((2-(dimethylamino)ethyl)methylamino)ethyl methacrylate
DCM	-	dichloromethane
DCTB	-	<i>trans</i> -2-[3-(4- <i>tert</i> -Butylphenyl)-2-methyl-2-propenylidene] malononitrile
DDS	-	drug delivery system
D _h	-	hydrodynamic diameter
D.I.	-	dispersity index (light scattering)
DLS	-	dynamic light scattering
DMAc	-	dimethyl acetamide
DMAEMA	-	dimethyl aminoethyl methacrylate
DMF	-	dimethyl formamide
DMSO	-	dimethyl sulfoxide

Glossary

DNA	-	desoxyribonucleic acid
DP	-	degree of polymerization
Dq	-	quaternized PDMAEMA
EBIB	-	ethyl 2-bromoisobutyrate
EDC	-	<i>N</i> -(3-dimethylaminopropyl)- <i>N'</i> -ethylcarbodiimide hydrochloride
eGFP	-	enhanced green fluorescent protein
ENB	-	Elite Network of Bavaria
EPR	-	enhanced permeation and retention
FCS	-	fetal calf serum
GPC	-	gel permeation chromatography
HMTETA	-	1,1,4,7,10,10-hexamethyltriethylenetetramine
IC ₅₀	-	inhibitory concentration for 50 % of cells
<i>im</i> -IPEC	-	intracellular interpolyelectrolyte complex
IPEC	-	interpolyelectrolyte complex
LCC ₅₀	-	concentration of polyplex for 50 % of viable cells
LD ₅₀	-	lethal dose for 50 % of cells
l-PEI	-	linear polyethylene imine
MAA	-	methacrylic acid
MALDI-ToF-MS	-	matrix assisted laser desorption ionization time of flight mass spectrometry
MCM	-	multicompartment micelle
MFI	-	mean fluorescence intensity
Mic-PDMAEMA	-	micellar PDMAEMA
M _n	-	number average molecular weight
MTT	-	3-(4,5-dimethylthiazolyl-2)-2,5-diphenyl tetrazolium bromide
M _w	-	weight average molecular weight
MWCO	-	molecular weight cut off

Glossary

$N_{agg.}$	-	aggregation number
NMR	-	nuclear magnetic resonance
N/P (ratio)	-	nitrogen to phosphate ratio
P2VP	-	poly(2-vinyl pyridine)
P2VPq	-	poly(1-methyl-2-vinyl-pyridinium)
PB	-	polybutadiene
PB- <i>b</i> -PDMAEMA	-	polybutadiene- <i>block</i> -poly(2-(dimethylamino)ethyl methacrylate)
PBS	-	phosphate buffered saline
PDAMA	-	poly(2-((2-(dimethylamino)ethyl)methylamino)ethyl methacrylate)
PDAMAq	-	quaternized PDAMA
PDI	-	polydispersity index
PDLL- <i>b</i> -PEG	-	poly(D,L-lysine)- <i>block</i> -poly(ethylene glycol)
PDMAEMA	-	poly(2-(dimethylamino)ethyl methacrylate)
PDMAEMAq	-	quaternized PDMAEMA
pDNA	-	plasmid DNA
PDT	-	photodynamic therapy
PEG	-	poly(ethylene glycol)
PEI	-	poly(ethylene imine)
PEO	-	poly(ethylene oxide)
PI	-	propidium iodide
PLL- <i>b</i> -PEG	-	poly(L-lysine)- <i>block</i> -poly(ethylene glycol)
PMAA	-	poly(methacrylic acid)
PMANa	-	poly(sodium methacrylate)
PS	-	photosensitizer
PtBMA	-	poly(<i>tert</i> butyl methacrylate)
RAFT	-	reversible addition fragmentation chain transfer (polymerization)

Glossary

RES	-	reticuloendothelial system
R_h	-	hydrodynamic diameter
RNA	-	ribonucleic acid
ROS	-	reactive oxygen species
SD	-	standard deviation
SEC	-	size exclusion chromatography
Si-PDMAEMA	-	PDMAEMA from silsesquioxane initiator
siRNA	-	small interfering ribonucleic acid
tBMA	-	<i>tert</i> -butyl methacrylate
TE	-	transfection efficiency
TEM	-	transmission electron microscopy
THF	-	tetrahydrofurane

Chapter 1 – Introduction

“Nanomedicine” is a catchy name for recent efforts in the medical field to use materials of nanoscopic dimensions for the treatment or diagnosis of various diseases.^{1, 2} Although the definition is rather vague, the size of such systems is in between that of small molecule drugs (up to several nanometers) and micron-sized objects, resulting in specific beneficial properties. Nanomaterials are comparable in size to proteins, enzymes or viruses and are therefore well suited to specifically interact with biological systems on a cellular or sub-cellular level. Compared to small molecule drugs a higher degree of complexity is inherent to those materials, leading to a multi-functionality of the overall system. For example, in cancer therapy many drug delivery systems (DDS) have been developed from nanostructured materials, which show increased availability of the drug in the organism through a prolonged circulation time in the bloodstream, an enhanced accumulation in the targeted tissue through targeting mechanisms as well as selective release or activation of the drug at the desired site. All these properties of nanoscopic DDS can result in a more effective treatment or diagnosis as compared to conventional methods. Depending on what type of a material is used for the medical application they can be classified into three different categories, namely inorganic, organic or hybrid materials. Quantum dots are well-known examples for inorganic imaging agents in fluorescence microscopy³ and iron oxide nanoparticles are currently in clinical trials for magnetic resonance imaging⁴. Purely organic platforms can be found in the superstructures of self-assembled small molecules such as liposomes⁵ or in polymeric systems such as polymer micelles⁶ and polymer vesicles (polymersomes).⁷ Consequently, hybrids are a combination of both types of materials into a single DDS. In the following, polymeric systems capable of delivering therapeutically active substances will be described in more detail.

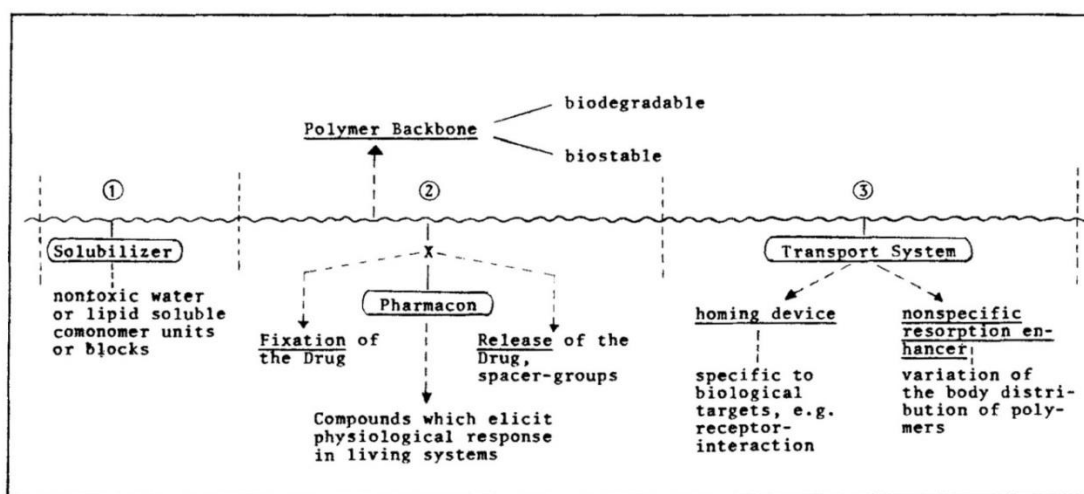
1. Polymer-Aided Drug Delivery

1.1. Polymer-Drug Conjugates

A pioneering idea for the use of polymers in therapeutic applications was introduced by Helmut Ringsdorf in 1975, when he proposed the concept of “polymer therapeutics”.⁸ In his approach a polymer chain is used to covalently connect several functional molecules,

such as a therapeutic drug and a targeting moiety, into one multi-functional macromolecule (**Scheme 1-1**).

The main advantage of such a combination as proposed by Ringsdorf was in the larger availability of the drug in the organism through an increase in blood circulation time due to the higher molecular weight and a better solubilization of poorly water-soluble drugs by linking them to hydrophilic macromolecules. The idea of attaching specific targeting molecules to increase the localization of the drug at the desired site was already included in this approach. Due to the ease of chemical modification of synthetic polymers, the original concept has been explored in much more detail and was considerably expanded to include a wide variety of macromolecular delivery systems for therapeutic applications.⁹⁻¹² The design of biocompatible¹³ and degradable polymers^{14, 15} together with the use of chemical linkers, which release the coupled drugs at appropriate conditions have pushed the field forward and several polymer-drug conjugate formulations are tested in clinical trials or have already been approved for therapeutic use in humans.^{2, 16}



Scheme 1-1. Ringsdorf's model for a pharmaceutically active polymer-drug conjugate. Reprinted with permission.⁸

1.2 Important Concepts in Drug Delivery: Stealth Effect and EPR

A highly successful synthetic material aiding in the transportation of drugs inside living organisms is poly(ethylene glycol) (PEG). Many DDS are ultimately formulations containing PEG in some form. It is an uncharged, water-soluble polymer that is

extensively used in many kinds of consumer products, such as shampoos, crèmes, gels, etc. and is synthesized by anionic polymerization of ethylene oxide. Therefore, PEG is also referred to as poly(ethylene oxide) (PEO) and both names are used regularly. For therapeutic applications PEG is an ideal polymer, because it is non-toxic, biocompatible and has protein repellent properties. Compared to other polymers with similar properties, *i.e.* polyoxazolines,¹⁷ it has the advantage of FDA (U.S. Food and Drug Administration) approval for many applications, consequently triggering an extensive use of PEG polymers in therapeutic problems and resulting in its status as “gold standard”.¹⁸ Originally, the term of PEGylation referred to the conjugation of therapeutically active molecules (small molecule drugs, proteins, peptides, DNA, etc.) to PEG chains in order to increase the solubility in water and to protect the respective molecule from degradation, *e.g.* by enzymes, or immunogenic recognition.¹⁹ In the meantime, however, the term is being broadly applied to many kinds of PEG containing structures used in a medical context, for example organic and inorganic nanoparticles, surface coatings and polymeric micelles.^{20, 21} Many of the desired properties found for PEG-drug conjugates are also occurring for PEGylated particles, where the PEG coating leads to increased circulation time in the bloodstream and a reduction of non-specific interactions especially with proteins, which is summarized in a so-called “shielding” or “stealth effect” of PEG. Depending on the designated application, the molecular weight and grafting density (mushroom or brush conformation²²) of PEG chains have to be adjusted.

Connected to the beneficial properties conferred by PEG on DDS, a passive targeting mechanism occurring for solid tumors in cancer therapy, known as the *enhanced permeation and retention (EPR) effect*, has been largely responsible for the success of nanoscopic DDS in that field.²³ It was first described by Maeda *et al.*²⁴ in 1984 and is based on the specific vascular structure in solid tumors, characterized by a high vascular permeability together with an impaired lymphatic drainage as compared to normal tissue, which allows DDS of a specific size range to preferentially accumulate inside the tumor tissue. In order to make use of the EPR effect, the nanoscopic carrier system needs to have a prolonged blood circulation time in the order of several hours, usually associated with a size in between approximately 10 – 500 nm and a dense shielding layer preventing protein adsorption.²⁵ Molecules with a size below 10 nm are rapidly cleared through the kidney, while larger particles up to 15 μm primarily accumulate in liver and spleen and are cleared through the reticuloendothelial system (RES).²⁶ However, if both the surface

coating, *e.g.* PEGylation, and the size of the drug carrying system are appropriately chosen, already a significant improvement of therapeutic efficacy can be observed due to increased tumor accumulation originating from the passive targeting by EPR.²⁷

1.3 Polymer Micelles and Vesicles

Apart from employing covalent polymer drug conjugates, the use of polymeric carrier systems which physically encapsulate active molecules can have certain benefits. Amphiphilic block copolymers self-assemble into micellar aggregates with a hydrophobic core and a hydrophilic shell in aqueous solution, similar to micelles from small molecule amphiphiles. At appropriate hydrophobic to hydrophilic balance in the block copolymer, the formation of polymer vesicles, also called polymersomes, is favored. These structures have a hydrophobic membrane encapsulating a large water-filled compartment and resemble liposomes or cellular structures. In contrast to micelles from surfactant molecules, the molar critical micelle concentration (cmc) of polymeric micelles is lower by several orders of magnitude and their stability against dissociation is consequently significantly higher.²⁸ The core of the micelles is well suited to incorporate drug molecules, protecting them from degradation or unwanted interaction with the organism, *i.e.*, systemic toxicity. Typically, the size of such polymeric micelles is in the range of 20 – 200 nm and therefore ideal to make use of the EPR effect, mentioned above. A dense brush formed by the water-soluble polymer chains in the corona of the micelles prevents agglomeration of the micelles with each other through steric repulsion and hinders recognition by the RES, *e.g.* in case of PEG. Consequently, by incorporating drugs into micellar carrier systems the pharmacokinetic properties can be significantly altered as compared to the free drug.²⁸

In systems suitable for the transportation of hydrophobic drugs, drug-incorporation is based only on hydrophobic interactions. Therefore, a given diblock copolymer can in principle be used for the transportation of many different kinds of hydrophobic drugs, which makes the system more versatile than a polymer-drug-conjugate. In cancer therapy, doxorubicin and paclitaxel are two examples for drugs commonly used in polymeric micelle carrier systems, where some formulations are currently undergoing clinical trials.²

Polymersomes are well-suited to carry large amounts of hydrophilic drugs in their aqueous compartment. Additionally, hydrophobic drugs can be incorporated into the polymersomal membrane offering additional options for the delivery of active agents or reporter molecules.²⁹ Additional complexity can be achieved, when smaller vesicular structures are incorporated inside a larger polymersome, mimicking cellular compartments.⁵ Polymersomes have been prepared from a number of different diblock copolymers, usually amphiphilic diblock copolymers. However, several examples exist using polyion complex formation of double hydrophilic copolymers with oppositely charged homopolymers or diblock copolymers for vesicle formation.^{30, 31} These systems are often also called PICsomes and are promising candidates for delivering both anti-cancer drugs and nucleic acids.

Besides hydrophobic cargo, polymer micelles can also be used to interact with ionic guest molecules, such as ionic drugs, proteins or polynucleotides. Generally, double hydrophilic diblock copolymers with one ionic block are utilized in this approach and a complex between guest molecule and ionic block of the block copolymer forms the core of the micelle. The group of Kazunori Kataoka has contributed significantly to the field with micelles from PEG-*block*-poly(amino acid) diblock copolymers. By using a PEG-*block*-poly(glutamic acid) block copolymer the group could incorporate amine-containing platinum drugs (**Figure 1-1**), which are selectively released in the slightly acidic environment of lysosomes in cancerous cells.^{27, 32}

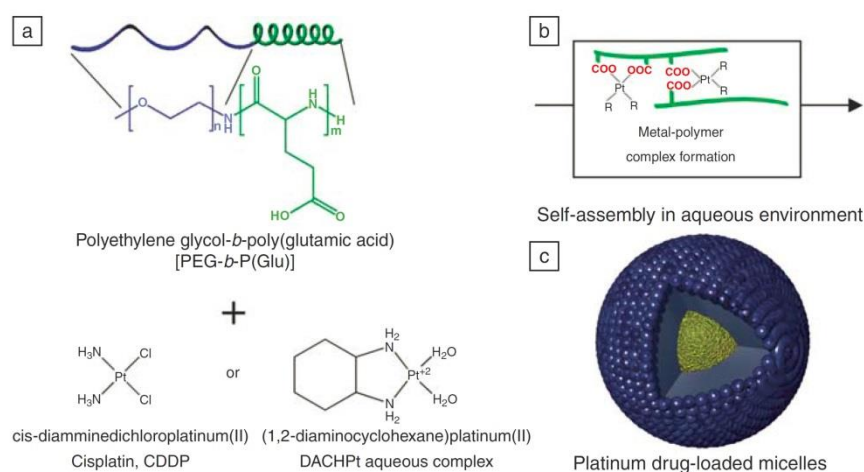


Figure 1-1. Schematic diagram for the formation of platinum drug carrying micelles. PEG-*b*-P(Glu) mixed with platinum drugs (A) forms a metal polymer complex (B), which self-assembles to drug loaded micelles (C) in aqueous solution. Reprinted with permission.³²

A substantial benefit of using synthetic polymer DDS in therapeutic applications is the high versatility, which stems from the rather easy chemical modification of synthetic polymers. Material properties can be tailored to the desired application through the correct choice of monomers constituting the polymer. However, chemical versatility is much greater than just a good selection of the materials creating the main chain of the polymer. Through post-polymerization modification reactions further functionalities or additional properties can be introduced to an already existing polymer system, thereby greatly enhancing the usefulness of the DDS. One such example is the conjugation of targeting functions to polymer micelles. While passive targeting is based on the inherent properties of the carrier system and the target tissue, *i.e.*, the special vascular structure in solid tumors utilized by particles of a certain size range in case of the EPR effect, the conjugation of specific targeting molecules allows very selective recognition of tissues or cell types. This is due to preferential binding of the target function to complementary recognition sites (*e.g.* cell receptors) on the targeted cell type. As a consequence, not only is the accumulation in the target tissue enhanced, but it can also occur in a much more selective fashion in a complex biological environment. Through the binding event of a DDS bearing targeting functions, an enhanced uptake into the cells can be induced. An inefficient cellular uptake is one of the drawbacks occurring in long-term circulating DDS, exactly because they are not recognized by the RES but neither by the cells to be treated. Several types of targeting functions have been tested both *in vitro* and *in vivo* so far, and these include peptides, proteins, sugars, antibodies and small molecules.⁶ In all of these cases the targeted cell line overexpresses certain receptors allowing for a preferential binding of the polymer micelles with the correct targeting moiety. Typically, the targeting molecule is conjugated to a terminal functional group at the periphery of the water-soluble corona to minimize sterical hindering.

Other chemical modifications can help to further increase the efficacy of DDS. For example, chemical crosslinking can enhance the stability of polymer micelles against dissociation, when injected into the bloodstream. By using disulfide bonds as part of the crosslinking connection the DDS becomes more stable in a regular medium, but can selectively disassemble in a reductive environment found inside targeted cancer cells.^{33, 34} Creating DDS that are sensitive to their environment in such a way that they selectively release their cargo through an external triggering event would be very useful in controlling the location and dose of a delivered drug molecule. Various approaches have

been reported for the creation of environmentally sensitive polymer micelles, which can disassemble upon external triggers, facilitating a fast drug release.^{15, 35} Using triggering events that are either a part of the natural biological environment of the targeted tissue (specific pH³⁶ or reductive environment) or that can be applied minimal-invasively (light irradiation, magnetic fields, ultrasound or temperature) by an external source have been successfully implemented into polymeric micelle carriers.⁶

1.4 Photodynamic Therapy

Photodynamic therapy (PDT) is one example for a minimal-invasive treatment approach using an external triggering event (light). Specific molecules, so-called photosensitizers (PS), can create a cellular toxicity upon illumination with light of appropriate wavelength.^{37, 38} The method is still under development, but shows great promise for the treatment of certain types of cancer (skin-, lung- and colon cancer) as well as some dermatological disorders.³⁹ Amongst others, the expected benefits from PDT as an anti-cancer therapy are the localized and externally controlled cytotoxicity due to light activation as well as having new drug molecules to overcome drug-resistance of certain tumors. A brief explanation of the PDT mechanism is given in the following.

Through light absorption, the PS molecule reaches an excited state and can return to the ground state by creating reactive oxygen species (ROS). These ROS can be produced either through direct interaction between the PS and oxygen molecules (Type II reaction) or by first abstracting hydrogen from cellular components (Type I reaction), creating radicals, which in turn lead to the formation of ROS. ROS are strongly cytotoxic because of their high reactivity, which disrupts essential cellular functions through the attack on proteins, enzymes and other cellular molecules. Once created, the ROS quickly reacts with any molecule in its vicinity, leading to a spatially limited radius of action. By precisely controlling the dimension of the illuminated area, *e.g.* through the use of lasers, the method produces a strictly localized toxic effect. Non-illuminated areas, even in the presence of PS show only negligible toxicity. A successful PDT therefore needs three components, namely PS accumulation inside the target tissue, light of the appropriate wavelength reaching the desired site and a supply of oxygen, typically dissolved in the aqueous environment. From these criteria some of the drawbacks of PDT also become apparent. The PS needs to accumulate at the target tissue in a homogeneous fashion and a

large effort has been made at rendering the typically hydrophobic PS molecules more hydrophilic in order to improve their bioavailability.⁴⁰ Humans treated with PDT drugs showed skin irritation, because of unspecific accumulation in the whole skin and had to avoid sunlight for weeks after the treatment. Since light must be able to reach the targeted area, only those types of tissue and organs can be treated, that are easily accessible with a light source either directly (skin) or with endoscopic methods (colon, bladder and lung). The penetration depth of the light has to be sufficiently high and PS of the new generation usually absorb light between 600 – 800 nm, where the absorption of the tissue is low and penetration depth can be increased. Finally, the oxygen supply can become problematic, especially for very efficient ROS producing drugs, because diffusion from the surrounding tissue is typically slower than the oxygen consumption due to ROS production. Only a few PDT drug formulations have been approved for use on humans so far,⁴¹ but the method opens up many attractive possibilities for a new cancer therapy, when the above mentioned drawbacks are finally overcome. Incorporating PDT drugs into polymer micelles might be one step towards that goal.⁴²

1.5 Complex Drug Delivery Systems: Multicompartment Micelles

Thus, with the many possibilities to introduce different functions or physical properties in polymer micelles, this type of delivery system rapidly developed from a simple encapsulation agent helping to solubilize a single drug to a multi-functional and highly sophisticated nanomedical device tailored to effectively treat the respective disease. In this context, the option to deliver two or more different active molecules simultaneously is an important feature of a truly multifunctional DDS.⁴³⁻⁴⁵ By delivering two drug types for the same disease a synergistic effect can occur, *e.g.* from delivering both a gene and an anti-cancer drug to a tumor, and this can lead to improved treatment efficiency and strongly reduced tumor growth.⁴⁶ If a reporter molecule and a drug are transported simultaneously, such a DDS can be used for concurrent diagnostics and treatment. Recently, such systems combining both therapeutic and diagnostic properties were termed as “theranostic” devices to emphasize their dual role in a therapeutic approach.^{25, 47-50} In principle, any kind of diagnostic technique can be combined in a carrier system with an appropriate drug. In some cases already the drug molecule combines both these features, *i.e.* a fluorescent anti-cancer drug (for example all PDT drugs).

Often, different active molecules can be problematic to incorporate in the same part of a simple core-shell micelle. Specific environments need to exist inside of such a device to accommodate each active agent. Multicompartment micelles (MCMs) have great potential of fulfilling these criteria and were first proposed by Ringsdorf.^{51, 52} Segregated compartments are formed, when immiscible polymer blocks are forced together in micellar structures.^{53, 54} One way to ensure the phase separation to occur on a microscopic level is by using triblock terpolymers. Consequently, the first published examples used fluorocarbon and hydrocarbon blocks in triblock terpolymers, due to the strong phase separation between the two water-insoluble blocks.^{55, 56} In the meantime, however, also triblock terpolymers without fluorinated blocks have been shown to form similar structures.^{57, 58} The different chemical environments inside the phase separated core of such complex structures allow for the incorporation of chemically different guest molecules.^{59, 60} Besides a pure therapeutic use of such structures, MCMs have great potential as a templating material for example in nanoparticle synthesis,⁶¹ as nano-reactors for chemical reactions⁶² and as building blocks in a hierarchical self-assembly⁶³ to mesoscopic materials. So far, only very few examples of an actual therapeutic use of MCMs from triblock terpolymers with more than one guest molecule exist. This is probably due to the synthetic effort necessary to produce triblock terpolymers with adequate homogeneity and in sufficient quantity. The group of Christine Jérôme used MCMs from miktoarm star terpolymers made of poly(ethylene oxide)-*star*-poly(2-vinylpyridine)-*star*-poly(ϵ -caprolactone) (PEO-P2VP-PCL) to incorporate a hydrophobic dye as a model drug, while simultaneously using the pH-sensitive P2VP block for exposing in acidic environment a targeting function conjugated to that block.⁶⁴ They studied the uptake behavior of the micelles in dependence of the protonation state of the pH sensitive block *in vitro* as well as the drug release kinetics in diluted conditions. Also, Yamauchi et al.⁶⁵ recently reported on the use of a polystyrene-*block*-poly(acrylic acid)-*block*-poly(ethylene glycol) triblock terpolymer for the preparation of MCMs which carry a hydrophobic fluorescent dye in the core and a platinum drug in the poly(acrylic acid) compartment, while the PEG corona stabilizes the overall micelle. They demonstrated a dose-dependent decrease of the cell viability *in vitro* and tracked the micelles through the fluorescent dye. In summary, multicompartment micelles have great potential for tackling some of the open challenges in efficient drug delivery, especially in the field of combinatorial therapy where multifunctional drug carriers, capable of delivering several

drugs at once are needed. For the synthetic effort necessary in creating such systems to be worthwhile, the full potential of a selective drug release of several drugs independent of each other and in specific cellular locations must be realized in the future.

2. Delivery of Genes

“Gene therapy” summarizes a therapeutic approach for the treatment of inheritable or acquired diseases, where defective or missing genes are replaced by an appropriate exogenous gene introduced into the cell.^{66, 67} Also the down-regulation (silencing) of overactive genes by means of RNA interference can offer promising and previously unavailable therapeutic tools.⁶⁸ A human gene therapy approach is especially promising for certain types of diseases that are otherwise difficult or even impossible to treat so far. These include genetic diseases like severe combined immunodeficiency, hemophilia or cystic fibrosis, but also acquired illnesses like cancer or AIDS could potentially be addressed with gene therapy.⁶⁶ One of the biggest challenges for gene therapy is the effective introduction of foreign genetic material into the target cell, because several hurdles exist that protect against just such an event. Consequently, significant efforts have been made in creating delivery vehicles (“vectors”) for nucleic acids that can effectively overcome the different cellular barriers and successfully deliver their cargo to the target (nucleus or cytosol). Inevitably, the delivery of genes for fighting disease in patients will need delivery vehicles capable of delivering their cargo in a complex living organism and not just in cell culture. This environment offers special conditions, which additionally complicate the process of gene delivery before the vector has even reached the target cell and encounters its inherent defense mechanisms. It follows that the same challenges discussed above for *in vivo* drug delivery apply here as well.

However, the intentional modification of cells, summarized under the title of genetic engineering, by introducing recombinant DNA *in vitro* is an important field in its own right. Many drug molecules are difficult to produce by fully synthetic means because of multi-step procedures requiring protective groups, stereo-selective catalysis and multiple purification steps. Cells can produce these drugs by enzymatic means with absolute stereo-selectivity and in high quantity when genetically engineered to do so. Since the cells are cultivated in cell culture in a bioreactor, many of the restrictions that apply to an *in vivo* delivery system are absent for this application. Therefore, even vectors which might not be suitable for a gene therapy approach can still be very effective for the delivery of genes *in vitro* where matters of delivery efficiency and production cost might be more important than blood circulation times or organ distribution.

All delivery vehicles, regardless of their final use, are usually divided in two categories, namely viral and non-viral vectors. Some significant differences between the two types exist, leading to specific challenges that need to be overcome before a widespread use can take place.

2.1 Viral Vectors

Viruses are heavily used as delivery vehicles for genetic material, because they evolved specifically to introduce their own genome into the host cell. As a result, the delivery efficiency of viral vectors is very high and in many cases specific towards a certain cell line. In addition, viruses can stably incorporate the transported DNA sequence into the host cell genome ensuring continued gene expression, which can be beneficial in the treatment of certain diseases. However, some drawbacks exist for viral vectors. The most significant drawback is the possibility of an immune response of the organism, posing a significant risk to the patient. Also, a repeated application of viral carriers in the same patient could result in a loss of transfection efficiency, due to recognition of the virus by the immune system. Furthermore, large-scale production and chemical modification of the virus capsid is challenging, the latter potentially leading to a change in the self-assembly of the three dimensional virus structure. Some restrictions on the size of the transported DNA can also apply, due to the highly defined structure of the virus. Nevertheless, most clinical trials performed on gene therapy so far have used viral vectors.^{69, 70}

2.2 Non-Viral Vectors

Alternative transfection methods, often based on synthetic molecules or artificial particles, have been developed in recent years to overcome the above-mentioned drawbacks of viral vectors. Amongst those are electroporation, the “gene gun” - metal nanoparticles coated with DNA that are shot into the cells - as well as cationic molecules such as lipids and polymers.⁷¹ All of these methods are generally considered to be less effective and selective in delivering their genetic cargo as compared to their viral competitors and in most cases only a transient expression of genes can be achieved, since they are lacking mechanisms to permanently introduce the transported DNA sequence

into the host genome. For some non-viral systems, but especially in polymeric vectors, a significant cellular toxicity is observed in many cases. Still, significant effort has been put into improving the performance of non-viral vectors, aided by the ease with which chemical modifications can be made on the systems.

2.3 Barriers to a Successful Delivery of Genes

The process of a successful delivery of nucleic acids to the target site in the cell with special consideration of the barriers encountered *en route* is exemplarily described in the following by example of a polycationic non-viral gene delivery vector.

On its own, the uptake of free DNA in cells is inefficient, because of the size and negative charge of the DNA. Consequently, methods that make use of delivery mechanisms inherent to the cell (liposomes and polymers) rather than brute force (gene gun and electroporation) first need to compact the DNA to particles of smaller size and neutralize the negative charge of the DNA phosphate groups. Both processes occur when polycations form polyion complexes with nucleic acids (**Figure 1-2, I**). Such complexes are also termed as “polyplexes” or “inter-polyelectrolyte complexes” (IPECs) and additionally protect the DNA against enzymatic degradation. The properties of polyplexes like size and charge are mostly influenced by the choice of the polycation and do not strongly depend on the DNA used, but even if these physicochemical parameters of polyplexes are known, it is not possible to predict their transfection behavior.⁷⁰ When mixing DNA and polycations to form polyplexes, generally, an excess of polycation (calculated as the ratio of positive to negative charges or nitrogen over phosphorus, N/P) is used and this leads to the formation of polyplexes with an overall positive charge. These can now efficiently bind to the negatively charged cell membrane, significantly enhancing their cellular uptake *in vitro* (**Figure 1-2, II**). Cellular uptake of the polyplexes depends on a multitude of factors such as size, charge, surface chemistry, the presence of targeting functions and possibly also mechanical properties of the polyplexes. It constitutes one of the most critical steps in gene delivery, although a high polyplex uptake is by no means a guarantee for a strong transgene expression. The uptake behavior is also known to vary with cell type, where different pathways may be used, which complicates matters further.⁷² An uptake through an endosomal pathway is the most common mechanism of polyplex entry into cells.

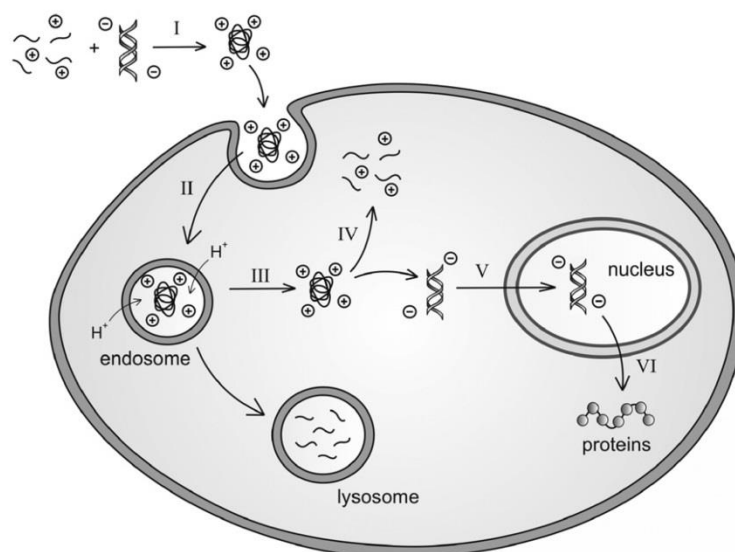


Figure 1-2. Barriers to gene delivery – Design requirements for gene delivery systems include the ability to (I) package therapeutic genes; (II) gain entry into cells; (III) escape the endo-lysosomal pathway; (IV) effect DNA/vector release; (V) traffic through the cytoplasm and into the nucleus; (VI) enable gene expression; and (VII) remain biocompatible. Reprinted with permission.⁷²

Once the polyplex is inside of an endosomal compartment in the cell, it needs to be released into the cytosol and further travel to the nucleus in case of DNA delivery (**Figure 1-2, III**), while for siRNA delivery reaching the cytosol is often sufficient. During the transport of endosomes to lysosomes ATP-mediated proton pumps acidify the interior of the endosome, finally leading to the activation of nucleases capable of degrading the DNA. Several polymeric vectors make use of this acidification for an endosomal escape. This can be either through a controversially discussed⁷³ process called “proton sponge effect” (PSE)^{74, 75} where the high buffering capacity of polycations like poly(ethylene imine) (PEI) leads to a water influx and finally bursting of the endosome. Other polymeric systems have used cell penetrating peptide sequences⁷⁶ or synthetic functions⁷⁷ mimicking these peptides for interrupting the endosomal membrane and facilitating a release of the polyplex from the endosome. Also the co-delivery of small molecules assisting in endosomal escape has been shown.

Even after a polyplex has successfully entered the cytosol of the target cell, there are still several barriers to overcome, before the DNA has reached its designated destination. The mobility of macromolecules and particles, such as polyplexes, is strongly hindered in the cytosol, *i.e.*, due to the cytoskeleton and the high viscosity of the cytosol originating from

the high protein content. Viral vectors can rely on active transport mechanisms such as microtubules, which are generally not available for polymeric vectors unless still enclosed in the endosome. Instead polymeric vectors have to form complexes of small size to increase mobility. Nucleic acid degradation is a reoccurring problem in the cytosol and a premature release of the DNA from the complex is detrimental for transfection efficiency mainly for reasons of rapid DNA degradation. However, for the genetic information of the DNA to be accessible it must eventually be released from the polyplex, otherwise transgene expression is hindered. Finding a system with a balanced binding strength towards the DNA, where on the one hand stable complexes that protect the DNA from degradation are formed while still allowing for a release at the correct timepoint, is critical.

The final barrier for DNA delivery to eukaryotic cells is the nucleic membrane and the DNA has to cross it in order to induce a successful expression of the desired gene (**Figure 1-2, V**). Pore complexes can actively transport even large molecules through the membrane and into the nucleus, but appropriate targeting ligands have to be presented in order to activate these pore complexes. Another possibility is during cellular division, where the nucleic membrane breaks down for a short period of time. The lack of pore complex activating peptides is the reason why many polymeric vectors are only efficient in dividing cell lines, while transfection performance drops severely in non-dividing cell lines.

Many of the processes involved in the successful delivery of exogenous genetic material to a target cell are not fully understood yet. It is therefore difficult to make any prediction on the transfection performance of a new polymer vector and in many cases careful mapping of the parameter space is necessary to find optimal transfection conditions. Since performance can vary strongly with each different cell line and also depends on factors like the presence or absence of serum proteins *in vitro*, this process has to be repeated for each vector when applied to a new target.

As mentioned above, the delivery of genes under *in vivo* conditions constitutes a formidable challenge for most transfection systems, especially for non-viral ones. Polyplex stability can be a problem under physiological conditions (increased salt concentration, competing polyions, serum proteins, etc.) and dissociation of the complex

can lead to DNA degradation, while an aggregation of polyplexes or the association with proteins in the bloodstream can lead to fast clearance. For intravenous injection of polyplexes the problem of sufficient accumulation at the target site and avoidance of recognition, already discussed for anti-cancer-drug carrying polymer micelles, arises as well. Some solutions are found in the charge neutralization and shielding of the polyplexes, for example through PEGylation, although this generally results in lower uptake efficiency in the target cells. A direct injection of the polyplexes to the target tissue can overcome the problems associated with insufficient accumulation; however, it does not automatically guarantee a successful gene transfection.

2.4 Polymeric Vectors

Many different polymers with positive charges have been tested for their potential in transfection. Most of these polymers have amino groups as the charge bearing species and some typical representatives of polymeric non-viral carriers are depicted in **Figure 1-3**. Polylysine was one of the first polymers to be used for the transfection of cells and has reached pre-clinical trials as a block copolymer with PEG.^{78, 79} PEI in both its branched and linear architectures has shown remarkably high transfection efficiency and is considered as the “gold standard” for polymeric gene delivery.⁷⁵ Many chemical modifications have been proposed to further increase the transfection efficiency and especially at addressing the problem of its rather high cytotoxicity.⁸⁰ Several commercially available transfection reagents such as ExGen500 and jetPEI use linear PEI in their formulations. Szoka et al. first used poly(amido amine) dendrimers for nucleic acid transport and several different dendritic molecules have been studied in detail because of their branched architecture and highly defined structure.^{81, 82} Recently, some reports used phosphonium containing polymers as an alternative material, proving their principal capability for the delivery of genes *in vitro*, while exhibiting rather low cytotoxicity as compared to ammonium containing polymers.⁸³⁻⁸⁵

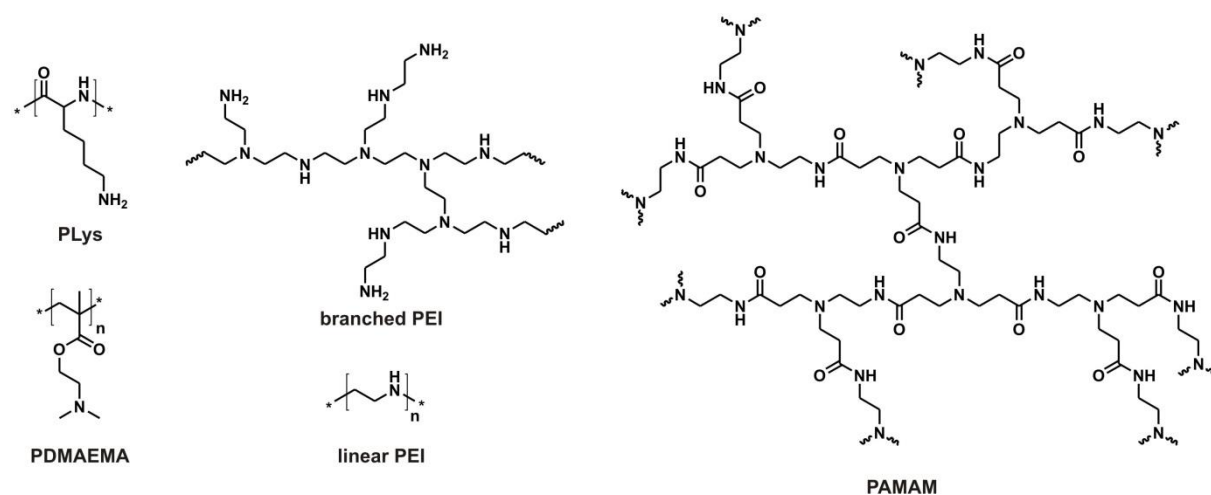


Figure 1-3. Polymer structures of polycations regularly used as non-viral transfection agents.

To better understand the individual mechanisms that govern a successful delivery of genes to the target cell, it is a necessity to have well-defined starting materials. Almost all synthetic polymers have a distribution of their molecular weight and therefore represent a mixture of individual polymer chains of varying length. Furthermore, reproducibility is only given up to a certain point, since both molecular weight and molecular weight distribution can vary significantly between individual batches. If the distribution of a polymer sample is broad, it becomes difficult to discern between the individual contributions of the different chains making up the overall mixture. Therefore, polymers with a narrow molecular weight distribution, a good control over the molecular weight and high reproducibility between batches is to be preferred. Additionally, access to different polymer architectures can be interesting, since material properties can be significantly influenced through the three-dimensional connection of the monomers in a polymer. By using monomers that can be polymerized with controlled or living polymerization methods, such different polymer architectures in combination with narrow molecular weight distributions have become available.^{86, 87} With the resulting polymers of defined molecular weight and controllable architecture, the aim is to establish structure-property relationships for polymeric vectors and possibly even define some guidelines for the design of successful polymeric gene carriers.⁸⁸

Poly(2-(dimethylamino)ethyl methacrylate) (PDMAEMA) is a polycation that can be easily prepared by living polymerization methods like reversible addition fragmentation chain transfer (RAFT) polymerization,⁸⁹ atom transfer radical polymerization (ATRP),⁹⁰

as well as anionic polymerization⁹¹ and has shown promising performance as a non-viral gene carrier.⁹² Similar to many other polymeric gene transfection agents an increase in cytotoxicity that is coupled with an increase in transfection efficiency could be observed. Several studies on the influence of the molecular weight on transfection efficiency and toxicity have also been performed.^{93, 94} Much effort has been put into decoupling an effective transfection from a significant cytotoxicity. At the very least a decrease of the toxicity to bearable levels, while maintaining a high transfection efficiency has been the aim of several studies. It is believed that part of the toxicity stems from the non-degradable nature of the PDMAEMA. Several groups have therefore prepared DMAEMA containing polymers that can be cleaved into smaller building blocks under physiological conditions, albeit with ambiguous results on both transfection efficiency and toxicity.⁹⁵⁻⁹⁸ A copolymerization of PDMAEMA with other monomers or conjugating PEG to PDMAEMA could successfully reduce the toxic effects of the polymers in many cases. However, not in all cases did a reduction of the toxicity also lead to an increase in transfection efficiency.⁹⁹ The influence of architectural changes to the PDMAEMA structure was also tested for improving gene delivery efficacy. Non-linear polymer architectures can be synthesized for PDMAEMA for example by using multi-functional initiator molecules. Both star-shaped¹⁰⁰⁻¹⁰², branched^{103, 104} and cylindrical brush-like¹⁰⁵ polymers were subsequently tested for their transfection performance and showed superior results as compared to their linear counterparts. Georgiou *et al.* were the first to use star-shaped PDMAEMAs for gene transfection. They prepared the polymer through an “arm-first” method with a crosslinking monomer introduced into the group transfer polymerization of DMAEMA.¹⁰⁶⁻¹⁰⁸ Several other groups have made use of such branched structures in the meantime. In summary, PDMAEMA offers many possibilities to elucidate the mechanisms of gene transfection, due to its chemical versatility.

Despite these tremendous improvements in controlling the polymer architecture and molecular weight distribution, many open questions remain unanswered for the moment. Controversial and even conflicting results are repeatedly reported in the literature. In many cases a comparison between different studies is difficult, because transfection protocols, cell lines, reporter genes and material characterization methods are chosen based on preference or availability by the respective groups rather than by standardized rules. This is a major drawback that needs to be addressed in the future in order to better coordinate the individual efforts of each group.

As an outlook for nanomedicine, polymeric materials have a good chance of significantly contributing to the field in the future. Polymers are chemically versatile and can easily be tailored to their respective use by skilled synthetic chemists. However, to be able to correctly design the materials, polymer chemists and material scientists in general need to closely collaborate with scientists from other disciplines like biology, biochemistry, pharmaceutical and medical sciences, who have a deep understanding of the processes and related challenges specific to living organisms. Only through a clever design of materials that takes into account all the available knowledge of the different disciplines will a significant improvement become possible, rather than hoping for a “lucky shot” from a single discipline.

3. Aim of this Thesis

The motivation of this thesis was to explore the potential of polyelectrolyte nano-structures especially for therapeutic applications.

In polymeric gene delivery, we investigated structure-property relationships of branched polycations in gene delivery, in particular of star-shaped architectures. A better mechanistic understanding of the relevant processes involved in the transport of nucleic acids by means of polymeric vectors would help to improve the material performance. With controlled radical polymerization methods and multi-functional initiator molecules, a vast library of polymeric structures was accessible that was previously nearly unexplored for transfection. Information about the influence of macromolecular parameters like molecular weight or degree of branching on transfection results might yield some general “design rules” for improving non-viral gene delivery.

Multicompartment micelles are a relatively new class of nanostructured materials, which have potential use in several fields. Here, we wanted to investigate MCMs from BVqMAA triblock terpolymers, and were particularly interested in expanding the functionality of this system as well as creating new MCM structures. The incorporation of new, additional compartments in the micelles would increase the complexity and could lead to previously unknown micelle structures. Using individual compartments for the incorporation of active molecules opens many possibilities for therapeutic applications, especially if more than one functional aspect of the MCM is put to use. Applying the MCM system from BVqMAA triblock terpolymer to a therapeutic application was the ultimate goal.

4. References

1. Peer, D.; Karp, J. M.; Hong, S.; Farokhzad, O. C.; Margalit, R.; Langer, R., *Nature Nanotechnology* **2007**, 2, (12), 751-760.
2. Wang, R.; Billone, P. S.; Mullett, W. M., *Journal of Nanomaterials* **2013**, 2013, 12.
3. Medintz, I. L.; Uyeda, H. T.; Goldman, E. R.; Mattoussi, H., *Nature Materials* **2005**, 4, (6), 435-446.
4. Colombo, M.; Carregal-Romero, S.; Casula, M. F.; Gutierrez, L.; Morales, M. P.; Boehm, I. B.; Heverhagen, J. T.; Prosperi, D.; Parak, W. J., *Chemical Society Reviews* **2012**, 41, (11), 4306-4334.
5. Marguet, M.; Bonduelle, C.; Lecommandoux, S., *Chemical Society Reviews* **2013**, 42, (2), 512-529.
6. Mahmud, A.; Xiong, X.-B.; Aliabadi, H. M.; Lavasanifar, A., *Journal of Drug Targeting* **2007**, 15, (9), 553-584.
7. Levine, D. H.; Ghoroghchian, P. P.; Freudenberg, J.; Zhang, G.; Therien, M. J.; Greene, M. I.; Hammer, D. A.; Murali, R., *Methods* **2008**, 46, (1), 25-32.
8. Ringsdorf, H., *Journal of Polymer Science Part, C-Polymer Symposium* **1975**, (51), 135-153.
9. Duncan, R.; Kopecek, J., *Advances in Polymer Science* **1984**, 57, 51-101.
10. Haag, R.; Kratz, F., *Angewandte Chemie-International Edition* **2006**, 45, (8), 1198-1215.
11. Maeda, H., *Advanced Drug Delivery Reviews* **2001**, 46, (1-3), 169-185.
12. Qiu, L. Y.; Bae, Y. H., *Pharmaceutical Research* **2006**, 23, (1), 1-30.
13. Duncan, R., *Advanced Drug Delivery Reviews* **2009**, 61, (13), 1131-1148.
14. Binauld, S.; Stenzel, M. H., *Chemical Communications* **2013**, 49, (21), 2082-2102.
15. Wei, H.; Zhuo, R.-X.; Zhang, X.-Z., *Progress in Polymer Science* **2013**, 38, (3-4), 503-535.
16. Larson, N.; Ghandehari, H., *Chemistry of Materials* **2012**, 24, (5), 840-853.
17. Adams, N.; Schubert, U. S., *Advanced Drug Delivery Reviews* **2007**, 59, (15), 1504-1520.
18. Knop, K.; Hoogenboom, R.; Fischer, D.; Schubert, U. S., *Angewandte Chemie-International Edition* **2010**, 49, (36), 6288-6308.
19. Roberts, M. J.; Bentley, M. D.; Harris, J. M., *Advanced Drug Delivery Reviews* **2012**, 64, Supplement, (0), 116-127.
20. Jokerst, J. V.; Lobovkina, T.; Zare, R. N.; Gambhir, S. S., *Nanomedicine* **2011**, 6, (4), 715-728.
21. Ikeda, Y.; Nagasaki, Y., *Polymers in Nanomedicine* **2012**, 247, 115-140.
22. de Gennes, P. G., *Macromolecules* **1980**, 13, (5), 1069-1075.
23. Maeda, H.; Wu, J.; Sawa, T.; Matsumura, Y.; Hori, K., *Journal of Controlled Release* **2000**, 65, (1-2), 271-284.
24. Iwai, K.; Maeda, H.; Konno, T., *Cancer Research* **1984**, 44, (5), 2115-2121.
25. Koo, H.; Huh, M. S.; Sun, I.-C.; Yuk, S. H.; Choi, K.; Kim, K.; Kwon, I. C., *Accounts of Chemical Research* **2011**, 44, (10), 1018-1028.
26. Petros, R. A.; DeSimone, J. M., *Nature Reviews Drug Discovery* **2010**, 9, (8), 615-627.
27. Murakami, M.; Cabral, H.; Matsumoto, Y.; Wu, S.; Kano, M. R.; Yamori, T.; Nishiyama, N.; Kataoka, K., *Science Translational Medicine* **2011**, 3, (64), 64ra2.

28. Savic, R.; Eisenberg, A.; Maysinger, D., *Journal of Drug Targeting* **2006**, 14, (6), 343-355.
29. Discher, D. E.; Ahmed, F., *Annual Review of Biomedical Engineering* **2006**, 8, (1), 323-341.
30. Anraku, Y.; Kishimura, A.; Oba, M.; Yamasaki, Y.; Kataoka, K., *Journal of the American Chemical Society* **2010**, 132, (5), 1631-1636.
31. Plamper, F. A.; Gelissen, A. P.; Timper, J.; Wolf, A.; Zevin, A. B.; Richtering, W.; Tenhu, H.; Simon, U.; Mayer, J.; Borisov, O. V.; Pergushov, D. V., *Macromolecular Rapid Communications* **2013**, ASAP, DOI: 10.1002/marc.201300053.
32. Tong, R.; Christian, D. A.; Tang, L.; Cabral, H.; Baker, J. R.; Kataoka, K.; Discher, D. E.; Cheng, J., *MRS Bulletin* **2009**, 34, (06), 422-431.
33. Matsumoto, S.; Christie, R. J.; Nishiyama, N.; Miyata, K.; Ishii, A.; Oba, M.; Koyama, H.; Yamasaki, Y.; Kataoka, K., *Biomacromolecules* **2009**, 10, (1), 119-127.
34. Jia, Z.; Wong, L.; Davis, T. P.; Bulmus, V., *Biomacromolecules* **2008**, 9, (11), 3106-3113.
35. Zhang, Q.; Ko, N. R.; Oh, J. K., *Chemical Communications* **2012**, 48, (61), 7542-7552.
36. Bae, Y.; Fukushima, S.; Harada, A.; Kataoka, K., *Angewandte Chemie-International Edition* **2003**, 42, (38), 4640-4643.
37. Dolmans, D.; Fukumura, D.; Jain, R. K., *Nature Reviews Cancer* **2003**, 3, (5), 380-387.
38. Henderson, B. W.; Dougherty, T. J., *Photochemistry and Photobiology* **1992**, 55, (1), 145-157.
39. Palumbo, G., *Expert Opinion on Drug Delivery* **2007**, 4, (2), 131-148.
40. Nishiyama, N.; Morimoto, Y.; Jang, W.-D.; Kataoka, K., *Advanced Drug Delivery Reviews* **2009**, 61, (4), 327-338.
41. O'Connor, A. E.; Gallagher, W. M.; Byrne, A. T., *Photochemistry and Photobiology* **2009**, 85, (5), 1053-1074.
42. Nishiyama, N.; Jang, W.-D.; Kataoka, K., *New Journal of Chemistry* **2007**, 31, (7), 1074-1082.
43. Khan, M.; Ong, Z. Y.; Wiradharma, N.; Attia, A. B. E.; Yang, Y.-Y., *Advanced Healthcare Materials* **2012**, 1, (4), 373-392.
44. Lee, A. L. Z.; Wang, Y.; Cheng, H. Y.; Pervaiz, S.; Yang, Y. Y., *Biomaterials* **2009**, 30, (5), 919-927.
45. Nishiyama, N.; Iriyama, A.; Jang, W.-D.; Miyata, K.; Itaka, K.; Inoue, Y.; Takahashi, H.; Yanagi, Y.; Tamaki, Y.; Koyama, H.; Kataoka, K., *Nature Materials* **2005**, 4, (12), 934-941.
46. Wang, Y.; Gao, S.; Ye, W.-H.; Yoon, H. S.; Yang, Y.-Y., *Nature Materials* **2006**, 5, (10), 791-796.
47. Cabral, H.; Nishiyama, N.; Kataoka, K., *Accounts of Chemical Research* **2011**, 44, (10), 999-1008.
48. Kelkar, S. S.; Reineke, T. M., *Bioconjugate Chemistry* **2011**, 22, (10), 1879-1903.
49. Kim, J.; Piao, Y.; Hyeon, T., *Chemical Society Reviews* **2009**, 38, (2), 372-390.
50. Lammers, T.; Aime, S.; Hennink, W. E.; Storm, G.; Kiessling, F., *Accounts of Chemical Research* **2011**, 44, (10), 1029-1038.
51. Ringsdorf, H.; Lehmann, P.; Weberskirch, R., *Abstracts of Papers of the American Chemical Society*, Anaheim, USA, **1999**, 217, (1-2), U657, BTEC-001.

52. Weberskirch, R.; Ringsdorf, H., *Abstracts of Meeting of HCM network*, Patras, Greece, **1995**.
53. Du, J.; O'Reilly, R. K., *Chemical Society Reviews* **2011**, 40, (5), 2402-2416.
54. Moughton, A. O.; Hillmyer, M. A.; Lodge, T. P., *Macromolecules* **2012**, 45, (1), 2-19.
55. Kubowicz, S.; Baussard, J. F.; Lutz, J. F.; Thunemann, A. F.; von Berlepsch, H.; Laschewsky, A., *Angewandte Chemie-International Edition* **2005**, 44, (33), 5262-5265.
56. Li, Z. B.; Kesselman, E.; Talmon, Y.; Hillmyer, M. A.; Lodge, T. P., *Science* **2004**, 306, (5693), 98-101.
57. Schacher, F.; Walther, A.; Müller, A. H. E., *Langmuir* **2009**, 25, (18), 10962-10969.
58. Schacher, F.; Walther, A.; Ruppel, M.; Drechsler, M.; Müller, A. H. E., *Macromolecules* **2009**, 42, (10), 3540-3548.
59. Lodge, T. P.; Rasdal, A.; Li, Z.; Hillmyer, M. A., *Journal of the American Chemical Society* **2005**, 127, (50), 17608-17609.
60. Xia, J.; Zhong, C., *Macromolecular Rapid Communications* **2006**, 27, (19), 1654-1659.
61. Schacher, F.; Betthausen, E.; Walther, A.; Schmalz, H.; Pergushov, D. V.; Müller, A. H. E., *ACS Nano* **2009**, 3, (8), 2095-2102.
62. Longstreet, A. R.; McQuade, D. T., *Accounts of Chemical Research* **2012**, 46, (2), 327-338.
63. Gröschel, A. H.; Schacher, F. H.; Schmalz, H.; Borisov, O. V.; Zhulina, E. B.; Walther, A.; Müller, A. H. E., *Nature Communications* **2012**, 3.
64. Cajot, S.; van Butsele, K.; Paillard, A.; Passirani, C.; Garcion, E.; Benoit, J. P.; Varshney, S. K.; Jérôme, C., *Acta Biomaterialia* **2012**, 8, (12), 4215-4223.
65. Bastakoti, B. P.; Wu, K. C. W.; Inoue, M.; Yusa, S.-i.; Nakashima, K.; Yamauchi, Y., *Chemistry – A European Journal* **2013**, ASAP, DOI: 10.1002/chem.201203958.
66. Verma, I. M.; Somia, N., *Nature* **1997**, 389, (6648), 239-242.
67. Mulligan, R. C., *Science* **1993**, 260, (5110), 926-932.
68. Song, C.-Z., In *Gene Therapy for Cancer*, Hunt, K. K.; Vorburger, S. A.; Swisher, S. G., Eds. Humana Press: Totowa, NJ, **2007**; pp 185-196.
69. Crystal, R. G., *Science* **1995**, 270, (5235), 404-410.
70. Mintzer, M. A.; Simanek, E. E., *Chemical Reviews* **2009**, 109, (2), 259-302.
71. Nishikawa, M.; Huang, L., *Human Gene Therapy* **2001**, 12, (8), 861-870.
72. Wong, S. Y.; Pelet, J. M.; Putnam, D., *Progress in Polymer Science* **2007**, 32, (8-9), 799-837.
73. Won, Y.-Y.; Sharma, R.; Konieczny, S. F., *Journal of Controlled Release* **2009**, 139, (2), 88-93.
74. Behr, J. P., *Chimia* **1997**, 51, (1-2), 34-36.
75. Boussif, O.; Lezoualch, F.; Zanta, M. A.; Mergny, M. D.; Scherman, D.; Demeneix, B.; Behr, J. P., *Proceedings of the National Academy of Sciences of the United States of America* **1995**, 92, (16), 7297-7301.
76. Funhoff, A. M.; van Nostrum, C. F.; Lok, M. C.; Kruijtzter, J. A. W.; Crommelin, D. J. A.; Hennink, W. E., *Journal of Controlled Release* **2005**, 101, (1-3), 233-246.
77. Sanjoh, M.; Miyata, K.; Christie, R. J.; Ishii, T.; Maeda, Y.; Pittella, F.; Hiki, S.; Nishiyama, N.; Kataoka, K., *Biomacromolecules* **2012**, 13, (11), 3641-3649.

78. Christie, R. J.; Matsumoto, Y.; Miyata, K.; Nomoto, T.; Fukushima, S.; Osada, K.; Halnaut, J.; Pittella, F.; Kim, H. J.; Nishiyama, N.; Kataoka, K., *ACS Nano* **2012**, 6, (6), 5174-5189.
79. Itaka, K.; Yamauchi, K.; Harada, A.; Nakamura, K.; Kawaguchi, H.; Kataoka, K., *Biomaterials* **2003**, 24, (24), 4495-4506.
80. Neu, M.; Fischer, D.; Kissel, T., *The Journal of Gene Medicine* **2005**, 7, (8), 992-1009.
81. Dufes, C.; Uchegbu, I. F.; Schatzlein, A. G., *Advanced Drug Delivery Reviews* **2005**, 57, (15), 2177-2202.
82. Haensler, J.; Szoka, F. C., *Bioconjugate Chemistry* **1993**, 4, (5), 372-379.
83. Hemp, S. T.; Allen, M. H., Jr.; Green, M. D.; Long, T. E., *Biomacromolecules* **2012**, 13, (1), 231-238.
84. Hemp, S. T.; Smith, A. E.; Bryson, J. M.; Allen, M. H., Jr.; Long, T. E., *Biomacromolecules* **2012**, 13, (8), 2439-2445.
85. Ornelas-Megiatto, C.; Wich, P. R.; Fréchet, J. M. J., *Journal of the American Chemical Society* **2012**, 134, (4), 1902-1905.
86. Hawker, C. J., *Angewandte Chemie-International Edition in English* **1995**, 34, (13-14), 1456-1459.
87. Matyjaszewski, K., *Macromolecules* **2012**, 45, (10), 4015-4039.
88. Xu, F. J.; Yang, W. T., *Progress in Polymer Science* **2011**, 36, (9), 1099-1131.
89. Sahnoun, M.; Charreyre, M.-T.; Veron, L.; Delair, T.; D'Agosto, F., *Journal of Polymer Science, Part A-Polymer Chemistry*, **2005**, 43, (16), 3551-3565.
90. Plamper, F. A.; Schmalz, A.; Penott-Chang, E.; Drechsler, M.; Jusufi, A.; Ballauff, M.; Müller, A. H. E., *Macromolecules* **2007**, 40, 5689-5697.
91. Rungsardthong, U.; Deshpande, M.; Bailey, L.; Vamvakaki, M.; Armes, S. P.; Garnett, M. C.; Stolnik, S., *Journal of Controlled Release* **2001**, 73, (2-3), 359-380.
92. Schallon, A.; Jerome, V.; Walther, A.; Synatschke, C. V.; Müller, A. H. E.; Freitag, R., *Reactive & Functional Polymers* **2010**, 70, (1), 1-10.
93. Layman, J. M.; Ramirez, S. M.; Green, M. D.; Long, T. E., *Biomacromolecules* **2009**, 10, (5), 1244-1252.
94. van de Wetering, P.; Cherng, J. Y.; Talsma, H.; Hennink, W. E., *Journal of Controlled Release* **1997**, 49, (1), 59-69.
95. Dai, F.; Sun, P.; Liu, Y.; Liu, W., *Biomaterials* **2010**, 31, (3), 559-569.
96. Guo, S.; Huang, Y.; Wei, T.; Zhang, W.; Wang, W.; Lin, D.; Zhang, X.; Kumar, A.; Du, Q.; Xing, J.; Deng, L.; Liang, Z.; Wang, P. C.; Dong, A.; Liang, X.-J., *Biomaterials* **2011**, 32, (3), 879-889.
97. Jiang, X.; Lok, M. C.; Hennink, W. E., *Bioconjugate Chemistry* **2007**, 18, (6), 2077-2084.
98. Zhang, Y.; Zheng, M.; Kissel, T.; Agarwal, S., *Biomacromolecules* **2011**, 13, (2), 313-322.
99. van de Wetering, P.; Cherng, J. Y.; Talsma, H.; Crommelin, D. J. A.; Hennink, W. E., *Journal of Controlled Release* **1998**, 53, (1-3), 145-153.
100. Xiu, K. M.; Yang, J. J.; Zhao, N. N.; Li, J. S.; Xu, F. J., *Acta Biomaterialia* **2013**, 9, (1), 4726-4733.
101. Nemoto, Y.; Borovkov, A.; Zhou, Y. M.; Takewa, Y.; Tatsumi, E.; Nakayama, Y., *Bioconjugate Chemistry* **2009**, 20, (12), 2293-2299.
102. Pafiti, K. S.; Mastroiannopoulos, N. P.; Phylactou, L. A.; Patrickios, C. S., *Biomacromolecules* **2011**, 12, (5), 1468-1479.

103. Xu, F. J.; Ping, Y.; Ma, J.; Tang, G. P.; Yang, W. T.; Li, J.; Kang, E. T.; Neoh, K. G., *Bioconjugate Chemistry* **2009**, 20, (8), 1449-1458.
104. Yu, S.; Chen, J.; Dong, R.; Su, Y.; Ji, B.; Zhou, Y.; Zhu, X.; Yan, D., *Polymer Chemistry* **2012**, 3, (12), 3324-3329.
105. Kuehn, F.; Pietrowski, E.; Fischer, K.; Luhmann, H.; Schmidt, M., *Abstracts of Papers of the American Chemical Society*, Boston, USA, **2010**, 240, 328-POLY.
106. Georgiou, T. K.; Phylactou, L. A.; Patrickios, C. S., *Biomacromolecules* **2006**, 7, (12), 3505-3512.
107. Georgiou, T. K.; Vamvakaki, M.; Patrickios, C. S.; Yamasaki, E. N.; Phylactou, L. A., *Biomacromolecules* **2004**, 5, (6), 2221-2229.
108. Georgiou, T. K.; Vamvakaki, M.; Phylactou, L. A.; Patrickios, C. S., *Biomacromolecules* **2005**, 6, (6), 2990-2997.

Chapter 2 - Overview over the Thesis

This thesis consists of seven chapters including five publications, which are presented in **Chapters 3 to 7**.

Structural characterization of polyelectrolyte nanostructures in aqueous solution and the therapeutic use arising from these materials is the common topic unifying the different chapters. Two different types of polymeric materials were used in the work, which can be divided into star-shaped polycations on one side and multicompartment micelles (MCMs) from ionic triblock terpolymers on the other.

In close collaboration with the group of Process Biotechnology at the University of Bayreuth, we explored the biological properties of star-shaped polycations for the delivery of genetic material (transfection) into eukaryotic cells. To better understand the relationship between chemical modifications on the molecular level and biological properties relevant to the transfection process, *i.e.*, cytotoxicity and transfection efficiency (TE) were the main criteria of interest, I synthesized a variety of different polymer structures that were subsequently tested against several types of cell lines. We found general design criteria for star-shaped vectors (**Chapter 3 and 4**) and could use them to create materials with significantly enhanced transfection properties (**Chapter 4**) as compared to previously used polymers.

In the second part of the thesis, from a starting material consisting of MCMs from triblock terpolymers which have a negatively charged corona in aqueous solution, I investigated the possibilities to alter the micellar structure towards higher complexity through the interaction with oppositely charged (block co-)polymers. Creating new compartments or changing the surface chemistry of the micelles by means of interpolyelectrolyte complex (IPEC) formation was of particular interest (**Chapter 5 and 6**). Some of these new MCMs were then used to investigate the influence of the corona chemistry on biological properties, while simultaneously demonstrating good drug carrying capacity sufficient for anti-cancer therapy *in vitro* and *in vivo* (**Chapter 7**).

The most important results from each of the different parts are discussed in the following.

1. Influence of Polymer Architecture and Molecular Weight of Poly(2-(Dimethylamino)ethyl Methacrylate) Polycations on Transfection Efficiency and Cell Viability in Gene Delivery

Poly(2-(dimethylamino)ethyl methacrylate) (PDMAEMA) is an ideal candidate for investigating structure-property relationships in non-viral gene delivery, because well-defined polymers with varying morphologies can be synthesized by means of controlled polymerization methods such as atom transfer radical polymerization (ATRP).¹ Star-shaped polycations have only recently been used in gene transfection and there was some evidence for a superior transfection performance of this specific polymer architecture reported in the literature.^{2, 3} We were especially interested how structural parameters, such as the arm number and arm length of star-shaped polycatione, influence their transfection properties. By using ATRP, I prepared a material library consisting of linear, 3-arm-, and 5-arm-star polymers with different molecular weights for each type of polymer. The two star-shaped DMAEMA polymers were polymerized in a “core-first” approach using multifunctional initiator molecules on the basis of sugars (glucose and saccharose). The final polymer library contained twelve polymers in total and covered a molecular weight range from 16 to 158 kDa (see **Table 2-1**).

Table 2-1: Nomenclature and molecular characterization of the linear, 3-arm and 5-arm DMAEMA polymers synthesized with ATRP.

Architecture	Name	N / Molecule ^a	M _n [kDa] ^b	PDI ^c
Linear	L ₁₁₀	108	17.1	1.12
	L ₅₂₀	518	81.7	-
	L ₈₈₀	881	138.7	1.73
	L ₁₀₀₀	1003	157.9	1.80
3-Arm	S-3 ₉₅	95	15.9	1.26
	S-3 ₂₁₀	210	34.0	1.16
	S-3 ₃₀₀	296	47.5	1.12
	S-3 ₆₀₀	596	94.7	1.12
	S-3 ₇₁₀	710	112.6	1.13
5-Arm	S-5 ₅₈₀	575	91.9	1.09
	S-5 ₇₀₀	699	111.4	1.12
	S-5 ₉₂₀	919	146.0	1.10

^acalculated from the NMR-molecular weight; ^bdetermined from NMR conversion data; ^cmeasured *via* SEC with DMAc as eluent and poly(methyl methacrylate) as standard.

The same polymerization conditions were used for all three types of polymer architectures and well-defined star-shaped PDMAEMAs with narrow molecular weight distributions were obtained. Then, polyplexes were formed with plasmid DNA (pDNA) in increasing ratios of PDMAEMA-nitrogen/DNA-phosphate (N/P ratio) to test them for their cytotoxicity as well as TE in Chinese Hamster Ovary (CHO-K1) cells. For ease of data analysis, the concentration dependent cytotoxicity data for each polymer sample was converted into a single value, defined as the lethal complex concentration for 50 % of the cells (LCC₅₀) which could then be plotted against the molecular weight (**Figure 2-1a**). Interestingly, a trend was found that points towards a reduced cytotoxicity (high LCC₅₀ value) with increasing degree of branching for comparable molecular weights, *i.e.*, 5-arm stars are less toxic than 3-arm stars which in turn are less toxic than linear polymers.

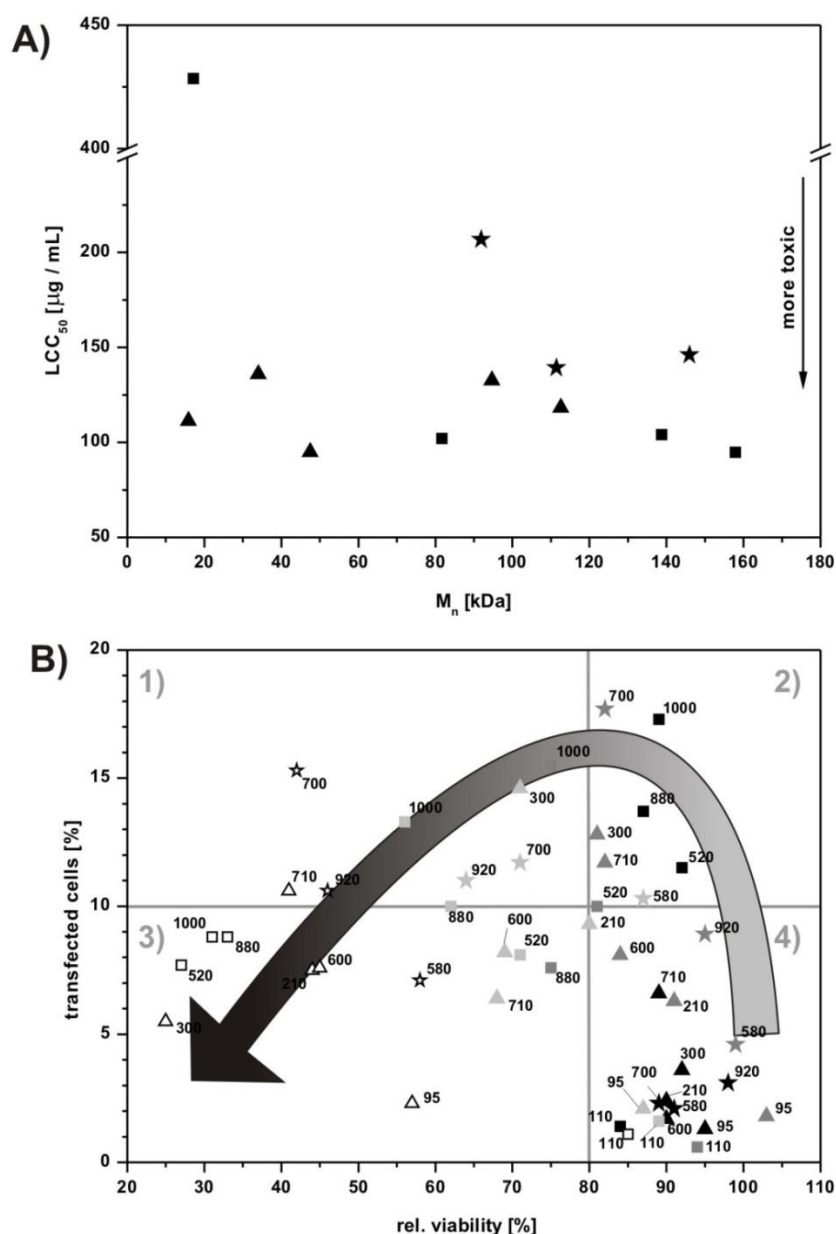


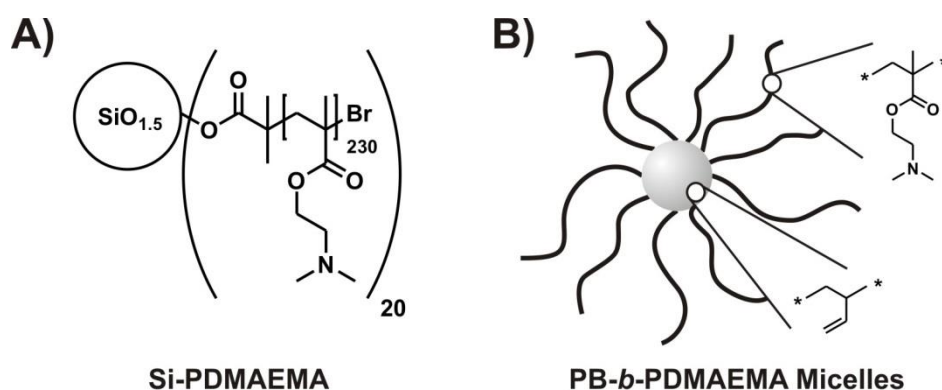
Figure 2-1: (A) Plot of the LCC₅₀-values of various PDMAEMAs against the molecular weight of the polymer. LCC₅₀-values were calculated from MTT experiments using CHO-K1 cells. The symbols represent linear (squares), 3-arm star (triangles) and 5-arm star (stars) PDMAEMA. (B) Fraction of transfected cells plotted against the relative viability for the polyplexes from PDMAEMA polymers at N/P ratios 2 (black), 5 (dark grey), 10 (light grey) and 20 (open symbols). The average number of monomers per polycation is given next to each entry. Data represent mean value of three independent experiments. The arrow represents the general course of a polycation through the graph with increasing N/P ratio (from grey = low to black = high N/P ratio).

Cellular toxicity can have a direct influence on the TE, as cell death decreases the production of reporter genes. It is therefore reasonable to directly connect the toxicity of a

given N/P ratio with the corresponding TE. To have both of these important parameters visualized in one graph, we introduced a plot of the TE against relative viability for all N/P ratios in the polymer library as depicted in **Figure 2-1b**. This new type of graph allows the reader to quickly identify the polymeric material and N/P ratio with ideal transfection properties, *i.e.* the data points that appear in the upper right quadrant number 2. Additionally, this type of graph nicely illustrates the effect of increasing the N/P ratio for a certain DMAEMA polymer, starting with low toxicity and TE, then going through a tradeoff region between increasing TE and toxicity, while finally the toxicity dominates and results in a decreased TE. This behavior is illustrated by the arrow in **Figure 2-1b**. From the dataset we could further find that polymers below a critical molecular weight of approximately 20 kDa (corresponding to 130 monomer units in case of PDMAEMA), exhibit no significant transfection, suggesting that polymers with an intermediate molecular weight and a branched architecture would be good candidates for gene delivery.

2. Nano-Particulate Non-Viral Agent for the Effective Delivery of pDNA and siRNA to Differentiated Cells and Primary Human T Lymphocytes

With the knowledge from the polymer library containing linear, 3- and 5-arm star DMAEMA polymers described in **Chapter 2.1**, we then tested the transfection properties of a star-shaped PDMAEMA with 20 arms (Si-PDMAEMA). This polymer had been obtained again by ATRP “core-first” method using a multifunctional silsesquioxane nanoparticle as the initiator (**Scheme 2-1a**).



Scheme 2-1. (A) Chemical structure of star-shaped Si-PDMAEMA synthesized *via* “core-first” method by ATRP; (B) Star-like PDMAEMA micelle self-assembled from amphiphilic PB-*b*-PDMAEMA diblock copolymer.

Despite its large molecular weight ($M_n = 730$ kg/mol), we could achieve very good cellular viability coupled with extremely high transfection efficiencies in CHO-K1 cells (74 % TE) with 93 % rel. viability on average that surpassed the best results from the “gold standard” poly(ethylene imine) (PEI) (50 % TE with 94 % rel. viability on average). In various cell lines that are generally considered to be more difficult to transfect than CHO-K1 cells, the Si-PDMAEMA performed better relative to PEI as is exemplarily shown for C2C12 cells (**Figure 2-2**). These cells stop dividing when the culture plate is densely populated (confluent), which significantly hinders successful transfection for most polymeric vectors. Furthermore, the confluent C2C12 cells could easily be differentiated into myotubes through a change of the culture medium composition. In all of the cases Si-PDMAEMA (**Figure 2-2**, open symbols) gave higher TE for every single transfection experiment as compared to PEI (**Figure 2-2**, closed symbols).

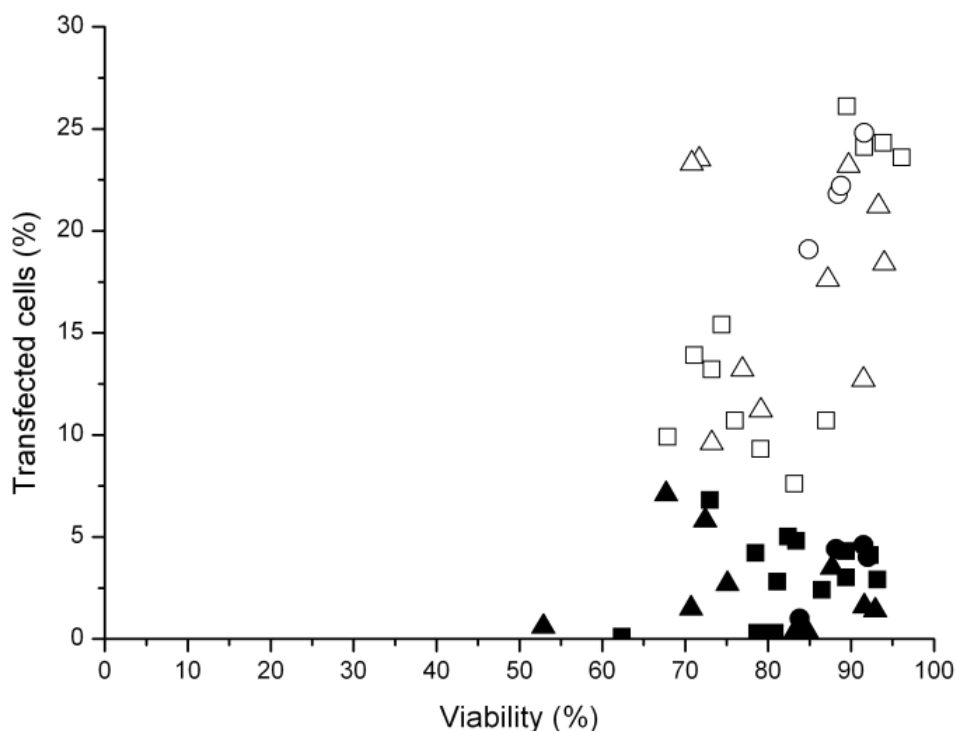


Figure 2-2. Analysis of the percentage of transfected cells against the relative viability after transfection in C2C12 cells. Transfection efficiencies in dividing (●, ○), non-dividing myoblasts (■, □) and myotubes (▲, △) are plotted against the viability. Black symbols: PEI, white symbols: Si-PDMAEMA. Data shown are from individual transfections.

The superior transfection performance of Si-PDMAEMA is based on its general architecture, where a multitude of polymeric arms emanate from a common center, rather than the specific polymer sample: When polymeric micelles from an amphiphilic diblock copolymer (polybutadiene-*block*-PDMAEMA; PB-*b*-PDMAEMA) comprising a PB core and PDMAEMA corona, which resemble a star-shaped architecture (**Scheme 2-1b**), were used for gene delivery, a comparable performance to that of Si-PDMAEMA was found. Both types of nanostructures could also transfect human T lymphocytes with pDNA more efficiently as compared to the standard method of electroporation for these cell types. Additionally, RNA interference could also successfully be performed with both polymeric vectors of star-like architecture, reaching up to 40 % silencing efficiency of the targeted gene in human T lymphocytes. The remarkable transfection performance of this class of polymers, combined with the large number of different cell lines it can be applied to, especially for non-dividing or differentiated cells, makes these star-like polymers highly interesting materials for *in vitro* gene delivery.

3. Double-Layered Micellar Interpolyelectrolyte Complexes – How Many Shells to a Core?

MCMs are highly complex nanostructures with possible applications in templating, as nanoreactors, for carrying catalysts and in biomedical drug delivery or imaging. By using triblock terpolymers, it is possible to obtain MCMs with two chemically different compartments in the core of the resulting micelles. However, increasing the number of distinguishable compartments to more than two is generally very difficult.

Here, we established a new route for the formation of distinguishable and chemically different compartments in MCMs from ionic triblock terpolymers by using the negatively charged corona of those micelles for IPEC formation with oppositely charged polyions. The original MCMs used in this work formed through self-assembly of poly(butadiene)-*block*-poly(1-methyl-2-vinyl pyridinium)-*block*-poly(methacrylic acid) (BVqMAA) in aqueous solution. The MAA corona stabilizes the micelles and is easily accessible for further reactions. First, we used quaternized PDMAEMA (PDMAEMAq), which retains its positive charge even at high pH values (pH = 10) where PMAA is fully deprotonated. Upon mixing the polycation solution with BVqMAA micelles, an IPEC was immediately formed, which collapsed onto the core of the micelles. This new IPEC compartment (2nd IPEC) comprising PDMAEMAq and PMAA could be distinguished in cryogenic transmission electron microscopy (cryo-TEM) measurements from the original intramicellar IPEC shell (Vq/MAA). Furthermore, a complete second layer was formed (**Figure 2-3**, left side) leading to an onion-type morphology. Non-complexed MAA from the original micellar corona served to stabilize the micelles in solution below a critical complexation ratio. The 2nd IPEC layer was found for 3 different block lengths of the MAA block in BVqMAA micelles, ranging from 345 to 550 units. The length of the two DMAEMAq homopolymers (157 and 820 units) used for complex formation did not significantly affect structure formation. If complexation ratios close to charge neutrality were reached, a macroscopic phase separation with precipitation of the MCMs was found.

This macroscopic precipitation at high complexation ratio was avoided when instead of a homopolymer the double hydrophilic diblock copolymer of PEG-*b*-PDMAEMAq was used for IPEC formation (**Figure 2-3**, right side). The new layered compartment from PDMAEMAq/MAA IPEC developed as before, but the colloidal stability of the particles

was retained even at charge neutralization, because the PEG segment served as stabilizing corona chains.

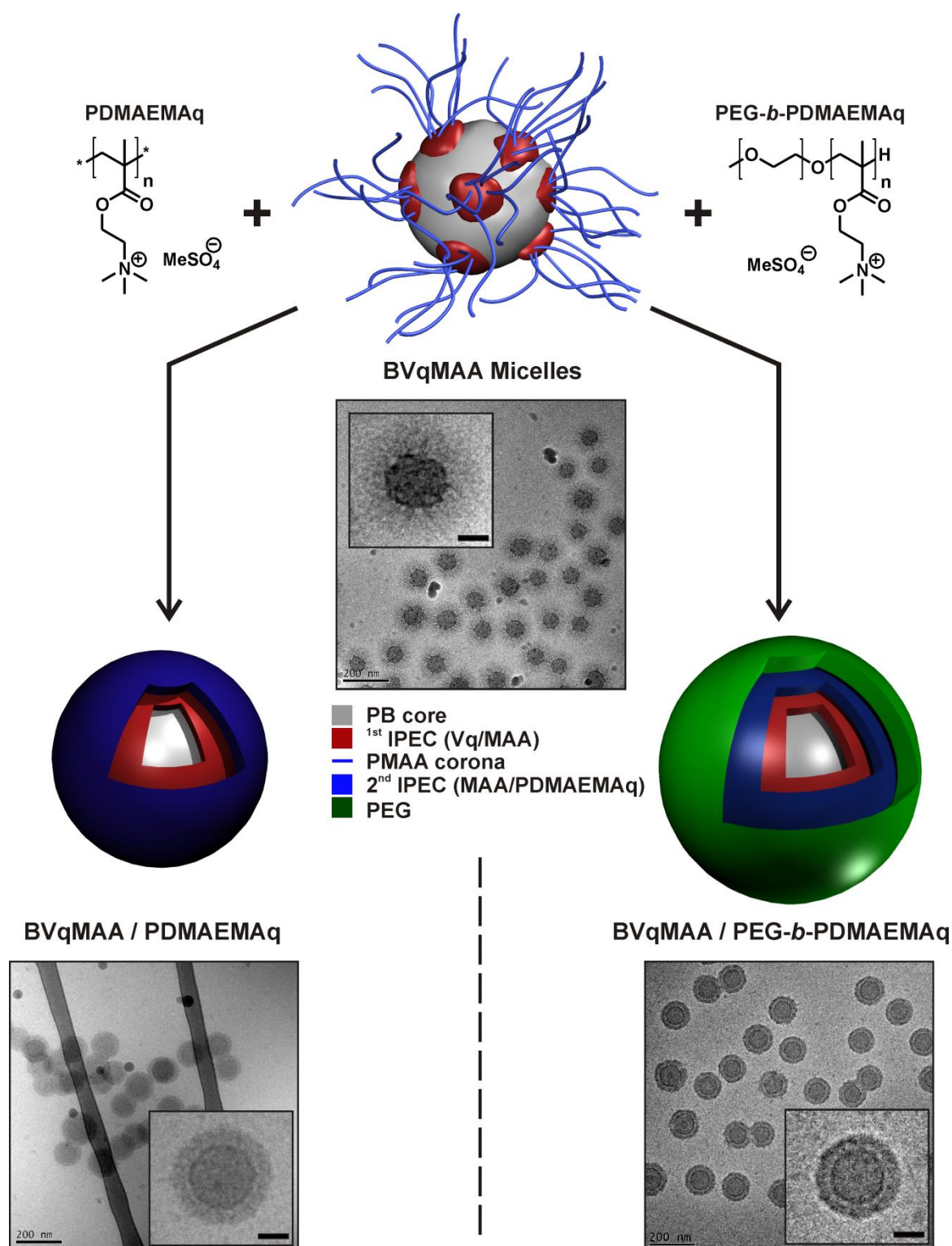


Figure 2-3: Schematic pathway for the formation of double-layered IPECs from BVqMAA triblock terpolymer micelles and either PDMAEMAq homopolymers (left) or a PEG-*b*-PDMAEMAq diblock copolymer (right). Scale bars in the insets represent 40 nm.

4. Micellar Interpolyelectrolyte Complexes With a Compartmentalized Shell

Next, we used BVqMAA micelles with a very long MAA corona of 1350 units and otherwise nearly identical block lengths of the remaining two blocks for the complex formation with oppositely charged polycations. There, we found a novel arrangement of the newly created compartment instead of the previously layered one in micelles with short to medium MAA block length.

The original incentive behind using BVqMAA micelles with a very long corona (**Figure 2-4a**) was to create more than one additional compartment in an onion-type arrangement, through the consecutive addition of different polycations. By using a very long corona of 1350 units as compared to a maximum of 550 units that were previously used, colloidal stability even with multiple layers of IPEC compartments should be achieved. In that sense, the proposed approach would be similar to a layer-by-layer procedure, without alternating between the addition of positively and negatively charged polyions. Additionally, we were interested to see whether an increase in the charge density of the polycation would lead to a change in the IPEC compartment structure, *i.e.*, a more dense compartment. For this purpose a new polycation, poly(2-((2-(dimethylamino)ethyl)methylamino)ethyl methacrylate) (PDAMA), with a similar structure to that of PDMAEMA but carrying two amino groups per repeating unit, was synthesized by reversible addition fragmentation (RAFT) polymerization and subsequently quaternized to give PDAMAq.

After analyzing the complexes from long-corona BVqMAA micelles with PDAMAq by electron microscopy, we found that complex formation had successfully occurred, but the new compartment was anisotropically distributed around the original core of the micelles (**Figure 2-4b**). Instead of a layered structure, up to three individual patches of newly formed IPEC decorated the core. The structures are not kinetically trapped, but even reform when dialyzed from high salt conditions where the IPEC compartment disintegrates (**Figure 2-4c**) to low salt conditions (**Figure 2-4d**). Essentially, the same structures as for direct mixing at low salt conditions were found again.

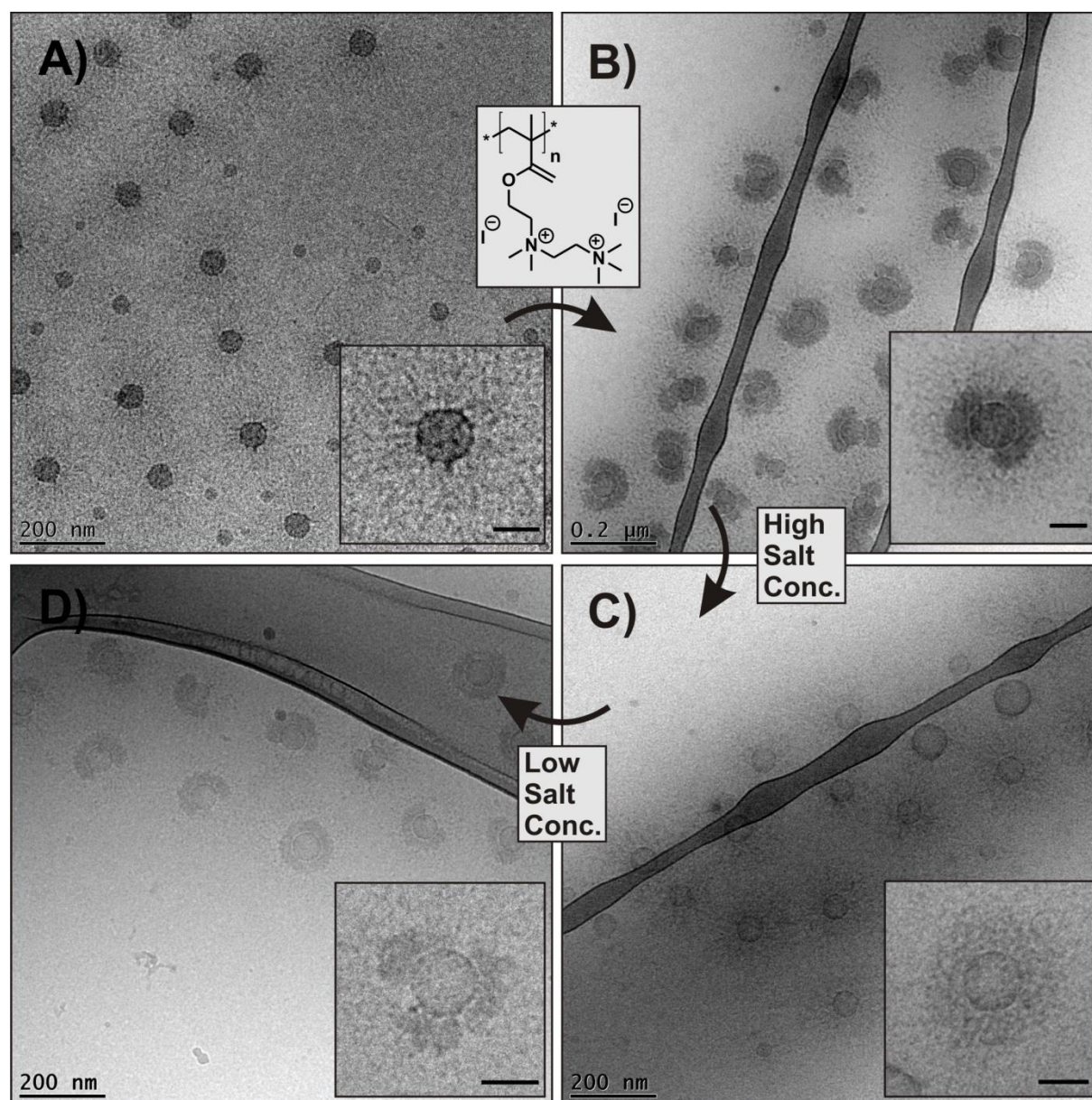


Figure 2-4. cryo-TEM micrographs of BVqMAA₁₃₅₀ micelles (A) in pH 10 buffer; (B) after the complex formation with PDAMAq; (C) after further addition of 500 mM NaCl; (D) after dialysis back to original pH 10 buffer. The scale bars of the insets represent 50 nm.

The patchy IPEC compartment structure was also independent of the polycation used for complexation, as demonstrated by using PDMAEMAq. Finally, we identified the corona length as the determining factor for the occurrence of this specific structure: In micelles with a MAA-block length of only 400 units, again a layered arrangement of the new IPEC compartment was observed. We explain the formation of both types of structures (layered and patchy IPEC) through the interfaces generated between the new IPEC compartment and both the original micellar core and the solvent. For micelles with a short corona, a

patchy arrangement of the newly formed IPEC would quickly lead to an interface between IPEC and solvent, which could then lead to further aggregation of the structures and loss of colloidal stability. The long MAA corona in the micelles used here permits a stabilization of the micelles even for anisotropic arrangements of the IPEC compartment. Such a patch instead of a layered morphology allows for an energy minimization of the interface between new IPEC and original core, which is not possible in the case of short corona micelles.

5. Multicompartment Micelles with Adjustable Poly(ethylene glycol) Shell for Efficient *in Vivo* Photodynamic Therapy

In the last part of this thesis I explored the capacity of MCMs based on BVqMAA micelles to act as a drug delivery system (DDS). For this, I spent time in the laboratory of Prof. Kazunori Kataoka in Tokyo, Japan, and the results presented in the following were obtained in collaboration with his group.

A hydrophobically modified porphyrazine derivate was chosen as a model hydrophobic drug for the encapsulation in BVqMAA micelles. This drug can create reactive oxygen species (ROS) when illuminated with light in the near infrared region and is therefore capable of acting as a photosensitizer (PS) in photodynamic cancer therapy (PDT). The drug was incorporated into the polybutadiene core during the self-assembly step of the BVqMAA triblock terpolymers. The MCM system allowed us to investigate the influence of the corona composition on the biological properties of the DDS, by taking advantage of the complex formation with a double hydrophilic and positively charged diblock copolymer poly(L-lysine)-*block*-poly(ethylene glycol) (PLL-*b*-PEG) in the same approach as discussed in **Chapter 2.3**. Simply by adjusting the mixing ratio of the added diblock copolymer, we were able to gradually change the composition of the micellar corona from pure MAA to PEG.

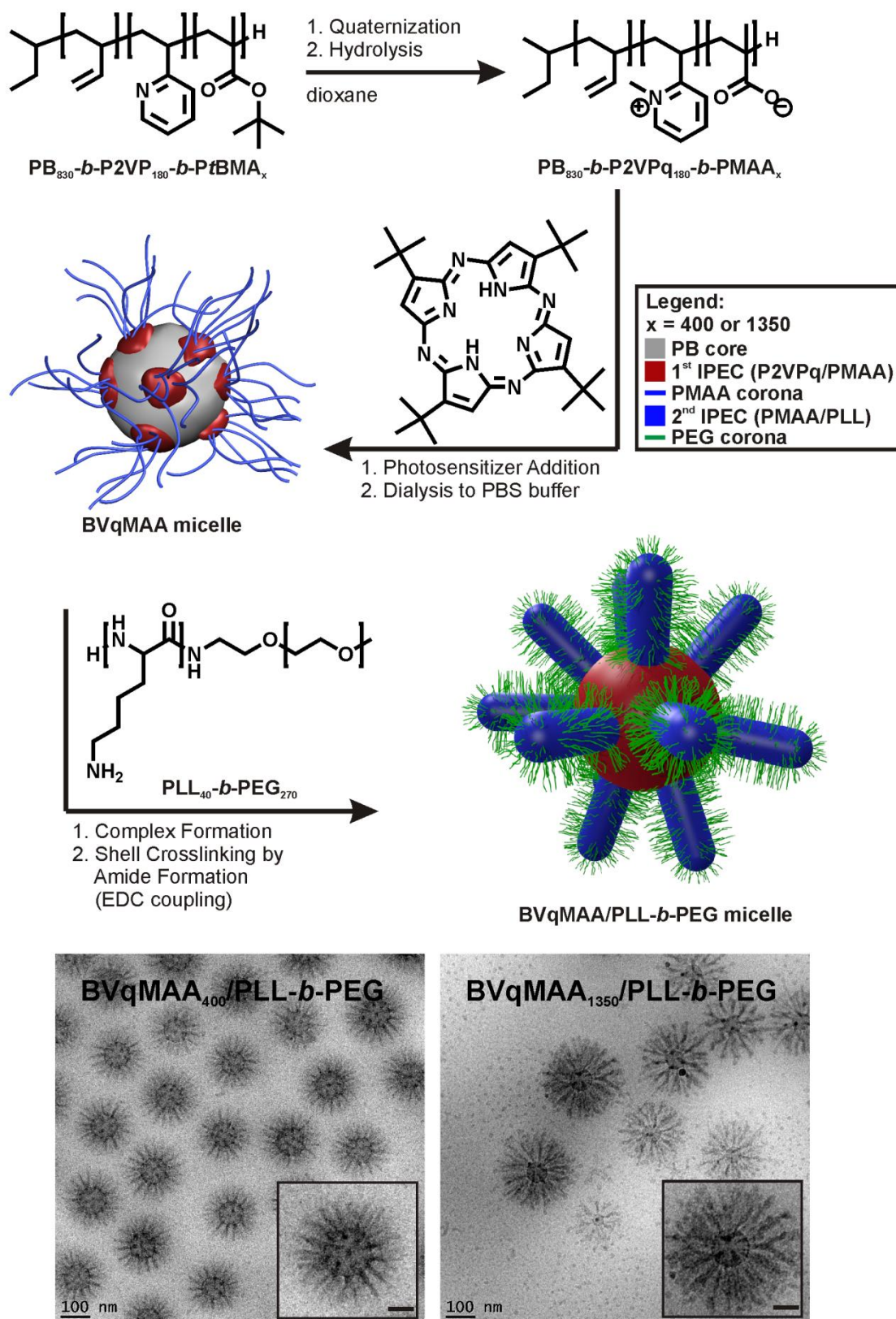


Figure 2-5. Preparation of porphyrazine derivate containing BVqMAA micelles from BVT triblock terpolymer, followed by corona modification with PLL-*b*-PEG diblock copolymers and cryo-TEM micrographs for the resulting structures of two BVqMAA/PLL-*b*-PEG complex micelles. The scale bars in the insets represent 50 nm.

At high complexation ratios close to charge neutrality we found a novel micellar morphology of the MCMs, where the newly formed IPEC is of cylindrical shape and oriented perpendicular to the surface of the micellar core (**Figure 2-5**). The reason for this new morphology was identified as the very short block length of the PLL block (40 units) as compared to the MAA blocks (400 and 1350 units). At high complexation ratios the system is forced into a cylindrical bottlebrush structure to accommodate the large PEG chains (270 monomer units) of PLL-*b*-PEG, which would not be possible in a layered arrangement of the PLL/MAA IPEC.

Using PLL as the cationic block with its primary amines – in contrast to the quaternary amines in PDMAEMAq or PDAMAq – further allowed a facile fixation of the corona composition through amide formation *via* activated esters. After fixation, BVqMAA/PLL-*b*-PEG micelles retained their cylinder-on-sphere morphology even under highly challenging conditions (high salt concentration), indicating a stability of micellar structure even when getting in contact with serum-containing medium or when injected into the bloodstream.

For the evaluation of their drug carrying capabilities and biological properties, the micelles were first tested in cell culture. Human lung cancer cells (A549) were treated with micelles having an increasing degree of PEGylation. A strong decrease of the relative viability (*i.e.* increase in toxicity) was observed for all drug carrying micelles upon illumination (**Figure 2-6a**), while non-illuminated micelles resulted only in minor toxicity, proving the photodynamic activity of the DDS. Non-drug carrying micelles, on the other hand, did not contribute significantly to the overall toxicity. A strong dependence of the photo-induced toxicity on the corona composition was found, where non-PEGylated micelles showed highest toxicity that gradually decreased with increasing degree of PEGylation. We found that the uptake behavior into the cells can be controlled through the corona composition (**Figure 2-6b**) and non-PEGylated micelles had the highest uptake into A549 cells decreasing with increasing PLL-*b*-PEG complexation ratio, correlating well with trends in toxicity.

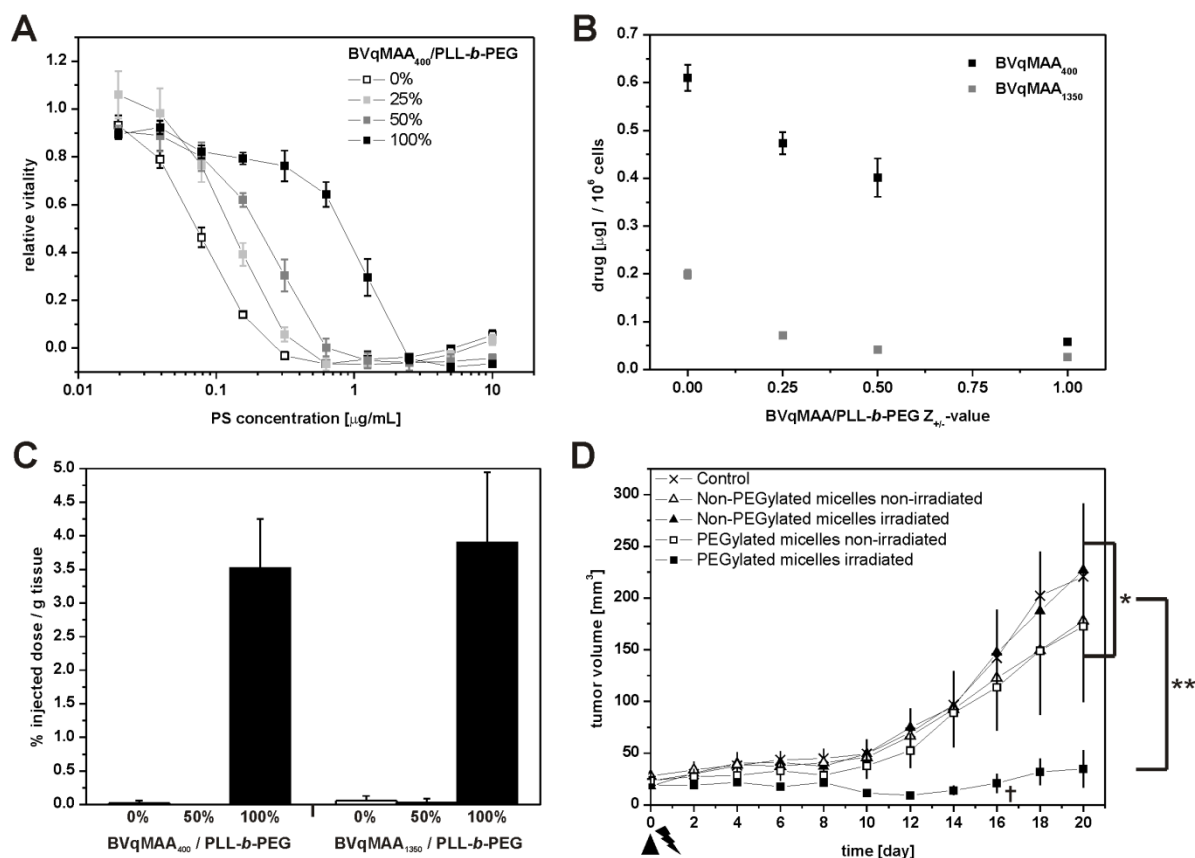


Figure 2-6. (A) *In vitro* PDT effect. Relative viability of A549 cells after treatment with BVqMAA₄₀₀/PLL-*b*-PEG micelles and 15 min photoirradiation. (B) *In vitro* uptake of drug in A549 cells after 24 h incubation. (C) *In vivo* drug accumulation in subcutaneous A549 tumor model 24 h post injection of BVqMAA/PLL-*b*-PEG micelles (n = 4). (D) *In vivo* PDT efficacy study (n = 5). Evolution of the tumor volume with time (Illumination at tumor site on day 0. †: 1/5 tumor regression. *p > 0.05; **p < 0.001.).

A strong influence of the corona composition on the behavior of the MCMs in animals was also seen in the subsequent *in vivo* study. Only fully PEGylated micelles with a near-neutral ζ -potential and dense PEG shell showed a prolonged blood circulation time in female balb-c nu/nu mice in the range of several hours. Non- or partially PEGylated micelles were almost completely cleared from the bloodstream within the first hour after intravenous injection. Long-circulating micelles could successfully accumulate in subcutaneous A549 tumor models in these mice 24 h after injection by passive targeting *via* the enhanced permeation and retention (EPR) effect, as shown in **Figure 2-6c**. The amount of drug delivered to the tumor by the BVqMAA/PLL-*b*-PEG micelles was sufficient to suppress tumor growth up to 21 days after a single dose injection and photoirradiation step (**Figure 2-6d**). We could therefore successfully demonstrate the

drug carrying capacity and therapeutic efficacy of BVqMAA MCMs, while the interactions of the micelles in biological surroundings could be tuned by controlling the corona composition.

6. Individual Contributions to Joint Publications

The results presented within this thesis were obtained in collaboration with other persons and were previously published. In the following the individual contributions of each co-author are specified. The asterisk indicates the corresponding author(s) of the respective publication.

Chapter 3

This work has been published in *Biomacromolecules* 12, pp. 4247-4255 (2011) under the title:

“Influence of Polymer Architecture and Molecular Weight of Poly(2-(dimethylamino)ethyl methacrylate) Polycations on Transfection Efficiency and Cell Viability in Gene Delivery”

by Christopher V. Synatschke, Anja Schallon, Valérie Jérôme, Ruth Freitag*, and Axel H. E. Müller*

This work was conducted in collaboration with the chair of “Process Biotechnology” at the University of Bayreuth. I synthesized all materials, conducted their physicochemical characterization and wrote the manuscript, except that:

A. Schallon was involved in the planning of the experiments, performed all of the cell-culture experiments and corrected the manuscript.

V. Jérôme, R. Freitag and A.H.E. Müller were involved in scientific discussions and correcting the manuscript.

Chapter 4

This work has been published in *Biomacromolecules* 13, pp. 3463–3474 (2012) under the title:

“Nanoparticulate Non-Viral Agent for the Effective Delivery of pDNA and siRNA to Differentiated Cells and Primary Human T Lymphocytes”

by Anja Schallon, Christopher V. Synatschke, Valérie Jérôme, Axel H. E. Müller , and Ruth Freitag*

This work was conducted in collaboration with the chair of “Process Biotechnology” at the University of Bayreuth. I synthesized all materials, conducted their physico-chemical characterization and wrote parts of the manuscript, except that: A. Schallon was involved in the planning of the experiments, performed of the cell-culture experiments and wrote parts of the manuscript.

V. Jérôme and R. Freitag were involved in scientific discussions, planning of the cell-culture experiments and wrote parts of the manuscript.

A.H.E. Müller was involved in scientific discussions and corrected the manuscript.

Chapter 5

This work has been published in *Soft Matter* 7, pp. 1714-1725 (2011) under the title:

“Double-Layered Micellar Interpolyelectrolyte Complexes-How Many Shells to a Core?”

by Christopher V. Synatschke, Felix H. Schacher*, Melanie Förtsch, Markus Drechsler and Axel H. E. Müller*

I conducted all of the experiments and wrote parts of the manuscript, except that:

F.H. Schacher synthesized the BVT triblock terpolymers, wrote parts of the manuscript and was involved in the planning of the experiments.

M. Förtsch and M. Drechsler conducted all of the cryo-TEM measurements.

A.H.E. Müller was involved in scientific discussions and corrected the manuscript.

Chapter 6

This work has been published in *Macromolecules* 46, pp. 6466-6474 (2013) under the title:

“Micellar Interpolyelectrolyte Complexes With a Compartmentalized Shell”

by Christopher V. Synatschke, Tina I. Löbling, Melanie Förtsch, Andreas Hanisch, Felix H. Schacher*, and Axel H. E. Müller*,

I synthesized the BVT and BVqMAA polymers, was involved in the planning of the experiments and wrote the manuscript, except that:

T.I. Löbling performed all other synthesis, physico-chemical characterization and corrected the manuscript.

M. Förtsch conducted all of the cryo-TEM measurements.

A. Hanisch assisted with BVT synthesis and corrected the manuscript.

F.H. Schacher and A.H.E. Müller were involved in scientific discussions and corrected the manuscript.

Chapter 7

This work has been published in *ACS Nano* (DOI: 10.1021/nn4028294) under the title:

“Multicompartment Micelles with Adjustable Poly(ethylene glycol) Shell for Efficient *in vivo* Photodynamic Therapy”

by Christopher V. Synatschke, Takahiro Nomoto, Horacio Cabral, Melanie Förtsch, Kazuko Toh, Yu Matsumoto, Kozo Miyazaki, Andreas Hanisch, Felix H. Schacher, Akihiro Kishimura, Nobuhiro Nishiyama, Axel H. E. Müller*, and Kazunori Kataoka*

This work was done in collaboration with the group of Prof. Kazunori Kataoka at the University of Tokyo, Japan. I conducted all of the experiments and wrote the manuscript, except that:

T. Nomoto was involved in planning of the experiments, conducted some of fluorescence microscopy measurements and corrected the manuscript.

H. Cabral conducted part of the animal experiments, was involved in the planning of experiments and corrected the manuscript.

M. Förtsch conducted all of the cryo-TEM measurements.

K. Toh and Y. Matsumoto conducted fluorescence microscopy measurements on animals.

K. Miyazaki assisted with *in vivo* PDT efficacy measurements and corrected the manuscript.

A. Hanisch assisted with BVT synthesis and corrected the manuscript.

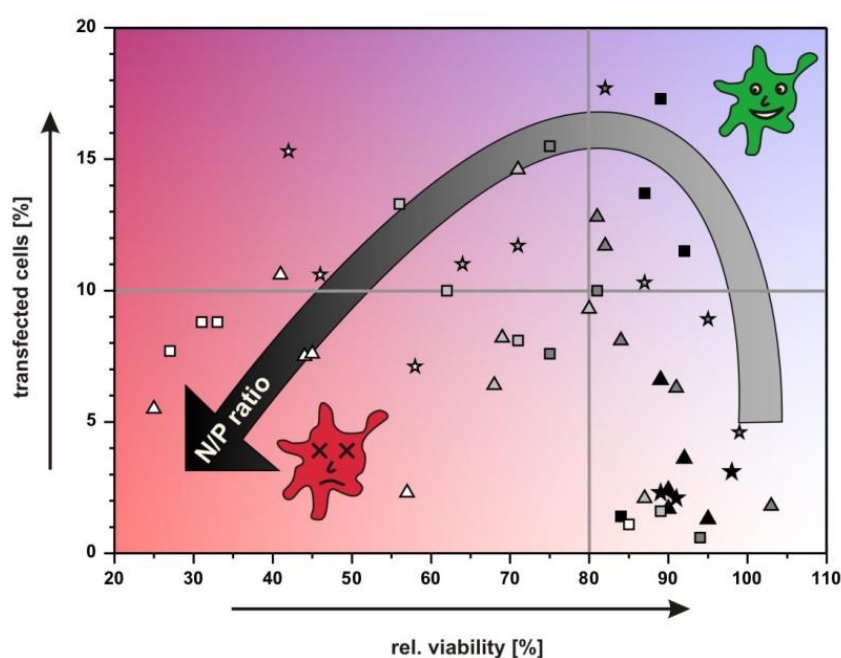
F.H. Schacher, A. Kishimura, N. Nishiyama, A.H.E. Müller and K. Kataoka were involved in scientific discussions and corrected the manuscript.

7. References

1. Matyjaszewski, K., *Macromolecules* **2012**, 45, (10), 4015-4039.
2. Nakayama, Y.; Masuda, T.; Nagaishi, M.; Hayashi, M.; Ohira, M.; Harada-Shiba, M., *Current Drug Delivery* **2005**, 2, (1), 53-57.
3. Nemoto, Y.; Borovkov, A.; Zhou, Y. M.; Takewa, Y.; Tatsumi, E.; Nakayama, Y., *Bioconjugate Chemistry* **2009**, 20, (12), 2293-2299.

Chapter 3

Influence of Polymer Architecture and Molecular Weight of Poly(2-(Dimethylamino)ethyl Methacrylate) Polycations on Transfection Efficiency and Cell Viability in Gene Delivery



The results of this chapter have been published in *Biomacromolecules* as:

“Influence of Polymer Architecture and Molecular Weight of Poly(2-(Dimethylamino)ethyl Methacrylate) Polycations on Transfection Efficiency and Cell Viability in Gene Delivery”

by Christopher V. Synatschke, Anja Schallon, Valérie Jérôme, Ruth Freitag, and Axel H. E. Müller

Reprinted with permission from *Biomacromolecules* **2011**, *12*, 4247-4255. Copyright 2011 American Chemical Society.

Abstract

Nonviral gene delivery with the help of polycations has raised considerable interest in the scientific community over the last decades. Herein, we present a systematic study on the influence of the molecular weight and architecture of poly(2-(dimethylamino)ethyl methacrylate) (PDMAEMA) on the transfection efficiency and the cytotoxicity in CHO-K1 cells. A library of well defined homopolymers with a linear and star-shaped topology (3- and 5-arm stars) was synthesized *via* atom transfer radical polymerization (ATRP). The molecular weights of the polycations ranged from 16 to 158 kDa. We found that the cytotoxicity at a given molecular weight decreased with increasing number of arms. For a successful transfection a minimum molecular weight was necessary, since the polymers with a number-average molecular weight, M_n , below 20 kDa showed negligible transfection efficiency at any of the tested polyelectrolyte complex compositions. From the combined analysis of cytotoxicity and transfection data, we propose that polymers with a branched architecture and an intermediate molecular weight are the most promising candidates for efficient gene delivery, since they combine low cytotoxicity with acceptable transfection results.

Introduction

The transport of foreign genetic material into eukaryotic cells, or DNA transfection, by means of non-viral vectors has been an active field of interdisciplinary research for several decades.¹⁻⁵ With efficient vectors it should be possible to find new ways of treatment for genetic diseases or significantly improve the production of therapeutic proteins.⁶ The use of viruses, although widespread in DNA medicine, as delivery vehicles raised some concerns in terms of immunogenicity, pathogenicity and oncogenicity.^{7, 8} Furthermore, viruses show limitations in the size of the DNA that can be transported and chemical modifications as well as large-scale production can be difficult. Synthetic vectors can potentially overcome those limitations, while achieving acceptable, albeit at present much lower transfection results compared to their viral competitors. Therefore, a lot of effort has been put into the development of non-viral vectors, including polycations and their derivatives. One of the most efficient polycations for gene delivery, which is also considered to be the “gold standard” in this particular area, is poly(ethylene imine) (PEI) either in its branched or linear form, mostly with a molecular weight around 25 kDa.⁹⁻¹² Another promising candidate is poly(2-(dimethylamino)ethyl methacrylate) (PDMAEMA). A vast amount of articles have been published on the use of PDMAEMA or its copolymers for the delivery of genetic material.¹³⁻¹⁹ For systematic studies, this material is better suited than branched PEI, since the monomer can be polymerized in a controlled manner, e.g. through group transfer- and anionic polymerization^{20, 21} or with controlled radical polymerization methods like atom transfer radical polymerization²² (ATRP) and reversible addition (chain) transfer polymerization.²³ By using such controlled polymerization procedures, narrow molecular weight distributions are obtained and more complex polymeric architectures, including star-shaped or branched polymers, can be produced.²⁴⁻²⁷ Such well-defined structures with a maximum of homogeneity are mandatory for establishing structure – property relationships. This is of particular importance, since evidence is building up in the pertinent literature, that non-linear polymers show better transfection properties than their linear counterparts.²⁸

Star-shaped polycations, in particular, have recently raised considerable interest as gene-delivery agents. By connecting the arms of the molecule to a central core, a more dense structure is obtained in solution compared to the corresponding linear polymer. Georgiou *et al.* were the first to use star-shaped PDMAEMA and some copolymers as a mimic of dendritic structures for gene delivery.²⁹⁻³¹ In their works, they used group

transfer polymerization to first synthesize the arms and subsequently, through the addition of a bifunctional crosslinker, connected these arms to a common center, thereby creating the star polymers. This so-called arm-first method allows good control over the length of the arms and is especially appealing because the synthesis of multifunctional initiators is not necessary. A drawback of this method is the retention of linear precursors, probably due to a lowering of solution viscosity, reduced chain mobility or termination reactions.³² Also, the final number of arms is hard to control, *i.e.* it is difficult to obtain large libraries of polymeric samples with similar arm-numbers. In their first publication on PDMAEMA stars,³⁰ Georgiou *et al.* compared seven star-shaped samples where the arm-number varied between 20 – 70. Since then, other groups also reported on their results with star-shaped PDMAEMA,³³ often using the core-first approach for the preparation of the materials.³⁴⁻³⁷ For example, Li *et al.* used a functionalized cyclodextrin as an ATRP initiator to create star-shaped polymers from different cationic monomers. They found the primary and tertiary amine containing polymers to be more effective than quaternized ones, but none of the materials was able to reach transfection levels of PEI.³⁴ Clearly, parameters such as the molecular weight, but also the architecture can have a significant influence on the outcome of a transfection experiment.

However, systematic studies of these parameters on the transfection characteristics to our knowledge only exist for linear DMAEMA (co-)polymers, but not for star-shaped architectures. Linear homopolymers prepared from free radical polymerization with a number average molecular weight between 2.5 – 131 kDa were analyzed with regard to their toxicity and transfection by van de Wetering *et al.* and more recently by Layman *et al.* (M_n from 2.5 to 400 kDa).^{18, 38} The uptake as well as the toxicity of linear PDMAEMA up to a molecular weight of 40 kDa was studied with fluorescently labeled polymers prepared from ATRP, although no genetic material was transported.³⁹ Finally, three individual groups investigated the influence of polymer architecture by preparing copolymers of DMAEMA with poly(ethylene glycol) or methacrylate derivatives thereof.^{13, 40, 41}

In this study, we systematically analyze the effect of both molecular weight and polymer architecture on critical parameters for gene delivery. A library of three polymer architectures containing linear, 3-arm stars and 5-arm stars, with molecular weights ranging from 16 to 158 kDa, was synthesized *via* ATRP. The polymers were then

evaluated in their ability to transfect Chinese Hamster Ovary (CHO-K1) cells together with their cytotoxicity for these cells.

Experimental Part

Materials

Anisole (p.a., 99 %), copper(I) bromide (CuBr, 99.999 %), 2-(dimethylamino)ethyl methacrylate (DMAEMA, 98 %), ethyl 2-bromoisobutyrate (EBIB, 98 %) 1,1,4,7,10,10-hexamethyltriethylenetetramine (HMTETA, 97 %) and trioxane (≥ 99 %) were purchased from Sigma-Aldrich (Steinheim, Germany). Copper(II) bromide (CuBr_2 , ≥ 99 %) was from Fluka. Dioxane and acetone (both p.a. grade) were obtained from Fisher Scientific (Leicestershire, UK) and VWR International (Ismaning, Germany), respectively. The DMAEMA monomer was passed through an aluminium oxide (basic, Sigma-Aldrich) column prior to use in order to remove the stabilizer. EBIB was distilled under vacuum and stored under nitrogen atmosphere at 4 °C before use. All other chemicals were used as received. For dialysis a Spectra/Por 3 (MWCO = 3500, Spectrumlabs, Rancho Dominguez, Canada) dialysis membrane from regenerated cellulose was used. 3-(4,5-dimethylthiazolyl-2)-2,5-diphenyl tetrazolium bromide (MTT) and Hoechst 33258 were from Sigma Aldrich (Taufkirchen, Germany). Milli-Q water was used for the preparation of all aqueous solutions. Polymers were prepared as 0.5 mM stock solution in Milli-Q water. Cell culture materials, cell culture media and solutions were from PAA (Cölbe, Germany). Serum reduced medium OptiMEM was from Invitrogen (Carlsbad, California, USA). Plasmid DNA was prepared by using the EndoFree Plasmid Kit from Qiagen (Hilden, Germany) and diluted in Milli-Q.

Synthesis

All polymer samples were prepared by ATRP. A detailed description of the synthesis of the star-shaped ATRP initiators based on glucose and saccharose is published elsewhere.⁴² Briefly, for the star-shaped polymers DMAEMA (50 g, 0.318 mol, 160 eq.), CuBr (228 mg, $1.59 \cdot 10^{-3}$ mol, 0.8 eq.), CuBr_2 (88.8 mg, $3.98 \cdot 10^{-4}$ mol, 0.2 eq.), trioxane (5 g, 0.056 mol) and anisole (145 g, 1.34 mol) (flask 1) as well as the respective initiator

(here glucose-based initiator with five initiation sites per molecule, 368 mg, $3.98 \cdot 10^{-4}$ mol, 1 eq. of initiation sites), HMTETA (458 mg, $1.99 \cdot 10^{-3}$ mol, 1 eq.) and anisole (5 g, 0.046 mol) (flask 2) were weighed into sealable flasks and separately degassed with nitrogen for 15 minutes. The initiator solution (flask 2) was then transferred with the help of a syringe and minimal contact to air to the monomer solution (flask 1). The polymerization was started by stirring the reaction mixture in a thermostated oil bath at 60 °C. For the determination of the conversion NMR spectroscopy was used and the integrals of the vinyl protons (6.2 and 5.6 ppm) were compared to the integral of the trioxane signal (5.15 ppm). At appropriate conversion, samples were withdrawn from the reaction mixture under nitrogen atmosphere, then opened to air, diluted with dioxane and dialyzed against a mixture of dioxane and Milli-Q water. The highest conversions that were reached in this manner were up to 60 %. In order to remove anisole, residual monomer, copper salts and other low molecular weight impurities the dialysis solution was subsequently changed from low to high water contents (9:1; 7:3; 1:1 and 1:2). Complete dialysis lasted for at least four days under continuous stirring and frequent exchange of the solvent. The pure polymers were obtained as white powder after freeze-drying.

To reach high molecular weights for the linear PDMAEMA the polymerization was carried out with acetone as the solvent for the ATRP. Earlier attempts in our group, where anisole was used as the solvent, had resulted in broad molecular weight distributions and insufficient molecular weights. Here, DMAEMA (100 g, 0.636 mol, 3000 eq.), CuBr (121.7 mg, $8.48 \cdot 10^{-4}$ mol, 4 eq.), CuBr₂ (9.5 mg, $4.24 \cdot 10^{-5}$ mol, 0.2 eq.), trioxane (10 g, 0.111 mol) and acetone (295 g, 5.08 mol) were weighed into a sealable flask. EBIB (41.4 mg, $2.12 \cdot 10^{-4}$ mol, 1 eq.), HMTETA (205.2 mg, $8.91 \cdot 10^{-4}$ mol, 4.2 eq.) and acetone (5 g, 0.086 mol) were mixed in a separate sealable flask and both solutions were degassed with nitrogen for 15 minutes. The initiator solution was then transferred under a nitrogen atmosphere to the monomer solution and the polymerization was started by heating the final mixture to 40 °C. Again, conversion was monitored with the help of NMR spectroscopy and samples were drawn at appropriate conversions. The highest conversion that was reached for the final sample was 40 %. Purification of the linear PDMAEMA was performed analogously to the star-shaped samples.

Characterization

NMR spectroscopy. All NMR spectra were recorded on a Bruker Avance (Ultrasield) 300 instrument (300 MHz) in deuterated chloroform (Deutero GmBH, Kastellaun, Germany) as solvent. The signal of CHCl₃ was used for calibration (7.26 ppm for ¹H).

Size exclusion chromatography (SEC). The apparent molecular weights and their distributions of the PDMAEMA samples after dissolving them overnight were determined with a SEC system using dimethylacetamide (DMAc) with 0.05 % lithium bromide as eluent at a flow rate of 0.8 mL/min. The equipment consisted of one pre-column and two analytical columns (PSS GRAM, 10² and 10³ Å pore size, 7 mm particle size) and a refractive index (RI) detector. The measurements were performed at 60 °C and linear PMMA standards with a narrow molecular weight distribution and methyl benzoate as internal standard were used for calibration.

Plasmid DNA

Plasmid pEGFP-N1 (4.7 kb) (Clontech Laboratories, Mountain View, California USA) encoding for the eGFP (green fluorescent protein), was used in all transfection experiments. The plasmid was amplified in *Escherichia coli* DH5 alpha strain in TB medium to sufficient quantities by using standard molecular biology techniques, including harvesting and purification *via* Qiagen's Giga-Prep kits. Plasmid DNA (pDNA) concentration and quality were determined by A_{260/280} ratio and by agarose gel electrophoresis, respectively.

Mammalian Cell Line and Culture Conditions

The Chinese Hamster Ovary CHO-K1 (CCL-61, ATCC) cell line used in the transfection experiments was maintained in RPMI 1640 cell culture medium supplemented with 10 % FCS, 100 µg/mL streptomycin, 100 IU/mL penicillin, and 2 mM L-glutamine (Growth medium). Cells were cultivated at 37 °C in a humidified 5 % CO₂ atmosphere.

Complex Formation

pDNA/polymer polyplexes were prepared at room temperature using 3 μg pDNA and varied amounts of the respective polycation stock solution to achieve the indicated PDMAEMA-nitrogen/DNA-phosphate (N/P) ratios. For this purpose, the pDNA was diluted in a final volume of 200 μL of 150 mM NaCl-solution. The required polymer solution was added in a single drop to the pDNA solution and the mixture was immediately vortexed for 10 sec at full speed, followed by incubation at room temperature for 30 min.

Transfection of Mammalian Cells

Cells were seeded in 2 mL growth medium at a density of 2×10^5 cells/well in 6-well plates 24 h prior to transfection. One hour prior to transfection, cells were rinsed with PBS and supplemented with 2 mL OptiMEM. The polyplex suspension (200 μL) was added to the cells and the plates were centrifuged for 5 min at 200 g and placed for 4 h in the incubator. Afterwards, the medium was removed, 2 mL of fresh growth medium were added, and the cells were further incubated for 20 h. Cells were harvested by trypsinization and resuspended in PBS. The relative expression of eGFP fluorescence of 1×10^4 cells was quantified *via* flow cytometry using a Cytomics FC 500 equipped with the CXP Analysis research software (Beckman Coulter, Krefeld, Germany). The parameters of the device were set, so that the fluorescence intensity value of the control cells (non-treated) was below 100. All cells showing a fluorescence intensity above this value were recorded as transfected.

MTT Assay (Cytotoxicity Studies)

The cytotoxicity of the polyplexes at various N/P-ratios was evaluated in 96-well microtitre plates by the MTT assay following essentially the transfection protocol. The CHO-K1 cells were seeded in growth medium at a density of 2×10^4 cells/well 24 h prior to the experiment. One hour prior to the experiment, the medium was discarded and serum-free growth medium was added. Cells were incubated with the indicated polyplex preparation for 4 h, then the medium was replaced by serum-containing medium (analogously to the transfection protocol above). After 20h incubation, cells were rinsed with PBS and further incubated in 200 μL MTT solution (0.5 mg/mL in PBS) for 2 h. The

solution was aspirated, replaced with 200 μ L DMSO and mixed at 150 rpm for 5 min to dissolve the formazan crystals produced in the reaction. Absorbance was then measured at 580 nm in a microplate reader (Genios Pro, Tecan GmbH, Crailsheim, Germany) with untreated cells serving as controls. The lethal complex concentration (LCC₅₀) was defined as polymer concentration of the complex at which 50 % of metabolic activity could be measured.

Statistical Analysis

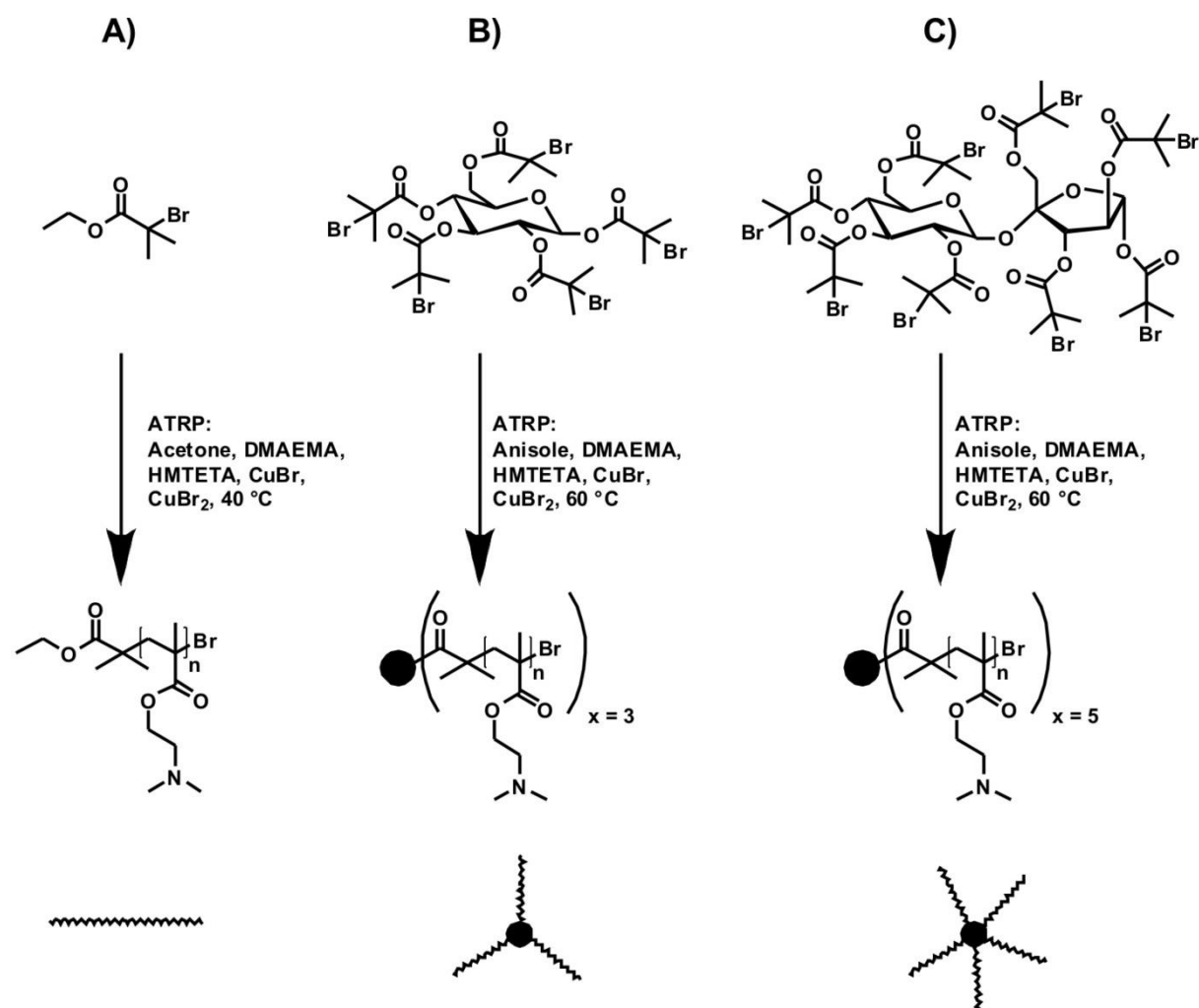
Group data are reported as mean \pm SD. For transfection results, the Student's t-test was used to determine whether data groups differed significantly from each other. Statistical significance was defined as having P-values < 0.05 for significance and P-values < 0.01 for great significance. To determine the significance of more than two groups of data, ANOVA was used with a defined P-value < 0.05 for significant differences.

Results and Discussion

The aim of this work was to study the influence of polymer architecture and molecular weight on both transfection efficiency (TE) and cytotoxicity of DMAEMA-based polymers in gene delivery experiments. For this purpose, a library of three different polymer architectures, namely linear, 3-arm- and 5-arm stars, was synthesized by means of ATRP. We chose this controlled radical polymerization method, as it allows a precise control of the molecular weight of the resulting polymers, while ensuring narrow molecular weight distributions. This is in contrast to many other studies published in the pertinent literature, where the PDMAEMA used for the transfection experiments is frequently prepared *via* free radical polymerization. Such polymers typically have a broad molecular weight distribution, especially in case of larger molecules.^{18, 38} With such polydisperse samples it is almost impossible to discern the influence of the individual species. Instead meaningless average values are determined. Any systematic investigation of the influence of molecular parameters (architecture, molecular weight, etc.) on the gene delivery ability requires instead polymers with a minimal heterogeneity in these parameters. This becomes even more important for architectures with a higher complexity such as stars. Furthermore, when ATRP is used to prepare the polycations, functional end-groups remain on the polymer chains, which can be used for subsequent modifications such as fluorophore labelling, as was demonstrated in an earlier publication.²⁸

Polymer Synthesis and Characterization

The polymerization process of the linear and star-shaped samples is depicted in **Scheme 3-1**. We used a core-first approach with functionalized sugars (glucose⁴³ and saccharose⁴⁴) as initiators for the star polymers (**Scheme 3-1B** and **C**, respectively). Due to steric hindrance, the actual arm number per molecule is lower than the number of initiation sites. In our experience, the average arm-number for the glucose-based polymers is around three arms per molecule and we confirmed this for the S-3₃₀₀ sample through alkaline cleavage of the arms, where an average number of arms of 3.1 was determined. PDMAEMA from the saccharose-based initiator usually has slightly more than five arms (5.4 – 5.6).²² A detailed description of the synthesis of the initiators and synthetic procedure for the cleavage of the arms has been published previously.^{42, 45}



Scheme 3-1: Synthesis of the PDMAEMA samples with linear (A), 3-arm (B) and 5-arm (C) star-shaped architecture, from the respective initiators *via* ATRP. Due to steric hindrance not all initiating sites of the star initiators can form polymer chains. The bottom line shows a schematic representation of the respective polymer architecture.

Table 3-1: Nomenclature and molecular characterization of the linear, 3-arm and 5-arm DMAEMA polymers synthesized with ATRP. Molecular weight averages were calculated from NMR conversion data and PDI was determined with SEC.

Architecture	Name	N / Molecule ^a	M _n [kDa] ^b	PDI ^c
Linear	L ₁₁₀	108	17.1	1.12
	L ₅₂₀	518	81.7	-
	L ₈₈₀	881	138.7	1.73
	L ₁₀₀₀	1003	157.9	1.80
3-Arm	S-3 ₉₅	95	15.9	1.26
	S-3 ₂₁₀	210	34.0	1.16
	S-3 ₃₀₀	296	47.5	1.12
	S-3 ₆₀₀	596	94.7	1.12
	S-3 ₇₁₀	710	112.6	1.13
5-Arm	S-5 ₅₈₀	575	91.9	1.09
	S-5 ₇₀₀	699	111.4	1.12
	S-5 ₉₂₀	919	146.0	1.10

^acalculated from the NMR-molecular weight; ^bdetermined from NMR conversion data; ^cmeasured *via* SEC with DMAc as eluent and poly(methyl methacrylate) as standard.

As shown in **Table 3-1**, for each architecture we synthesized a series of polymers with increasing average molecular weights. The name of each sample is given as the polymer architecture in capital letters, while the subscripts denote the average number of monomers per molecule as determined from the NMR conversion data. SEC measurements confirmed controlled polymerization conditions, as polymers show a rather narrow molecular weight distribution, at least for the star-shaped polymers. One of the linear polymers (L₅₂₀) could not be detected in the SEC measurements, even at high polymer concentrations (> 5 mg / mL). The reason for this remains obscure. Additionally, the polydispersity indices (PDI) of the linear polymers are considerably higher than those of the star-shaped samples. This could be an indication of an uncontrolled polymerization of the linear samples, caused for example through a complex formation between the growing polymer chains and the copper catalyst. Also, PDMAEMA is known to interact with the column material during size exclusion chromatography, which has to be suppressed through the addition of salt to the eluent. An interaction of the sample with the column material would also result in a broadening of the molecular weight distribution

and should be more pronounced for the linear samples, because of their less dense structure and increased hydrodynamic radius compared to the branched structures. For all further discussions, in particular the nomenclature of the polymers, the molecular weight determined *via* NMR was used.

Cytotoxicity Studies by MTT Assay

The polycation library was then used to systematically study the effect of both molecular weight and polymer architecture on cytotoxicity and gene delivery efficiency in mammalian cells. All experiments were performed using Chinese Hamster Ovary (CHO-K1) cells, as this cell line is well established in our group and also commonly used for recombinant protein production in the biopharmaceutical industry. The cytotoxicity of the polyplexes from the indicated polymers at different N/P ratios was determined by MTT assay. The results are shown in **Figure 3-1**, where the average of the three experiments is given as the residual cell viability relative to an untreated cell population.

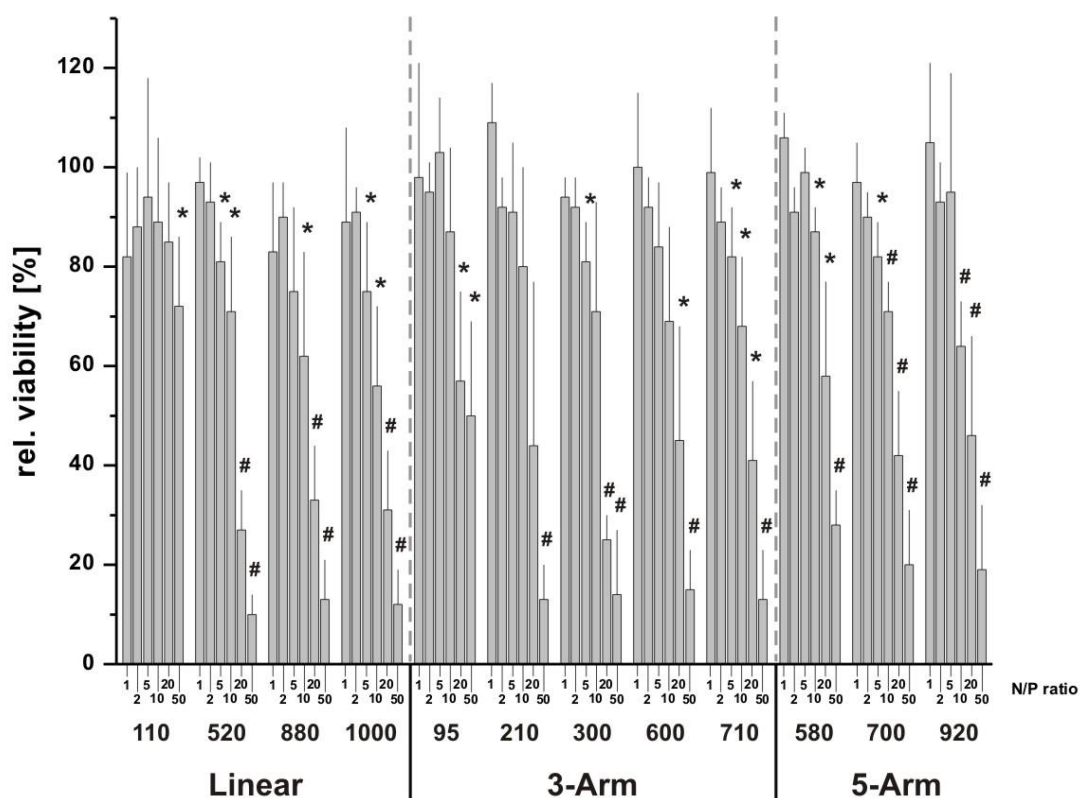


Figure 3-1: Relative viability of CHO-K1 cells incubated with polyplexes made of linear, 3-arm and 5-arm PDMAEMA of varying molecular weights at increasing N/P ratios (1, 2, 5, 10, 20 and 50). Incubation period was 4 h with polyplexes in serum-free media and 20 h in growth media at a cell seeding density of 2×10^4 cells/well. The results are expressed as a percentage of the control cell culture. Data represent mean \pm SD, $n \geq 3$. The Students t-test was used to determine the N/P ratios that significantly differ from 100 % viability (*, $P < 0.05$; #, $P < 0.01$).

As shown in **Figure 3-1**, all polyplexes became toxic at a sufficiently high concentration of the polycation (N/P ratio), as can be seen from the decreasing average relative viability of the cells. A decrease of viability with increasing N/P ratio can be seen for all polymers used for complex formation except the ones with the lowest molecular weights, namely L₁₁₀ and S-3₉₅, which show the lowest cytotoxicity (highest residual cell viability) at intermediate N/P ratios. Both low molecular weight polymers showed no significant cytotoxicity ($P < 0.01$) in the Students t-test. Only at N/P = 50 for L₁₁₀ and at N/P = 20 for S-3₉₅ a significant difference ($P < 0.05$) was observed in the Students t-test compared to 100 % viability, indicating a slightly toxic behavior. Polycations in general are toxic to cells as they interact with various important anionic species found in biological systems including the membrane lipids, (poly)nucleotides and many proteins.^{39, 46, 47} As the N/P-ratio increases, the fraction of non-complexed polycations in the

preparation and hence the cytotoxicity increases. The smallest polycations included in our investigation on the other hand show low general toxicities and can be considered quasi non-toxic in the investigated range.

In order to simplify the amount of data and allow a better comparison between the individual polymers as well as the different architectures, the LCC_{50} (50 % lethal concentration of complexes at a fixed DNA concentration) value was determined for each polyplex solution. The LCC_{50} value then indicates the polycation concentration where the viability compared to the control cells reached 50 %. The value was extrapolated from a plot of the viability against the polymer concentration (see Schallon *et al.*²⁸ for details). In **Figure 3-2** the LCC_{50} values are plotted against the molecular weight of each polymer in a double logarithmic scale. A smaller LCC_{50} -value represents a more toxic polymer, since a lower molar polycation concentration is necessary to reduce viable cell numbers to 50 %. A steady decrease of the LCC_{50} value with increasing molecular weight of the polycations can be seen from **Figure 3-2**.

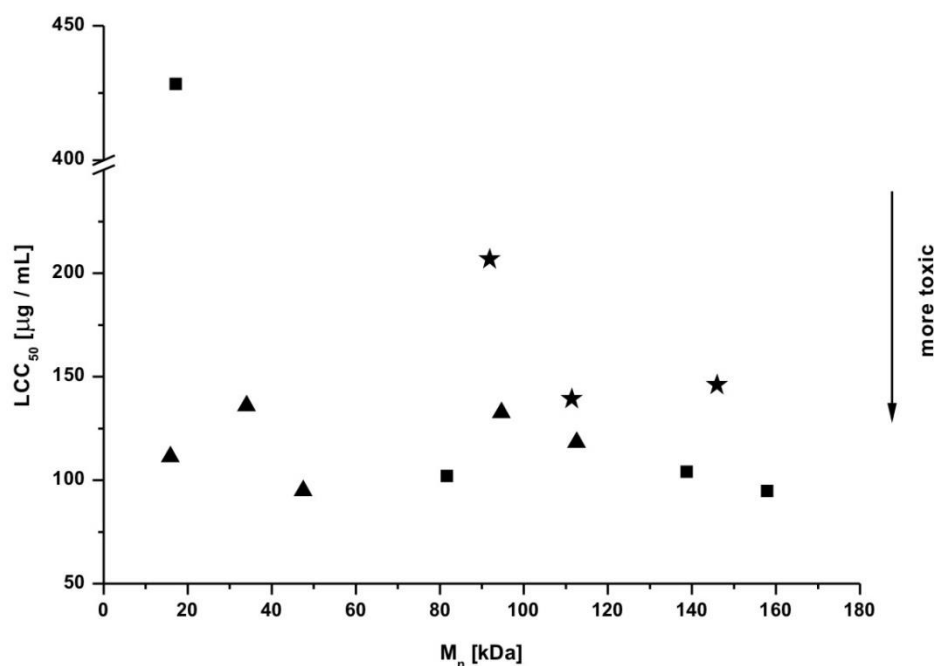


Figure 3-2: Plot of the LCC_{50} -values (50 % lethal complex concentration) of various PDMAEMAs against the molecular weight of the polymer in a double logarithmic scale. The symbols represent linear (square), 3-arm star (triangle) and 5-arm star (star) PDMAEMA. LCC_{50} -values were calculated from MTT experiments with CHO-K1 cells.

More importantly, when the different architectures are compared for a similar molecular weight, the 5-arm star polymers show the lowest toxicities, followed by the 3-arm stars and finally the linear polymers. Our data therefore hints towards a decrease of cytotoxicity of PDMAEMA with increasing arm-number. In this context, a study by Newland *et al.* is of interest.⁴⁸ The authors describe a highly branched PDMAEMA prepared through the copolymerization of DMAEMA with ethylene glycol dimethacrylate. In their experiments, they observed a decrease in the cytotoxicity of irregularly branched PDMAEMA compared to linear PDMAEMA, which suggests that polycation cytotoxicity may decrease not only with increasing arm-number as indicated by our results, but in general as a consequence of increased branching. Similar trends were also described by Xu *et al.* for different types of branched DMAEMA polymers.^{25, 26, 37}

The reasons for the cytotoxicity of polycations in general and PDMAEMA in particular, have been investigated in several studies. It was found that polycations have a tendency to interact with the cellular membrane and membrane proteins.^{18, 46} A decrease in the membrane potential was observed, which points towards the formation of holes in the cellular membrane.⁴⁹ Furthermore, an interaction of the polycation with important proteins and RNA in the cytosol has been speculated upon.¹¹ The general conception is that polymers carrying more charges per molecule, e.g. larger polycations, are more toxic, because they have a stronger tendency to bind negatively charged peptides and eventually precipitate within the cytosol.^{17, 18} In a recent study with well-defined linear PDMAEMA from ATRP it was found that these polymers induce cytotoxicity through a cooperative effect from both membrane disruption and apoptosis.³⁹ However, the specific mechanism may also depend on the cell type.⁴⁷ As a consequence of this observation, several groups have synthesized degradable polycations made from small building blocks, which indeed showed a reduced cytotoxicity compared to their non-degradable analogues.⁵⁰⁻⁵³

However, such an explanation cannot be applied here, since the polymers used in this study are not biodegradable. The reduced cytotoxicity is therefore very likely a result of the unique star-shaped architecture of those molecules. A star-shaped molecule has the highest density in the core, which decreases with increasing distance from the core.⁵⁴ The interaction of the various positively charged nitrogen atoms in such a star with rather flexible polyanions such as pDNA should not be hampered significantly. In fact little differences can be observed in the stability of polyplexes from the same type of

polycation, regardless of its architecture.⁵⁵ In case of a putative interaction with a globular protein molecule or even more importantly the phospholipids in the cellular membrane, however, we propose that not all nitrogens in a star-shaped polymer can participate in the interaction, since those from the inner part of the star would be sterically excluded. Since interaction with the phospholipids and the concomitant formation of holes in the membrane is an important mediator of cellular cytotoxicity, branched and in particular star-shaped and dendritic polymers should be less toxic than their linear counterparts, while transfection efficiency would not necessarily be affected.

Transfection Studies

In order to investigate the structure-function-relationship in regard to gene transfer capability, the polycations were then evaluated as transfection agents. We chose the eGFP transgene and flow cytometry for analysis, since the choice of a reporter gene assay proved not to be crucial for the experimental outcome, as recently reviewed by van Gaal *et al.*⁵⁶ In order to successfully transport genetic material into the nucleus of eukaryotic cells, several barriers have to be overcome.⁷ First, the DNA has to be condensed by the polycation into small and positively charged particles, so called polyplexes. These polyplexes then have to be transported into the cell through the cellular membrane. The commonly accepted mechanism for the uptake of polyplexes by cells is *via* endocytosis.^{19, 57} Alternatively, it was proposed that some polycations (e.g. dendrimers) have the ability to directly penetrate the cellular membrane, as could be shown in experiments on model membranes.⁵⁸ In any case, after crossing the cellular membrane the polyplex needs to protect the genetic material from degradation. Furthermore, the polyplex has to be transported to the nucleus before the genetic material crosses the nuclear membrane.

When all of these barriers have successfully been overcome, the genetic information can be processed leading to the expression of transgenes. In our case, the transgene was the enhanced green fluorescent protein (eGFP). Successfully transfected cells appear green in this case and thus are easily detected by flow cytometry. From these data, the transfection efficiency (TE) was calculated as percentage of green fluorescent cells within the total cell population analyzed, **Figure 3-3**. N/P ratios above values of 20 were not tested, as the cytotoxicity of the polycations at N/P = 20 increases (see **Figure 3-1**) generally resulting in a low TE.

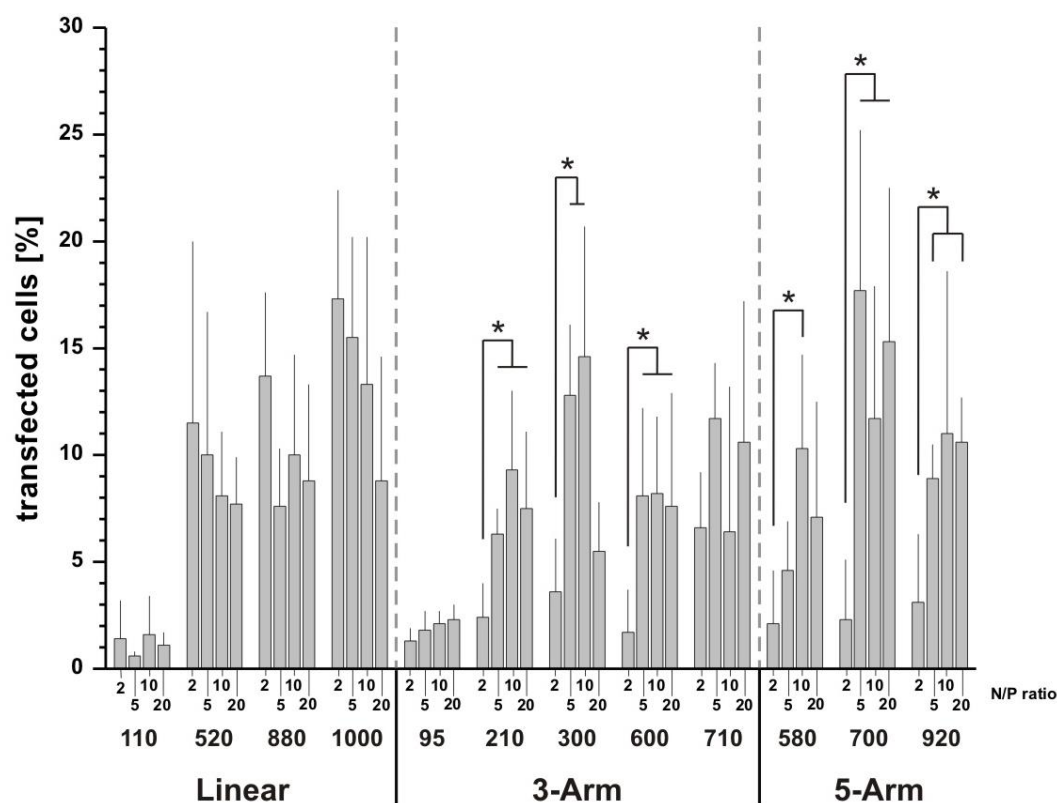


Figure 3-3: Average transfection efficiency (TE) of linear, 3-arm and 5-arm DMAEMA polymers of varying molecular weights using CHO-K1 as hosts and eGFP as reporter protein. Cells were used at a seeding density of 2×10^5 per well in 6-well plates. The transfection efficiency was determined for increasing N/P ratios (2, 5, 10 and 20) for each polymer and N/P ratio combination. Statistical significance was tested by ANOVA and Students t-test and TEs showing differences ($P < 0.05$) were denoted (*). Data represent mean values of five independent experiments \pm SD.

The average TE was compared at various N/P ratios for polymers with different molecular weights and architectures (**Figure 3-3**). The lowest TE-values determined were close to 1 % (L₁₁₀ with N/P = 5 and S-3₉₅ with N/P = 2), these polycations can be considered almost non-transfecting. Higher N/P ratios were also tested, leading to an increased cytotoxicity without any significant change of the TE (data not shown). Possibly, small polycations cannot form sufficiently stable complexes with the DNA in order to condense and protect it from degradation. An insufficient buffering capacity of small polycations in the context of the proton sponge effect could also be a possible reason.^{59, 60} The highest TE values were around 17 – 18 % (L₁₀₀₀ at N/P = 2 and S-5₇₀₀ at N/P = 5). A direct comparison with published studies on the TE of PDMAEMA is difficult, because most prior studies discuss a relative fluorescence intensity of the expressed proteins and do not disclose the absolute number of transfected cells. The first

publication on PDMAEMA stars by Georgiou *et al.*³⁰ indeed is one of the few examples where the percentage of transfected cells is determined and they achieved maximum efficiencies close to 20 %, which is very close to our own results.

A closer analysis of the results showed only a partial influence of the N/P ratio on the TE. Optimal N/P ratios leading to the highest transfection were generally between 5 and 10. In that range, major differences between all other 3- and 5-arm star polymers were not observed. We also analysed the mean fluorescence intensity (MFI) in the eGFP expressing cell population, but could not detect any significant differences of the expression level of the transgene (see **Figure 3-S1**). Therefore, in case of a successful transfection the transgene expression per cell seems to be independent of the DMAEMA polymer used here. Thus, TE values are sufficient to assess the efficiency of the delivery of the pDNA to the cell. Within one polymer sample, N/P = 2 displayed a significantly ($P < 0.05$) lower TE than all other tested ones. For S-3₃₀₀ a bell-shaped dependence of the transfection with the N/P ratio was found. For the other star-shaped samples the overall transfection may also decrease at higher N/P ratios, thus completing the bell-shaped dependence. However those N/P ratios were not tested, because they lead to rather high cytotoxicity (**Figure 3-1**). Bell-shaped patterns have often been described for PDMAEMA in the literature. Potential explanations given are on the one hand an insufficient condensation of the DNA leading to an ineffective penetration of the membrane at low N/P ratios. On the other hand, a large excess of polymer induces cytotoxicity and hence a decrease of TE.^{14, 17, 18}

For the linear architecture the N/P ratio seems to be less important as long as the cytotoxicity stays below ~30 %. The molecular weight has a much bigger influence. L₁₁₀ did not transfect at any N/P ratio tested. Values comparable to the best TE obtained for the star polymers could be achieved by increasing the degree of polymerization (*i.e.* 520 – 1000). In contradiction to published data showing that TE increased with molecular weight of linear polymers,^{18, 38} we never saw significant differences between the TE of L₅₂₀, L₈₈₀ and L₁₀₀₀. A slight tendency towards more efficient transfection at low N/P ratios correlating with low cytotoxicity was observed, but it did not reach statistical significance ($P > 0.05$).

In contrast to the linear polymers, the stars need a higher N/P ratio for efficient transfection. An explanation might be that the accessibility of nitrogens in the core of the

star-shaped polymers is decreased. Consequently, not all nitrogens would be able to interact with the DNA and a larger quantity of polymer would be necessary to compensate for the negative charge. Therefore, better results were achieved at higher N/P ratios for the star-shaped architectures.

Transfection Efficiency against Viability

The differences in trends of the TE with molecular weight and N/P-ratio discussed above makes an interpretation of the influence of the molecular architecture for polycations of a given molecular weight difficult. Moreover, for optimal results, TE should be considered together with cytotoxicity. In reality, the most efficient polymers for gene delivery are often also quite toxic. The gold standard PEI can be seen as a general example for this.⁴⁶ **Figure 3-4** shows an evaluation of the polymers used in this study according to both TE and cytotoxicity at varying N/P ratios.

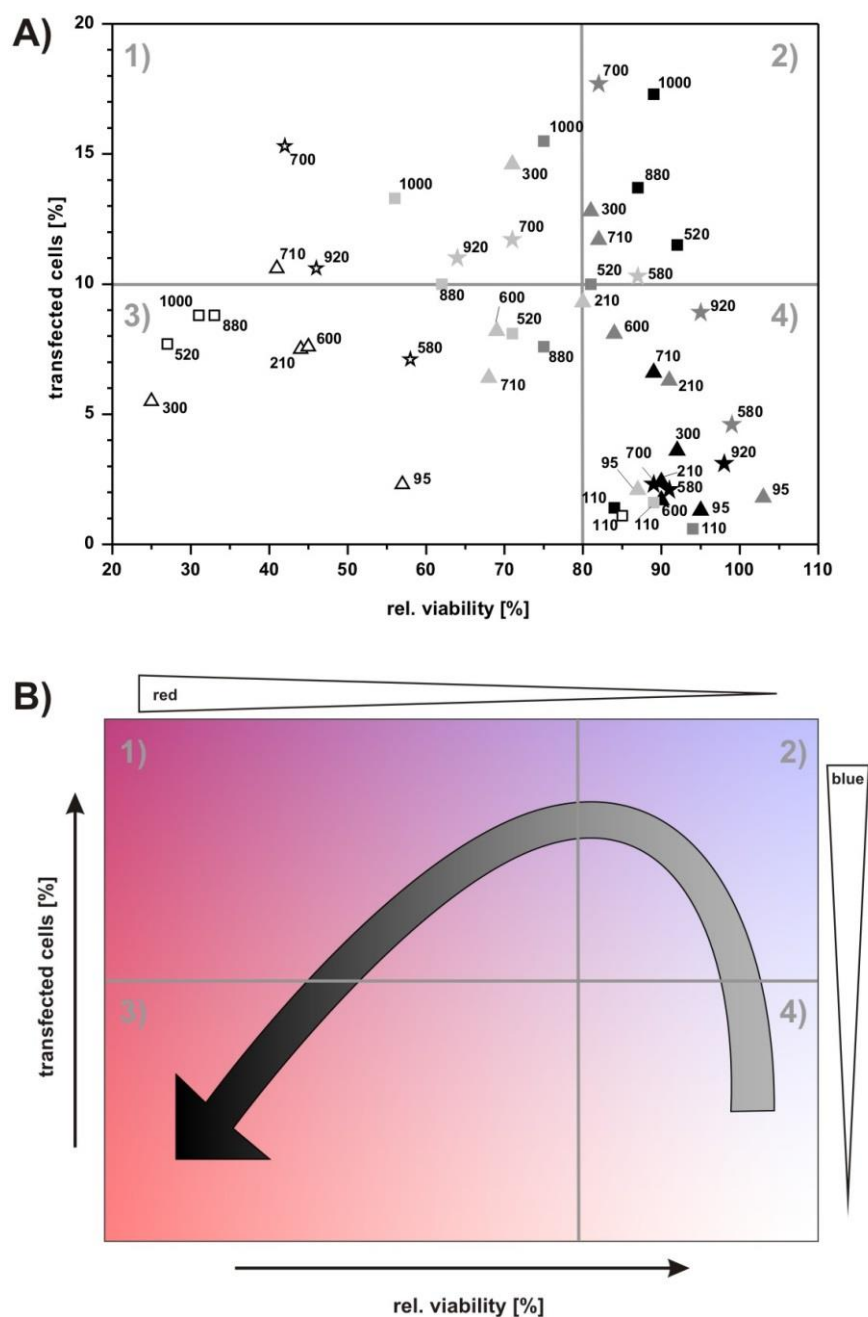


Figure 3-4: (A) Percent of transfected cells plotted against the relative viability for the polyplexes from linear (squares), S-3 (triangles) and S-5 (stars) DMAEMA polymers at N/P ratios 2 (black), 5 (dark grey), 10 (light grey) and 20 (open symbols). Percent of transfected cells were defined as amount of cells expressing the transgene related to all cells. The relative viability was calculated as metabolic activity of treated cells compared to untreated control cells. The average number of monomers per polycation is given next to each entry. Data represent mean value of three independent experiments. (B) Schematic representation of the evolution of the combination of TE and relative viability of PDMAEMA polycations with increasing N/P ratio. The darker color in the arrow represents the gradual increase in N/P ratio, where as an increasing blue staining in the background indicates more transfected cells and increasing red staining more dead cells. Plots are divided into four quadrants, 1: high cytotoxicity, high TE; 2: low cytotoxicity, high TE; 3: high cytotoxicity, low TE; 4: low cytotoxicity, low TE.

For an easier understanding and in order to categorize the entries, **Figure 3-4A** was further divided into four quadrants according to the following criteria: Transfection above 10 % was defined as “efficient”, while a relative viability above 80 % was defined as an acceptable range. In consequence, the most effective gene delivery vehicles tested are found in quadrant 2, *i.e.* they combined a high TE with low cytotoxicity. The two most effective polymers identifiable from **Figure 3-4A** are L₁₀₀₀ at N/P ratio of 2 and S-5₇₀₀ at an N/P ratio of 5. The two other linear polycations with a high molecular weight L₈₈₀ and L₅₂₀ at N/P ratio of 2 also fall in this quadrant, but show a slightly lower TE. From the S-3 series, both S-3₃₀₀ and S-3₇₁₀ at N/P ratio of 5 show efficient transfections with still acceptable cytotoxicity.

The non-transfecting but also non-toxic polymers are located in quadrant 4 (**Figure 3-4A**). Interestingly, these are all star-shaped polymers at N/P ratio of 2, indicating that at least for the star-shaped polymers a certain N/P ratio has to be surpassed, before transfection can take place, as described above. Some star-shaped polymers of varying molecular weight and arm numbers at N/P ratio of 5 are also located in quadrant 4, but show a little higher transfection capability, *i.e.* TEs between 5 and 10 %. For these polymers the optimal N/P ratio probably lies somewhere between 5 and 10, since at an N/P ratio of 10 their TE is higher, but the cytotoxicity also increases, shifting them to the middle of the diagram. Also in this segment are the low molecular weight polymers L₁₁₀ and S-3₉₅ at all N/P ratios (except S-3₉₅ at N/P = 20, which is found in quadrant 3) tested. Therefore, we propose that a certain critical molecular weight or alternatively a critical amount of nitrogens per molecule exists below which a successful transfection cannot take place. This critical value was observed for both linear and star-shaped PDMAEMAs, indicating an independence of the polymer architecture. Since this study used only one type of polymer, it was impossible to distinguish between the effect of molecular weight and number of nitrogens per molecule. However, from the literature it is known that PEI gives excellent transfection results at an average molecular weight of 25 kDa (~580 nitrogens per molecule), while 2 kDa PEI (~47 nitrogens per molecule) is rather inefficient.⁶¹ Although not explicitly tested, we would expect a rather poor performance from a 25 kDa PDMAEMA (~160 nitrogens per molecule), pointing towards a greater importance of the number of nitrogens rather than the molecular weight.

In quadrant 3, undesirable properties of the polycations in regard to gene delivery are combined, as those polymers show both a low TE and a high cytotoxicity. Not

surprisingly, the majority of the entries in this segment come from polyplexes at N/P 20. This is consistent with the increased cytotoxicity at increasing N/P ratio. The transfection efficiency decreases, since a large amount of cells is killed through the influence of the polymers at high concentrations. As discussed before, the polymers at N/P ratio of 10 that end up in this quadrant probably signify the upper limit for an effective transfection, as the cytotoxicity of the polymers starts to play a more important role in the whole process.

With increasing N/P ratios the entries in **Figure 3-4A** move through the different quadrants. This is schematically visualized in **Figure 3-4B**. Generally, at low N/P ratio the polymers show no transfection (linear polymers may be an exception to this) and negligible cytotoxicity. With increasing N/P ratio (approximately N/P ratio 5), at first the transfection also increases, while the cytotoxicity stays at acceptable levels. At an even higher N/P ratio of 10 the cytotoxicity of the polymers starts to play a major role and a shift to the left side of the diagram can be seen. Finally, at the highest tested N/P ratio of 20, both viability and TE decrease again, moving the entries for this N/P ratio to the lower left corner. Interestingly, the maximum TE value of each polymer is found at a relative viability between 70 – 90 %, indicating that a certain cytotoxicity cannot be avoided in a successful transfection.

From these results, we propose that the most efficient polycations for gene delivery should have a branched architecture together with an intermediate molecular weight. The former ensuring a comparatively low cytotoxicity for a given molecular weight (higher LCC₅₀ value) compared to the linear analogues. Noticeably, the architecture of the polymer has no detectable influence on the TE as long as the minimum molecular weight required for efficient transfection is reached. Therefore, branched polymeric architectures might be a promising tool for achieving an optimal balance between a maximum number of transfected cells together with a minimal cytotoxicity.

Conclusions

With increased branching, e.g. arm number, a trend to less toxic behavior at a given molecular weight of the respective polycations could be seen. The transfection experiments were more difficult to interpret, since they gave a high variance. We found, however, that there is a certain minimal molecular weight necessary in order to reach a

significant transfection. Additionally, at least for the star-shaped polymers, an increase in molecular weight does not necessarily result in an improved gene delivery. Our data suggests, that an ideal combination between low cytotoxicity and high transfection should be achievable with a branched structure displaying an intermediate molecular weight. In the future, it needs to be clarified, whether star-shaped polymers with more than 5 arms can further reduce the cytotoxicity, which could lead to an increase in transfection efficiency. Also, other structures of e.g. irregularly branched polymers should be tested.

Acknowledgements

C. V. Synatschke gratefully acknowledges funding by the state of Bavaria through a BayEFG scholarship and ongoing support by the Elite Network of Bavaria (ENB). The authors would like to thank D. V. Pergushov (Moscow), A. Kishimura (Tokyo) and C. B. Tsvetanov (Sofia) for helpful discussions. M. Böhm is acknowledged for performing the SEC measurements.

References

1. de Smedt, S. C.; Demeester, J.; Hennink, W. E *Pharmaceutical Research* **2000**, *17*, 113-126.
2. He, C.-X.; Tabata, Y.; Gao, J.-Q. *International Journal of Pharmaceuticals* **2010**, *386*, 232-242.
3. Jeong, J. H.; Kim, S. W.; Park, T. G. *Progress in Polymer Science* **2007**, *32*, 1239-1274.
4. Treco, D. A.; Selden, R. F. *Molecular Medicine Today* **1995**, *1*, 314-321.
5. Wong, S. Y.; Pelet, J. M.; Putnam, D. *Progress in Polymer Science* **2007**, *32*, 799-837.
6. Godbey, W. T.; Mikos, A. G. *Journal of Controlled Release* **2001**, *72*, 115-125.
7. Mintzer, M. A.; Simanek, E. E. *Chemical Reviews* **2009**, *109*, 259-302.
8. Verma, I. M.; Somia, N. *Nature* **1997**, *389*, 239-242.
9. Boussif, O.; Lezoualch, F.; Zanta, M. A.; Mergny, M. D.; Scherman, D.; Demeneix, B.; Behr, J. P. *Proceedings of the National Academy of Science of the United States of America* **1995**, *92*, 7297-7301.
10. Godbey, W. T.; Wu, K. K.; Mikos, A. G. *Journal of Controlled Release* **1999**, *60*, 149-160.
11. Parhamifar, L.; Larsen, A. K.; Hunter, A. C.; Andresen, T. L.; Moghimi, S. M *Soft Matter* **2010**, *6*, 4001-4009.
12. von Gersdorff, K.; Sanders, N. N.; Vandenbroucke, R.; de Smedt, S. C.; Wagner, E.; Ogris, M. *Molecular Therapy* **2006**, *14*, 745-753.
13. Deshpande, M. C.; Davies, M. C.; Garnett, M. C.; Williams, P. M.; Armitage, D.; Bailey, L.; Vamvakaki, M.; Armes, S. P.; Stolnik, S. *Journal of Controlled Release* **2004**, *97*, 143-156.
14. Dubruel, P.; Schacht, E. *Macromolecular Bioscience* **2006**, *6*, 789-810.
15. Funhoff, A. M.; van Nostrum, C. F.; Lok, M. C.; Kruijtzter, J. A. W.; Crommelin, D. J. A.; Hennink, W. E. *Journal of Controlled Release* **2005**, *101*, 233-246.
16. Lam, J. K. W.; Armes, S. P.; Stolnik, S. *Journal of Drug Targeting* **2011**, *19*, 56-66.
17. van de Wetering, P.; Cherng, J. Y.; Talsma, H.; Crommelin, D. J. A.; Hennink, W. E. *Journal of Controlled Release* **1998**, *53*, 145-153.
18. van de Wetering, P.; Cherng, J.-Y.; Talsma, H.; Hennink, W. E. *Journal of Controlled Release* **1997**, *49*, 59-69.
19. van der Aa, M.; Huth, U. S.; Hafele, S. Y.; Schubert, R.; Oosting, R. S.; Mastrobattista, E.; Hennink, W. E.; Peschka-Suss, R.; Koning, G. A.; Crommelin, D. J. A. *Pharmaceutical Research* **2007**, *24*, 1590-1598.
20. Creutz, S.; Teyssie, P.; Jerome, R. *Macromolecules* **1997**, *30*, 6-9.
21. Rungtsardthong, U.; Deshpande, M.; Bailey, L.; Vamvakaki, M.; Armes, S. P.; Garnett, M. C.; Stolnik, S. *Journal of Controlled Release* **2001**, *73*, 359-380.
22. Plamper, F. A.; Schmalz, A.; Penott-Chang, E.; Drechsler, M.; Jusufi, A.; Ballauff, M.; Müller, A. H. E. *Macromolecules* **2007**, *40*, 5689-5697.
23. Sahnoun, M.; Charreyre, M.-T.; Veron, L.; Delair, T.; D'Agosto, F. *Journal of Polymer Science, Part A: Polymer Chemistry* **2005**, *43*, 3551-3565.
24. Heath, W. H.; Senyurt, A. F.; Layman, J.; Long, T. E. *Macromolecular Chemistry and Physics* **2007**, *208*, 1243-1249.
25. Wang, Z. H.; Li, W. B.; Ma, J.; Tang, G. P.; Yang, W. T.; Xu, F. J. *Macromolecules* **2011**, *44*, 230-239.

26. Xu, F. J.; Ping, Y.; Ma, J.; Tang, G. P.; Yang, W. T.; Li, J.; Kang, E. T.; Neoh, K. G. *Bioconjugate Chemistry* **2009**, *20*, 1449-1458.
27. Xu, F. J.; Yang, W. T. *Progress in Polymer Science* **2011**, *36*, 1099-1131.
28. Schallon, A.; Jerome, V.; Walther, A.; Synatschke, C. V.; Müller, A. H. E.; Freitag, R. *Reactive and Functional Polymers* **2010**, *70*, 1-10.
29. Georgiou, T. K.; Phylactou, L. A.; Patrickios, C. S. *Biomacromolecules* **2006**, *7*, 3505-3512.
30. Georgiou, T. K.; Vamvakaki, M.; Patrickios, C. S.; Yamasaki, E. N.; Phylactou, L. A. *Biomacromolecules* **2004**, *5*, 2221-2229.
31. Georgiou, T. K.; Vamvakaki, M.; Phylactou, L. A.; Patrickios, C. S. *Biomacromolecules* **2005**, *6*, 2990-2997.
32. Pafiti, K. S.; Mastroyiannopoulos, N. P.; Phylactou, L. A.; Patrickios, C. S. *Biomacromolecules* **2011**, *12*, 1468-1479.
33. Dai, F.; Sun, P.; Liu, Y.; Liu, W. *Biomaterials* **2010**, *31*, 559-569.
34. Li, J. S.; Guo, Z. Z.; Xin, J. Y.; Zhao, G. L.; Xiao, H. N. *Carbohydrate Polymers* **2010**, *79*, 277-283.
35. Loh, X. J.; Zhang, Z. X.; Mya, K. Y.; Wu, Y. L.; He, C. B.; Li, J. *Journal of Materials Chemistry* **2010**, *20*, 10634-10642.
36. Nemoto, Y.; Borovkov, A.; Zhou, Y. M.; Takewa, Y.; Tatsumi, E.; Nakayama, Y. *Bioconjugate Chemistry* **2009**, *20*, 2293-2299.
37. Xu, F. J.; Zhang, Z. X.; Ping, Y.; Li, J.; Kang, E. T.; Neoh, K. G. *Biomacromolecules* **2009**, *10*, 285-293.
38. Layman, J. M.; Ramirez, S. M.; Green, M. D.; Long, T. E. *Biomacromolecules* **2009**, *10*, 1244-1252.
39. Cai, J. G.; Yue, Y. A.; Rui, D.; Zhang, Y. F.; Liu, S. Y.; Wu, C. *Macromolecules* **2011**, *44*, 2050-2057.
40. Üzgün, S.; Akdemir, O.; Hasenpusch, G.; Maucksch, C.; Golas, M. M.; Sander, B.; Stark, H.; Imker, R.; Lutz, J.-F.; Rudolph, C. *Biomacromolecules* **2009**, *11*, 39-50.
41. Venkataraman, S.; Ong, W. L.; Ong, Z. Y.; Loo, S. C. J.; Ee, P. L. R.; Yang, Y. Y. *Biomaterials* **2011**, *32*, 2369-2378.
42. Plamper, F. A.; Becker, H.; Lanzendorfer, M.; Patel, M.; Wittemann, A.; Ballauff, M.; Müller, A. H. E. *Macromolecular Chemistry and Physics* **2005**, *206*, 1813-1825.
43. Haddleton, D. M.; Edmonds, R.; Heming, A. M.; Kelly, E. J.; Kukulj, D. *New Journal of Chemistry* **1999**, *23*, 477-479.
44. Stenzel-Rosenbaum, M. H.; Davis, T. P.; Chen, V. K.; Fane, A. G. *Macromolecules* **2001**, *34*, 5433-5438.
45. Plamper, F. A.; Ruppel, M.; Schmalz, A.; Borisov, O.; Ballauff, M.; Müller, A. H. E. *Macromolecules* **2007**, *40*, 8361-8366.
46. Fischer, D.; Li, Y.; Ahlemeyer, B.; Krieglstein, J.; Kissel, T. *Biomaterials* **2003**, *24*, 1121-1131.
47. Rawlinson, L.-A. B.; O'Brien, P. J.; Brayden, D. J. *Journal of Controlled Release* **2010**, *146*, 84-92.
48. Newland, B.; Tai, H.; Zheng, Y.; Velasco, D.; Di Luca, A.; Howdle, S. M.; Alexander, C.; Wang, W.; Pandit, A. *Chemical Communications* **2010**, *46*, 4698-4700.
49. Prevet, L. E.; Mullen, D. G.; Banaszak Holl, M. M. *Molecular Pharmaceutics* **2010**, *7*, 2370-2370.

50. Deng, R.; Yue, Y.; Jin, F.; Chen, Y. C.; Kung, H. F.; Lin, M. C. M.; Wu, C. *Journal of Controlled Release* **2009**, *140*, 40-46.
51. Luten, J.; van Nostrum, C. F.; de Smedt, S. C.; Hennink, W. E. *Journal of Controlled Release* **2008**, *126*, 97-110.
52. Wen, Y. T.; Pan, S. R.; Luo, X.; Zhang, X.; Zhang, W.; Feng, M. *Bioconjugate Chemistry* **2009**, *20*, 322-332.
53. You, Y.-Z.; Manickam, D. S.; Zhou, Q.-H.; Oupický, D. *Journal of Controlled Release* **2007**, *122*, 217-225.
54. Borisov, O.; Zhulina, E.; Leermakers, F.; Ballauff, M.; Müller, A. *Self Organized Nanostructures of Amphiphilic Block Copolymers I*; Springer: Berlin/Heidelberg, 2011; Vol. 241, pp 1-55.
55. Schallon, A.; Synatschke, C. V.; Pergushov, D. V.; Jerome, V.; Müller, A. H. E.; Freitag, R. *Langmuir* **2011**, *27*, 12042-12051.
56. van Gaal, E. V. B.; van Eijk, R.; Oosting, R. S.; Kok, R. J.; Hennink, W. E.; Crommelin, D. J. A.; Mastrobattista, E. *Journal of Controlled Release* **2011**, *154*, 218-232.
57. Elouahabi, A.; Ruyschaert, J.-M. *Molecular Therapeutics* **2005**, *11*, 336-347.
58. Ainalem, M. L.; Campbell, R. A.; Khalid, S.; Gillams, R. J.; Rennie, A. R.; Nylander, T. *Journal of Physical Chemistry B* **2010**, *114*, 7229-7244.
59. Akinc, A.; Thomas, M.; Klibanov, A. M.; Langer, R. *Journal of Genetic Medicine* **2005**, *7*, 657-663.
60. Yang, S.; May, S. *Journal of Chemical Physics* **2008**, *129*, 185105.
61. Godbey, W. T.; Wu, K. K.; Mikos, A. G. *Journal of Biomedical Materials Research, Part A* **1999**, *45*, 268-275.

Supplementary Material

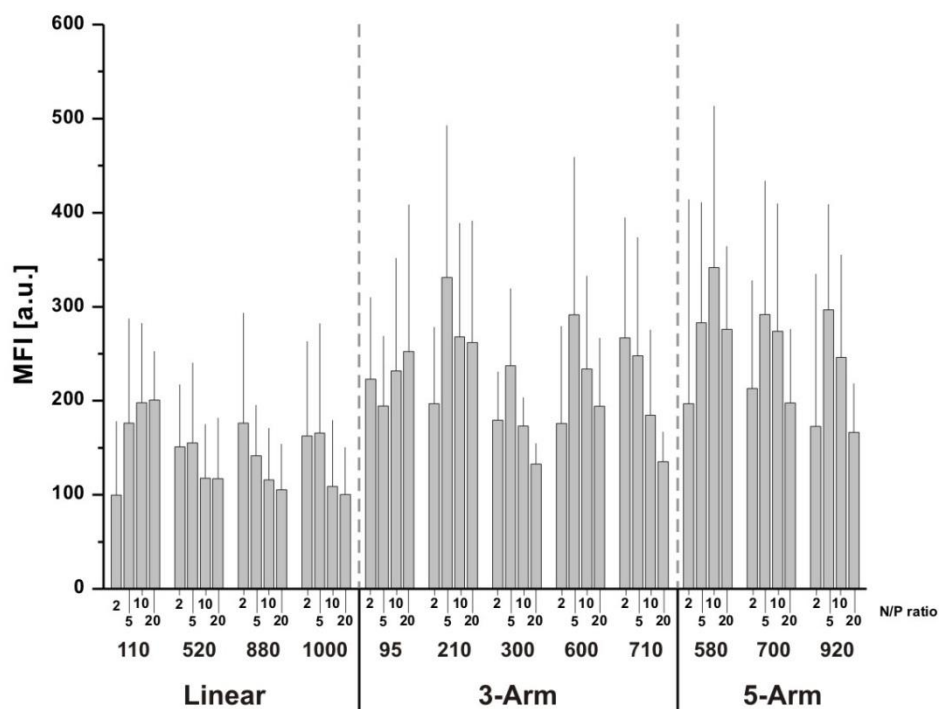
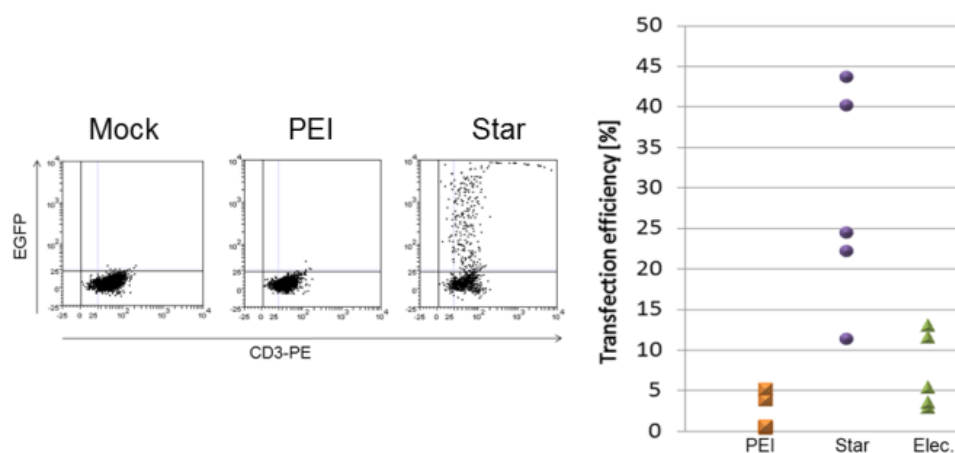


Figure 3-S1: Mean fluorescence intensity (MFI) for the transfection efficiency data shown in **Figure 3-3**. Statistical significance was tested by ANOVA. Data represent mean values of five independent experiments \pm SD.

Chapter 4

Nano-Particulate Non-Viral Agent for the Effective Delivery of pDNA and siRNA to Differentiated Cells and Primary Human T Lymphocytes



The results from this chapter have been published in *Biomacromolecules* as:

“Nano-Particulate Non-Viral Agent for the Effective Delivery of pDNA and siRNA to Differentiated Cells and Primary Human T Lymphocytes”

by Anja Schallon, Christopher V. Synatschke, Valérie Jérôme, Axel H. E. Müller and Ruth Freitag*.

Reprinted with permission from *Biomacromolecules* **2012**, *13*, 3463–3474. Copyright 2012 American Chemical Society.

Abstract

Delivery of polynucleotides such as plasmid DNA (pDNA) and siRNA to non-dividing and primary cells by non-viral vectors presents a considerable challenge. In this contribution, we introduce a novel type of PDMAEMA-based star-shaped nanoparticles that (i) are efficient transfection agents in clinically relevant and difficult-to-transfect human cells (Jurkat T cells, primary T lymphocytes) and (ii) can efficiently deliver siRNA to human primary T lymphocytes resulting to more than 40 % silencing of the targeted gene. Transfection efficiencies achieved by the new vectors in serum-free medium are generally high and only slightly reduced in the presence of serum, while cytotoxicity and cell membrane disruptive potential at physiological pH are low. Therefore, these novel agents are expected to be promising carriers for non-viral gene transfer. Moreover, we propose a general design principle for the construction of polycationic nanoparticles capable of delivering nucleic acids to the above-mentioned cells.

Introduction

The interest in designing fully synthetic non-viral vectors for gene delivery has never waned,¹ although in the past the application range of such agents was limited. Compared to viral vectors,^{2, 3} transfection efficiencies of non-viral vectors in general are low and none of the known agents can efficiently transfect non-dividing and/or differentiated cells.⁴ For some innovative medical therapies, e.g. RNA interference (siRNA), delivery is still considered a substantial bottleneck.^{5, 6} Currently used non-viral delivery agents are typically based on cationic polymers, polypeptides, or lipids,⁷⁻¹⁰ with poly(ethylene imine), PEI, being a major player in the field of commercial products.

The performance of non-viral transfection agents is typically discussed based on the various stages of the delivery process. The poor performance of non-viral vectors in transfecting suspension or non-dividing cells has been linked to problems in transfection complex attachment to the cellular membrane leading to inefficient endocytosis¹¹ and to a presumed inability to transgress the intact nuclear membrane,¹² respectively.

In recent years, we have nevertheless seen a number of studies, which link size and structure of non-viral polycationic transfection agents to their performance.^{12, 13} Increasing size of the polycation often correlates with improved transfection efficiency, but also with an increase in cytotoxicity; the latter being presumably due to a more pronounced disruptive interaction with the cellular membrane.^{14, 15} Concomitantly evidence is building up that non-linear polymer structures are more efficient transfection agents than linear polymers of the same size.^{2, 16-19} In this context, poly(2-(dimethylamino)ethyl methacrylate) (PDMAEMA), first described in the mid-90's by Cherng and co-workers,²⁰ has become an important probe molecule in transfection studies, since PDMAEMA can be synthesized by a number of controlled polymerization methods (e.g., anionic polymerization and atom transfer radical polymerization (ATRP)). Thus, rather homogeneous polycations of different topologies (e.g. linear, branched) become available. In this context, suitable methods for the core-first synthesis of nano-particular multi-armed DMAEMA stars using ATRP have recently become available,^{21, 22} extending the basis for detailed investigation of structure-function relationships. In addition, such star shaped architectures can also be produced by using block copolymers which can self-assemble to micelles structures given suitable solvents.²³ The resulting

polymeric micelles have a low critical micelle concentration (cmc), leading to a high stability in aqueous solutions, showing many advantages in biomedical applications.²⁴

Analysis of transfection and cytotoxicity data as a function of polycation size and structure published by several groups including our own in the past,^{18, 19, 25, 26, 27, 28} led to the hypothesis that polycations with star-shaped architecture constitute promising candidates for efficient transfection agents, although in general for a given structure, PEI-based structures were superior to, e.g., PDMAEMA-based ones. Georgiou et al. found that for optimal polymer architecture with ideal pK value star PDMAEMA homopolymers are transfection agents comparable to the dendrimer SuperFect®.²⁹ Recently, Xu and co-workers reported similar transfection efficiency and reduced cytotoxicity for star-shaped PDMAEMA homopolymers with a cyclodextrin core compared to branched PEI (b-PEI).³⁰ However, all these data were obtained in standard cell lines, neither non-dividing cells nor human primary T lymphocytes were ever tested in this context. Moreover, it is commonly assumed that the transfection of such cell types is difficult or nearly impossible using polycationic agents.⁴

Although PDMAEMA and several of its copolymer variants have been widely studied as transfection agents for plasmid DNA with varying results (see above), only recently have researchers begun to focus on siRNA delivery³¹⁻³³ mediated by PDMAEMA-based polymers.³⁴⁻³⁹ A comparative study has, e.g., shown that micelle architecture, based on triblock copolymers, facilitates an overall release of siRNA compared to the PDMAEMA homopolymer or a PEGylated formulation of this polycation, thereby resulting in a potent gene silencing effect.⁴⁰ Recently, PEGylated polycaprolactone nanoparticles with grafted short PDMAEMA-arms on the surface were reported as being more efficient than PEI and Lipofectamine® in delivering siRNA *in vitro* and *in vivo* (*i.e.*, in HeLa cell line and the corresponding tumor model).⁴¹ The only existing agent for efficient siRNA-based gene knock-down, in human primary T lymphocytes, is Nucleofection®,⁴² which is on the other hand intrinsically restricted to *in vitro* and *ex vivo* applications. In this context, as recently shown by Weber and co-workers,⁴³ gene knock-down and delivery do not always correlate.

In this contribution, we introduce novel polycationic nanoparticles (Si-PDMAEMA: star with 20 arms emanating from a silsesquioxane initiator core; Mic-PDMAEMA: self-assembly of an amphiphilic polybutadiene-*block*-poly(2-(dimethylamino)ethyl

methacrylate) diblock copolymer) based on multi PDMAEMA-arms emanating from a common center. This structure shows, to our knowledge, a never observed capability for the transfection of primary and non-dividing cells by adequate biocompatibility. Moreover, the Si-PDMAEMA shows also improved transfection efficiency (compared to PEI) in non-adherent Jurkat cells, *i.e.*, a suspension cell line known as difficult-to-transfect and in standard cell lines such as CHO-K1, HEK 293. The novel agents can furthermore efficiently deliver siRNA into primary human T lymphocytes and into recombinant CHO cells. As far as we ascertain, our data show, for the first time, that a polycation can be used successfully to deliver siRNA into human primary T lymphocytes and leading to the specific knock-down of the targeted gene.

Experimental Section

Materials

Milli Q water was used to prepare aqueous solutions and for dialysis. Anisole (99 %), CuBr (99.999 %), CuBr₂ (>99 %), 1,1,4,7,10,10-hexamethyltriethylenetetramine (HMTETA, 97 %), iodomethane (>99 %), tetrahydrofuran (THF, >99.9 %), (trimethylsilyl)diazomethane (2 M solution in diethyl ether) and 1,3,5-trioxane (>99 %) were from Sigma-Aldrich (Munich, Germany) and used as received. Dioxane (p.a. quality) was from Fisher Scientific GmbH (Schwerte, Germany). The 2-(dimethylamino)ethyl methacrylate monomer (DMAEMA, 98 %, Sigma-Aldrich) was passed through an aluminum oxide column (basic, Sigma-Aldrich) prior to use in order to remove the stabilizer. 3-(4,5-dimethylthiazolyl-2)-2,5-diphenyl tetrazolium bromide, Hoechst 33258, and branched poly(ethylene imine) (b-PEI, 25 kDa) were from Sigma Aldrich, linear PEI (l-PEI, 25 kDa) from Polysciences Europe GmbH (Eppelheim, Germany). Polycation stock solutions were 500 μM in Milli Q water. PB₂₉₀-b-PDMAEMA₂₄₀ (M_n = 53,500 g/mol, PDI = 1.07), prepared as described elsewhere,⁴⁴ was kindly donated by Felix Schacher, Macromolecular Chemistry II, University of Bayreuth. Cell culture materials, media, and solutions were from PAA Laboratories (Cölbe, Germany). Serum reduced medium Opti-MEM was from Life Technologies GmbH (Darmstadt, Germany). The PE-conjugated anti-CD3, FITC-conjugated anti-CD4 and FITC-conjugated isotype control antibodies used for immunostaining were from BD Biosciences (Heidelberg, Germany). Blood was obtained from the Bavarian Red Cross.

Plasmid pEGFP-N1 (4.7 kb, Clontech, USA) encoding for the enhanced green fluorescent protein (EGFP) driven by the cytomegalovirus immediate early promoter was used in most of the transfection experiments. The pIVEX2.3-UK plasmid (4.3 kb, Roche Applied Science, Germany), encoding for the human urokinase under the control of a T7 promoter, was used in control transfection as “non-EGFP expression” plasmid. The plasmids were amplified in *E. coli* DH5 alpha strain in LB medium to sufficient quantities using standard molecular biology techniques, including for harvesting and purified using the EndoFree Plasmid Kit (Giga Prep) from Qiagen (Hilden, Germany).

Polymer Synthesis

For the synthesis of Si-PDMAEMA, 34.4 mg (2.867×10^{-6} mol) of the silsesquioxane initiator (synthesis and detailed characterization as published elsewhere⁴⁵⁻⁴⁷ were mixed with 46 μ L (1.691×10^{-4} mol) HMTETA and 5 g anisole in a glass flask and sealed with a rubber septum (Solution 1). In a separate flask 4.9 g (0.0312 mol) DMAEMA, 19.3 mg (1.346×10^{-4} mol) CuBr, 7.2 mg (3.223×10^{-5} mol) CuBr₂, 0.53 g trioxane, and 7 g anisole were mixed and the flask was sealed with a rubber septum (Solution 2). Both solutions were degassed with nitrogen for at least 15 min. Solution 1 was then transferred under nitrogen to Solution 2 with a syringe. The mixture was briefly stirred, a sample for NMR conversion analysis was withdrawn, and the polymerization started by heating the mixture to 60°C in an oil bath. Progress of the polymerization was monitored by following the monomer consumption *via* ¹H-NMR by comparing the integrals of the signals of the two vinyl protons of DMAEMA (6.21 ppm and 5.61 ppm) with that of the internal standard signal of trioxane at 5.14 ppm. After 205 min a conversion of 42 % had been reached and the polymerization was quenched by cooling and opening the flask to air. For purification the reaction mixture was dialyzed against a dioxane/water mixture (initial composition 9:1). Dioxane contents were lowered subsequently to 7:3, 1:1, and 1:2, and finally to pure water. Dialysis lasted for four days under continuous stirring and the final polymer was obtained by freeze-drying.

Star-like polymer micelles (Mic-PDMAEMA) were prepared by dissolving 144 mg PB₂₉₀-*b*-PDMAEMA₂₄₀ (2.7×10^{-6} mol, $M_n = 53500$ g/mol, PDI = 1.07) in 6 mL THF in a glass flask (40 mL), equipped with a magnetic stirrer bar. 10 mL of PBS buffer were added drop-wise to induce micelle formation. THF was allowed to partially evaporate through stirring the open flask overnight at 25°C and any residual THF was then removed

through dialysis against PBS for 6 d with regular exchange of the dialysis solution. The final polymer concentration was 10.65 g/L.

Polymer Characterization

GPC measurements for PB₂₉₀-*b*-PDMAEMA₂₄₀ were performed on a Waters instrument with four PSS-SDV gel columns (5 μm) with a porosity range from 10² to 10⁴ Å (PSS Mainz, Germany) and THF containing 0.25 wt. % tetrabutylammonium bromide as eluent. A differential refractometer was used for detection and narrowly distributed polystyrene standards for calibration. The determination of the hydrodynamic radius, R_h, of Si-PDMAEMA (Milli Q water; 1 g/L polymer conc.) and Mic-PDMAEMA (PBS buffer; 10 g/L polymer conc.) was performed by dynamic light scattering (DLS) in sealed cylindrical scattering cells (d = 10 mm) at an angle of 90° using an ALV DLS/SLS-SP 5022F instrument consisting of an ALV-SP 125 laser goniometer with an ALV 5000/E correlator and a He-Ne laser with the wavelength λ = 632.8 nm. Prior to the measurement, the solution was filtered through a 5 μm pore size filter to remove any dust particles. The CONTIN algorithm was applied to analyze the obtained correlation functions. Apparent z-average hydrodynamic radii were calculated according to the Stokes-Einstein equation. The <R_h>_{z, app.} was taken as the average of three individual measurements. The copper content of the Si-PDMAEMA was determined by inductively coupled plasma optical emission spectroscopy (ICP-OES) using a Varian Vista-Pro radial machine. For the determination of the arm number and size in Si-PDMAEMA a previously published procedure was used,²¹ *i.e.* the arms were cleaved off and analyzed *via* GPC as linear polymers.

Potentiometric Titration

Measurements were performed on an automatic titration machine (Titrand 809, Metrohm) equipped with a pH electrode (Unitrode, Metrohm, 6.0258.000) and calibrated with Merck buffer solutions. Titrations were performed with 0.1 N HCl solution (Titrisol, Merck) in triplicate on 35 mL of polymer solution (0.5 mg/mL in MilliQ water) previously adjusted to a pH of 11.5. HCl solution was added dynamically (increment of addition was automatically adjusted between 5 μL – 100 μL depending on the steepness of the curve for optimal resolution) and under continuous stirring every 30 seconds until a

final pH of 2.8 was reached. The respective apparent pK_a values were taken as the pH value at a protonation degree of 50 % ($\alpha = 0.5$) from the potentiometric titration curves.

Zeta Potential Measurement

For zeta-potential measurements, polyplexes were prepared in 1 mL of a 150 mM aqueous NaCl-solution containing a total of 15 μ g pDNA, following otherwise the ‘transfection protocol’ indicated below. Zeta-potential measurements were performed in triplicate using the standard capillary electrophoresis cell (DTS 1060) of the Zetasizer Nano ZS (Malvern Instruments, Ltd., UK) at room temperature.

Cell Lines and Culture Conditions

CHO-K1 (CCL-61, ATCC), CHO-EGFP-VEGFA (recombinant CHO cells constitutively expressing EGFP⁴⁸), HEK-293 (CRL-1573, ATCC), and Jurkat (TIB-152, ATCC) cells were maintained in RPMI 1640 culture medium, A549 (CCL-185, ATCC) and C2C12 (CRL-1772, ATCC) cells in DMEM culture medium, Wi-38 (CCL-75, ATCC) and L929 (CCL-1, ATCC) in MEM cell culture medium all supplemented with 10 – 20 % fetal calf serum (FCS) (as recommended by ATCC), 100 μ g/mL streptomycin, 100 IU/mL penicillin, and 2 - 4 mM L-glutamine. Cells were cultivated at 37°C in a humidified 5 % CO₂ atmosphere. For induction of differentiation, C2C12 cells were grown near to confluence in growth medium and the medium was switched to DMEM supplemented with 10 % horse serum. The differentiation, verified by the appearance of multinucleated and elongated myotubes, occurs after 2 to 4 days. To assess the homogeneity of growth-arrested and differentiated C2C12 cells, approximately 1×10^6 fixed cells were analyzed by flow cytometry. For this purpose, the cell pellet obtained after centrifugation for 5 min at 200 g was resuspended in 2 mL Dulbecco-PBS (DPBS), 2 mL ice-cold 70 % ethanol were added drop-wise and the mixture stored for at least 2 hours at -20°C. Cells were stained with 2 μ g/mL Hoechst 33258 and analyzed in a Cytomics FC 500 flow cytometer (Beckman Coulter, Krefeld, Germany) equipped with a violet (405 nm) laser.

Isolation and Cultivation of Human Primary T Lymphocytes

Peripheral blood mononuclear cells (PBMCs) were isolated from the blood of healthy donors by Ficoll™ density gradient centrifugation (Lymphocyte separation medium LSM 1077, PAA Laboratories), according to the supplier's instructions. The interface cells (containing typically 70 – 100 % lymphocytes according to the supplier) were washed three times with DPBS by centrifugation for 10 min at 300 g. The freshly isolated peripheral blood lymphocytes (PBLs) were seeded at 4×10^6 cells per mL in QPBL medium (PAA Laboratories), which contains phytohemagglutinin (PHA) and stimulates the growth of T cells. Two to five days cultivation in this medium was sufficient to reach ~ 95 % CD3⁺ cells with blasted morphology. CD3 expression was analyzed by immunostaining using a PE-conjugated anti-CD3 antibody (according to manufacturer's instructions). Immunofluorescence was analyzed by flow cytometry.

Transfection of pDNA

For transfection of the adherent cell lines, cells were seeded at a density of 2×10^5 cells per well in 6-well plates 20 h prior to transfection. One hour prior to transfection, cells were rinsed with DPBS and supplemented with 2 mL Opti-MEM medium. For transfection of CHO cells in the presence of serum, Opti-MEM was replaced by RPMI 1640 supplemented with 10 % FCS. Polyplexes were prepared by mixing 3 µg pDNA in a final volume of 200 µL of aqueous 150 mM NaCl-solution with sufficient amounts of the respective polycation stock solution, added in a single drop, to achieve the intended N/P-ratio (polymer N/DNA P-ratio). Solutions were vortexed for 10 sec and incubated for 20 min at room temperature for polyplex formation. The polyplex suspension (200 µL) was added to the cells and the plates were centrifuged for 5 min at 200 g and placed for 4 h in the incubator. Afterwards, the supernatant was removed by aspiration, 2 mL of fresh growth medium were added, and the cells were further incubated for 20 h. For transfection of the suspension cells (Jurkat), two hours prior to transfection, cells were rinsed with DPBS and seeded at 5×10^5 cells per well in 1.5 mL Opti-MEM medium (6-well plates). The polyplex suspension (200 µL prepared as described above) was then added to the cells and the plates were centrifuged for 5 min at 200 g and placed for 4 h in the incubator. Afterwards, 0.5 mL of the medium was removed taking care not to disturb

the cells, 2 mL of pre-warmed fresh growth medium were added, and the cells were further incubated for 20 h.

For primary human T lymphocytes, transgene delivery was carried out 3 to 5 days after PBMC preparation and cultivation in QPBL medium. 5×10^5 cells were placed in 1.5 mL Opti-MEM medium per well in 6-well plates. 200 μ L of the polyplex suspension prepared as described above were added and the plate placed for 4 h in the incubator. Afterwards, 0.5 mL of the medium was removed taking care not to disturb the cells, 2 mL of pre-warmed fresh QPBL medium were added, and the cells were further incubated for 48 h. Electroporation of T lymphocytes was performed as previously described.⁴² Briefly, 20 μ g DNA were pulsed with 5.0×10^6 cells in Opti-MEM at 250 V, 950 μ F (BioRad Gene Pulse X Cell). Immediately after electroporation, cells were incubated for 10 min at 37°C followed by transfer into pre-warmed fresh QPBL medium (2 mL) in a 6-well plate.

For analysis, adherent cells were harvested by trypsinization and suspension cells by centrifugation and resuspended in DPBS. For determination of the viability, dead cells were identified *via* counterstaining with propidium iodide (PI) or trypan blue. The relative expression of EGFP fluorescence of 1×10^4 cells was quantified *via* flow cytometry. Cells were initially evaluated by scatter properties (FSC/SSC) in order to select a region representing single non-apoptotic cells (elimination of dead cells, debris and cellular aggregations). This gated region (R0) was further analyzed for fluorescence (PI/EGFP). Dot plots with log of the red fluorescence intensity (PI) on the x-axis and log of the green fluorescence intensity (EGFP) on the y-axis were used to estimate the percentage of EGFP-expressing cells in the main non-apoptotic cell population (gate R0). Negative controls (N/P 0, non-transfected cells or cells transfected with an irrelevant pDNA) were used to set the position of quadrants separating GFP-positive living cells (upper left), GFP-positive dead cells (upper right), GFP-negative living cells (lower left) and GFP-negative dead cells (lower right). These quadrants were applied for the analysis of transfected cells and percentage cell number / total cell number in the gated region were calculated for each quadrant.

Delivery of siRNA

siRNAs were: hCD4-siRNA (sense) 5'- GCAAUUGCUGAGUGUUCGGAUUGACUGC - 3', (anti-sense), 5' – GCAGUCAAUCCGAACACUAGCAAUUGC - 3'; EGFP-siRNA⁵⁰ (sense) 5' – AAGCUGACCCUGAAGUUCAUCUGCACC - 3', (antisense), 5' – GGUGCAGAUGAACUUCAGGGUCAGCUU - 3' (all Eurofins MWG Operon). The siRNAs were obtained as duplex and solubilized into 1x siMAX universal buffer (6 mM HEPES, 20 mM KCl, 200 μ M MgCl₂, pH 7.3; Eurofins MWG Operon). EGFP-siRNA and hCD4-siRNA were used as negative control in the experiments involving CD4 knockdown in T lymphocytes and EGFP knockdown in CHO-EGFP-VEGFA cells, respectively. For siRNA delivery into EGFP expressing CHO cells (CHO-EGFP-VEGFA cells⁴⁸), cells were seeded at a density of 0.25×10^5 cells per well in 24-well plates 20 h prior to delivery. One hour prior to delivery, cells were rinsed with DPBS and supplemented with 0.2 mL Opti-MEM medium. siRNA-polyplexes were prepared by diluting siRNAs stock solution (10 μ M) in a total volume of 50 μ L Opti-MEM to the indicated final concentration and adding sufficient amounts of the polycation stock solution to reach the desired N/P ratio. The mixture was immediately mixed by vortexing at full speed followed by incubation at room temperature for 15 min. The polyplex suspension (50 μ L) was added to the cells, the plates were centrifuged for 5 min at 200 g, and placed for 4 h in the incubator. Afterwards, the supernatant was removed by aspiration, 1 mL of fresh growth medium was added, and the cells were further incubated for 20 h (Si-PDMAEMA) and 30 h (Si-PDMAEMA and Mic-PDMAEMA). The relative expression of EGFP fluorescence of 1×10^4 cells was quantified. For determination of the viability, dead cells were identified *via* counterstaining with propidium iodide. Cells were initially evaluated by scatter properties (FSC/SSC) in order to select a region representing single non-apoptotic cells (elimination of dead cells, debris and cellular aggregations). This gated region (R0) was further analyzed for fluorescence (PI/EGFP). To assess the efficiency of the siRNA to knockdown the EGFP expression, the median fluorescence intensity (FI) values were compared.

For siRNA delivery to T lymphocytes, cells were washed twice with DPBS and plated in 250 μ L Opti-MEM in 24-well plates at 5×10^5 cells per well for 1 h prior to transfection. Polyplexes were prepared and added to the wells as described above. The plates were centrifuged for 5 min at 200 g and placed for 4 h in the incubator. Afterwards, 700 μ L of pre-warmed fresh QPBL medium were added per well and the cells were further

incubated for at least 24 h without removing the complexes or replacing the medium until subsequent analysis by flow cytometry.

Analysis of CD4 Expression

For analysis of CD4 expression, cells were harvested by centrifugation (5 min, 200 g, 4 °C) and resuspended in DPBS. T lymphocytes expressing CD4 receptors were identified by immunofluorescence *via* staining the cells with FITC-conjugated anti-CD4 or FITC-conjugated isotype control antibodies (according to manufacturer's instructions) on the day of siRNA delivery and at least 24 h after delivery. Dead cells were identified *via* counterstaining with propidium iodide. The relative expression of CD4 was quantified *via* flow cytometry.

Cells were initially evaluated by scatter properties (FSC/SSC) in order to select a region representing single non-apoptotic cells and to eliminate debris which always compose a significant fraction in an activated primary lymphocyte cell culture (gate "lympho") and by (SSC/PI) in order to select the living cells (PI-negative population) (gate "living"). The expression of the CD4 protein was assessed in histogram plots (green fluorescence intensity on the x-axis and cell number on the y-axis) representing the intensity of the CD4-FITC fluorescence (CD4^{low}: fluorescence intensity between 70 and 170; CD4^{high}: fluorescence intensity > 170) in the living T lymphocytes (defined as a sub-population of gate "lympho" and gate "living").

Cytotoxicity / Vitality Assay (MTT)

The toxicity of the polycations was tested (concentration range 0.001 mg/mL to 5.0 mg/mL, 8 replicate experiments each) according to the ISO 10993-5 protocol by MTT assay using L929 murine fibroblasts, cultured in MEM supplemented with 10 % FCS, as test cells. The cells were seeded at a density of 1×10^5 cells per well 24 h prior to the experiment in 96-well plates. The concentration of the MTT stock solution was 1 mg/mL. As 100 % viability control, untreated cells were used. The absorbance was measured using a plate reader (Genios Pro, Tecan, Germany); wavelength 580 nm.

For T lymphocytes, the MTT assay was performed as follows. 5×10^5 human T lymphocytes in 500 μL Opti-MEM medium were transferred into 1.5 mL Eppendorf™ tubes. The polymer was added and the cells were incubated for 4 h at 37°C in the incubator. Then, the Opti-MEM medium was replaced by QPBL medium. All medium exchange and washing steps were done by centrifugation (5 min, 200 g, 4°C). The cells were further incubated for 20 h. Then cells were rinsed with DPBS and further incubated in 200 μL MTT solution (1.0 mg/mL in RPMI 1640 without phenol red) for 2 h. The tubes were centrifuged for 5 min at 600 g, the MTT solution was discarded and 200 μL isopropanol were added to the cell pellet. The tubes were mixed at 150 rpm for 5 min to dissolve the formazan crystals produced in the reaction. Absorbance was measured at 580 nm in the microplate reader with untreated cells serving as controls. For data evaluation, Origin 6.1 (OriginLab Corporation, Northampton, USA) software was used, the x-scale was plotted logarithmically and a nonlinear fit was used to obtain the LD₅₀ values.

Hemolysis Test

The membrane damaging properties of the polymers was quantified by analyzing the release of hemoglobin from human erythrocytes, according to Parnham and Wetzig.⁵¹ The erythrocytes-containing blood fraction obtained after Ficoll™ gradient separation was centrifuged at 700 g for 10 min. The obtained pellet was washed three times with cold DPBS pH 7.4 by centrifugation at 700 g for 10 min and re-suspension in the same buffer. Polymer solutions were prepared in DPBS buffer and 100 μL were added to the erythrocytes (100 μL) to give final concentrations in the range of 0.001 to 5.0 mg/mL and incubated for 60 min under constant shaking at 37°C. After centrifugation (700 g, 10 min), the supernatant was analyzed for released hemoglobin at 580 nm. The absorbance was measured using a plate reader (Genios Pro, Tecan, Germany). For comparison, collected erythrocytes were washed with DPBS and either lysed with 0.2 % Triton X-100 yielding the 100 % lysis control value (A_{100}) or resuspended in DPBS as reference (A_0). The analysis was repeated with blood from at least six independent donors. The hemolytic activity of the polycations was calculated as follow:

$$\% \text{ hemolysis} = 100 * (A - A_0) / (A_{100} - A_0)$$

with A: absorbance of the sample, A_{100} : absorbance at 100 % hemolysis, A_0 : absorbance at 0 % hemolysis.

Statistical Analysis

Group data are reported as mean \pm s.e.m. For transfection results, the Student's *t*-test was used to determine whether data groups differed significantly from each other. Statistical significance was defined as having $P < 0.05$.

Results and Discussion

Polymer Synthesis and Characterization

As basis for the investigation, a well-defined 20-armed star (Si-PDMAEMA) was synthesized *via* ATRP of DMAEMA, from a silsesquioxane initiator core (**Scheme 4-1a**) based on a procedure previously published by one of our groups.²¹ Progress of the polymerization was monitored by following the monomer consumption *via* ¹H-NMR as evidenced by the decrease in the integral of the two vinyl protons at 6.21 ppm and 5.61 ppm. Trioxane was added as an internal standard to the mixture, because it gives a characteristic signal at a chemical shift of 5.14 ppm and does not participate in the reaction. The polymerization was quenched at 42 % monomers conversion, which corresponds to an average degree of polymerization (DP, or number of DMAEMA units per molecule) of 4,570, or a number average molecular weight M_n of 730 kDa assuming that the monomers were homogeneously distributed among all growing particles. Due to steric hindrance, not all putative initiation sites of the silsesquioxane initiator can be expected to start a polymer chain²¹ and the number of arms per star is therefore below the theoretically possible 58. In order to determine the average number and length of the arms, these were cleaved off and their molecular weight distribution was determined by gel permeation chromatography (GPC). The number average M_n of the arms was 23,500 Da, and the weight average M_w was 33,500 Da, which corresponds to a polydispersity index (PDI) of 1.42 and a DP of 235 monomers per arm. From this, an average number of 19.5 arms was calculated for the produced Si-PDMAEMA. The number of arms is in good agreement with the values of 19 to 24 arms that have been determined for other star-shaped polymers prepared using the same initiator.²¹ A z-average hydrodynamic radius, $\langle R_h \rangle_z$, *app.*, of 37.2 ± 3.5 nm was determined for the Si-PDMAEMA by dynamic light scattering (DLS).

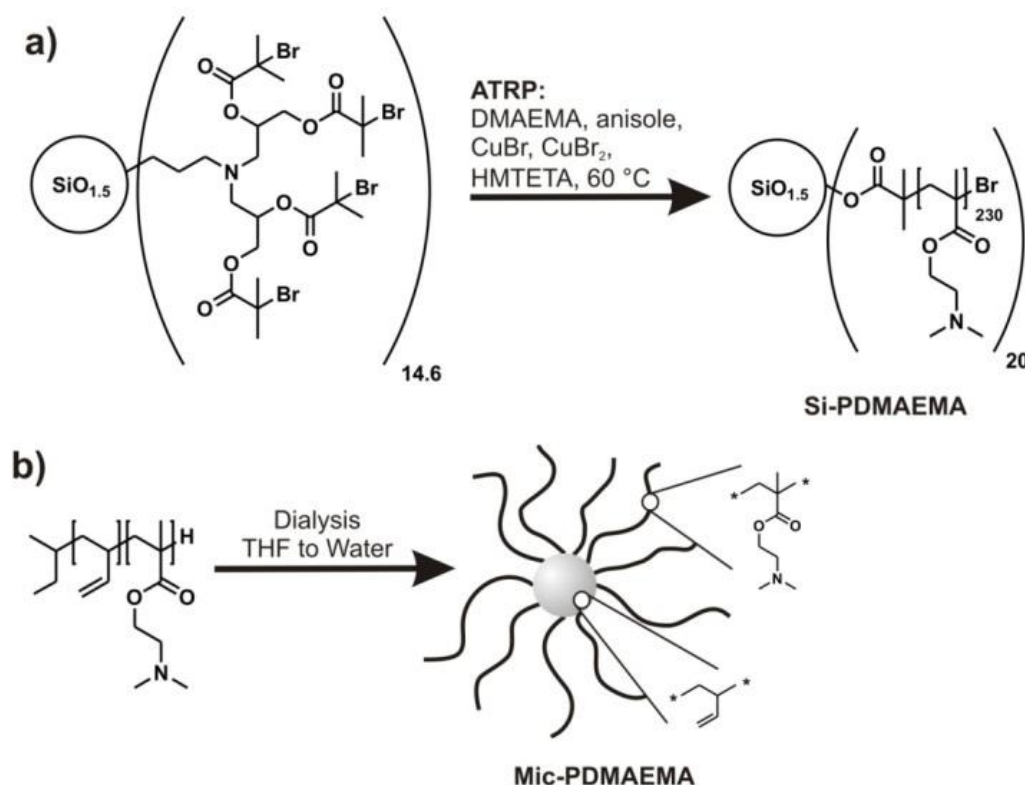
It is known that branched poly(ethylene imine) (b-PEI) shows a high buffering capacity, because of the large number of nitrogen atoms in its chemical structure. The so-called “proton sponge effect” is a result of this buffering capacity and it is said to result in an effective escape of PEI-based-polyplexes from the endosome, explaining the high transfection efficiency of this polymer.^{52, 53}

We conducted potentiometric titration experiments for the Si-PDMAEMA star-shaped polymer as well as for b-PEI. From the titration experiments apparent pK_a values of pK_a ,

$pK_{a, app.}(b\text{-PEI}) = 7.05$ and $pK_{a, app.}(\text{Si-PDMAEMA}) = 6.73$ were determined. The titration was performed at a mass concentration of 0.5 mg/mL in MilliQ water (corresponding to molar nitrogen concentration of 11.6 mM and 3.13 mM for b-PEI and Si-PDMAEMA, respectively) with 0.1M HCl solution. b-PEI had a larger buffering region ranging from pH 9.6 – 4.2 than Si-PDMAEMA, which showed a buffering effect from pH 8.9 – 4.6. The overall amount of buffered HCl was greater for b-PEI (2.61 mL) than for Si-PDMAEMA (1.25 mL), which is explained by the higher molar nitrogen concentration of b-PEI. In the buffering region relevant for the endosomal environment (pH 7.4 – 5) b-PEI shows a slightly better buffering capacity by mass concentration than Si-PDMAEMA, with 1.27 mL of buffered 0.1M HCl for b-PEI and 0.94 mL for Si-PDMAEMA.

Elemental analysis of the polycations indicated *inter alia* the presence of 15.55 ppm Cu, *i.e.* not all of the copper catalyst had been removed from the final product during dialysis, probably due to strong binding by the PDMAEMA arms. However, given the low cytotoxicity of Si-PDMAEMA, see below, significant release of copper ions during application is unlikely.

To demonstrate the general potential of multi-arm star-shaped polycationic nanoparticles as polynucleotide delivery vehicles, a second structure of similar design was produced *via* self-assembly (formation of star-like micelles) of an amphiphilic diblock copolymer. For this purpose, polybutadiene-*block*-poly(2-(dimethylamino)ethyl methacrylate) (PB₂₉₀-*b*-PDMAEMA₂₄₀) was synthesized *via* sequential living anionic polymerization as previously published.⁴⁴ The diblock copolymer had a number-average molecular weight, M_n , of 53,500 Da and a very narrow PDI of 1.07. A micellar, star-shaped gene delivery agent, Mic-PDMAEMA, was obtained *via* the self-assembly of PB₂₉₀-*b*-PDMAEMA₂₄₀ into micelles upon a change in solvent from THF, which solubilizes the entire diblock copolymer, to PBS, which only solubilizes the PDMAEMA block (**Scheme 4-1b**). An $\langle R_h \rangle_{z, app.}$ of 27 ± 3 nm was determined for the Mic-PDMAEMA by DLS. The hydrodynamic radii of the two delivery agents are thus in the same range.



Scheme 4-1. Synthetic procedure for Si-PDMAEMA preparation from multi-functional initiator *via* ATRP (a) and self-assembly of amphiphilic diblock copolymer PB₂₉₀-*b*-PDMAEMA₂₄₀ to Mic-PDMAEMA star-shaped micelles (b).

The first step in polynucleotides delivery is the formation of polyplexes between the polycationic delivery agent and the negatively charged polynucleotide. Surface charge of polyplexes is an important factor especially for unspecific uptake into cells by adsorptive endocytosis mediated by proteoglycans.⁵⁴ We determined the zeta potential of the Si-PDMAEMA and Mic-PDMAEMA polyplexes at various polymer N / DNA P-ratios (**Table 4-S1**). The zeta potential of the polyplexes increased with increasing N/P ratio and at N/P ratios equal to or larger than 5 positive values up to +10.5 mV were obtained.

pDNA Delivery by Si-PDMAEMA

The Si-PDMAEMA was tested by standardized transfection procedures, using EGFP as reporter gene, in a panel of model cell lines including adherent (CHO-K1, HEK-293, Wi-38, A549) and suspension (Jurkat) cells. In addition, C2C12 cells were used as model for non-dividing and differentiated cells and human T lymphocytes were used as example for primary cells. b-PEI (25 kDa), *i.e.* the standard non-viral transfection agent used in our

group, served as control. While depending on N/P-ratio and cell type, transfection efficiencies were consistently higher for Si-PDMAEMA than for b-PEI at slightly reduced cytotoxicities (**Table 4-1**). This included the Jurkat cells, where the best transfection efficiency was $46.1 \% \pm 3.7$ for Si-PDMAEMA compared to $6.2 \% \pm 2.6$ for b-PEI ($n \geq 5$). In order to exclude a false positive measurement, we also performed transfection with a blank pDNA (“control plasmid”). The data presented in **Table 4-1** and **Figure 4-S2** clearly demonstrate that the measured increase in fluorescence in the Si-PDMAEMA transfected cells is due to EGFP expression and not to an increased autofluorescence of the cells due to polymer accumulation. Jurkat cells are suspension cells, which are difficult to transfect with non-viral vectors because they sparsely internalize cationic complexes.¹¹ The low values obtained for b-PEI are in accordance with the data from the literature^{55, 56} and were thus expected, while the much better value obtained for Si-PDMAEMA were a first indication for a fundamentally different performance of this transfection agent.

Table 4-1. Transfection efficiency and cell viability after transfection with polyplexes based on b-PEI and Si-PDMAEMA.

Cell line		Transfection efficiency (%)		Viability (%)	
		PEI	Si-PDMAEMA	PEI	Si-PDMAEMA
CHO-K1	N/P 5	36.6 ± 12.0	59.8 ± 18.9	95.3 ± 3.7	93.7 ± 4.4
	N/P 10	49.1 ± 17.6	73.5 ± 8.0	94.4 ± 3.9	92.9 ± 3.0
	N/P 20	40.9 ± 20.6	70.5 ± 6.3	87.3 ± 8.7	91.6 ± 3.2
Control plasmid ^a	N/P 5	n. d.	0.2 ± 0.2	n. d.	98.5 ± 0.7
	N/P 10	n. d.	1.6 ± 1.1	n. d.	97.4 ± 2.8
	N/P 20	n. d.	0.8 ± 0.1	n. d.	95.0 ± 1.9
HEK-293	N/P 5	23.5 ± 9.7	33.9 ± 15.0	83.9 ± 10.1	88.0 ± 6.8
	N/P 10	36.1 ± 8.2	50.3 ± 15.1	82.7 ± 14.3	90.8 ± 5.9
	N/P 20	32.8 ± 7.7	55.2 ± 15.2	79.1 ± 17.7	83.4 ± 9.6
Wi-38	N/P 5	20.3 ± 3.1	9.8 ± 3.5	71.0 ± 6.5	76.8 ± 7.3
	N/P 10	19.2 ± 3.9	26.9 ± 5.5	66.6 ± 5.7	73.3 ± 6.4
	N/P 20	2.1 ± 1.7	20.9 ± 6.4	39.4 ± 16.6	53.8 ± 7.9
A549	N/P 5	21.7 ± 21.2	45.8 ± 28.0	93.2 ± 4.7	91.4 ± 4.0
	N/P 10	36.1 ± 14.2	48.6 ± 22.0	74.8 ± 7.9	86.0 ± 9.4
	N/P 20	20.0 ± 7.7	43.0 ± 9.8	48.7 ± 16.1	70.1 ± 21.3
Jurkat ^{b, c}	N/P 3	0.6 ± 0.4	24.1 ± 0.0	81.4 ± 2.9	76.6 ± 4.8
	N/P 5	2.0 ± 1.4	33.3 ± 2.7	84.3 ± 4.2	54.4 ± 0.6
	N/P 10	4.4 ± 3.1	46.1 ± 3.7	69.0 ± 19.3	44.2 ± 15.3
	N/P 20	6.2 ± 2.6	28.6 ± 16.3	39.9 ± 22.0	53.6 ± 17.7
Control plasmid ^a	N/P 5	n. d.	0.4 ± 0.1	n. d.	71.8 ± 3.5
	N/P 10	n. d.	0.3 ± 0.0	n. d.	60.6 ± 7.7
	N/P 20	n. d.	0.4 ± 0.2	n. d.	53.1 ± 2.4

The cells were transfected with pEGFP-N1 (EGFP expression plasmid) and in the case of CHO-K1 and Jurkat cells additional transfections were performed with a control plasmid (pIVEX2.3-UK, non-EGFP expression plasmid) to exclude that accumulation of polymer merely induces an increase of the cell autofluorescence. DNA concentration: 15 µg/mL. The EGFP expression was measured 24 h after transfection by flow cytometry and analyzed as described in the materials and methods section. The transfection efficiency data represent the percentage of living cells expressing EGFP in the non-apoptotic cell population defined by scatter properties as determined by flow cytometry analysis. For determination of the viability, dead cells were identified *via* counterstaining with propidium iodide. ^{a, b}: Representative flow cytometry dot plots are provided in the supplementary information (**Figure 4-S1** and **Figure 4-S2**). Data represent mean ± s.e.m., n ≥ 5, safe for ^c: n ≥ 3. n. d.: not determined.

C2C12 myoblast cells show growth arrest at confluency and differentiate into myotubes when cultivated in DMEM containing 10 % horse serum.⁵⁷ They are therefore a convenient cell model to compare the transfection efficiency of Si-PDMAEMA in dividing and non-dividing cells. The transfection of dividing C2C12 with PEI had previously been proven inefficient.⁵⁸ In our hands, Si-PDMAEMA was up to 9-fold more efficient in transfecting C2C12 cells than b-PEI, at similar or slightly improved viabilities. As shown in **Table 4-2**, transfection efficiencies between 20 and 30 % were achieved with Si-PDMAEMA in dividing C2C12. Values in the same range were previously only obtained with lipid-based transfection reagents; although in most of these cases higher toxicities were recorded.⁵⁹⁻⁶¹

Table 4-2. Transfection efficiency and cell viability after transfection with polyplexes based on b-PEI and Si-PDMAEMA in the C2C12 cell line at N/P ratios 5, 10, and 20.

Cell line		Transfection efficiency (%)		Viability (%)	
		PEI	Si-PDMAEMA	PEI	Si-PDMAEMA
Dividing	N/P 5	1.5 ± 2.3	12.9 ± 2.1	90.1 ± 3.1	92.7 ± 0.9
	N/P 10	4.8 ± 1.4	22.3 ± 2.0	88.3 ± 5.0	90.94 ± 1.7
	N/P 20	16.6 ± 4.1	27.7 ± 5.2	79.2 ± 3.3	81.7 ± 2.1
Non-dividing^a	N/P 5	0.8 ± 0.5	7.3 ± 3.9	88.6 ± 5.9	88.3 ± 6.0
	N/P 10	2.7 ± 1.6	15.8 ± 6.2	82.0 ± 7.3	83.4 ± 8.4
	N/P 20	2.7 ± 2.3	13.4 ± 6.9	63.7 ± 14.6	61.3 ± 17.5
Differentiated^b	N/P 5	1.3 ± 1.3	7.6 ± 3.2	85.6 ± 10.0	90.0 ± 4.9
	N/P 10	1.9 ± 1.2	18.8 ± 4.7	79.0 ± 10.0	83.8 ± 8.2
	N/P 20	1.4 ± 1.3	11.3 ± 6.8	49.7 ± 25.2	54.2 ± 16.4

The cells were transfected with pEGFP-N1. DNA concentration: 15 µg/mL. 48 h prior to transfection, C2C12 cells were cultivated in RPMI supplemented with 10 % FCS (dividing), let grow to confluency in this medium (non-dividing) or cultivated in DMEM supplemented with 10 % horse serum (differentiated). Prior to transfection, the cell cycle distribution of the “non-dividing” and “differentiated” cells was assess by flow cytometry (^a: sub-G1: 0.5 %, G1: 81.3 %, S: 15.3 %, G2/M: 0.5 %, ^b: sub-G1: 7.7 %, G1: 87.5 %, S: 5.1 %, G2/M: 0.2 %). The EGFP expression was measured 24 h after transfection by flow cytometry. Representative flow cytometry dot plots are provided in the supplementary information (**Figure 4-S3**). The transfection efficiency data represent the percentage of living cells expressing EGFP in the non-apoptotic cell population defined by scatter properties as determined by flow cytometry analysis. For determination of the viability, dead cells were identified *via* counterstaining with propidium iodide. Data represent mean ± s.e.m., n ≥ 9.

Moreover, while transfection efficiencies of b-PEI decreased considerably, when C2C12 cells were, prior to transfection, growth-arrested or differentiated into myotubes, this was

not the case for Si-PDMAEMA (Table 4-2 and Figure 4-1). Most importantly, Si-PDMAEMA was not only better than PEI in average but also for every individual transfection at a N/P ratio of 10 as shown in Figure 4-1.

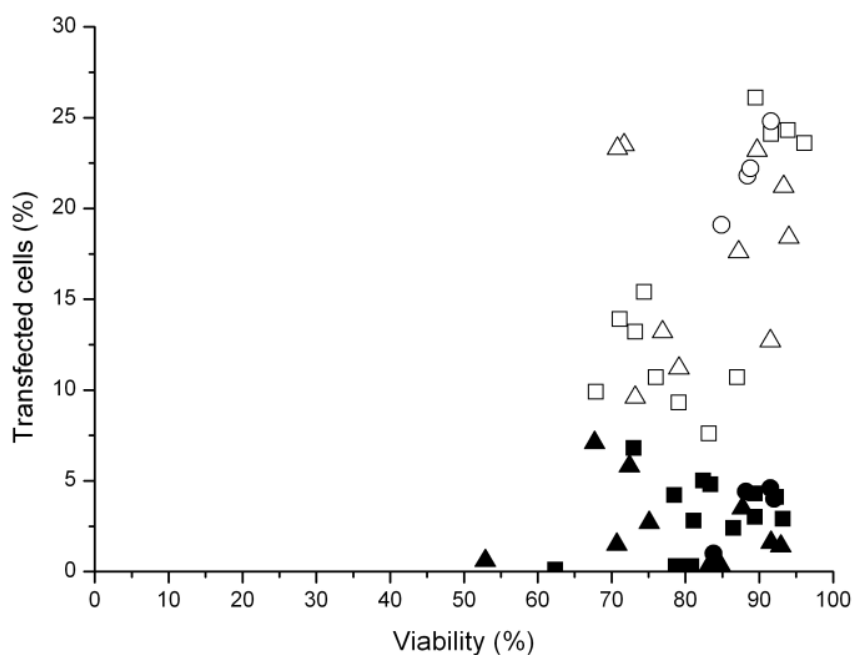


Figure 4-1. Analysis of the percentage of transfected cells against the relative viability after transfection in C2C12 cells. Prior to transfection, C2C12 cells were cultivated in growth medium (“dividing”), or growth arrested (evaluated by cell cycle analysis) by culturing the cells to confluency (“non-dividing”) or differentiated into myotubes (evaluated from the appearance of elongated, multinucleate cells) by culturing the cells in DMEM containing 10 % horse serum for 2 days (“differentiated”). For transfection polyplexes were formed with either b-PEI or Si-PDMAEMA and 15 $\mu\text{g}/\text{mL}$ pEGFP-N1 at a N/P ratio of 10. 24 h post-transfection, the cells were counterstained with propidium iodide to identify dead cells and analyzed for EGFP expression by flow cytometry. Representative flow cytometry dot plots are given in the supplementary information (Figure 4-S3). Transfection efficiencies in dividing (●, ○), non-dividing myoblasts (■, □) and myotubes (▲, △) are plotted against the viability. Black symbols: b-PEI, white symbols: Si-PDMAEMA. Data shown are from individual transfections.

To our knowledge, this is the first time that such efficient gene transfer could be shown in C2C12 myotubes. The recognized route for nuclear entry of pDNA after PEI transfection, is during mitosis when the nuclear membrane breaks down.⁶² The data presented here on the successful transfection (*i.e.*, successful translocation of the pDNA into the nucleus) of non-dividing cells by Si-PDMAEMA imply that in contradistinction this transfection agent does not necessarily require breakdown of the nuclear envelope for delivery of exogenous pDNA into the nucleus.

Finally, we included human primary T lymphocytes in our panel, because efficient tools for their transfection are rare and would be of high interest not only for research, but also for medical applications. Most conventional methods fail to efficiently transfect T lymphocytes and Nucleofection[®], currently the most efficient method for this purpose, is restricted to *in vitro* applications.^{42, 63} For our study, peripheral blood T lymphocytes were isolated from human blood and transfected with b-PEI or Si-PDMAEMA at various N/P-ratios or electroporated. Whereas, in the initial experiment, b-PEI did not yield more than 1 % and electroporation never more than 10 % transfected T lymphocytes, Si-PDMAEMA performed best at N/P 10 yielded transfection efficiencies of up to 44 %. The robustness of Si-PDMAEMA as transfection reagent for human T lymphocytes was subsequently verified at N/P 2.5 to 10 with cells isolated from several independent donors. The transfection outcomes achieved at N/P 10 were the most successful in terms of EGFP expression (**Figure 4-2**). In these experiments, as before, electroporation led to slightly better results (3 – 12 % transfected cells) than b-PEI, but never reached the values achieved with Si-PDMAEMA (**Figure 4-2A - B**). Moreover, relative fluorescence intensities of Si-PDMAEMA transfected cells were slightly higher than for b-PEI transfected or electroporated ones, arguing for higher specific transgene expression (**Figure 4-2C**), albeit not of a statistical significance ($P=0.01$; t-test). Relative viabilities were almost independent of the transfection protocol and instead varied in a consistent manner with the individual blood donor. In some cases viabilities dropped to 50 %, although the majority of the polycation transfected cells showed a relative viability of ≥ 80 % (**Figure 4-2D**).

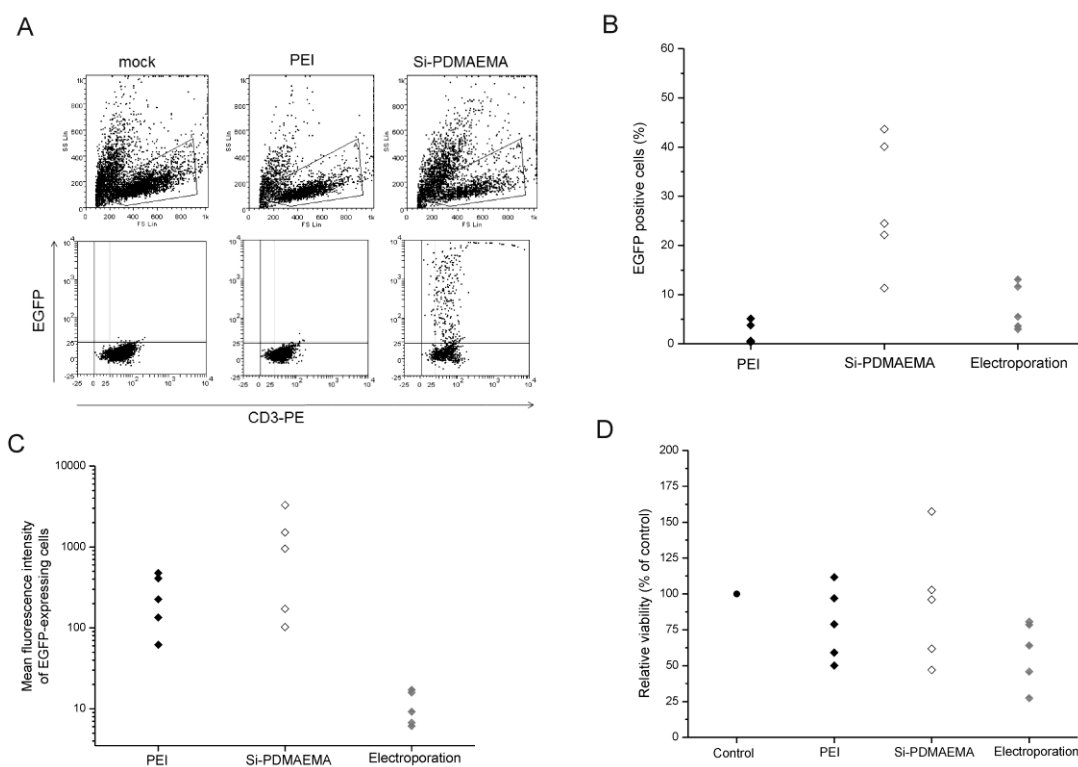


Figure 4-2. Analysis of the EGFP expression and relative viability after transfection in primary human T lymphocytes. Prior to transfection, peripheral blood mononuclear cells (PBMCs) were cultivated for 2 – 3 days in QPBL medium to stimulate proliferation of the T lymphocytes. On the day of transfection the cells were $\geq 95\%$ CD3⁺ with blast morphology. For transfection, polyplexes were formed with either b-PEI or Si-PDMAEMA and 15 $\mu\text{g}/\text{mL}$ pEGFP-N1 at a N/P ratio of 10. 24 h post-transfection, the cells were analyzed for EGFP expression by flow cytometry. Data shown are from individual transfections. Dot plots with log of the red fluorescence intensity (CD3-PE) on the x-axis and log of the green fluorescence intensity (EGFP) on the y-axis were used to estimate the percentage of EGFP-expressing cells in the non-apoptotic cell population (gate A) defined by scatter properties (FSC/SSC). The EGFP-expressing lymphocytes were identified as a subpopulation of the CD3⁺ cells. (A) Representative example for the analysis of the flow cytometry data. (B) Percentage of EGFP-expressing lymphocytes. (C) Mean fluorescence intensity (MFI) of the EGFP expressing lymphocytes. (D) Relative viability of the cells 24 h after transfection. The viability is given in percentage of living cells of transfected samples versus living cells of the non-transfected control. Data shown are from 5 individual PBMC samples, each obtained from a different donor. Results obtained after electroporation are given for comparison.

Biocompatibility of Si-PDMAEMA

The likely compatibility of Si-PDMAEMA transfection with *in vivo* applications was assessed by a set of standard methods, comprising transfection in the presence of serum, as well as cytotoxicity and hemolysis assays;² b-PEI was used for comparison. Serum proteins are known to interact with polycationic transfection agents and lower transfection efficiency considerably.⁶⁴ Due to its compact shape and its high arm density,

interaction with serum proteins is apparently reduced in the case of Si-PDMAEMA, which performed up to 5-fold better than b-PEI in the presence of 10 % serum (**Figure 4-3**).

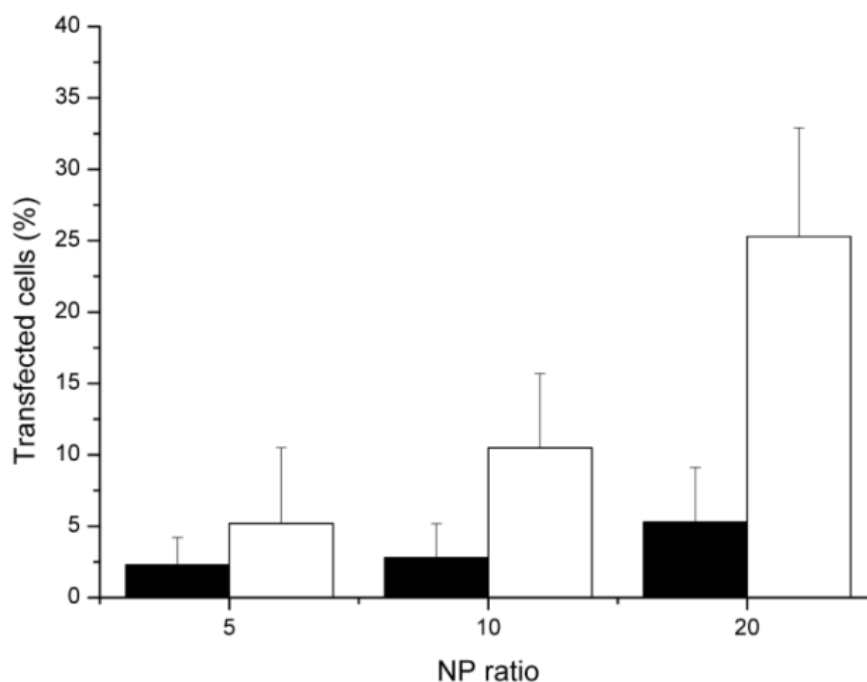


Figure 4-3. Analysis of the percentage of transfected cells after transfection, in the presence of serum, at various N/P ratio in CHO-K1 cells. CHO-K1 cells were transfected using b-PEI (black bars) or Si-PDMAEMA (white bars) in the presence of 10 % FCS at the indicated N/P ratio. For transfection, polyplexes were formed with either b-PEI or Si-PDMAEMA and 15 $\mu\text{g}/\text{mL}$ pEGFP-N1 at N/P ratios of 5, 10, and 20. 24 h post-transfection, the cells were counterstained with propidium iodide to identify dead cells and analyzed for EGFP expression by flow cytometry. The data represent the percentage of living cells expressing EGFP (“transfected cells”) in the non-apoptotic cell population defined by scatter properties as determined by flow cytometry analysis. Data represent mean \pm s.e.m. ($n \geq 3$). The measured cell viability was always $> 88 \%$.

The toxicities of the polycations were tested by MTT assay according to the ISO 10993-5 protocol using L929 mouse fibroblasts cultured in MEM supplemented with 10 % fetal bovine serum as test cells. In addition, cytotoxicity assays were also performed with human T lymphocytes.

Cytotoxicity was tested only for the non-complexed polycations (concentration range 0.001 mg/mL to 5.0 mg/mL), as these are considered to be more toxic than the DNA-containing polyplexes.¹⁴ Their investigation thus presents a worst-case setting. Both PEI and Si-PDMAEMA affected the metabolic activity in a concentration dependent manner

when they were added to the L929 cells in the indicated concentration range for up to 4 h. Above concentrations of 0.01 mg/mL (b-PEI) and 0.1 mg/mL (Si-PDMAEMA), the metabolic activities of the cells decreased significantly and concentrations above 0.1 mg / mL for b-PEI and 1.0 mg / mL for Si-PDMAEMA reduced the cell viability to nearly 20 %. In spite of its almost 30-fold higher molecular weight, Si-PDMAEMA was therefore considerably less toxic to the cells than the b-PEI. The LD₅₀ of 0.5 mg/mL calculated for Si-PDMAEMA in L929 cells corresponded to 77 times the concentration utilized in the subsequent transfection assays performed at a N/P ratio of 10. b-PEI, on the other hand, had an LD₅₀ of 0.06 mg/mL, which corresponds to 36 times the polymer concentration used in the standard transfection protocol (N/P 10). With an LD₅₀-Si-PDMAEMA of 0.27 mg/mL, compared to an LD₅₀-b-PEI of 0.03 mg/mL for b-PEI, Si-PDMAEMA also showed an order of magnitude better biocompatibility in contact with human T lymphocytes.

Compared to b-PEI, Si-PDMAEMA also performed better in the hemolysis assay (**Table 4-3**). It is thus possible that the comparatively low cytotoxicity of Si-PDMAEMA is due to its architecture, which reduces surface contact with the cell membrane and thus decreases membrane destabilization potential. The erythrocytes were incubated with eight different polymer concentrations in the range of 0.001 to 5.0 mg/mL for 1 h. Compared to b-PEI, which was found to completely lyse the erythrocytes at 5.0 mg/mL, Si-PDMAEMA showed only moderate hemolytic effects (< 35 %) at physiological pH over the entire tested concentration range. Its low hemolytic activity and thus presumably low disruptive potential for cell membranes in general augurs well for an eventual use of Si-PDMAEMA-based agents for the *in vivo* delivery of plasmid DNA. However, for *in vivo* applications, further modifications of the Si-PDMAEMA are required in order to mask the positive charges of the gene vector, which are responsible for unspecific interactions with blood components, vessel walls and rapid clearance of the polyplexes from the bloodstream.⁶⁵⁻⁶⁷ Toward this end, modifications such as “PEGylation”⁶⁸⁻⁷⁰ or as recently reported introduction of polysulfobetaine into the cationic agent⁷¹ could be done.

Table 4-3. Relative release of hemoglobin in percent (mean \pm s.e.m.) by human red blood cells after 60 min incubation with different concentrations of the cationic polymers at 37°C (n = 6).

Polymer	0.001 mg/mL	0.005 mg/mL	0.01 mg/mL	0.05 mg/mL	0.1 mg/mL	0.5 mg/mL	1.0 mg/mL	5.0 mg/mL
b-PEI	0.1 \pm 0.8	5.0 \pm 1.9	5.4 \pm 3.1	16.2 \pm 5.0	26.2 \pm 9.4	63.3 \pm 12.9	75.2 \pm 12.0	101.5 \pm 8.4
Si-PDMAEMA	1.4 \pm 2.1	0.9 \pm 1.9	0.9 \pm 0.2	7.1 \pm 1.9	13.2 \pm 5.8	22.0 \pm 1.5	23.4 \pm 5.0	34.1 \pm 7.2

siRNA-Mediated Knockdown of Gene Expression in Recombinant CHO Cells and T Lymphocytes

RNA interference (RNAi) represents a promising technology for gene-specific knockdown, e.g. in the context of developing new therapeutic approaches.⁷² However, a critical factor still limiting the use of siRNA as therapeutic is delivering siRNA to its intracellular target site as recently reviewed.^{32, 73} Recombinant CHO cells constitutively expressing EGFP⁴⁸ and human primary T lymphocytes were used to evaluate the potential of Si-PDMAEMA to deliver siRNA into the cells and mediate gene silencing. Prior to all silencing experiments, preliminary tests were performed in order to estimate the most suitable siRNA concentration and N/P ratio for gene silencing. Therefore, referring to published contributions,^{36, 74} 25 and 50 nM siRNA were tested in parallel to various charge ratios (N/P 3 to 20). Optimized conditions were found to be 25 or 50 nM siRNA and a N/P ratio of 10 gave the best results. A significant silencing effect was not detected for incubation time shorter than 30 h, probably due to the high stability of the targeted proteins (EGFP $t_{1/2} \geq 24$ h⁷⁵; CD4 $t_{1/2} = 20$ h⁷⁶) (data not shown). The results presented below were obtained under optimized conditions and reflect the maximal knockdown achieved so far. In the recombinant CHO cells, knockdown after incubation with the complexes containing 50 nM EGFP-siRNA was evaluated by flow cytometry analysis of the EGFP fluorescence in comparison to cells where delivery of siRNA had been attempted using b-PEI (**Table 4-4**). b-PEI/siRNA polyplexes achieved at most a 16 % reduction of the EGFP expression. This low knockdown efficiency of PEI is in agreement with data published elsewhere.^{77, 78} Si-PDMAEMA triggered a significantly higher knockdown (54.6 %). For both polycations, only a minimal effect on cell viability, which remained within 85 % of the non-transfected cells, was observed. Similar levels were observed in isolated cases for PDMAEMA/siRNA polyplexes in lung cancer cells.

^{79, 80}

Table 4-4. Gene silencing in recombinant CHO cells constitutively expressing EGFP.

	N/P ratio			
	0	5	10	15
naked siRNA	5.3	-	-	-
b-PEI	-	0.0	16.0	n.d.
Si-PDMAEMA	-	1.7	54.6	51.0

EGFP expression was determined by flow cytometry 30h after siRNA delivery using either b-PEI or Si-PDMAEMA. siRNA concentration: 50 nM at N/P 10. Data represent percentage of knockdown of EGFP expression compared to control cells. Viabilities were estimated by propidium iodide staining prior to flow cytometry analysis. n.d.: not determined

T lymphocytes are known to be particularly resistant to siRNA uptake enforced by conventional non-viral delivery methods excepting Nucleofection[®] 42 and antibody fragment-peptide fusion protein-based delivery.⁸¹ Based on the promising results obtained in the recombinant CHO cell line, we subsequently investigated the potential of Si-PDMAEMA for knockdown of CD4-expression in human T lymphocytes. In preliminary experiments, screening for optimized delivery conditions, we were able to show that Si-PDMAEMA-based delivery of hCD4-siRNA led to significantly higher silencing effect than the one obtained after b-PEI-based delivery (data not shown). In order to confirm this observation, siRNA delivery/knockdown was repeated with T lymphocytes isolated from another donor. In addition, linear PEI (l-PEI, 25 kDa) was used instead of b-PEI. Cells mock-delivered with EGFP-siRNA served as control. Knockdown after 30 h incubation with the complexes was evaluated by flow cytometry analysis. Delivery of the siRNA with l-PEI had no effect on the level of CD4 expression. Si-PDMAEMA, on the other hand, achieved a 2.3-fold decrease of CD4^{high} and a 2.3-fold increase of the CD4^{low} populations, respectively (**Table 4-5**). Viability was again within 85 % of the non-transfected cells in all cases. This is, to our knowledge, the first time that a PDMAEMA-based polycation were used successfully to deliver siRNA into human primary T lymphocytes and leading to the specific knock-down of the targeted gene.

Table 4-5. Analysis of CD4 expression 30 h after human T lymphocytes were either mock delivered (EGFP-siRNA) or delivered with hCD4-siRNA (25 nM each).

	hCD4-siRNA		EGFP-siRNA	
	CD4 ^{high}	CD4 ^{low}	CD4 ^{high}	CD4 ^{low}
I-PEI	77.5	22.5	79.9	20.1
Si-PDMAEMA	29.6	70.3	69	31

The siRNA was delivered complexed with I-PEI or Si-PDMAEMA (N/P ratio 10). Data represent the percentage of CD4^{high} and CD4^{low} cells within the viable CD4⁺ population. The viability was estimated by propidium iodide staining prior to flow cytometry analysis. For comparison: cells submitted to the same medium changes as the transfected ones, but not receiving any siRNA displayed 66.7 % CD4^{high} and 33.5 % CD4^{low}. Representative flow cytometry dot plots and histograms are provided in the supplementary information (**Figure 4-S4**).

Verification of the General Design Principle for Improved Non-Viral Transfection Agents

In order to verify our initial hypothesis that many arms emanating from a common center is a general design principle for the construction of efficient non-viral polynucleotide delivery vehicles, star-like polymer micelles (Mic-PDMAEMA) were produced and their efficiency as potential transfection reagent was explored under standard conditions in Jurkat cells. The micelle core-based structure was as efficient as Si-PDMAEMA as shown by the achieved transfection efficiency ranging from 11 to 35 % transfected cells depending on the N/P ratio, although transfection at N/P ratio of 20 led to high cytotoxicity (**Table 4-6**).

Table 4-6. Summary of the Jurkat cells transfection with star-like PDMAEMA-based micelles (Mic-PDMAEMA) in serum-free medium.

N/P ratio	Transfection efficiency (%)	Viability (%)
N/P 3	11.5 ± 1.4	88.1 ± 3.2
N/P 5	31.0 ± 3.0	76.2 ± 13.3
N/P 10	21.2 ± 0.0	79.4 ± 0.4
N/P 20	35.0 ± 17.4	32.4 ± 20.9

The cells were transfected with pEGFP-N1 (EGFP expression plasmid). DNA concentration: 15 µg/mL. Polymer concentrations were adjusted to the indicated N/P ratios. The EGFP expression was measured 24 h after transfection by flow cytometry. The transfection efficiency data represent the percentage of living cells expressing EGFP in the non-apoptotic cell population defined by scatter properties as determined by flow cytometry analysis. The viability was estimated by propidium iodide staining prior to flow cytometry analysis. Data represent mean ± s.e.m. (n ≥ 3); representative flow cytometry dot plots are provided in the supplementary information (**Figure 4-S5**).

Recently, we have in addition published data showing that magnetic core-shell nanoparticles displaying similar architecture, can efficiently deliver pDNA to CHO-K1 cells yielding more than 50 % transfected cells.⁸² Taken together, these results sustain our initial hypothesis that star-shaped architectures with a large number of arms irradiating from the core are efficient non-viral vectors. Additional fine tuning of the composition of the co-polymers to enhance endosomal release could further increase the transfection efficiency of the star-like micelles as recently demonstrated in one monocyte cell line by Manganiello and co-workers.⁸³

The ability of Mic-PDMAEMA to deliver siRNA was tested using the EGFP knockdown in the recombinant CHO cells stably expressing this protein as test system. Here also, preliminary screening of the optimum for siRNA concentration and N/P ratio was performed (data not shown) and the results presented below reflect data obtained under these optimized conditions. Knockdown after 30 h incubation with the polyplexes (N/P ratio of 20) containing either EGFP-siRNA or hCD4-siRNA (used as control) was evaluated by flow cytometry (**Figure 4-4**).

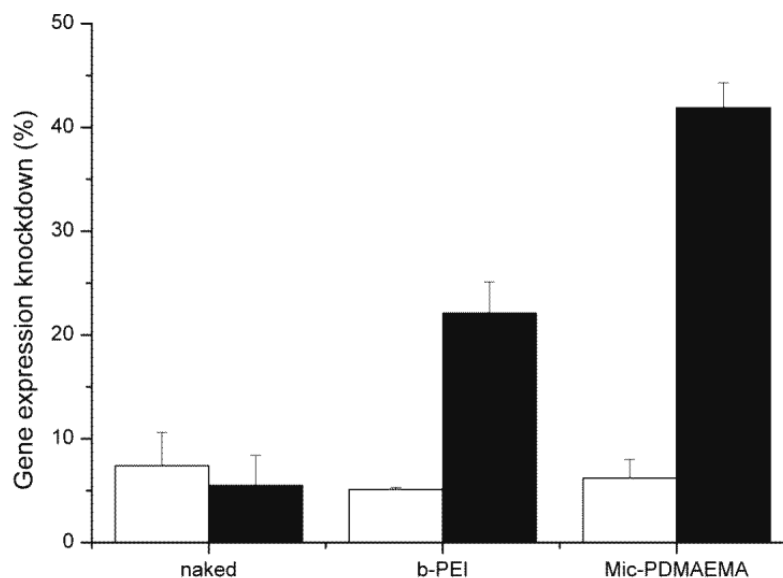


Figure 4-4. siRNA mediated silencing of the EGFP-expression in recombinant CHO cells constitutively expressing this protein determined after delivery with b-PEI or Mic-PDMAEMA; siRNA concentration: 25 nM, N/P ratio: 20. CHO-EGFP-VEGF cells were either mock delivered (hCD4siRNA, white bars) or delivered with EGFP-siRNA (black bars). 30 h post-transfection, the cells were counterstained with propidium iodide to identify dead cells and analyzed for EGFP expression by flow cytometry. Data represent percentage of knockdown of EGFP expression in viable cells compared to non-treated control cells (mean \pm s.e.m., $n \geq 3$).

Whereas b-PEI/siRNA polyplexes achieved at most a 20 % reduction in the fluorescence geometric mean, Mic-PDMAEMA delivery resulted in a 43.6 % knockdown and thus performed almost in the same range as Si-PDMAEMA (**Table 4-4**). As before, cell viability was only minimally affected (> 85 % in all cases).

Conclusions

The large polycationic nanoparticles introduced here display, to our knowledge, a never before observed capability to deliver nucleic acids to human primary T lymphocytes and to non-dividing cells and thus, have considerable advantages over conventional polycations for gene delivery. In particular, the proposed new transfection reagent synthesized from an inorganic core (Si-PDMAEMA) displays high potentiality for transfection of primary, non-dividing and differentiated cells as well as a broad compatibility with established cell lines. An additional construct, produced along the same design principle and containing a polybutadiene core (Mic-PDMAEMA), also showed more efficient pDNA-deliveries than PEI to CHO and Jurkat cells. Furthermore, we established a first proof of principle that Si-PDMAEMA and Mic-PDMAEMA can be used for gene silencing using small interfering RNA (siRNA) in CHO cells and human primary T lymphocytes. In this context, polymers based on diblock copolymers are of particular interest because their production is easy and further modification, e.g., including a targeting sequence, would be possible. As far as we know, star-like architectures reported before were generally less efficient than conventional transfection reagents for gene delivery in particular when “hard-to-transfect” cells were concerned. This work establishes that the design principle of many arms emanating from a common center results in efficient polynucleotide delivery vehicles independent of the core material and therefore offers advanced possibilities for the development improved gene vectors in particular for primary cells. Moreover, due to its low disruptive potential for cell membranes (hemolytic activity) at physiological pH and its ability to transfect cells in the presence of serum, Si-PDMAEMA might become an attractive system for further *in vivo* evaluations.

Acknowledgments

The authors would like to thank Prof. Förster (Physical Chemistry I and Bayreuth Center for Colloids and Interfaces, University of Bayreuth) for access to the Zetasizer. C. V. Synatschke acknowledges funding through a BayEFG scholarship and support from the Elite Network of Bavaria. PB₂₉₀-*b*-PDMAEMA₂₄₀ block polymers were kindly supplied by F. Schacher (Macromolecular Chemistry II, University of Bayreuth, Germany). Alexandra Rinkenauer is acknowledged for performing some of the siRNA delivery experiments.

References

1. Grigsby, C. L.; Leong, K. W. *Journal of the Royal Society Interface* **2010**, 7 Suppl 1, 67-82.
2. Mintzer, M. A.; Simanek, E. E. *Chemical Reviews* **2009**, 109, (2), 259-302.
3. Verma, I. M. *Molecular Medicine* **1994**, 1, (1), 2-3.
4. van Gaal, E. V.; van Eijk, R.; Oosting, R. S.; Kok, R. J.; Hennink, W. E.; Crommelin, D. J.; Mastrobattista, E. *Journal of Controlled Release* **2011**, 154, (3), 218-232.
5. Shegokar, R.; Al Shaal, L.; Mishra, P. R. *Pharmazie* **2011**, 66, (5), 313-318.
6. Sliva, K.; Schnierle, B. S. *Virology Journal* **2010**, 7, 248.
7. Donkuru, M.; Badea, I.; Wettig, S.; Verrall, R.; Elsabahy, M.; Foldvari, M. *Nanomedicine* **2010**, 5, (7), 1103-1127.
8. Elsabahy, M.; Nazarali, A.; Foldvari, M. *Current Drug Delivery* **2011**, 8, (3), 235-244.
9. Laufer, S. D.; Restle, T. *Current Pharmaceutical Design* **2008**, 14, (34), 3637-3655.
10. Midoux, P.; Pichon, C.; Yaouanc, J. J.; Jaffres, P. A. *British Journal of Pharmacology* **2009**, 157, (2), 166-178.
11. Labat-Moleur, F.; Steffan, A. M.; Brisson, C.; Perron, H.; Feugeas, O.; Furstenberger, P.; Oberling, F.; Brambilla, E.; Behr, J. P. *Gene Therapy* **1996**, 3, (11), 1010-1017.
12. Pathak, A.; Patnaik, S.; Gupta, K. C. *Biotechnology Journal* **2009**, 4, (11), 1559-1572.
13. Gao, X.; Kim, K. S.; Liu, D. *AAPS Journal* **2007**, 9, (1), E92-104.
14. Fischer, D.; Li, Y.; Ahlemeyer, B.; Krieglstein, J.; Kissel, T. *Biomaterials* **2003**, 24, (7), 1121-1131.
15. Hunter, A. C. *Adv. Drug Delivery Reviews* **2006**, 58, (14), 1523-1531.
16. Al-Dosari, M. S.; Gao, X. *AAPS Journal* **2009**, 11, (4), 671-681.
17. Nakayama, Y. *Accounts of Chemical Research* **2012**, 45, (7), 994-1004.
18. Schallon, A.; Jérôme, V.; Walther, A.; Synatschke, C. V.; Müller, A. H. E.; Freitag, R. *Reactive and Functional Polymers* **2010**, 70, 1-10.
19. Synatschke, C. V.; Schallon, A.; Jérôme, V.; Freitag, R.; Müller, A. H. E. *Biomacromolecules* **2011**, 12, 4247 - 4255.
20. Cherng, J.-Y.; van de Wetering, P.; Talsma, H.; Crommelin, D. J. A.; Hennink, W. E. *Pharmaceutical Research* **1996**, 13, (7), 1038-1042.
21. Plamper, F. A.; Schmalz, A.; Penott-Chang, E.; Drechsler, M.; Jusufi, A.; Ballauff, M.; Müller, A. H. E. *Macromolecules* **2007**, 40, (16), 5689-5697.
22. Wang, J. S.; Greszta, D.; Matyjaszewski, K. *Abstract Papers, Joint Conference – Chemical Institute of Canada and American Chemical Society* **1995**, 210, 227-PMSE.
23. Harada, A.; Kataoka, K. *Progress in Polymer Science* **2006**, 31, (11), 949-982.
24. Miyata, K.; Christie, R. J.; Kataoka, K. *Reactive and Functional Polymers* **2011**, 71, (3), 227-234.
25. Newland, B.; Tai, H.; Zheng, Y.; Velasco, D.; Di Luca, A.; Howdle, S. M.; Alexander, C.; Wang, W.; Pandit, A. *Chemical Communications* **2010**, 46, (26), 4698-4700.
26. Zhong, Z.; Song, Y.; Engbersen, J. F.; Lok, M. C.; Hennink, W. E.; Feijen, J. *Journal of Controlled Release* **2005**, 109, (1-3), 317-329.

27. Layman, J. M.; Ramirez, S. M.; Green, M. D.; Long, T. E. *Biomacromolecules* **2009**, 10, (5), 1244-1252.
28. van de Wetering, P.; Cherng, J. Y.; Talsma, H.; Crommelin, D. J. A.; Hennink, W. E. *Journal of Controlled Release* **1998**, 53, (1-3), 145-153.
29. Georgiou, T. K.; Vamvakaki, M.; Patrickios, C. S.; Yamasaki, E. N.; Phylactou, L. A. *Biomacromolecules* **2004**, 5, (6), 2221-2229.
30. Xu, F. J.; Zhang, Z. X.; Ping, Y.; Li, J.; Kang, E. T.; Neoh, K. G. *Biomacromolecules* **2009**, 10, (2), 285-293.
31. Aliabadi, H. M.; Landry, B.; Sun, C.; Tang, T.; Uludağ, H. *Biomaterials* **2012**, 33, (8), 2546-2569.
32. Scholz, C.; Wagner, E. *Journal of Controlled Release* **2012**, 161, (2), 554-565.
33. Zhang, S.; Zhao, Y.; Zhi, D.; Zhang, S. *Bioorganic Chemistry* **2012**, 40, (0), 10-18.
34. Benoit, D. S.; Henry, S. M.; Shubin, A. D.; Hoffman, A. S.; Stayton, P. S. *Molecular Pharmaceutics* **2010**, 7, (2), 442-455.
35. Convertine, A. J.; Benoit, D. S. W.; Duvall, C. L.; Hoffman, A. S.; Stayton, P. S. *Journal of Controlled Release* **2009**, 133, (3), 221-229.
36. Convertine, A. J.; Diab, C.; Prieve, M.; Paschal, A.; Hoffman, A. S.; Johnson, P. H.; Stayton, P. S. *Biomacromolecules* **2010**, 11, (11), 2904-2911.
37. Kong, W.-H.; Sung, D.-K.; Shim, Y.-H.; Bae, K. H.; Dubois, P.; Park, T. G.; Kim, J.-H.; Seo, S.-W. *Journal of Controlled Release* **2009**, 138, (2), 141-147.
38. Pafiti, K. S.; Patrickios, C. S.; Georgiou, T. K.; Yamasaki, E. N.; Mastroiannopoulos, N. P.; Phylactou, L. A. *European Polymer Journal* **2012**, 48, (8), 1422-1430.
39. Zhu, C.; Jung, S.; Luo, S.; Meng, F.; Zhu, X.; Park, T. G.; Zhong, Z. *Biomaterials* **2010**, 31, (8), 2408-2416.
40. Gary, D. J.; Lee, H.; Sharma, R.; Lee, J. S.; Kim, Y.; Cui, Z. Y.; Jia, D.; Bowman, V. D.; Chipman, P. R.; Wan, L.; Zou, Y.; Mao, G.; Park, K.; Herbert, B. S.; Konieczny, S. F.; Won, Y. Y. *ACS Nano* **2011**, 5, (5), 3493-4505.
41. Lin, D.; Huang, Y.; Jiang, Q.; Zhang, W.; Yue, X.; Guo, S.; Xiao, P.; Du, Q.; Xing, J.; Deng, L.; Liang, Z.; Dong, A. *Biomaterials* **2011**, 32, (33), 8730-8742.
42. Goffinet, C.; Keppler, O. T. *The FASEB Journal* **2006**, 20, (3), 500-502.
43. Weber, N. D.; Merkel, O. M.; Kissel, T.; Munoz-Fernandez, M. A. *Journal of Controlled Release* **2012**, 157, (1), 55-63.
44. Schacher, F.; Müllner, M.; Schmalz, H.; Müller, A. H. E. *Macromolecular Chemistry and Physics* **2009**, 210, (3-4), 256-262.
45. Mori, H.; Müller, A. H. E.; Klee, J. E. *Journal of the American Chemical Society* **2003**, 125, (13), 3712-3713.
46. Mori, H.; Walther, A.; Andre, X.; Lanzendorfer, M. G.; Müller, A. H. E. *Macromolecules* **2004**, 37, (6), 2054-2066.
47. Muthukrishnan, S.; Plamper, F.; Mori, H.; Müller, A. H. E. *Macromolecules* **2005**, 38, (26), 10631-10642.
48. Freimark, D.; Jérôme, V.; Freitag, R. *Biotechnology Journal* **2010**, 5, (1), 24-31.
49. Chou, L.-F.; Chou, W.-G. *Cell Biology International* **1999**, 23, (10), 663-670.
50. Kim, D.-H.; Behlke, M. A.; Rose, S. D.; Chang, M.-S.; Choi, S.; Rossi, J. J. *Nature Biotechnology* **2005**, 23, (2), 222-226.
51. Parnham, M. J.; Wetzig, H. *Chemistry and Physics of Lipids* **1993**, 64, (1-3), 263-274.

52. Boussif, O.; Lezoualc'h, F.; Zanta, M. A.; Mergny, M. D.; Scherman, D.; Demeneix, B.; Behr, J. P. *Proceedings of the National Academy of Science of the United States of America* **1995**, 92, (16), 7297-7301.
53. Jeon, O.; Lim, H. W.; Lee, M.; Song, S. J.; Kim, B. S. *Journal of Drug Targeting* **2007**, 15, (3), 190-198.
54. Mislick, K. A.; Baldeschwieler, J. D. *Proceedings of the National Academy of Science of the United States of America* **1996**, 93, (22), 12349-12354.
55. Guillem, V. M.; Tormo, M.; Moret, I.; Benet, I.; Garcia-Conde, J.; Crespo, A.; Alino, S. F. *Journal of Controlled Release* **2002**, 83, (1), 133-146.
56. Wang, D.-A.; Narang, A. S.; Kotb, M.; Gaber, A. O.; Miller, D. D.; Kim, S. W.; Mahato, R. I. *Biomacromolecules* **2002**, 3, (6), 1197-1207.
57. Atherton, G. T.; Travers, H.; Deed, R.; Norton, J. D. *Cell Growth and Differentiation* **1996**, 7, (8), 1059-1066.
58. Ehrhardt, C.; Schmolke, M.; Matzke, A.; Knoblauch, A.; Will, C.; Wixler, V.; Ludwig, S. *Signal Transduction* **2006**, 6, (3), 179-184.
59. Balci, B.; Dincer, P. *Biotechnology Journal* **2009**, 4, (7), 1042-1045.
60. Billiet, L.; Gomez, J.-P.; Berchel, M.; Jaffrès, P.-A.; Le Gall, T.; Montier, T.; Bertrand, E.; Cheradame, H.; Guégan, P.; Mével, M.; Pitard, B.; Benvegna, T.; Lehn, P.; Pichon, C.; Midoux, P. *Biomaterials* **2012**, 33, (10), 2980-2990.
61. Dodds, E.; Dunckley, M. G.; Naujoks, K.; Michaelis, U.; Dickson, G. *Gene Therapy* **1998**, 5, (4), 542-551.
62. Grosse, S.; Thévenot, G.; Monsigny, M.; Fajac, I. *Journal of Gene Medicine* **2006**, 8, (7), 845-851.
63. Hamm, A.; Krott, N.; Breibach, I.; Blindt, R.; Bosserhoff, A. K. *Tissue Engineering* **2002**, 8, (2), 235-245.
64. Guo, W.; Lee, R. J. *Journal of Controlled Release* **2001**, 77, (1-2), 131-138.
65. Kircheis, R.; Wightman, L.; Wagner, E. *Advanced Drug Delivery Reviews* **2001**, 53, (3), 341-358.
66. Laga, R.; Carlisle, R.; Tangney, M.; Ulbrich, K.; Seymour, L. W. *Journal of Controlled Release* **2012**, 161, (2), 537-553.
67. Merdan, T.; Kopeček, J.; Kissel, T. *Advanced Drug Delivery Reviews* **2002**, 54, (5), 715-758.
68. Ogris, M.; Brunner, S.; Schuller, S.; Kircheis, R.; Wagner, E. *Gene Therapy* **1999**, 6, (4), 595-605.
69. Üzgün, S.; Akdemir, O.; Hasenpusch, G.; Maucksch, C.; Golas, M. M.; Sander, B.; Stark, H.; Imker, R.; Lutz, J.-F.; Rudolph, C. *Biomacromolecules* **2010**, 11, (1), 39-50.
70. Verbaan, F. J.; Oussoren, C.; van Dam, I. M.; Takakura, Y.; Hashida, M.; Crommelin, D. J.; Hennink, W. E.; Storm, G. *International Journal of Pharmaceutics* **2001**, 214, (1-2), 99-101.
71. Dai, F.; Liu, W. *Biomaterials* **2011**, 32, (2), 628-638.
72. Castanotto, D.; Rossi, J. J. *Nature* **2009**, 457, (7228), 426-433.
73. Takahashi, Y.; Nishikawa, M.; Takakura, Y. *Advanced Drug Delivery Reviews* **2009**, 61, (9), 760-766.
74. Cuccato, G.; Polynikis, A.; Siciliano, V.; Graziano, M.; di Bernardo, M.; di Bernardo, D. *BMC Systems Biology* **2011**, 5, (19), 1-12.
75. Maliyekkel, A.; Davis, B. M.; Roninson, I. B. *Cell Cycle* **2006**, 5, (20), 2390-2395.

76. Novina, C. D.; Murray, M. F.; Dykxhoorn, D. M.; Beresford, P. J.; Riess, J.; Lee, S.-K.; Collman, R. G.; Lieberman, J.; Shankar, P.; Sharp, P. A. *Nature Medicine* **2002**, 8, (7), 681-686.
77. Hassani, Z.; Lemkine, G. F.; Erbacher, P.; Palmier, K.; Alfama, G.; Giovannangeli, C.; Behr, J. P.; Demeneix, B. A. *Journal of Gene Medicine* **2005**, 7, (2), 198-207.
78. Mao, S.; Germershaus, O.; Fischer, D.; Linn, T.; Schnepf, R.; Kissel, T. *Pharmaceutical Research* **2005**, 22, (12), 2058-2068.
79. Varkouhi, A. K.; Lammers, T.; Schiffelers, R. M.; van Steenberg, M. J.; Hennink, W. E.; Storm, G. *European Journal of Pharmaceutics Biopharmaceutics* **2011**, 77, (3), 450-457.
80. Varkouhi, A. K.; Mountrichas, G.; Schiffelers, R. M.; Lammers, T.; Storm, G.; Pispas, S.; Hennink, W. E. *European Journal of Pharmaceutical Sciences* **2012**, 45, (4), 459-466.
81. Kumar, P.; Ban, H. S.; Kim, S. S.; Wu, H.; Pearson, T.; Greiner, D. L.; Laouar, A.; Yao, J.; Haridas, V.; Habiro, K.; Yang, Y. G.; Jeong, J. H.; Lee, K. Y.; Kim, Y. H.; Kim, S. W.; Peipp, M.; Fey, G. H.; Manjunath, N.; Shultz, L. D.; Lee, S. K.; Shankar, P. *Cell* **2008**, 134, (4), 577-586.
82. Majewski, A. P.; Schallon, A.; Jérôme, V.; Freitag, R.; Müller, A. H. E.; Schmalz, H. *Biomacromolecules* **2012**, 13, (3), 857-866.
83. Manganiello, M. J.; Cheng, C.; Convertine, A. J.; Bryers, J. D.; Stayton, P. S. *Biomaterials* **2012**, 33, (7), 2301-2309.

Supporting Information

Table 4-S1 Evolution of the zeta potential with increasing N/P ratio for Si-PDMAEMA and Mic-PDMAEMA polyplexes prepared with a total of 15 μg pDNA in 1 mL of a 150 mM NaCl solution. Data, given in mV, represent mean \pm s.e.m., n = 3.

Sample	-	N/P 3	N/P 5	N/P 10	N/P 20
Si-PDMAEMA	n.d.	-30.7 ± 2.1	-0.4 ± 4.0	7.4 ± 1.8	10.1 ± 1.2
Mic-PDMAEMA	n.d.	0.0 ± 0.1	7.3 ± 1.0	8.8 ± 1.3	10.5 ± 0.6
Plasmid	-26.9 ± 3.2	-	-	-	-

n.d. = not determined

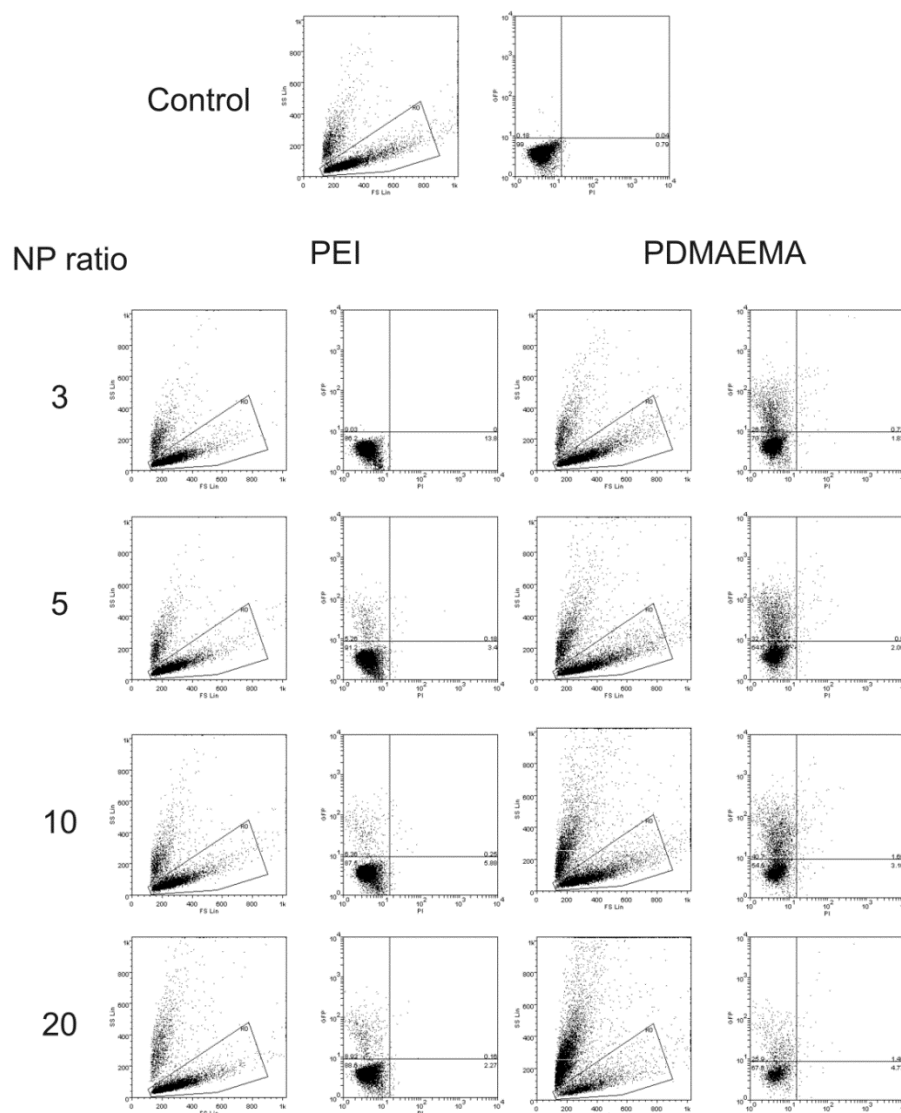


Figure 4-S1 Green fluorescent protein FACS analysis after transfection of Jurkat cells with b-PEI and Si-PDMAEMA. For transfection polyplexes were formed with either b-PEI or Si-PDMAEMA and 15 $\mu\text{g}/\text{mL}$ pEGFP-N1 at N/P 3 to 20. 24 h post-transfection, the cells were analyzed for EGFP expression. Cells were initially evaluated by scatter properties (FSC/SSC) in order to select a region representing single non-apoptotic cells. This gated region (R0) was further analyzed for fluorescence (PI/EGFP). Dot plots with log of the red fluorescence intensity (PI) on the x-axis and log of the green fluorescence intensity (EGFP) on the y-axis were used to estimate the percentage of EGFP-expressing cells in the main non-apoptotic cell population (gate R0). Negative controls (control; non-transfected cells) were used to set the position of quadrants separating GFP-positive living cells (upper left), GFP-positive dead cells (upper right), GFP-negative living cells (lower left) and GFP-negative dead cells (lower right). These quadrants were applied for the analysis of transfected cells and percentage cell number / total cell number in the gated region were calculated for each quadrant.

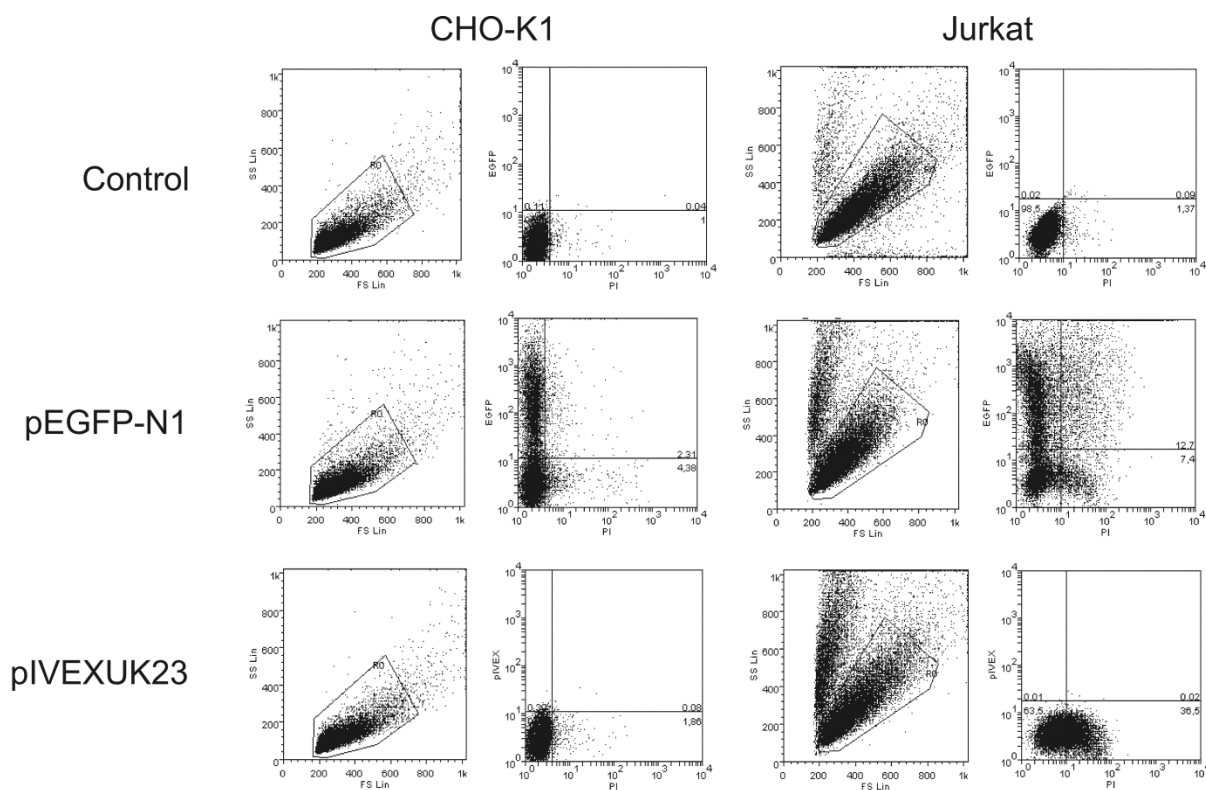


Figure 4-S2 Transfection of CHO-K1 and Jurkat cells with EGFP encoding (pEGFP-N1) and control (pIVEXUK23) plasmids. For transfection polyplexes were formed with either b-PEI or Si-PDMAEMA and 15 $\mu\text{g}/\text{mL}$ pEGFP-N1 or pIVEXUK23 at N/P 10. 24 h post-transfection, the cells were analyzed for EGFP expression. Cells were initially evaluated by scatter properties (FSC/SSC) in order to select a region representing single non-apoptotic cells. This gated region (R0) was further analyzed for fluorescence (PI/EGFP). Dot plots with log of the red fluorescence intensity (PI) on the x-axis and log of the green fluorescence intensity (EGFP) on the y-axis were used to estimate the percentage of EGFP-expressing cells in the main non-apoptotic cell population (gate R0). Negative controls (Control; non-transfected cells) were used to set the position of quadrants separating GFP-positive living cells (upper left), GFP-positive dead cells (upper right), GFP-negative living cells (lower left) and GFP-negative dead cells (lower right). These quadrants were applied for the analysis of transfected cells and percentage cell number / total cell number in the gated region were calculated for each quadrant.

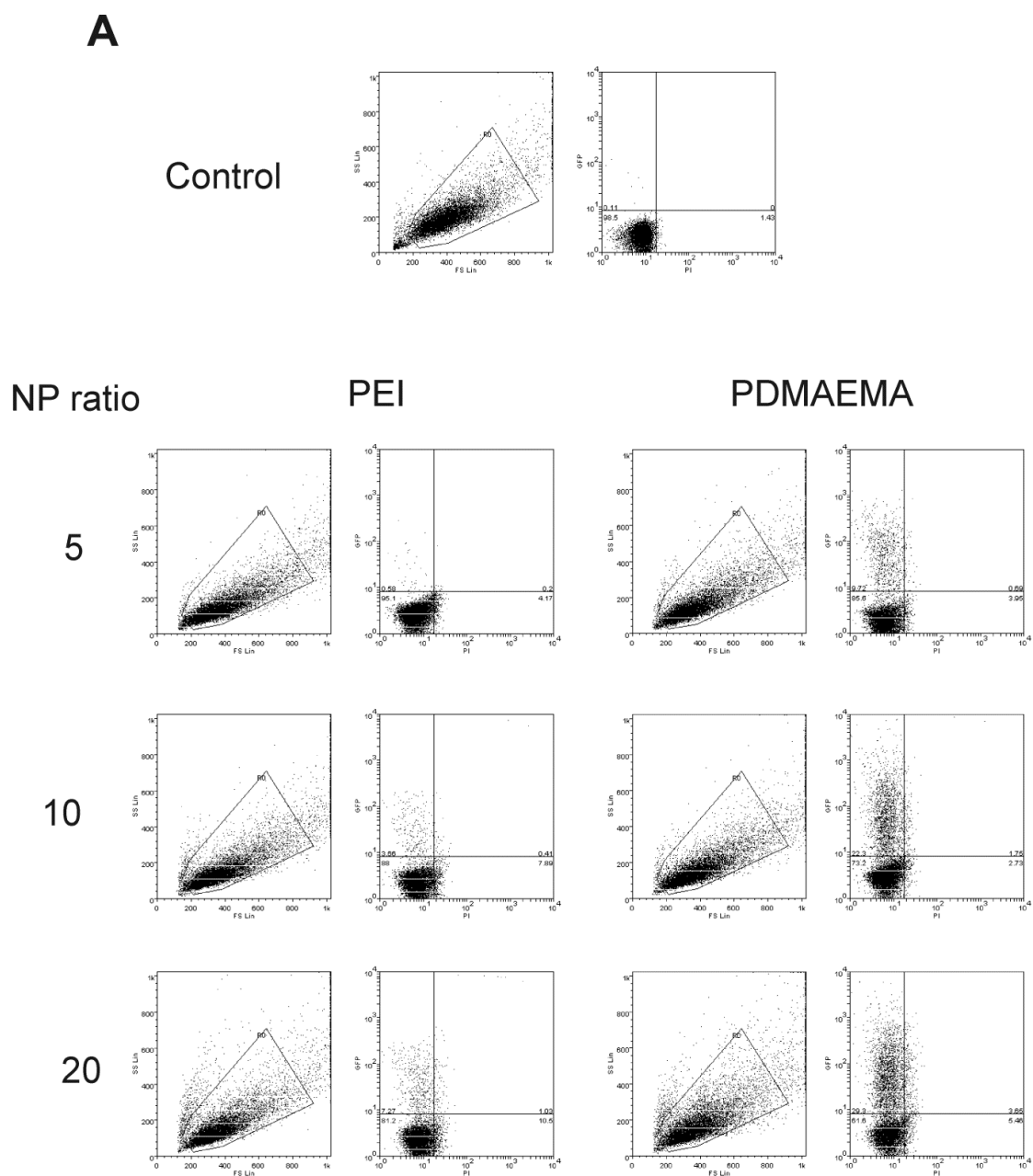


Figure 4-S3, Part 1

B

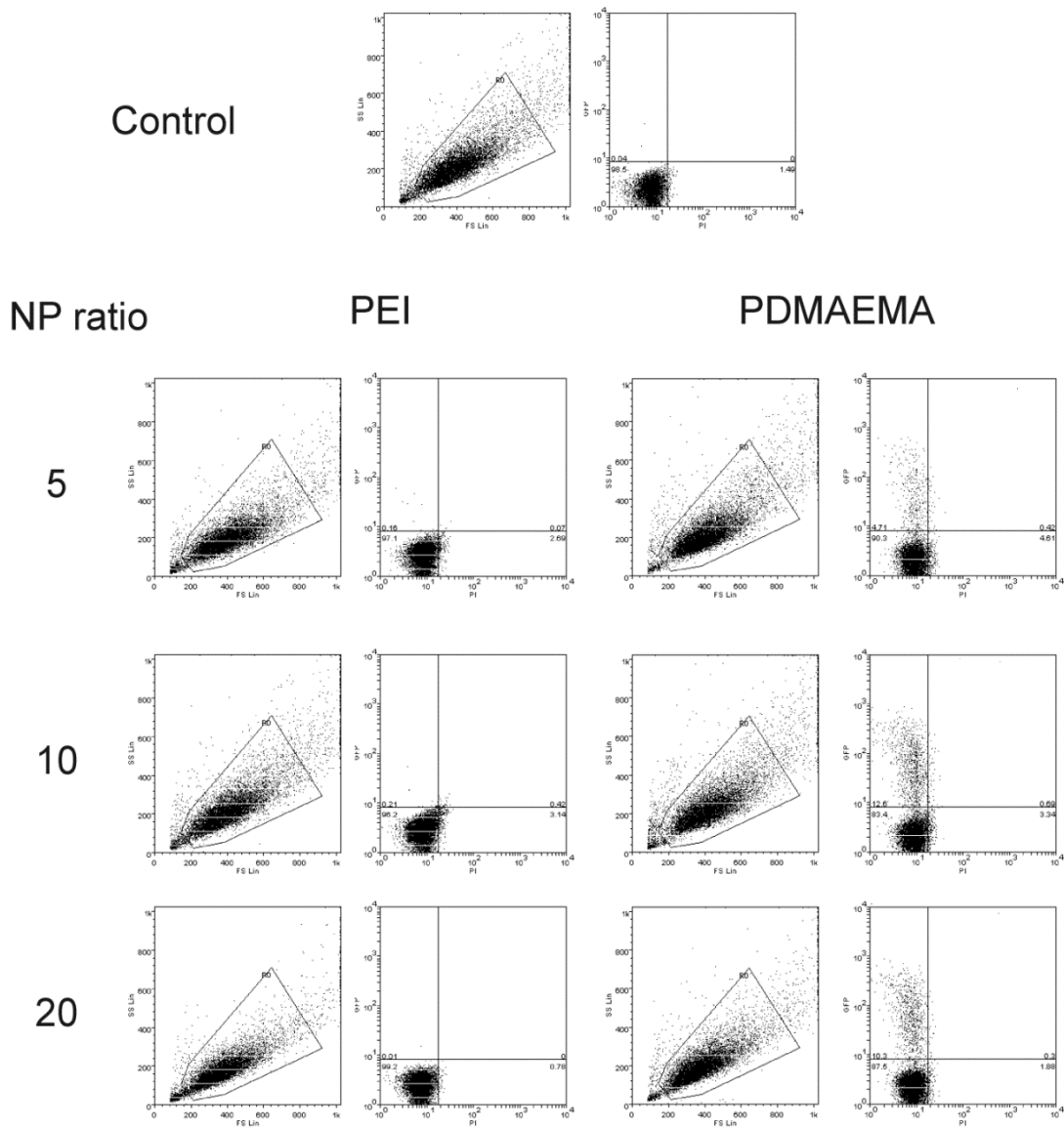


Figure 4-S3, Part 2

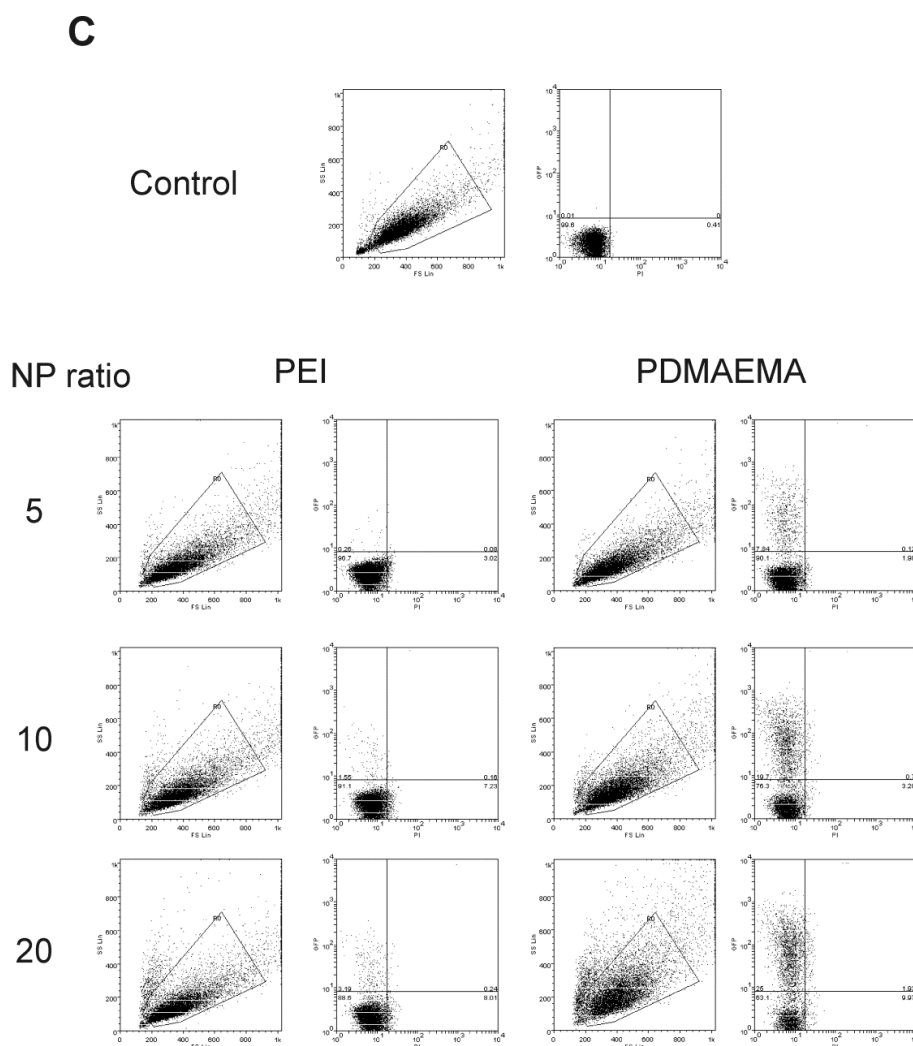


Figure 4-S3, Part 3: Green fluorescent protein FACS analysis after transfection of C2C12 myoblasts and myotubes with b-PEI and Si-PDMAEMA. Prior to transfection, C2C12 cells were cultivated in growth medium (A; “dividing”), or growth arrested (evaluated by cell cycle analysis) by culturing the cells to confluency (B; “non-dividing”) or differentiated into myotubes (evaluated from the appearance of elongated, multinucleate cells) by culturing the cells in DMEM containing 10 % horse serum for 2 – 3 days (C; “differentiated”). For transfection polyplexes were formed with either b-PEI or Si-PDMAEMA and 15 $\mu\text{g}/\text{mL}$ pEGFP-N1 at N/P 5, 10, and 20. 24 h post-transfection, the cells were analyzed for EGFP expression. Cells were initially evaluated by scatter properties (FSC/SSC) in order to select a region representing single non-apoptotic cells. This gated region (R0) was further analyzed for fluorescence (PI/EGFP). Dot plots with log of the red fluorescence intensity (PI) on the x-axis and log of the green fluorescence intensity (EGFP) on the y-axis were used to estimate the percentage of EGFP-expressing cells in the main non-apoptotic cell population (gate R0). Negative controls (control; non-transfected cells) were used to set the position of quadrants separating GFP-positive living cells (upper left), GFP-positive dead cells (upper right), GFP-negative living cells (lower left) and GFP-negative dead cells (lower right). These quadrants were applied for the analysis of transfected cells and percentage cell number / total cell number in the gated region were calculated for each quadrant.

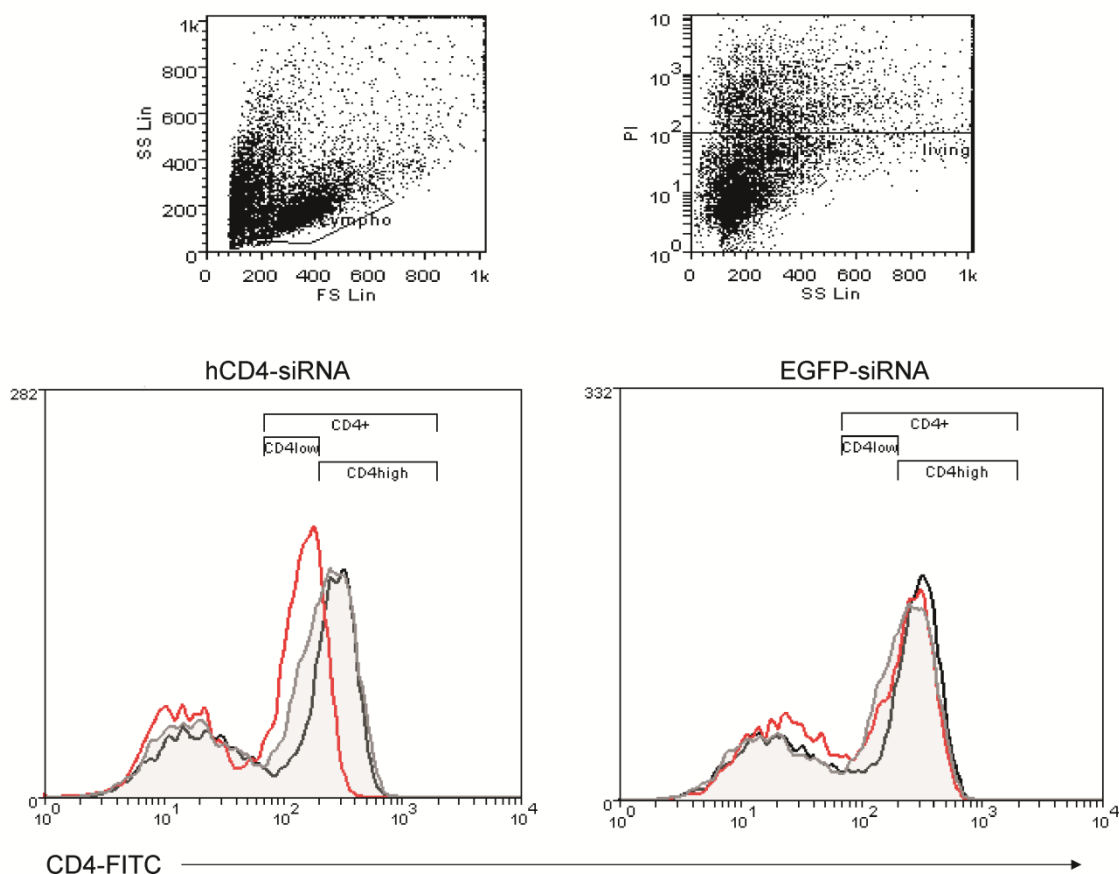


Figure 4-S4 Analysis of CD4 expression after human T lymphocytes were either mock delivered (EGFP-siRNA) or delivered with hCD4-siRNA. Prior to transfection, Peripheral blood mononuclear cells (PBMCs) were cultivated for 2 – 3 days in QPBL medium to stimulate proliferation of the T lymphocytes. On the day of transfection the cells are $\geq 95\%$ $CD3^+$ with blast morphology. For transfection, polyplexes were formed with either b-PEI or Si-PDMAEMA and 25 nM siRNA at a N/P ratio of 10. 30 h post-transfection, the cells were stained with CD4-FITC antibody, counterstained with propidium iodide for estimation of the dead cells and then analyzed for CD4 expression by flow cytometry. Cells were initially evaluated by scatter properties (FSC/SSC) in order to select a region representing single non-apoptotic cells (gate “lympho”) and for scatter and fluorescence (SSC/PI) in order to select the living cells (gate “living”). Non-treated cells (“control”), otherwise similarly treated were used to set the regions defined as “ $CD4^{high}$ ” and “ $CD4^{low}$ ”. The expression of the CD4 protein was assessed in histogram plots (green fluorescence intensity on the x-axis and cell number on the y-axis) representing the intensity of the CD4-FITC fluorescence ($CD4^{low}$: fluorescence intensity between 70 and 170; $CD4^{high}$: fluorescence intensity > 170) in the living T lymphocytes (defined as a sub-population of gate “lympho” and gate “living”). The data are presented as histograms overlays (“control cells”: line and fill color gray; “l-PEI”: black line; “Si-PDMAEMA”: red line).

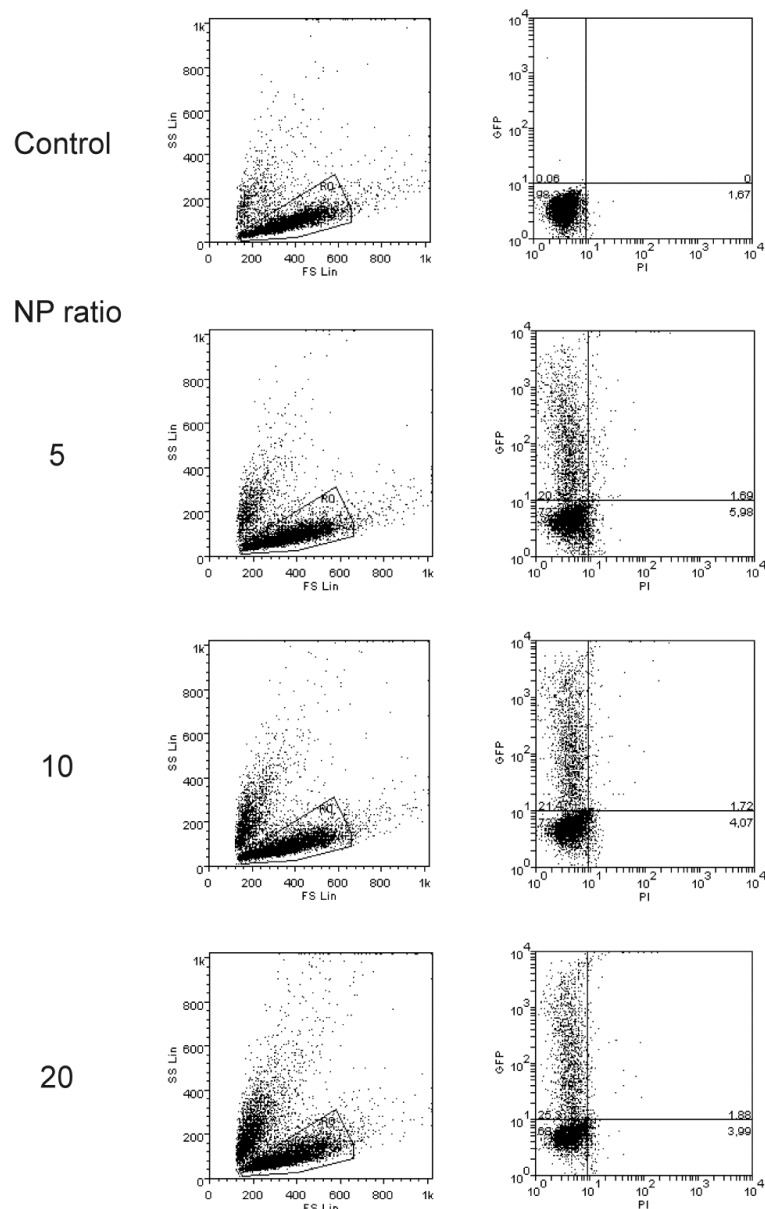
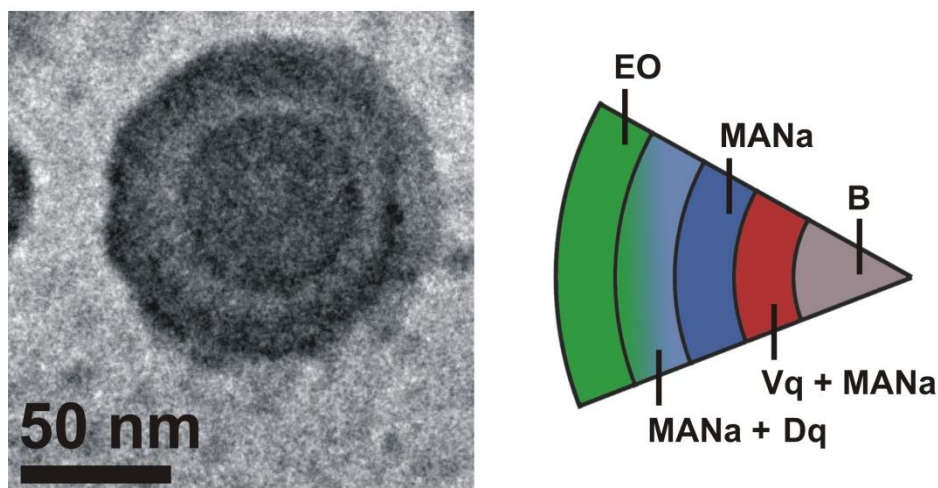


Figure 4-S5 Green fluorescent protein flow cytometry analysis after transfection of Jurkat cells with Mic-PDMAEMA. For transfection polyplexes were formed with Mic-PDMAEMA and 15 $\mu\text{g}/\text{mL}$ pEGFP-N1 at N/P 5, 10, and 20. 24 h post-transfection, the cells were analyzed for EGFP expression. Cells were initially evaluated by scatter properties (FSC/SSC) in order to select a region representing single non-apoptotic cells. This gated region (R0) was further analyzed for fluorescence (PI/EGFP). Dot plots with log of the red fluorescence intensity (PI) on the x-axis and log of the green fluorescence intensity (EGFP) on the y-axis were used to estimate the percentage of EGFP-expressing cells in the main non-apoptotic cell population (gate R0). Negative controls (control; non-transfected cells) were used to set the position of quadrants separating GFP-positive living cells (upper left), GFP-positive dead cells (upper right), GFP-negative living cells (lower left) and GFP-negative dead cells (lower right). These quadrants were applied for the analysis of transfected cells and percentage cell number / total cell number in the gated region were calculated for each quadrant.

Chapter 5

Double-Layered Micellar Interpolyelectrolyte Complexes – How Many Shells to a Core?



The results from this chapter have been published in *Soft Matter* as:

“Double-Layered Micellar Interpolyelectrolyte Complexes – How Many Shells to a Core?”

by Christopher V. Synatschke, Felix H. Schacher,* Melanie Förtsch, Markus Drechsler, and Axel H. E. Müller*

Abstract

We report on the formation of double-layered micellar interpolyelectrolyte complexes (IPECs) from ABC triblock terpolymer precursor micelles and hydrophilic homo- or block copolymers. Polybutadiene-*block*-poly(1-methyl-2-vinyl pyridinium)-*block*-poly(sodium methacrylate) (PB-*b*-P2VPq-*b*-PMANa) block terpolymers form micelles in aqueous solution at high pH exhibiting a PB core, a P2VPq/PMANa intramicellar IPEC (*im*-IPEC) shell, and a PMANa corona, which is negatively charged. Upon mixing with either positively charged, quaternized poly(*N,N*-dimethylaminoethyl methacrylate) (PDMAEMA_q) homopolymers or its double-hydrophilic block copolymer with poly(ethylene oxide) (PEO-*b*-PDMAEMA_q), a further IPEC shell is formed, rendering core-shell-shell-corona aggregates. The effects of the ratio of positive to negative charges, $Z_{+/-}$, the composition of the block terpolymer micelles, and the length of the added D_q block were investigated. We show that within a certain $Z_{+/-}$ regime stable complex micellar IPECs featuring two distinguishable IPEC shells are formed. The so-formed complex particles were analyzed by dynamic light scattering and cryogenic transmission electron microscopy.

Introduction

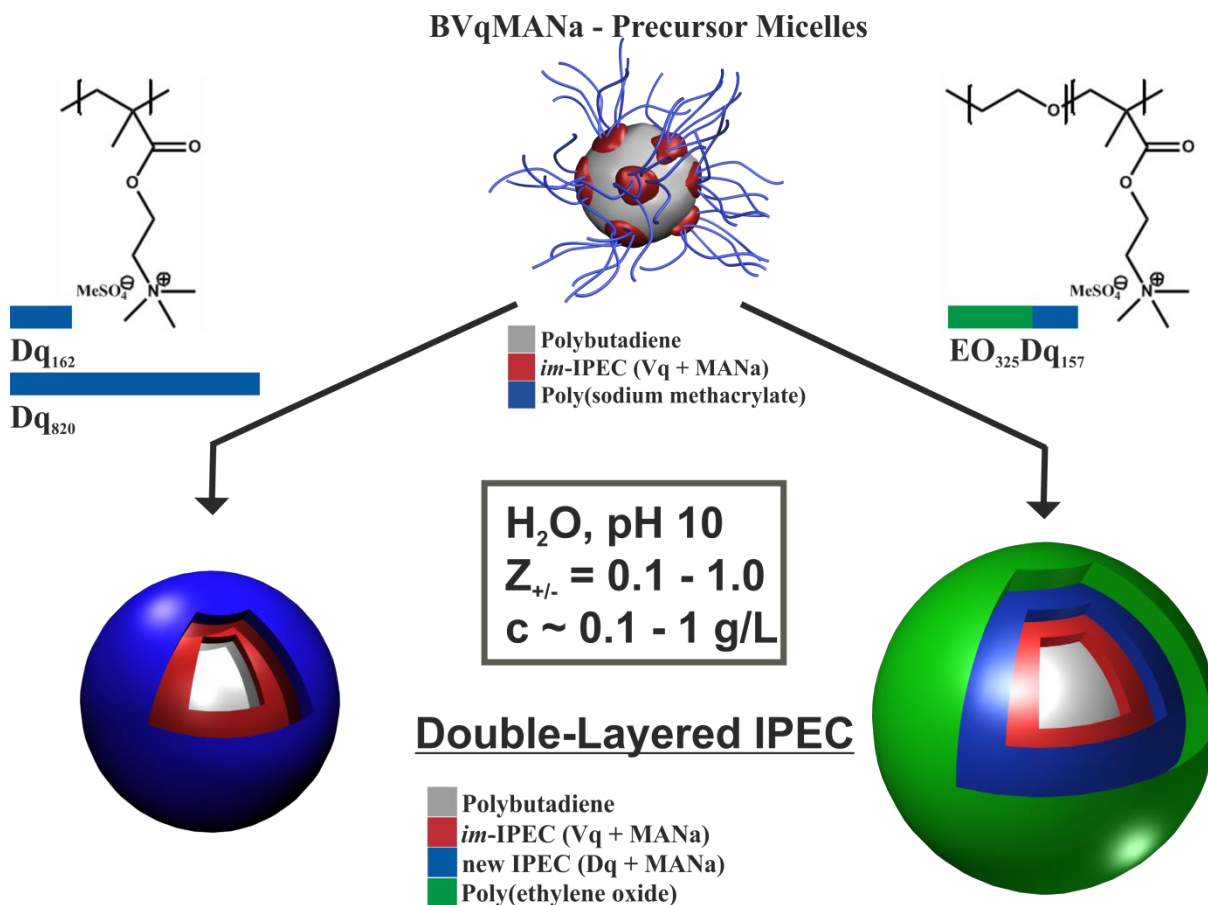
Self-assembly of block co- and terpolymers in solution has received considerable interest during the past decade.^{1, 2} Typically, such processes lead to the formation of spherical micelles,^{3, 4} cylindrical or rod-like aggregates,⁵⁻⁷ or vesicles.⁸ Particular interest is devoted to the control of size, size distribution, shape, or the number or type of functional groups present on the surface of such particles. This can be achieved by controlling the kinetics of the self-assembly process,⁹ through changing the polymer composition or architecture,¹⁰ or *via* the variation of external parameters like the employed solvent,^{11, 12} pH,¹³ salinity,¹⁴ or temperature.¹⁵

Another possibility to influence self-assembly processes in solution is to employ block copolymers with charged compartments, or polyelectrolyte segments.^{16, 17} Such polyelectrolytes can be natural (e.g., polynucleic acids) or synthetic polyanions or -cations and can be further subdivided into weak (e.g., poly(methacrylic acid), PMAA) or strong (e.g., poly(styrene sulfonate)) species.¹⁸ Recent research interest in such materials has been primarily based on intrinsic properties such as water solubility, very strong inter- and intra-chain interactions, ionic conductivity, and surface activity.¹⁹

Mixing of two different block copolymers with polyelectrolyte segments bearing opposite charges in aqueous solution leads to electrostatic co-assembly and the formation of interpolyelectrolyte complexes (IPECs).²⁰⁻²² The driving force is the entropy gain from the release of the counterions. Such IPECs are hydrophobic yet are still able to participate in dynamic polyion exchange reactions in aqueous media.^{23, 24} If weak polyelectrolytes like PMAA are used, the complex formation is pH-dependent.²⁵ In addition, the IPEC formation is reversible: the addition of large amounts of salt leads to a screening of the charges and to a breakup of the complexes.^{20, 26} If preformed micelles with a charged corona are mixed with oppositely charged polyelectrolytes, an elegant route towards complex micellar architectures is opened. This has been demonstrated for micelles exhibiting a soft polyisobutylene core and a PMAA corona^{25, 26} or for more complex core-compartmentalized block terpolymer micelles.²⁷

Within this contribution we demonstrate for the first time the formation of two distinctly different adjacent IPEC shells within the same complex micellar aggregate. As starting material we employ multicompartiment micelles exhibiting a soft polybutadiene (PB) core, a discontinuous shell consisting of an intramicellar IPEC (*im*-IPEC) between

quaternized poly(2-vinylpyridine) (P2VPq) and poly(sodium methacrylate) (PMANa), and a corona of excess PMANa, thus rendering colloidal objects with a negative surface charge. These micelles are formed if ampholytic block terpolymers, polybutadiene-*block*-poly(1-methyl-2-vinyl pyridinium)-*block*-poly(sodium methacrylate) (PB-*b*-P2VPq-*b*-PMANa), self-assemble in aqueous solution at pH 10, conditions where methacrylic acid is negatively charged.²⁸ To this is added another solution containing a positively charged polyelectrolyte, being either quaternized poly(*N,N*-dimethylaminoethyl methacrylate) (PDMAEMAq) homopolymers of different chain length or the corresponding double-hydrophilic block copolymer with poly(ethylene oxide) (PEO-*b*-PDMAEMAq). This then results in further IPEC formation between the PMANa corona and PDMAEMAq and the generation of a second IPEC shell. The whole process is shown in **Scheme 5-1**.



Scheme 5-1: Schematic pathway for the formation of double-layered IPECs from PB-*b*-P2VPq-*b*-PMANa block terpolymer micelles and either PDMAEMAq homopolymers (left) or a PEO-*b*-PDMAEMAq diblock copolymer (right).

In case of PEO-*b*-PDMAEMA_q, the PEO chains then serve as the corona of the generated core-shell-shell-corona particle and maintain a good solubility in aqueous media. We investigated two PDMAEMA_q homopolymers of different chain length, in short: Dq₁₆₂ and Dq₈₂₀, and one double-hydrophilic block copolymer, EO₃₂₅Dq₁₅₇, the subscripts denoting the degree of polymerization of the corresponding block. As precursor micelles three different block terpolymers, PB₈₀₀-*b*-P2VPq₁₉₀-*b*-PMANa₃₄₅, PB₈₀₀-*b*-P2VPq₁₉₀-*b*-PMANa₄₆₅, and PB₈₀₀-*b*-P2VPq₁₉₀-*b*-PMANa₅₅₀, were used. In the following sections a shorter nomenclature, BVqMANa_x, will be used for the precursor micelles, as the first two blocks (B and Vq) have the same degree of polymerization in all cases shown in this manuscript. The complexations were performed at different Z_{+/-} values. We define Z_{+/-} by dividing the number of cationic Dq monomer units added to the micellar solution divided by the number of free (non-complexed) anionic MANa units present, as shown in equation (5-1).

$$Z_{+/-} = \frac{n_{Dq}}{n_{MANa} - n_{Vq}} \quad (5-1)$$

The structure and the stability of the formed micellar IPECs were analyzed using dynamic light scattering (DLS) and cryogenic transmission electron microscopy (cryo-TEM).

Experimental

Synthesis

Materials. The solvents for the preparation of the micellar solutions were purchased in p.a. grade and used as delivered. Dimethyl sulfate (Me₂SO₄, >99 %, Aldrich) and hydrochloric acid (32 %) were used as received. Buffer solutions with pH 10 (H₃BO₃/KCl/NaOH) were obtained from Fluka and contained about 0.3 wt. % salt. The initiator for ATRP, ethylbromo isobutyrate (EBIB) was distilled and stored under nitrogen. HMTETA was distilled prior to use. Anisole (p.a. grade, Fluka) and CuBr (>99 %, Aldrich) were used as received.

*Synthesis of the PB-*b*-P2VP-*b*-PtBMA block terpolymers.* The linear block terpolymers were synthesized *via* sequential living anionic polymerization in THF at low temperatures using *sec*-butyl lithium as initiator. A detailed description of the synthetic procedure and a comprehensive investigation of PB-*b*-P2VP-*b*-PtBMA block terpolymers with different volume fractions is reported elsewhere.²⁹

*Synthesis of PEO-*b*-PDMAEMA (EO₃₂₅D₁₅₇).* EO-*b*-D was prepared *via* sequential living anionic polymerization in THF using 1,1-diphenyl-3-methylpentyllithium (DPMPLi) as initiator. A combination of MALDI-ToF mass spectrometry and ¹H-NMR yielded the composition EO₃₂₅D₁₅₇. More details about the synthesis and characterization can be found elsewhere.³⁰

Synthesis of PDMAEMA (D₁₆₂ and D₈₂₀). D₁₆₂ was prepared with Atom Transfer Radical Polymerization (ATRP) in anisole using an earlier reported protocol.³¹ The ratio of monomer to initiator was 500:1 and the reaction was quenched at ~ 40 % conversion (followed by ¹H-NMR). D₁₆₂ has a molecular weight of $M_{\text{NMR}} = 25.500$ g/mol and a PDI of 1.26, measured with THF-SEC with additional 0.25 wt. % *tetra*-butyl ammonium bromide (TBAB). Polystyrene standards were used for calibration ($M_{\text{n, SEC}} = 29.300$ g/mol). The ATRP of D₈₂₀ was accomplished in acetone at 60 °C. The ratio of initiator : CuBr : HMTETA : monomer was 1 : 4 : 4 : 1200 and the polymerization was stopped at a conversion of 68 % as determined by NMR. The polymer exhibited a molecular weight $M_{\text{NMR}} = 130.000$ g/mol and a PDI of 1.51.

Quaternization of the P2VP block. PB-*b*-P2VP-*b*-PtBMA block terpolymers were dissolved in dioxane at a concentration of 1 g/L. Afterwards, Me₂SO₄ (10 eq corresponding to the 2-vinyl pyridine groups) was added and the solution was stirred for at least 72 hours at 40 °C. The resulting solution of polybutadiene-*block*-poly(*N*-methyl-2-vinyl pyridinium)-*block*-poly(*tert*-butyl methacrylate) PB-*b*-P2VPq-*b*-PtBMA was directly used for the subsequent hydrolysis of the ester moiety of the PtBMA block. From IR measurements and iodometric titrations with diluted AgNO₃ solutions we determined an approximate degree of quaternization of 70-90 %. The quaternization of D or the EO-*b*-D diblock copolymer was performed in an analogous way. Here, a quantitative quaternization was achieved as proven by ¹H-NMR spectroscopy.³¹

Dialysis. Dialysis membrane tubing (MWCO 3.500 g/mol, regenerated cellulose ester) was purchased from Spectra/Por. Prior to use, the tubes were immersed in de-ionized water for 1 h to open the pores.

Hydrolysis of the PtBMA block. Solutions of PB-*b*-P2VP_q-*b*-PtBMA in dioxane ($c = 1$ g/L) were treated with a 5-fold excess of hydrochloric acid relative to the ester moieties. Afterwards, the reaction mixture was refluxed at 120 °C for 24 hours. Full conversion of the hydrolysis reaction was confirmed with IR spectroscopy *via* the disappearance of the *tert*-butyl (1393 cm^{-1} and 1367 cm^{-1}) and carbonyl (1722 cm^{-1}) signals.

*Preparation of the PB-*b*-P2VP_q-*b*-PMANa (BVqMANa) micellar solutions.* Directly after hydrolysis of the PtBMA block, micellar stock solutions ($c \sim 1$ g/L) were prepared *via* dialysis against pH 10 buffer solution.

Complexation reactions: Dq₁₆₇, Dq₈₂₀ and EO₃₂₅Dq₁₅₇ were dissolved in a pH 10 buffer solution (VWR®, AVS Titrimorm) at a respective concentration of 5 g/L. Afterwards, the corresponding volumes to reach a certain $Z_{+/-}$ -value (for the definition of $Z_{+/-}$ see the Introduction) were added to micellar solutions of BVqMANa₃₄₅, BVqMANa₄₆₅, or BVqMANa₅₅₀ (all 1 g/L) in small glass vials and stirred at ambient temperature. In general, measurements on the complexes were performed after one week of continuous stirring.

Characterization

Dynamic light scattering (DLS). All experiments were performed using approximately the same concentrations ($c = 1$ g/L). DLS measurements were performed in sealed cylindrical scattering cells ($d = 10$ mm) at an angle of 90° on an ALV DLS/SLS-SP 5022F equipment consisting of an ALV-SP 125 laser goniometer with an ALV 5000/E correlator and a He-Ne laser with the wavelength $\lambda = 632.8$ nm. The CONTIN algorithm was applied to analyze the obtained correlation functions. Apparent hydrodynamic radii were calculated according to the Stokes-Einstein equation. Prior to the light scattering measurements the sample solutions were filtered using Millipore nylon filters with a pore size of 1.2 μm (solutions of the quaternized Dq₁₆₂, Dq₈₂₀, or the double-hydrophilic EO₃₂₅Dq₁₅₇ in pH 10 buffer) or 5 μm (micellar precursors or the double-layered IPECs). The polydispersities were determined from unimodal peaks *via* the cumulant analysis.

Cryogenic Transmission Electron Microscopy (cryo-TEM): For cryo-TEM studies, a drop of the sample solution ($c \approx 0.1$ wt. %, 1 g/L) was placed on a lacey carbon-coated copper TEM grid (200 mesh, Science Services, München, Germany), where most of the liquid was removed with blotting paper, leaving a thin film stretched over the grid holes. The specimens were shock vitrified by rapid immersion into liquid ethane in a temperature-controlled freezing unit (Zeiss Cryobox, Zeiss NTS GmbH, Oberkochen, Germany) and cooled to approximately 100 K. The temperature was monitored and kept constant in the chamber during all the preparation steps. After freezing the specimens, they were inserted into a cryo-transfer holder (CT3500, Gatan, München, Germany) and transferred to a Zeiss EM922 Omega EFTEM instrument. Examinations were carried out at temperatures around 100 K. The microscope was operated at an acceleration voltage of 200 kV. Zero-loss filtered images ($\Delta E = 0$ eV) were taken under reduced dose conditions. All images were registered digitally by a bottom mounted CCD camera system (Ultrascan 1000, Gatan), combined and processed with a digital imaging processing system (Gatan Digital Micrograph 3.9 for GMS 1.4).

Zeta-potential. The zeta-potential was determined on a Malvern Zetasizer Nano ZS in conjunction with an MPT2 autotitrator (Malvern). The electrophoretic mobilities (u) were converted into ζ potentials *via* the Smoluchowski equation $\zeta = u\eta/\epsilon_0\epsilon$, where η denotes the viscosity and $\epsilon_0\epsilon$ the permittivity of the solvent, water.

Size Exclusion Chromatography (SEC). Four PSS-SDV gel columns (5 μm) with a porosity range from 10^2 to 10^5 Å (PSS, Mainz, Germany) were used together with a differential refractometer and a UV detector at $\lambda = 254$ nm. Measurements were performed in THF with a flow rate of 1 mL/min using toluene as internal standard. Narrowly distributed 1-4 polybutadiene were used as calibration standards.

SEC experiments for the PDMAEMA containing samples were performed using four PSS-SDV gel columns (5 μm) with a porosity range from 10^2 to 10^4 Å (PSS, Mainz, Germany) were used together with a differential refractometer and a UV detector at $\lambda = 254$ nm. Measurements were performed in THF with additional 0.25 wt. % tetrabutylammonium bromide (TBAB) as eluent and 0.5 ml/min as flow rate. Polystyrene standards were used for calibration.

¹H-NMR spectroscopy. The absolute number-average molecular weights, M_n , of the synthesized block copolymers were determined by ¹H-NMR in CDCl₃ (Bruker AC 250 spectrometer) using the M_n of the first block, as determined by MALDI-ToF MS or SEC, and suitable NMR signal areas of the corresponding blocks. For more details on the characterization of the block copolymers the reader is referred to the literature.³²

Results and Discussion

Characterization of the Precursor Micelles

In a recent publication we reported on the preparation of multicompartments-core micelles in aqueous media at high pH from polybutadiene-*block*-poly(1-methyl-2-vinyl pyridinium)-*block*-poly(sodium methacrylate) (BVqMANa) block terpolymers.²⁸ The micelles consisted of a soft B core, a discontinuous shell of an intramicellar IPEC (*im*-IPEC) between positively charged Vq and negatively charged poly(sodium methacrylate) (MANa at pH 10), and, depending on the length, a corona of MANa. They were shown to react on changes in pH and salinity in a dynamic way. These micelles were used as “precursor” materials for the results presented within this contribution. Three block terpolymer compositions were used. The first two blocks, B and Vq, are of the same length for all three polymers, while the length of the MANa block was varied. The solution characteristics of the precursor micelles in pH 10 buffer solution were determined by cryo-TEM, DLS and ζ -potential measurements (see **Table 5-1**).

Table 5-1: Molecular characterization of the BVqMANa_x block terpolymers and the micellar aggregates in aqueous solution at pH 10.

Polymer	Composition ^a	$10^{-3} M_n^b$ [g/mol]	$\langle R_{TEM} \rangle_n^c$ [nm]	$\langle R_h \rangle_{z, app}^d$ [nm]	PDI _{app} ^e	ζ -Potent. [mV]
1	B ₈₀₀ Vq ₁₉₀ MANa ₃₄₅	96	79.5 ± 7	170	0.18	-21
2	B ₈₀₀ Vq ₁₉₀ MANa ₄₆₅	106	93.5 ± 8	146	0.21	-30
3	B ₈₀₀ Vq ₁₉₀ MANa ₅₅₀	113	91 ± 11	88	0.05	-36

a: the subscripts denote the respective degrees of polymerization; b: calculated for the individual polymer chain without taking the counterions into account; c: determined from cryo-TEM images; d: determined *via* DLS at 1 g/L; e: determined *via* cumulant analysis.

Representative cryo-TEM images of the precursor micelles 1-3 are shown in **Figure 5-1**, where the proposed solution structure of multicompartments micelles can be confirmed. The BVqMANa_x polymers form micelles with a B core (dark grey), which is decorated with the *im*-IPEC consisting of Vq and MANa (small black dots), and a corona of the remaining MANa (light grey). With increasing length of the MANa block, the micelles appear more homogeneous in size and shape. Several micelles for BVqMANa₃₄₅ exhibit a

non-spherical shape, especially the core of the micelles shows deformations (see **Figure 5-1A**), whereas this cannot be seen for polymers with a longer water-soluble block (**Figures 5-1B** and **5-1C**). Furthermore, some of the BVqMANa₃₄₅ micelles seem to be interconnected by bridge-like structures (dark grey, shown at higher magnification in the inset of **Figure 5-1A**). Similar structures were previously observed in micellar systems prepared from amphiphilic miktoarm stars of polystyrene-*arm*-polybutadiene-*arm*-poly(2-vinyl pyridine) (μ SBV) block terpolymers in aqueous media and identified as hydrophobic B bridges, originating from the soft “liquid” cores of the aggregates.³³ For both BVqMANa₄₆₅ and BVqMANa₅₅₀, such effects were not observed. We attribute this to a superior stabilization of the micelles in aqueous solution with an increasing block length of the corona-forming block, MANa.

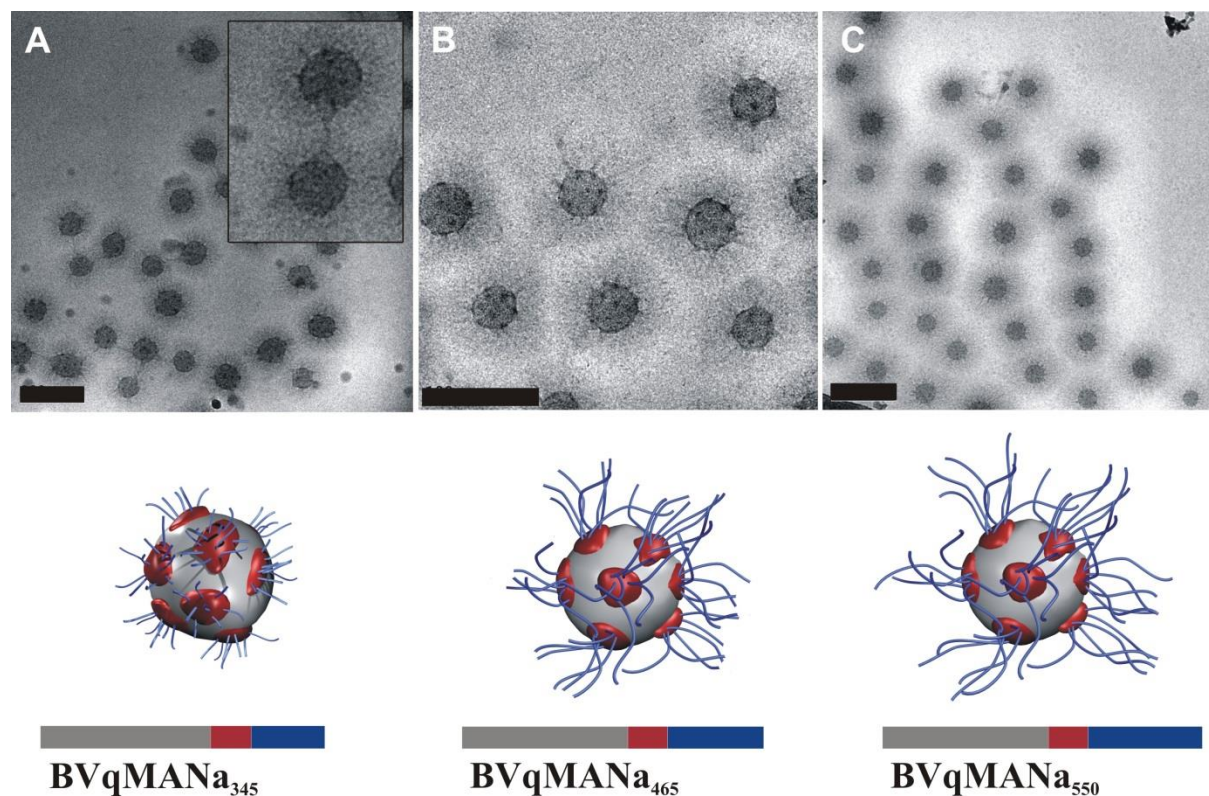


Figure 5-1: Cryo-TEM images of micelles formed from BVqMANa₃₄₅ (A, the inset shows hydrophobic bridges between two adjacent micelles at higher magnification), BVqMANa₄₆₅ (B), and BVqMANa₅₅₀ (C) at concentrations of 1 g/L in aqueous solution at pH 10, all scalebars correspond to 200 nm; below each cryo-TEM image are schematic depictions of the proposed solution structure.

The cryo-TEM images were subjected to a detailed image analysis to obtain average sizes of the individual compartments. For each micelle and compartment (core, *im*-IPEC and

corona) between 50 and 100 micelles were measured to calculate average values (**Table 5-2**).

Table 5-2: Average sizes of the individual compartments of the BVqMANa_x micelles as determined by image analysis of cryo-TEM data.

Compartment	BVqMANa₃₄₅ [nm]	BVqMANa₄₆₅ [nm]	BVqMANa₅₅₀ [nm]
R _{Micelle}	79.5 ± 7	93.5 ± 8	91 ± 11
R _{Core}	38 ± 5	37 ± 8	33.5 ± 4
D _{im-IPEC}	5 ± 2	3 ± 1	4 ± 1
D _{Corona}	40 ± 5	52 ± 6	53 ± 9
N _{agg} ^a	3,200	3,000	2,200

a: estimated with Eq. 5-2;

The smallest micelles are formed for BVqMANa₃₄₅ with an overall radius of 79.5 nm (**Table 5-2**), whereas both the aggregates found for BVqMANa₄₆₅ (93.5 nm) and BVqMANa₅₅₀ (91 nm) are larger. The diameter of the corona also increases with increasing length of the MANa block. The size of the *im*-IPEC stays constant at approximately 3-4 nm within the experimental error for all three samples discussed. However, the core radius seems to decrease with increasing length of the negatively charged block from 38 nm for BVqMANa₃₄₅ to 33.5 nm for BVqMANa₅₅₀, which points to a decrease in the aggregation number, N_{agg}. This is in accordance with Burkhardt *et al.*,³ who observed a decrease in N_{agg} with increasing hydrophilic block length in polyisobutylene-*block*-poly(methacrylic acid) micelles. They explained the decrease of N_{agg} with the increasing space occupied by the hydrophilic block leading to a repulsive force between the corona chains. Such a decrease in N_{agg} was also predicted by Borisov *et al.* in theoretical calculations for diblock-copolymer micelles with one ionic block.³⁴ A rough calculation of N_{agg} for our system based on the core diameter as observed in TEM (equation (2)) results in an approximate N_{agg} of 3200, 3000 and 2200 for BVqMANa₃₄₅, BVqMANa₄₆₅ and BVqMANa₅₅₀, respectively. We note that earlier static light scattering experiments on BVqMANa₅₅₀ gave a significantly lower value (N_{agg} = 234) and that we are not able to explain this discrepancy at the moment.²⁸

$$N_{agg.} = \frac{m_{core}}{m_{PB}^{chain}} = \frac{4\pi \cdot N_A \cdot \rho_{PB} \cdot R_{core}^3}{3 \cdot M_{PB}^{chain}} \quad (5-2)$$

with m_{core} : mass of the micellar core; m_{PB}^{chain} : mass of an individual PB chain; N_A : Avogadro constant; ρ_{PB} : density of polybutadiene; R_{core} : radius of the micellar core acc. to TEM; M_{PB}^{chain} : molecular weight of an individual PB chain.

If the aggregate sizes determined *via* cryo-TEM are compared to the data obtained from DLS measurements (**Table 5-1**), deviations are found for BVqMANa₃₄₅ and BVqMANa₄₆₅, whereas in case of BVqMANa₅₅₀ both methods are in good agreement. According to cryo-TEM (**Table 5-2, Figure 5-1**), BVqMANa₃₄₅ has an $\langle R_{TEM} \rangle_n = 79.5$ nm, while DLS experiments yield $\langle R_h \rangle_{z, app} = 170$ nm and a PDI of 0.18. We think that this difference can be tentatively explained by the bridges observed (inset in **Figure 5-1A**), masking the individual aggregate size. The reason for the difference in R for BVqMANa₄₆₅ (DLS: $\langle R_h \rangle_{z, app} = 146$ nm, PDI = 0.21 and cryo-TEM: $\langle R_{TEM} \rangle_n = 93.5$ nm) remains puzzling. In this case, hydrophobic bridges were not observed in cryo-TEM. Nevertheless, the increased value obtained by DLS might still hint towards aggregation of the micelles taking place in the stock solution. Furthermore, the values for R obtained *via* cryo-TEM represent a number average, whereas DLS gives a z-average. Especially for systems with higher PDI values, the differences between these two averages are expected to be significant.

Complexation and IPEC Formation

To generate an additional IPEC layer on top of the already existing *im*-IPEC shell, the BVqMANa_x micelles were mixed with positively charged polyelectrolytes in aqueous solution at pH 10. We have demonstrated this approach recently for the addition of poly(ethylene oxide)-*block*-poly(1-methyl-2-vinyl pyridinium) PEO-*b*-P2VPq diblock copolymers.²⁷ In this case, two identical IPEC shells were formed as both the “inner”, former *im*-IPEC, as well as the “outer”, newly generated IPEC, consisted of Vq and MANa. Here, we employed either quaternized PDMAEMA (Dq) or PEO-*b*-PDMAEMAq diblock copolymers as oppositely charged polyelectrolytes. The whole process is depicted in **Scheme 5-1**.

If cationic homopolymers (Dq₁₆₂, Dq₈₂₀) are used for further IPEC formation (**Scheme 5-1**, left part), core-shell-shell particles are formed where the previous MANa corona of the micelles is transformed into an IPEC layer consisting of MANa and Dq. Furthermore, the two IPECs are expected to form two distinctive layers due to immiscibility between Vq and Dq. Depending on the absolute ratio of positive to negative charges, $Z_{+/-}$, this would lead to uncharged polymer particles. It has been shown that such IPECs precipitate when a critical $Z_{+/-}$ value is reached.²⁶ When EO₃₂₅Dq₁₅₇ is used for this complexation step, core-shell-shell-corona particles are formed. In this case, even for $Z_{+/-} = 1$, the micellar IPECs are expected to remain water-soluble, stabilized through the PEO corona, depicted in green (**Scheme 5-1**, right part).

We will first discuss the results concerning the IPEC-formation of different BVqMANa precursor micelles with Dq₁₆₂ or Dq₈₂₀ at different $Z_{+/-}$ values. Afterwards, similar experiments will be discussed with EO₃₂₅Dq₁₅₇. Unless explicitly stated, the concentration of the precursor micelles was in between 0.1 and 1.0 g/L in pH 10 buffer solutions for the complexation reactions, a regime proven not to lead to further aggregation for BVqMANa₅₅₀.²⁸ However, in case of BVqMANa₃₄₅ and BVqMANa₄₆₅, a slight increase in hydrodynamic radius was observed with concentration ($\langle R_h \rangle_{z, app} = 172$ nm for 0.17 g/L and $\langle R_h \rangle_{z, app} = 195$ nm for 1.0 g/L for BVqMANa₃₄₅ and $\langle R_h \rangle_{z, app} = 146$ nm for 0.17 g/L and $\langle R_h \rangle_{z, app} = 191$ for 1 g/L for BVqMANa₄₆₅). Therefore, those were typically used at 0.17 g/L. The targeted amounts of quaternized homo- or diblock copolymers were added at a concentration of 5 g/L prepared in the same pH 10 buffer. The highest resulting polymer concentration prepared in that way (solutions of 1.0 g/L BVqMANa₅₅₀ micelles with EO₃₂₅Dq₁₅₇ at $Z_{+/-} = 1$) was roughly 1.7 g/L. The cationic homo- or diblock copolymer solution was added under vigorous stirring to the solution containing the precursor micelles. In general, the resulting micellar IPECs were examined after one week of continuous stirring.

Addition of Dq Homopolymers to BVqMANa_x Micelles

BVqMANa_x precursor micelles were mixed with Dq₁₆₂ or Dq₈₂₀ at different $Z_{+/-}$ ratios and analyzed by DLS. Exemplarily, the resulting CONTIN plots for BVqMANa₃₄₅ and Dq₁₆₂ at different $Z_{+/-}$ ratios are shown in **Figure 5-2**, while the results for all different combinations are summarized in **Table 5-3**.

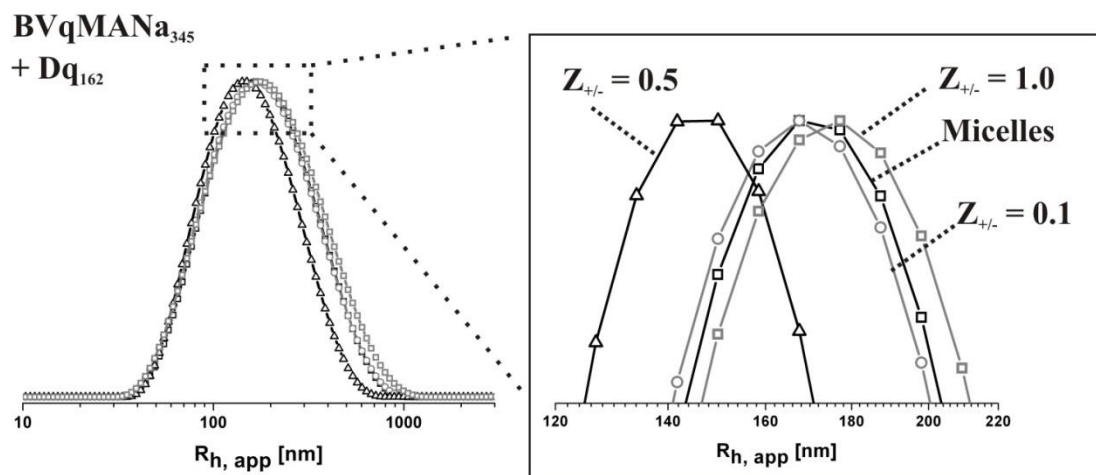


Figure 5-2: DLS CONTIN plots for BVqMANa₃₄₅ (-□-, black), and micellar IPECs with Dq₁₆₂ at $Z_{+/-}$ = 0.1 (-○-, grey), 0.5 (-Δ-, black) and 1.0 (-□-, grey) (A), the inset on the right shows an enlargement of the plot peak region.

Table 5-3: Apparent hydrodynamic radii of double-layered micellar IPECs prepared from BVqMANa_x block terpolymer micelles and Dq polymers as determined by DLS.

Entry	Sample	Z _{+/-} ^a	<R _h > _{z,app} ^b [nm]	PDI ^c
1	BVqMANa ₃₄₅	-	170	0.18
2	+ Dq ₁₆₂	0.1	172	0.27
3	+ Dq ₁₆₂	0.5	154	0.24
4	+ Dq ₁₆₂	1.0	184	0.34
5	+ Dq ₁₆₂	1.25	precipitation	
6	+ Dq ₈₂₀	0.5	162	0.27
7	+ Dq ₈₂₀	1.0	186	0.27
8	BVqMANa ₄₆₅	-	146	0.21
9	+ Dq ₁₆₂	0.1	145	0.18
10	+ Dq ₁₆₂	0.5	148	0.21
11	+ Dq ₁₆₂	0.75	170	0.25
12	+ Dq ₁₆₂	1.0	precipitation	
13	+ Dq ₈₂₀	0.1	115	0.12
14	+ Dq ₈₂₀	0.5	181	0.21
15	+ Dq ₈₂₀	0.75	precipitation	
16	BVqMANa ₅₅₀	-	88	0.05
17	+ Dq ₁₆₂	0.1	169	0.16
18	+ Dq ₁₆₂	0.25	128	0.17
19	+ Dq ₁₆₂	0.5	precipitation	
20	+ Dq ₈₂₀	0.1	110	0.13
21	+ Dq ₈₂₀	0.25	131	0.09
22	+ Dq ₈₂₀	0.5	precipitation	

a: ratio of added positive to remaining negative charges; b: determined *via* DLS; c: determined *via* cumulant analysis.

For all possible combinations of BVqMANa_x block terpolymer micelles and Dq homopolymers critical Z_{+/-} ratios, above which precipitation of the complexes occurred within several hours, were found. Interestingly, as can be seen from **Table 5-3**, the critical

$Z_{+/-}$ value decreases with increasing MANa block length. BVqMANa₃₄₅ micelles tolerated an addition of Dq polymers up to $Z_{+/-} = 1$, whereas for BVqMANa₅₅₀ precipitation already occurred at $Z_{+/-} = 0.5$, which is rather puzzling.

Remarkable differences are also observed if the hydrodynamic radii of the micellar IPECs after addition of oppositely charged Dq are compared: for BVqMANa₃₄₅ and BVqMANa₄₆₅, the micellar size does not significantly change if small amounts ($Z_{+/-} < 0.25$ for BVqMANa₃₄₅ and $Z_{+/-} < 0.5$ for BVqMANa₄₆₅) of Dq₁₆₂ are added. Upon further addition of Dq₁₆₂ the size increases until a critical $Z_{+/-}$ value is reached, where aggregation and finally precipitation occurs ($Z_{+/-} = 1.25$ for BVqMANa₃₄₅ and $Z_{+/-} = 1.0$ for BVqMANa₄₆₅). For BVqMANa₅₅₀, already the addition of 10 % of Dq₁₆₂ causes an increase in R_h from 88 nm to 169 nm. Increasing the $Z_{+/-}$ to 0.25 leads to a decrease in size of the micellar IPECs, before precipitation occurs at the critical $Z_{+/-}$ value of 0.5.

In theory, Dq₁₆₂ can interact with the negatively charged MANa corona in two possible ways: if all MANa chains of the corona are evenly neutralized, a collapse of the corona should occur. On the other hand, if only some MANa chains are fully neutralized and participate in the IPEC formation, the other uncomplexed MANa chains would retain their original length. This would lead to a less drastic change in corona size. This question was investigated by Borisov *et al.* in a recent publication, where molecular dynamics simulations on the structural organization of IPECs between oppositely charged linear and star-shaped polyelectrolytes were performed.³⁵ They found, that for star-shaped polyelectrolytes several arms were completely neutralized whilst others did not participate at all in the IPEC formation. A similar behavior was also found for small amounts of surfactant added to spherical polyelectrolyte brushes.³⁶ We assume that a similar mechanism is taking place here. This would explain the absence of significant changes in R_h for small $Z_{+/-}$ values in case of micellar IPEC formation for BVqMANa₃₄₅ and BVqMANa₄₆₅ with Dq₁₆₂. If larger amounts of Dq₁₆₂ are added, a drastic increase in the size of the structures indicates the formation of aggregates. This is simply caused through less and less “free” MANa being present to stabilize the particles in solution, until, finally, the aggregates precipitate.

If a longer cationic polyelectrolyte, Dq₈₂₀, is used for the complexation reactions, the situation is different. For small $Z_{+/-}$ values (0.1), a slight contraction of the micellar IPECs for BVqMANa₃₄₅ and BVqMANa₄₆₅ can be seen (**Table 5-3**, entries 6 and 13), while

BVqMANa₅₅₀ complexes again show an increase in R_h (**Table 5-3**, entry 20). A tentative explanation for the differences observed for BVqMANa₅₅₀ could be that with increasing MANa block length (and a longer polycationic chain, Dq₈₂₀) *inter*-micellar linkages are also formed to a certain extent. As shown for Dq₁₆₂, the addition of more Dq₈₂₀ eventually exceeds a critical $Z_{+/-}$ value in all cases and results in precipitation of the formed complexes. Considering the PDI of the resulting aggregates (according to DLS), in most cases the addition of Dq polymers leads to an increase for the complex micelles (exceptions are BVqMAA₄₆₅ micelles, entries 9 and 13 in **Table 5-3**). In general, the highest PDIs are observed for high $Z_{+/-}$ ratios, shortly before precipitation occurs. This observation is reasonable, as increasing complexation of the corona should result in poorly stabilized micelles, which in turn promotes aggregation and broadens the micellar size distribution. Even though both Dq polymers are moderately polydisperse (PDI(Dq₁₆₂) = 1.26; PDI(Dq₈₂₀) = 1.51), the effect of the $Z_{+/-}$ ratio seems to be more pronounced. This is in accordance with earlier work on star-shaped poly(acrylic acid) complexes with quaternized P4VPq homopolymers.³⁷

For a validation of a successful complexation and, hence, the formation of a second IPEC shell, cryo-TEM was performed for the complexes prepared from all BVqMANa_x block terpolymer micelles and the longer Dq₈₂₀ polycation. The results are shown in **Figure 5-3**.

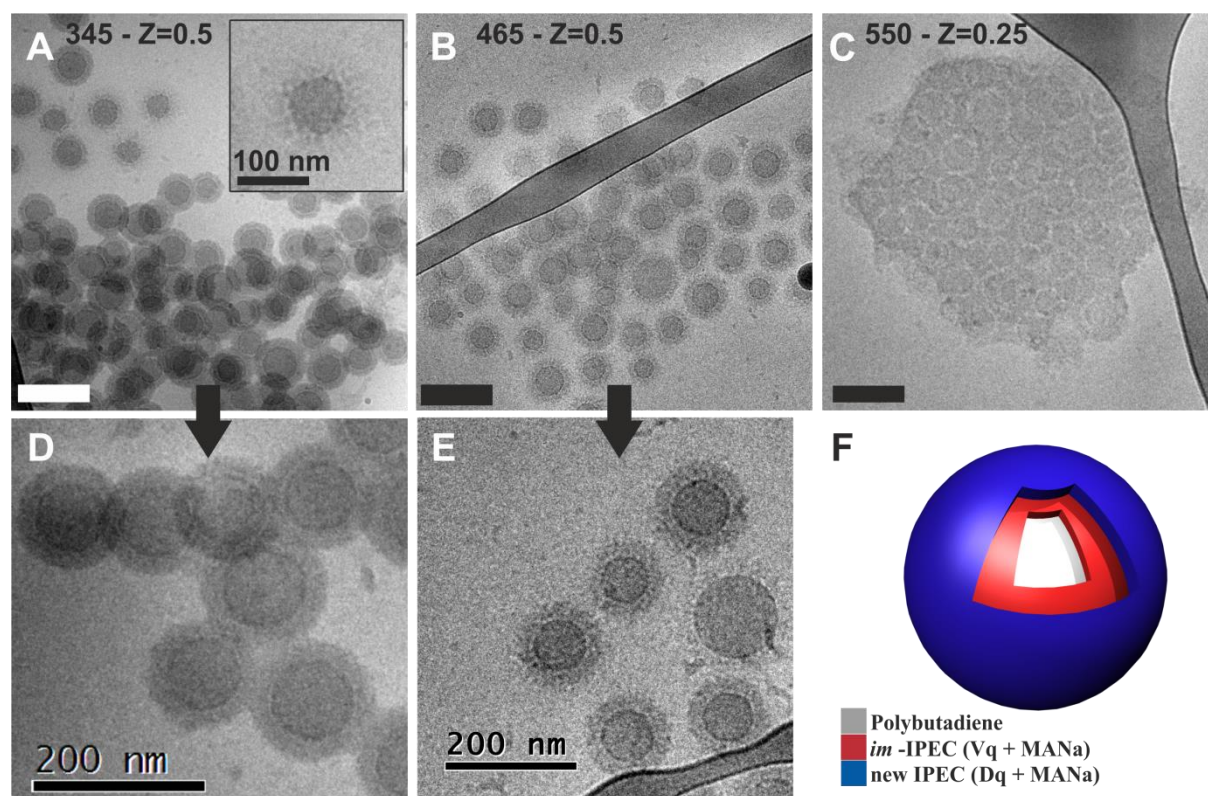


Figure 5-3: Cryo-TEM micrographs of complexes formed from precursor micelles and Dq₈₂₀ at different $Z_{+/-}$ ratios; BVqMANa₃₄₅ at $Z_{+/-} = 0.5$ (A, the inset shows a single precursor micelle, D shows a higher magnification); BVqMANa₄₆₅ at $Z_{+/-} = 0.5$ (B, E shows a higher magnification); BVqMANa₅₅₀ at $Z_{+/-} = 0.25$ (C); proposed solution structure of the resulting double-layered micellar IPECs (F); all scale-bars correspond to 200 nm.

The cryo-TEM images confirm the proposed core-shell-shell morphology of the complexes. Throughout all the samples, but especially for the complexes of BVqMANa₅₅₀ with Dq, highly aggregated particles were found in the cryo-TEM samples. This implicates that, although low $Z_{+/-}$ values are used, the particles are not significantly charged and do not repel each other anymore. The increase in R_h that is observed in the DLS for large $Z_{+/-}$ values could therefore be explained by clustering. One has to keep in mind, however, that in the cryo-TEM images a two-dimensional confinement of the particles takes place, which might further promote clustering of the particles. Moreover, a few precursor-like micelles were found for complexes of BVqMANa₃₄₅ (inset in **Figure 5-3A**) and BVqMANa₄₆₅ with Dq₈₂₀ at $Z_{+/-} = 0.5$. Some of these are depicted in the upper left corner of **Figure 5-3A** and also one shown on the right-hand side of **Figure 5-3E**. Such “precursor” micelles rather were an exception and we believe that these are a result of slow mixing during the addition of the Dq solutions.

The enlarged images in **Figure 5-3D** and **5-3E** nicely show the double-layered character of the micellar IPECs when compared to the original micelles. The grey B core is still surrounded by a thin, slightly darker shell. This is supposed to be the former discontinuous *im*-IPEC shell of the precursor micelles, consisting of Vq and MANa. Completely covering this part, a new continuous shell has been formed through the complexation of the MANa corona with Dq₈₂₀, depicted in blue in **Figure 5-3F**. Again, the overall size of the micelles as well as the size of the individual compartments was determined from the cryo-TEM images for complexes of BVqMANa₃₄₅ and BVqMANa₄₆₅ with Dq₈₂₀ and a Z_{+/-} ratio of 0.5. The averaged values from counting 50-100 particles in each case together with the corresponding standard deviations are shown in **Table 5-4**. Unfortunately, in case of micellar IPECs formed from BVqMANa₅₅₀ precursor micelles a detailed evaluation was not possible, due to the strong aggregation observed in the cryo-TEM images. Nevertheless, those solutions were stable over months.

Table 5-4: Average compartment dimensions for micellar IPECs from BVqMANa_x / Dq₈₂₀ as determined by analysis of 50-100 particles.

Compartment	BVqMANa ₃₄₅ [nm]	BVqMANa ₃₄₅ / Dq ₈₂₀ Z _{+/-} = 0.5 [nm]	BVqMANa ₄₆₅ [nm]	BVqMANa ₄₆₅ / Dq ₈₂₀ Z _{+/-} = 0.5 [nm]
R _{Micelle}	79.5 ± 7	65 ± 7	93.5 ± 8	61 ± 7
R _{Core}	38 ± 5	34.5 ± 5	37 ± 8	31 ± 4
D _{<i>im</i>-IPEC}	5 ± 2	8 ± 2	3 ± 1	6 ± 2
D _{Corona / 2nd IPEC- Shell}	40 ± 5	23 ± 3	52 ± 6	25 ± 4
N _{agg} ^a	3,200	2,400	3,000	1,700

a: estimated with Eq. 2;

If the overall radius is calculated according to the cryo-TEM micrographs by assuming it to be equal to half the core-to-core distance, a number-average $\langle R_{\text{TEM}} \rangle_n = 65$ nm for BVqMANa₃₄₅ and $\langle R_{\text{TEM}} \rangle_n = 61$ nm for BVqMANa₄₆₅ complexes is found (both were formed with Dq₈₂₀ at Z_{+/-} = 0.5, samples shown in **Figure 5-3**). This is again distinctly smaller than the size observed *via* DLS, where $\langle R_h \rangle_{z, \text{app}} = 162$ nm and $\langle R_h \rangle_{z, \text{app}} = 181$ nm were determined. This discrepancy between both methods, to our opinion, reflects

the tendency of these particles to aggregate after formation of the second IPEC shell, as also seen in some of the cryo-TEM images. Nevertheless, this did not seem to affect the stability of the micellar IPEC solutions. As a general observation from cryo-TEM, the overall size of the micelles seems to decrease after formation of the complexes with Dq₈₂₀. This decrease in the overall size is mainly due to a collapse of the MANa corona and the formation of a second IPEC shell. Also, a decrease in the core size was observed hinting to a decrease in $N_{agg.}$ by ~25 % (cf. Eq. 1) for BVqMANa₃₄₅ (2400 polymer chains / micelle) and ~45 % for BVqMANa₄₆₅ (1700 polymer chains / micelle). This change in $N_{agg.}$ points towards a dynamic behavior of the micelles upon complex formation. The micrographs were further submitted to a grayscale analysis. This is exemplarily shown for the complex of BVqMANa₃₄₅ with Dq₈₂₀ at $Z_{+/-} = 0.5$ in **Figure 5-4**.

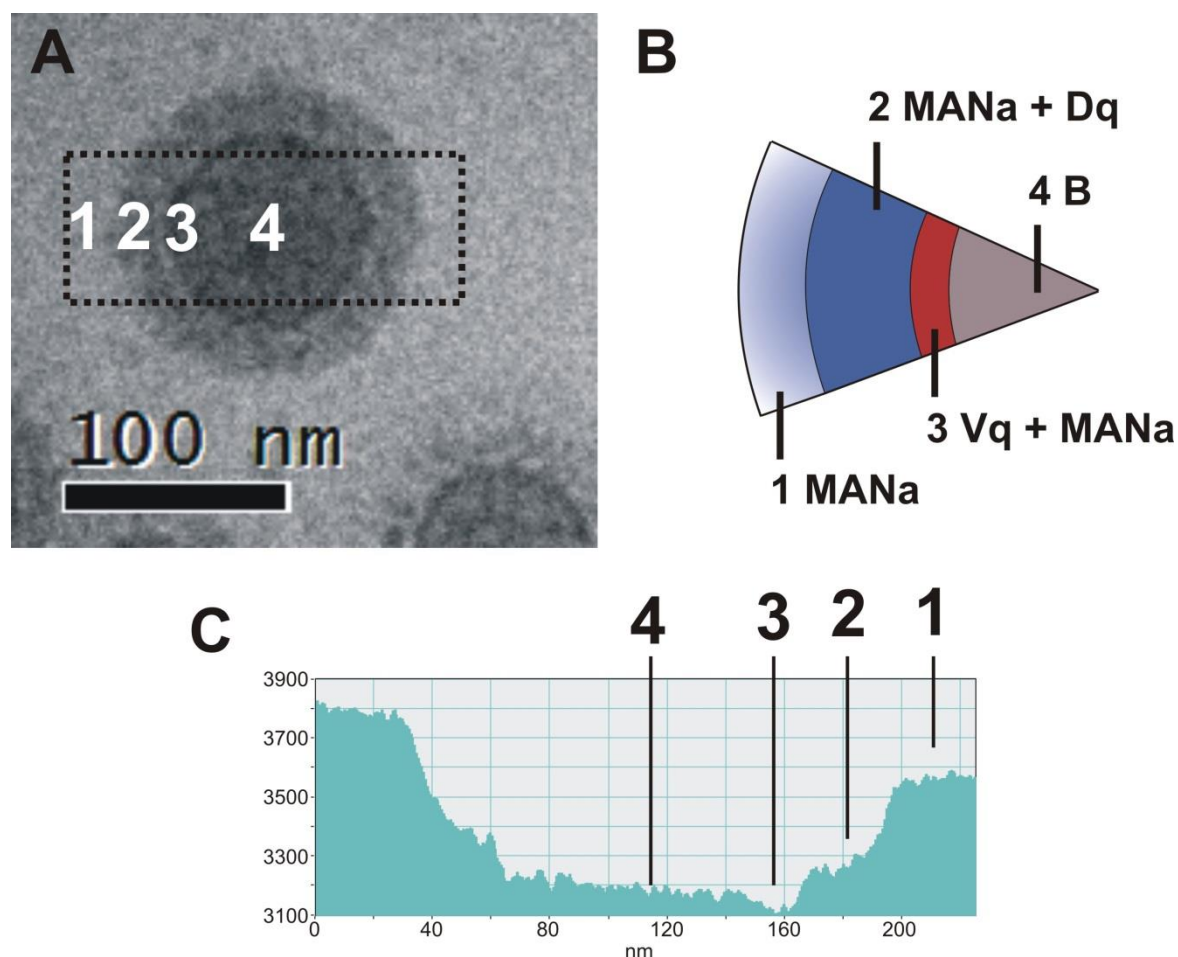


Figure 5-4: Cryo-TEM micrograph of a single micellar IPEC of BVqMANa₃₄₅ and Dq₈₂₀ at $Z_{+/-} = 0.5$; the black box highlights the area used for the greyscale analysis (A); circle segment showing the four different regions revealed *via* greyscale analysis (B); greyscale analysis of the particle in part A, the numbers correspond to the respective areas (C).

Figure 5-4A shows a single double-layered micellar IPEC particle. The rectangular black box shows the area used for the greyscale analysis in **Figure 5-4C**. The different compartments of the micellar IPEC are depicted in the segments of the drawing in **Figure 5-4B**. The B core exhibits a radius of 34.5 nm, and is surrounded by a thin, approx. 8 nm thick shell, resembling the former discontinuous *im*-IPEC shell of the precursor micelles. The newly formed IPEC shell, consisting of MANa and Dq, has a thickness of roughly 23 nm. As a $Z_{+/-}$ ratio of 0.5 was used, an uncomplexed MANa corona should emanate from the micellar IPEC. This is schematically shown in **Figure 5-4B** with a blue/white gradient and is not distinguishable in the cryo-TEM image. However, as many of the micelles can be found closely agglomerated, the repelling effect of any uncomplexed and, hence, still charged MANa seems to be negligible. The numbers shown in **Figure 5-4C** correspond to the different micellar compartments, also illustrated in **Figure 5-4A**. Ideally, the greyscale analysis of the double-layered IPEC should be completely symmetrical. However, as the enlarged micellar aggregate was not located right in the centre of the cryo-TEM image taken, the electron beam intensity is slightly decreasing from the lower right to the upper left corner of **Figure 4A**.

Addition of EO₃₂₅Dq₁₅₇ Diblock Copolymers to BVqMANa_x Micelles

If a double-hydrophilic block copolymer with one charged block (Dq) is used to generate core-shell-shell-corona structures from different BVqMANa_x precursor micelles, similar structures are supposed to form as shown earlier for Dq homopolymers. The only difference is that the other water-soluble block, EO, will serve as a solubilizing corona and, thus, further stabilize the resulting micellar IPECs. The micellar solutions were mixed with EO₃₂₅Dq₁₅₇ at different $Z_{+/-}$ ratios. Exemplarily, the DLS CONTIN plots for BVqMANa₃₄₅ and BVqMANa₄₆₅ at different $Z_{+/-}$ values are shown in **Figure 5-5**.

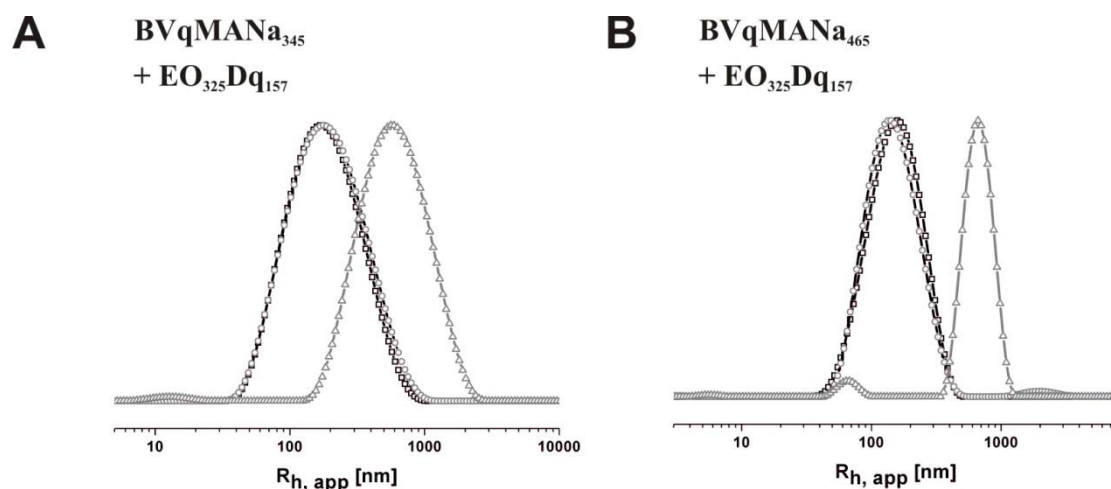


Figure 5-5: DLS CONTIN plots for BVqMANa₃₄₅ (-□-, black), and micellar IPECs with EO₃₂₅Dq₁₅₇ at $Z_{+/-} = 0.5$ (-○-, grey), and 1.0 (-Δ-, grey) (A); BVqMANa₄₆₅ (-□-, black), and micellar IPECs with EO₃₂₅Dq₁₅₇ at $Z_{+/-} = 0.5$ (-○-, grey), and 1.0 (-Δ-, grey) (B).

For an easier comparison, the results from the DLS measurements of all micellar complexes prepared using EO₃₂₅Dq₁₅₇ as the cationically charged part are also summarized in **Table 5-5**.

Table 5-5: Solution characteristics of double-layered micellar IPECs prepared from BVqMANa_x block terpolymer micelles and EO₃₂₅Dq₁₅₇ block copolymers.

Entry	Sample	$Z_{+/-}$ ^a	$\langle R_h \rangle_{z,app}$ ^b	PDI ^c
1	BVqMANa ₃₄₅	-	170	0.18
2	+ EO ₃₂₅ Dq ₁₅₇	0.5	184	0.28
3	+ EO ₃₂₅ Dq ₁₅₇	1.0	11; 610	-
4	BVqMANa ₄₆₅	-	146	0.21
5	+ EO ₃₂₅ Dq ₁₅₇	0.5	147	0.20
6	+ EO ₃₂₅ Dq ₁₅₇	1.0	6; 57; 660	-
7	BVqMANa ₅₅₀	-	88	0.05
8	+ EO ₃₂₅ Dq ₁₅₇	0.25	129	0.17
9	+ EO ₃₂₅ Dq ₁₅₇	0.5	10; 104; 1300	-

a: ratio of added positive to remaining negative charges; b: determined *via* DLS; c: determined *via* cumulant analysis, if applicable.

In general, two things are expected to happen when EO₃₂₅Dq₁₅₇ is added to solutions of BVqMANa_x precursor micelles: first, the complexation between MANa and Dq results in a corona contraction, like that observed when Dq homopolymers were added at different $Z_{+/-}$ ratios as described above; second, the EO compartment forms a new corona of the IPEC particles, stabilizing them in solution. The contraction of the former corona should be accompanied by an decrease in R_h whereas the new EO corona should have the opposite effect. As can be seen from **Figure 5-5** and the data in **Table 5-5**, for BVqMANa₃₄₅ and BVqMANa₄₆₅ a very slight increase in R_h can be observed for $Z_{+/-} = 0.5$ (170 to 184 nm and 146 to 147 nm). This might indicate that the corona contraction is almost completely compensated by the addition of a new corona-forming block, EO. Surprisingly, in both cases larger size distributions are found in DLS measurements if $Z_{+/-}$ approaches unity. This can be seen in the CONTIN plots in **Figure 5-5A** and **5-5B**, a new population is formed with an $R_h > 600$ nm. Again, the behavior observed for complexes of BVqMANa₅₅₀ and EO₃₂₅Dq₁₅₇ is different: at first ($Z_{+/-} = 0.25$), they increase in size (88 to 129 nm). Aggregation, according to DLS, for this particular system already occurs at $Z_{+/-} = 0.5$. This remains puzzling, as a sterical stabilization of the complex micelles would be anticipated due to the EO chains of the corona. One possible explanation would be that the intensity of the larger size distribution (entries 3, 6, and 9 in **Table 5-5**) is overestimated in DLS measurements as was demonstrated by Shibayama *et. al.* for multimodal distributions of colloidal particles and polymers in solution.³⁸ Further, another distribution at low $R_h = 10$ nm appears. We assume that this represents another micellar population, as it would be too large for EO₃₂₅Dq₁₅₇ unimers. To further investigate this, cryo-TEM was performed on micellar IPECs of all three BVqMANa_x / EO₃₂₅Dq₁₅₇ combinations at a representative $Z_{+/-}$ value. The results are shown in **Figure 5-6**.

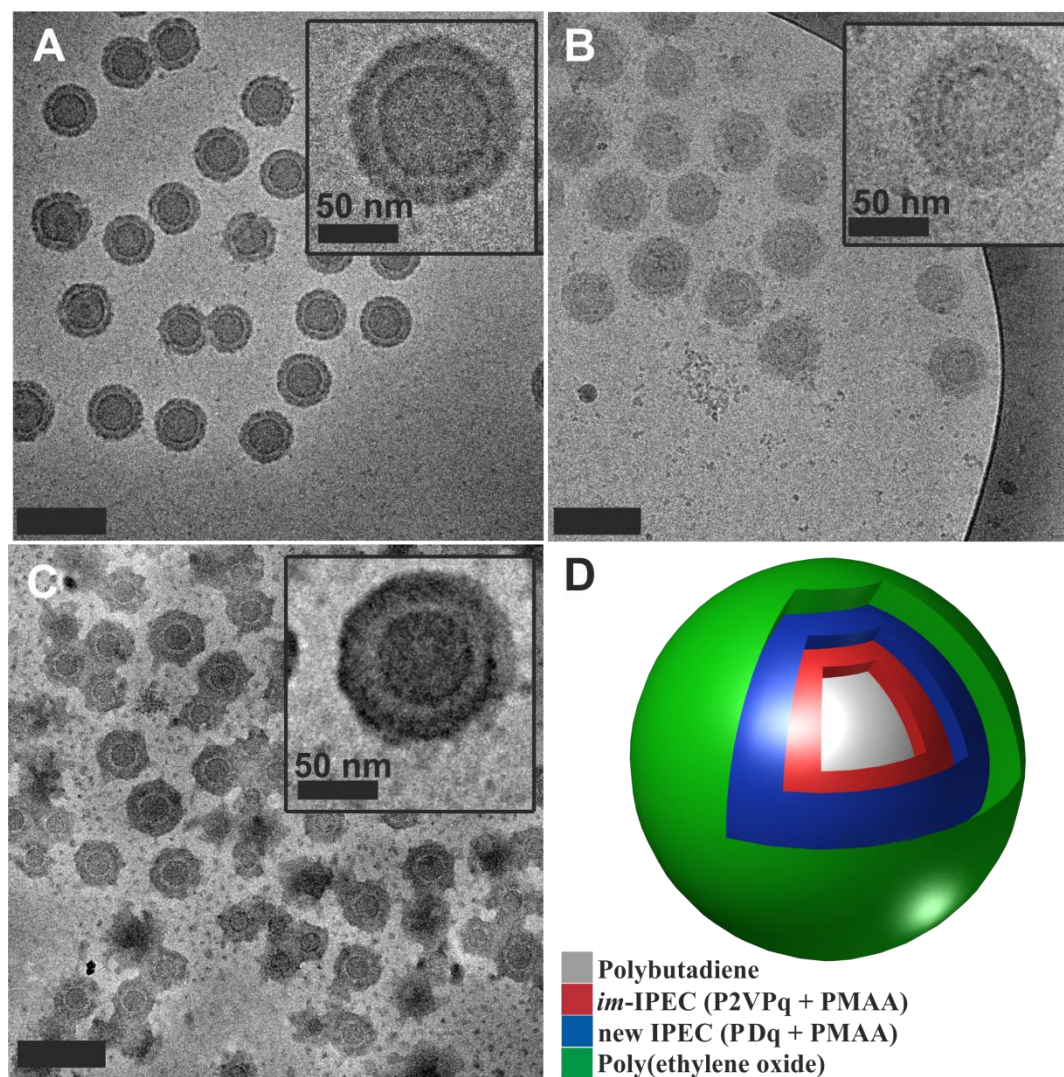


Figure 5-6: Cryo-TEM images for micellar IPECs of BVqMANa₃₄₅ / EO₃₂₅Dq₁₅₇ at $Z_{+/-} = 1.0$ (A); BVqMANa₄₆₅ / EO₃₂₅Dq₁₅₇ at $Z_{+/-} = 1.0$ (B); BVqMANa₅₅₀ / EO₃₂₅Dq₁₅₇ at $Z_{+/-} = 0.5$ (C); the insets in each part show a single double-layered particle at higher magnification; schematic depiction of the double-layered IPEC structure (D); all scalebars except for the insets correspond to 200 nm.

In general, the observed structures are similar, as shown in **Figure 5-6A-C**. In all images large, spherical objects with a grey core (B) and a thin, dark ring around the core (the former, patchy *im*-IPEC shell, Vq + MANa) are found. Both are surrounded by a lighter grey shell, followed by the newly formed second IPEC shell, appearing dark grey. The complex micelles of BVqMANa₃₄₅ and BVqMANa₄₆₅ show a rather homogeneous distribution, whilst BVqMANa₅₅₀ exhibits complexes at different stages of IPEC formation. For all three samples the double-layered character can be nicely confirmed. This is also shown in three insets in **Figure 5-6A-C**, each depicting a single IPEC particle. In case of BVqMANa₄₆₅ / EO₃₂₅Dq₁₅₇ (**Figure 5-6B**), the distinction between the

different shells is less pronounced than for the other two combinations. This could be due to ice-crystals that formed during the rapid vitrification of the sample for cryo-TEM measurement. Further, in **Figure 5-6C** (BVqMANa₅₅₀ / EO₃₂₅Dq₁₅₇), small dark dots can be seen. These aggregates exhibit an average core diameter of around 12 nm. This is far too small to refer to any of the used precursor micelles and could possibly represent the smallest distribution which was observed during DLS measurements. We tentatively try to explain this rather puzzling fact through aggregate formation from excess EO₃₂₅Dq₁₅₇. However, the driving force for such a behavior at the relatively low $Z_{+/-}$ value of 0.5 remains elusive. An alternative was to use a lower $Z_{+/-}$ ratio of 0.25. In this case, no such aggregates were found (**Figure 5-7 B**, for the DLS data also see **Table 5-5**, entries 2, 5 and 8).

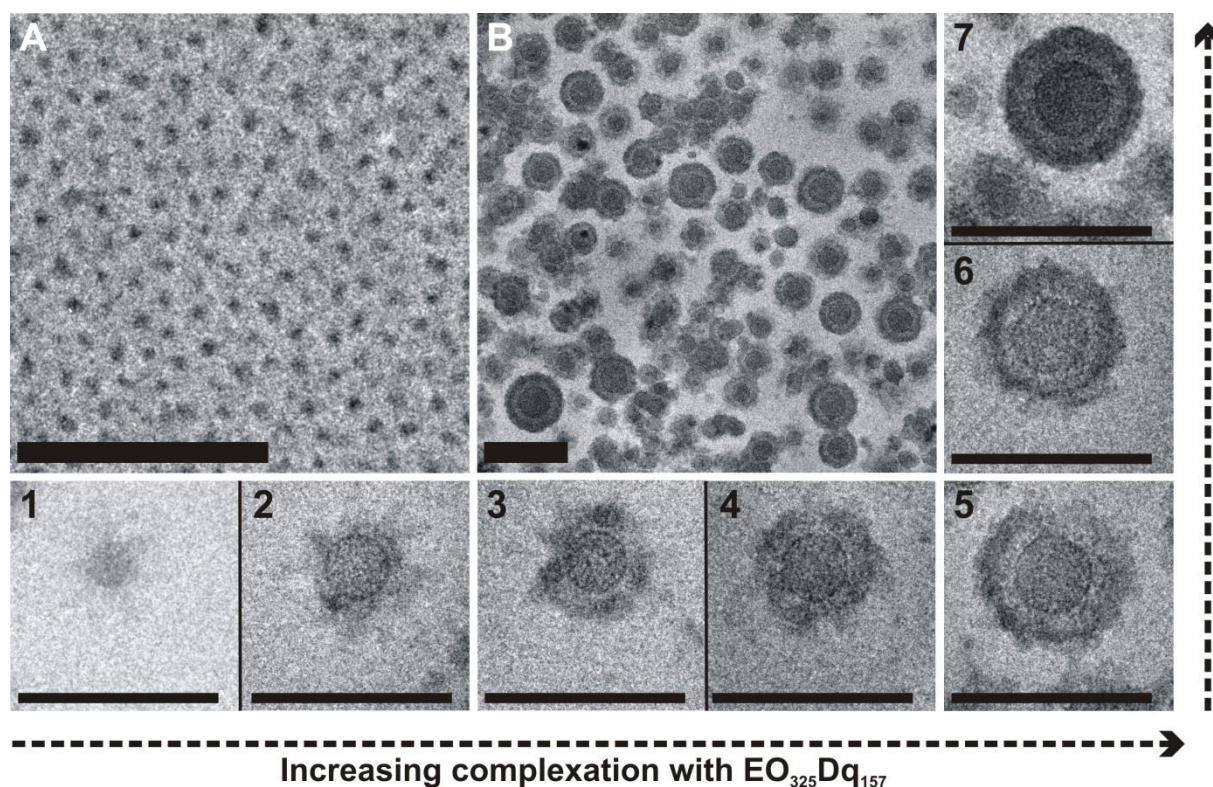


Figure 5-7: Cryo-TEM images of smaller aggregates formed for BVqMANa₅₅₀ / EO₃₂₅Dq₁₅₇ micellar IPECs at $Z_{+/-} = 0.5$ (A); BVqMANa₅₅₀ / EO₃₂₅Dq₁₅₇ at $Z_{+/-} = 0.25$ (B); the small micrographs (1-7, all were taken from the same sample) depict single micellar IPECs at different stages of complexation with EO₃₂₅Dq₁₅₇; all scalebars correspond to 200 nm.

Figure 5-7A shows the small aggregates formed for BVqMANa₅₅₀ / EO₃₂₅Dq₁₅₇ at $Z_{+/-} = 0.5$. If the amount of added EO₃₂₅Dq₁₅₇ is reduced ($Z_{+/-} = 0.25$, **Figure 5-7B**), micellar

IPECs at different stages of complexation are found, which is consistent with the increase in PDI as observed by DLS (**Table 5-5**, entries 7 and 8). We show a variety of examples, all found within the same cryo-TEM sample, shown in small micrographs 1-7 in **Figure 5-7** micrograph 1 depicts a precursor micelle of BVqMANa₅₅₀ (this was rather exceptional), and 2-6 then highlight different degrees of complexation and non-equilibrium 2nd IPEC shell formation. We believe that these structures represent non-equilibrium aggregates.

As already shown for the complexes with Dq homopolymers, the sizes of the individual compartments were estimated from the cryo-TEM images. The results are summarized in **Table 5-6**. It should be noted that, although for all three samples shown in **Figure 5-6A-C** hydrodynamic radii distributions of several hundred nm were found in DLS, structures of such dimensions were never observed during cryo-TEM. We therefore ascribe the DLS results again to a certain clustering of the micellar IPECs in solution.

Chapter 5 – Double-Layered Micellar Interpolyelectrolyte Complexes – How Many Shells to a Core?

Table 5-6: Average sizes determined for the individual compartments of BVqMANa_x / EO₃₂₅Dq₁₅₇ complexes as determined by analysis of the cryo-TEM images.

Compartment	BVqMANa ₃₄₅ [nm]	BVqMANa ₃₄₅ / EO ₃₂₅ Dq ₁₅₇ Z _{+/-} = 1.0 [nm]	BVqMANa ₄₆₅ [nm]	BVqMANa ₄₆₅ / EO ₃₂₅ Dq ₁₅₇ Z _{+/-} = 1.0 [nm]	BVqMANa ₅₅₀ [nm]	BVqMANa ₅₅₀ / EO ₃₂₅ Dq ₁₅₇ Z _{+/-} = 0.25 [nm]	BVqMANa ₅₅₀ / EO ₃₂₅ Dq ₁₅₇ Z _{+/-} = 0.5 [nm]
R _{Micelle}	79.5 ± 7	62.5 ± 7	93.5 ± 8	64 ± 7	91 ± 11	60.5 ± 8	61 ± 9
R _{Core}	38 ± 5	35 ± 3	37 ± 8	32 ± 5	33.5 ± 4	25 ± 5	23 ± 5
D _{im-IPEC}	5 ± 2	7 ± 2	3 ± 1	7.5 ± 2	4 ± 1	4.4 ± 1	5 ± 2
D _{Corona / 2nd IPEC Shell}	40 ± 5	24 ± 3	52 ± 6	27 ± 3	53 ± 9	28 ± 5	28 ± 6
N _{agg} ^a	3,200	2,500	3,000	1,900	2,200	900	700

a: estimated with Eq. 2;

According to the image analysis, the overall radius of all micellar IPECs after complexation reaches a value of around 60 nm, when EO₃₂₅Dq₁₅₇ is used for the formation of the outer IPEC shell. However, the size of the individual compartments does vary significantly. As already observed for the complexes with Dq homopolymers, the size of the B core decreases with increasing MANa block length (N_{agg} decreases), while the size of the outmost shell increases only marginally. Interestingly, here the size of the individual compartments is the same as for the Dq homopolymers within the experimental error. Compared to the precursor micelles, the size of the B core (and N_{agg} , if estimated with Eq. 2) decreases by 8 % (BVqMANa₃₄₅), 13.5 % (BVqMANa₄₆₅), and 25 % / 31 % (BVqMANa₅₅₀, $Z_{+/-} = 0.25 / 0.5$), respectively. Both the decrease in size observed for the micellar core and the collapse of the corona through the complex formation were also observed for the Dq complexes described earlier. This again indicates that such micellar particles are dynamic and “adjust” to changes in the surrounding conditions, *i.e.* to the formation of the 2nd IPEC shell.

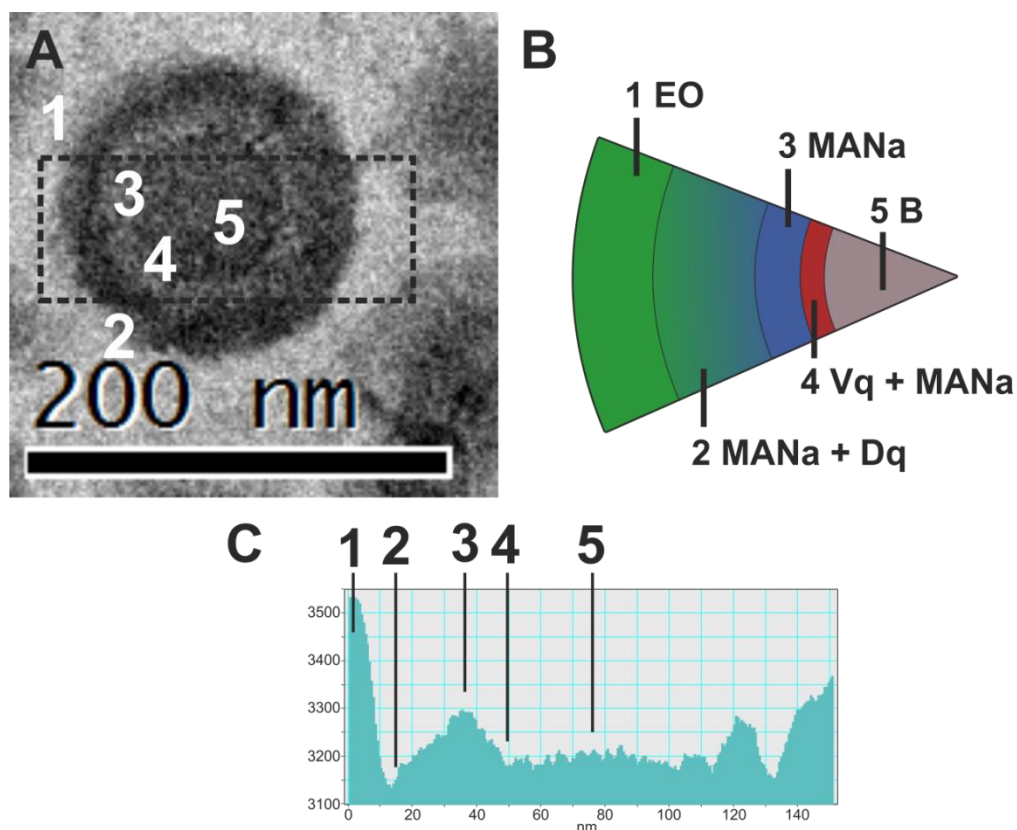


Figure 5-8: Cryo-TEM image of a single micellar IPEC of BVqMANa₅₅₀ / EO₃₂₅Dq₁₅₇ at $Z_{+/-} = 0.25$; the black box highlights the area used for the greyscale analysis (A); circle segment showing the five different regions identified *via* greyscale analysis (B); greyscale analysis of the particle in part A, the numbers correspond to the respective areas (C).

To our opinion the lighter grey shell, surrounding the former *im*-IPEC shell of the precursor micelles, resembles uncomplexed MANa. Covering this MANa shell, a dark grey ring, presumably the newly formed IPEC between Dq and MANa, can be seen. To further evaluate the multi-layered character of these complex micelles, the micrographs were submitted to grayscale analysis. This is shown in **Figure 5-8**.

A single double-layered IPEC micelle is shown in **Figure 5-8A**. Clearly, two different shells around the soft B core are visible. The box drawn around the aggregate was used for the grey-scale analysis, which is shown in **Figure 5-8C**. The grey-scale analysis identifies five different regions: region 1, with the lowest contrast, is the EO corona; 2, exhibiting the highest electron density, is presumably newly formed IPEC between Dq and MANa; 3, uncomplexed MANa; 4, formerly the discontinuous shell of the BVqMANa_x precursor micelles; and 5, the soft B core. The former patchy shell of the precursor micelles is rather thin with approx. 4 nm thickness, The newly formed shell(s) exhibit a combined thickness of around 28 nm. The core, with 50 nm diameter contracted, as compared to the precursor micelles in **Figure 5-1C**. The different compartments of the micellar IPECs are also schematically depicted in the circle segment in **Figure 5-8B**. Finally, the size of the surrounding EO corona cannot be estimated from the cryo-TEM micrographs as its electron density is too low. Eventually, the greyscale analysis also confirms the existence of double-layered micellar IPECs at this stage.

Conclusions

We showed that by mixing of different negatively charged BVqMANa_x block terpolymer precursor micelles with oppositely charged Dq or EO-*b*-Dq diblock copolymers in aqueous solution at pH 10 well-defined core-shell-shell-(corona) aggregates with two distinguishable IPEC shells can be prepared. We refer to these aggregates as double-layered IPECs, as both shells are formed as a result of the complexation between two oppositely charged polyelectrolytes. It turned out that the block terpolymer composition used for the preparation of the precursor micelles plays a crucial role as it affects the overall hydrophilic-to-hydrophobic balance of these aggregates.

If quaternized homopolymers (Dq) are used for the formation of the outer IPEC shell, stable micellar core-shell-shell-corona IPECs could be prepared up to a critical $Z_{+/-}$ ratio.

Here, remaining uncomplexed MANa serves as the corona. Above that critical $Z_{+/-}$ value, further aggregation of the particles occurred. Further, under the rather dilute conditions reported here, the length of the added Dq was not observed to be crucial. If similar complexation reactions were performed using EO₃₂₅Dq₁₅₇ diblock copolymers, surprisingly, large aggregates were found above the same critical $Z_{+/-}$ ratios, although a water-soluble EO corona was formed. Additionally, in samples of BVqMANa₅₅₀ treated with the double-hydrophilic diblock copolymer above $Z_{+/-} = 0.25$ small aggregates were observed in addition to the micellar IPECs, which we tentatively propose to consist of excess EO₃₂₅Dq₁₅₇. Overall, at optimized $Z_{+/-}$ ratios well-defined core-shell-shell-corona micellar IPECs were formed and the existence of a multi-layered structure was confirmed by cryo-TEM and greyscale analysis.

Some open questions remain: how does the dynamic character of the precursor micelles affect the formation of the outer IPEC layer? Can one make use of the different chemistries present in both adjacent IPEC shells (We could already show that within the IPEC formed between MANa and Vq the formation of narrowly dispersed gold nanoparticles is possible.²⁷)? Why does a truly double-hydrophilic block copolymer, EO₃₂₅Dq₁₅₇, form aggregates in dilute aqueous solutions? We are currently pursuing these issues and hope to be able to address all points in further contributions.

Acknowledgements

This work was supported by the *VolkswagenStiftung* within the framework “Complex Materials”. The authors would like to thank D.V. Pergushov for helpful discussions. E. Betthausen is acknowledged for the quaternization of PEO-*b*-PDMAEMA during her advanced lab course. C. V. Synatschke acknowledges a scholarship from the state of Bavaria under BayEFG as well as support from the Elite Network of Bavaria.

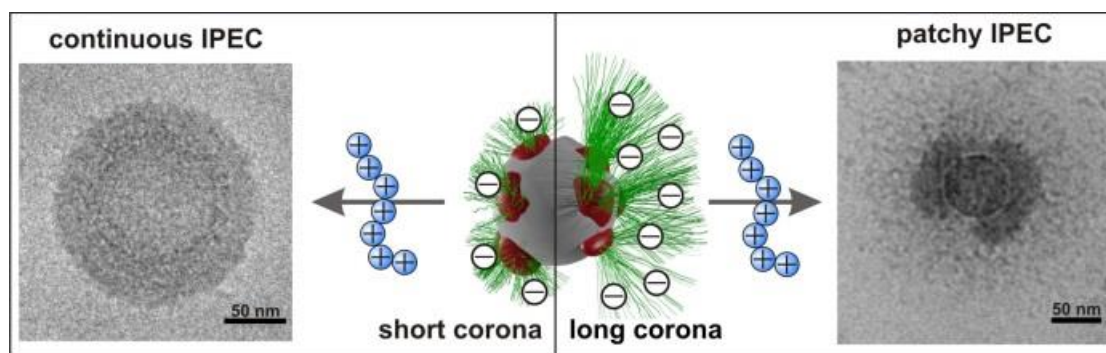
References

1. G. Riess, *Progress in Polymer Science* **2003**, *28*, 1107-1170.
2. C. A. Fustin, V. Abetz and J. F. Gohy, *European Physical Journal E* **2005**, *16*, 291-302.
3. M. Burkhardt, N. Martinez-Castro, S. Tea, M. Drechsler, I. Babin, I. Grishagin, R. Schweins, D. V. Pergushov, M. Gradzielski, A. B. Zezin and A. H. E. Müller, *Langmuir* **2007**, *23*, 12864-12874.
4. J. F. Gohy, N. Willet, S. Varshney, J.-X. Zhang and R. Jerome, *Angewandte Chemie – International Edition* **2001**, *40*, 3214-3216.
5. X. Wang, G. Guerin, H. Wang, Y. Wang, I. Manners and M. A. Winnik, *Science* **2007**, *317*, 644-647.
6. T. Gädt, N. S. Jeong, G. Cambridge, M. A. Winnik and I. Manners, *Nature Materials* **2009**, *8*, 144-150.
7. H. Schmalz, J. Schmelz, M. Drechsler, J. Yuan, A. Walther, K. Schweimer and A. M. Mihut, *Macromolecules* **2008**, *41*, 3235-3242.
8. D. E. Discher and A. Eisenberg, *Science* **2002**, *297*, 967-973.
9. H. Cui, Z. Chen, S. Zhong, K. L. Wooley and D. J. Pochan, *Science* **2007**, *317*, 647-650.
10. Z. Li, M. A. Hillmyer and T. Lodge, *Langmuir* **2006**, *22*, 9409-9417.
11. G. Njikang, D. Han, J. Wang and G. Liu, *Macromolecules* **2008**, *41*, 9727-9735.
12. A. Walther, A. S. Goldmann, R. S. Yelamanchili, M. Drechsler, H. Schmalz, A. Eisenberg and A. H. E. Müller, *Macromolecules* **2008**, *41*, 3254-3260.
13. S.-C. Chen, S.-W. Kuo, C.-S. Liao and F.-C. Chang, *Macromolecules* **2008**, *41*, 8865-8876.
14. Z. Zhu, J. Xu, Y. Zhou, X. Jiang, S. P. Armes and S. Liu, *Macromolecules* **2007**, *40*, 6393-6400.
15. F. A. Plamper, J. R. McKee, A. Laukkanen, A. Nykänen, A. Walther, J. Ruokolainen, V. Aseyev and H. Tenhu, *Soft Matter* **2009**, *5*, 1812-1821.
16. A. Harada and K. Kataoka, *Science*, **1999**, *283*, 65-67.
17. K. Kataoka, H. Togawa, A. Harada, K. Yasugi, T. Matsumoto and S. Katayose, *Macromolecules* **1996**, *29*, 8556-8557.
18. J. Koetz and S. Kosmella, *Polyelectrolytes and Nanoparticles*, Springer Verlag, Berlin, **2007**.
19. K. S. Schanze and A. H. Shelton, *Langmuir* **2009**, *25*, 13698-13702.
20. V. A. Kabanov, *Russian Chemical Reviews* **2005**, *74*, 3-20.
21. N. Lefevre, C. A. Fustin and J. F. Gohy, *Macromolecular Rapid Communications* **2009**, *30*, 1871-1888.
22. D. V. Pergushov, O. V. Borisov, A. B. Zezin and A. H. E. Müller, *Advances in Polymer Science* **2011**, *241*, 131-161.
23. P. S. Chelushkin, E. A. Lysenko, T. K. Bronich, A. Eisenberg, V. A. Kabanov and A. V. Kabanov, *Journal of Physical Chemistry B* **2007**, *111*, 8419-8425.
24. P. S. Chelushkin, E. A. Lysenko, T. K. Bronich, A. Eisenberg, V. A. Kabanov and A. V. Kabanov, *Journal of Physical Chemistry B* **2008**, *112*, 7732-7738.
25. M. Burkhardt, M. Ruppel, S. Tea, M. Drechsler, R. Schweins, D. V. Pergushov, M. Gradzielski, A. B. Zezin and A. H. E. Müller, *Langmuir* **2008**, *24*, 1769-1777.
26. D. V. Pergushov, E. V. Remizova, J. Feldthusen, A. B. Zezin, A. H. E. Müller and V. A. Kabanov, *Journal of Physical Chemistry* **2003**, *107*, 8093-8096.
27. F. Schacher, E. Betthausen, A. Walther, H. Schmalz, D. V. Pergushov and A. H. E. Müller, *ACS Nano* **2009**, *3*, 2095-2102.

28. F. Schacher, A. Walther and A. H. E. Müller, *Langmuir* **2009**, *25*, 10962-10969.
29. F. Schacher, J. Yuan, H. G. Schoberth and A. H. E. Müller, *Polymer* **2010**, *51*, 2021-2032.
30. F. Schacher, M. Müllner, H. Schmalz and A. H. E. Müller, *Macromolecular Chemistry and Physics* **2009**, *210*, 256-262.
31. F. A. Plamper, A. Schmalz, E. Penott-Chang, M. Drechsler, A. Jusufi, M. Ballauff and A. H. E. Müller, *Macromolecules* **2007**, *40*, 5689-5697.
32. F. Schacher, A. Walther, M. Ruppel, M. Drechsler and A. H. E. Müller, *Macromolecules* **2009**, *42*, 3540-3548.
33. A. Walther and A. H. E. Müller, *Chemical Communications* **2009**, 1127-1129.
34. O. V. Borisov and E. B. Zhulina, *Macromolecules* **2002**, *35*, 4472-4480.
35. S. V. Larin, A. A. Darinskii, E. B. Zhulina and O. V. Borisov, *Langmuir* **2009**, *25*, 1915-1918.
36. L. Samokhina, M. Schrunner and M. Ballauff, *Langmuir* **2007**, *23*, 3615-3619.
37. D. V. Pergushov, I. A. Babin, F. A. Plamper, A. B. Zezin and A. H. E. Müller, *Langmuir* **2008**, *24*, 6414-6419.
38. M. Shibayama, T. Karino and S. Okabe, *Polymer* **2006**, *47*, 6446-6456.

Chapter 6

Micellar Interpolyelectrolyte Complexes with a Compartmentalized Shell



The results presented in this chapter have been published in *Macromolecules* as:

“Micellar Interpolyelectrolyte Complexes with a Compartmentalized Shell”

by Christopher V. Synatschke, Tina I. Löblich, Melanie Förtsch, Andreas Hanisch, Felix H. Schacher,^{*} and Axel H. E. Müller^{*}

Reprinted with permission from *Macromolecules* **2013**, *46* (16), pp. 6466-6474.
Copyright 2013 American Chemical Society.

Abstract

We investigate the formation of micellar interpolyelectrolyte complexes (IPECs) from multicompartment micelles (MCMs) of polybutadiene-*block*-poly(1-methyl-2-vinylpyridinium methylsulfate)-*block*-poly(methacrylic acid) (BVqMAA) triblock terpolymers and polycations of opposite charge. As cationic material, predominantly a polymer with a high charge density is used: quaternized poly(2-((2-(dimethylamino)ethyl)methylamino)ethyl methacrylate) (PDAMAq), which carries two positive net charges per monomer unit. Upon IPEC formation at different charge stoichiometries, particles with a compartmentalized IPEC shell are formed. These rather unusual structures even form when both BVqMAA micelles and PDAMAq are mixed at rather high salinity, followed by dialysis, indicating that the structures formed are not kinetically trapped. Whereas the nature of the polycation seems to play a minor role, our studies suggest that the length of the PMAA corona is the key factor for the formation of a compartmentalized IPEC shell.

Introduction

Block copolymers have the ability to form a great variety of nanostructures both in the bulk and in solution through microphase separation originating from the intrinsic immiscibility between different polymer chains.¹ Understanding and controlling such self-assembly processes allows for the preparation of functional materials for various kinds of applications.² Some of these materials have been known for several decades, for example the use of ABA-type block copolymers as thermoplastic elastomers (Kraton[®]) or as polymeric emulsifiers (Pluronic[®]). In recent years, other fields have also demonstrated the potential of block copolymer nanostructures for different purposes. As such, semiconducting polymers with precisely tuned bandgaps can act as organic solar cells, transforming light into electricity or in the reverse process as organic light emitting diodes.³ Also, thin films of block copolymers have been used as templates for the deposition of inorganic materials⁴ and in lithographic applications,⁵ where well-defined domain sizes and periodic structures are desirable.^{6,7} In solution, block copolymers form well-defined micelles or vesicles, depending on the volume fraction of solvophobic and solvophilic segments. Apart from studying the underlying principles of structure formation,⁸ such particular systems have already been extensively used for the transportation of therapeutic cargos in biomedical applications. Often, hydrophobic drug molecules are enclosed in the core of such micelles, thereby enhancing solubility, circulation time, and bio-availability at the same time.⁹ Further, ionic cargo such as plasmid DNA,¹⁰⁻¹² small interference RNA^{13,14} and photosensitizers¹⁵ have been encapsulated as well, when ionic diblock copolymers were used for micellization.

The level of structural variety and complexity of the resulting structures increases dramatically as compared to diblock copolymers when ternary or even quaternary block copolymers are considered. Already for ABC triblock terpolymers, a vast library of bulk structures has been found.^{16,17} In solution-based structures, the additional segment can lead to further segregation of core or corona. Core-segregated micelles are often termed multicompartment micelles (MCM), and are an interesting class of materials, since they can combine different chemical environments in close proximity. Common examples for a compartmentalization of the core were achieved with triblock terpolymers containing a hydrocarbon and a fluorocarbon block.^{18,19} Janus particles can be seen as an extreme case of nanostructures with a phase separated corona, since it is strictly segregated into two hemispheres.²⁰⁻²³ MCMs are potentially useful as nanoreactors or multifunctional drug

carriers, as has been reviewed recently.²⁴ Individual MCMs from triblock terpolymers can further be used as building blocks for the formation of even larger superstructures, as has been shown in a controlled manner by controlling the kinetic pathway via suitable solvent sequences.²⁵

If more than three (core, shell, corona) individual compartments within micellar structures are targeted, one possibility would be the use of ABCD tetrablock quaterpolymers. However, their synthesis is challenging and often limited to certain block sequences. We have recently shown that interpolyelectrolyte complex (IPEC) formation between charged MCMs from amphiphilic and ampholytic triblock terpolymers and oppositely charged homopolymers or diblock copolymers can be used to generate well-defined and multi-layered soft nanoparticles. The IPEC formation is driven by both electrostatic interactions and a gain in entropy for the whole system *via* the release of low molecular weight counterions.^{26,27} Our initial system was based on polybutadiene-*block*-poly(1-methyl-2-vinylpyridinium)-*block*-poly(methacrylic acid) (BVqMAA) triblock terpolymers, which formed MCMs with a negatively charged poly(methacrylic acid) (PMAA) corona in aqueous media.²⁸⁻³⁰ The structures featured a soft and dynamic polybutadiene (PB) core and a patchy shell, consisting of intramicellar interpolyelectrolyte complexes (*im*-IPECs) between positively charged poly(1-methyl-2-vinylpyridinium) (P2VPq) and PMAA. We demonstrated that additional shells can be formed by adding either quaternized poly(2-(dimethylamino)ethyl methacrylate) (PDMAEMAq) or double hydrophilic block copolymers of P2VPq or PDMAEMAq with poly(ethylene oxide) (VqEO or DqEO).^{28,30} This facile approach can also be used to introduce new functionalities, e.g. a thermo-responsiveness, by using poly(sodium acrylate)-*block*-poly(*N*-isopropylacrylamide) as a complexing polymer to form a PNiPAAm corona to an MCM with inverse sequence of charges, polybutadiene-*block*-poly(sodium methacrylate)-*block*-poly(2-((methacryloyloxy)ethyl)trimethylammonium methylsulfate) (BMAADq).³¹

In the work presented here, we extend our concept to polycations with higher charge density, poly(2-((2-(dimethylamino)ethyl)methylamino)ethyl methacrylate) (PDAMAq), quaternized with methyl iodide, carrying two positive charges per monomer unit. Complex formation was carried out with two different BVqMAA systems, where PB and P2VPq are of the same length but with a shorter (DP = 400) and longer (DP = 1350) PMAA corona. In case of the long PMAA corona, we found rather unexpected structures with a compartmentalized IPEC shell for charge ratios, $Z_{+/-}$, below 0.7. The micellar IPECs were

in all cases characterized in detail by cryogenic transmission electron microscopy (cryo-TEM) and dynamic light scattering (DLS).

Experimental Part

Materials

trans-2-[3-(4-*tert*-Butylphenyl)-2-methyl-2-propenylidene]malononitrile (DCTB, 99.0 %, Aldrich), silver trifluoroacetate (AgTFA, 99.99 %, Aldrich), basic aluminum oxide (Sigma-Aldrich), ammonia solution (32 %, VWR International), HCl (37 %, VWR International) and pH 10 buffer solution (Titrimorm, VWR International) with an ionic strength of approximately 0.05 M were used as received. Dioxane, methanol, isopropanol, anisole and chloroform were of analytical grade and used as received. Deuterated chloroform and deuterated water were provided by Deutero (Kastellaun, Germany). For anionic polymerization THF (Sigma-Aldrich, p.a. quality) was first distilled over CaH₂ followed by a distillation over potassium and stored under N₂ before use. Butadiene (Rießner-Gase, 2.5) was purified by passing through columns filled with molecular sieves (4 Å) and basic aluminum oxide, before condensation into a glass reactor and storage over dibutylmagnesium. 2-Vinylpyridine (97 %, Aldrich) was de-inhibited by passing through a basic aluminium oxide column, subsequently stirred for 30 min with 2 mL of trioctylaluminium per 10 mL of 2-vinylpyridine and finally condensed to a sealable glass ampule under reduced pressure. *tert*-Butyl methacrylate (*t*BMA, 98 %, Aldrich) was stirred with 0.5 mL of trioctylaluminium per 10 mL of *t*BMA for 30 min and then condensed to a sealable ampule under reduced pressure. 1,1-Diphenylethylene (DPE, Aldrich, 97 %) was stirred with *sec*-Butyllithium (*sec*-BuLi) under N₂ and then distilled. *sec*-BuLi (Aldrich, 1.4 M in cyclohexane), dibutylmagnesium (Aldrich, 1M in heptane) and trioctylaluminum (Aldrich, 25 wt. % in hexane) were used as received. For the synthesis of the 2-((2-(dimethylamino)ethyl)methylamino)ethyl methacrylate (DAMA) monomer, 2-((2-(dimethylamino)ethyl)methylamino)ethanol (98 %, Aldrich), methacryloyl chloride (97 %, Fluka), triethyl amine (99 %, Merck) and dry pyridine were used without further purification. RAFT polymerization was achieved with 2-(2-cyanopropyl)dithio benzoate (CPDB, 97 %, Aldrich) as chain transfer agent and azobisisobutyronitrile (AIBN, 98 %, Aldrich) as initiator, which were used without further purification. Quaternization reactions were performed with either methyl iodide (99 %, Merck) in case of PDAMA or dimethyl sulfate (Me₂SO₄, >99 %, Aldrich) for 2-

vinylpyridine and were used without further purification. Milli-Q water purified with a Millipore filtering system was used in all cases. For dialysis, membranes made from regenerated cellulose (Spectrum Laboratories, Spectra/Por MWCO 3.5 kDa and 12-14 kDa) were used.

Synthesis of Polybutadiene-*block*-poly(2-vinylpyridine)-*block*-poly(*tert*-butyl methacrylate) (BVT) Block Terpolymers

Sequential living anionic polymerization with *sec*-BuLi as initiator and THF as solvent in a laboratory autoclave (2.5 L) at low temperatures was used for the synthesis of BVT triblock terpolymers. The procedure was carried out analogue to our previously published procedures (see **Scheme 6-S1**).^{16,32} During the polymerization of the *tert*-butyl methacrylate (*t*BMA) block, samples were withdrawn at different conversions, thereby creating polymers varying only in the block length of their final block, while both previous blocks are of the same length. In detail, 1.6 L of dry THF were placed in a 2.5 L laboratory autoclave (Büchi) and titrated at -20 °C with 1.6 mL of *sec*-BuLi solution (1.4 M in hexane) to remove any protic species that might terminate the polymerization and left to warm to room temperature overnight. The so-formed alkoxides exhibit stabilizing effects on the living chain end and in the case of *t*BMA well-defined polymers are accessible without addition of LiCl.³³ After cooling the reaction solution to -70 °C, 0.69 mL of *sec*-BuLi (1 eq., 9.66×10^{-4} mol) were added, followed by the addition of 63.5 mL of butadiene (41.91 g, 800 eq., 0.7748 mol) and polymerization for 8 h at -25 °C and further 2 h at -10 °C. 2-Vinylpyridine (21.68 g, 210 eq., 0.2062 mol) was added at -70 °C and stirred for 2 h, before 0.85 mL of DPE (5 eq., 4.815×10^{-3} mol) was injected and the solution stirred for 2.5 h at -50 °C. Then, at -70 °C, 167.9 g of *t*BMA (1200 eq., 1.181 mol) were added to the solution, which led to an immediate rise in the temperature to -60 °C. The reaction temperature was increased to -50 °C and approximately 1/3 of the reaction solution was withdrawn and quenched in degassed isopropanol (200 mL) after 40 min, 2 h and 8 h of reaction time, respectively. The final polymer was obtained after precipitation from THF containing butylated hydroxytoluene (BHT) as stabilizer into a 1/1 mixture of methanol and H₂O. The degrees of polymerization (DP) of each block were calculated from a combination of MALDI-ToF-MS of the polybutadiene block and ¹H NMR of the final triblock terpolymer and determined to be B₈₃₀V₁₈₀T₄₀₀ (40 min) and B₈₃₀V₁₈₀T₁₃₅₀ (8 h) for the two polymers used in this work, respectively. Size exclusion

chromatography (SEC) of the two polymers showed bimodal distributions in the elution curves of both polymers (**Figure 6-S1**), which come from a small amount of terminated BV diblock copolymer during the injection of *t*BMA monomer. The polydispersity indices (PDI) were determined to be 1.04 and 1.08 for B₈₃₀V₁₈₀T₄₀₀ and B₈₃₀V₁₈₀T₁₃₅₀, respectively.

Preparation of Polybutadiene-*block*-poly(1-methyl-2-vinylpyridinium methylsulfate)-*block*-poly(methacrylic acid) (BVqMAA) Precursor Micelles

In a typical reaction, 100 mg of the desired BVT triblock terpolymer were dissolved in 100 mL of dioxane and 200 eq. of Me₂SO₄ compared to the moles of 2-vinylpyridine units were added to the solution (**Scheme 6-S1**). After stirring at 40 °C for 5 d, 200 eq. of HCl (concentrated HCl, 37 %) per mol of *t*BMA units were added and the mixture was refluxed at 110 °C for 24 h and 48 h in case of the B₈₃₀V₁₈₀T₄₀₀ and B₈₃₀V₁₈₀T₁₃₅₀, respectively. Self-assembly of the resulting BVqMAA polymers was achieved through dialysis (MWCO = 12-14 kDa) to pH 10 buffer with an ionic strength of approximately 0.05 M over a period of at least three days.

Synthesis of 2-((2-(dimethylamino)ethyl)methylamino)ethyl methacrylate (DAMA)

In a 1 L 2-neck-flask equipped with a magnetic stir bar, 300 mL of dry pyridine, 67 mL of 2-((2-(dimethylamino)ethyl)methylamino)ethanol (0.414 mol, 1 eq.) and 115 mL of triethylamine (0.828 mol, 2 eq.) were mixed, sealed with a septum and purged with argon for 30 min. Then, the reaction mixture was cooled to 0 °C and 81 mL of methacryloyl chloride (0.828 mol, 2 eq.) was added slowly *via* a dropping funnel. The reaction mixture was allowed to warm to room temperature and stirred for 24 h before excess of methacryloyl chloride was converted to isopropyl methacrylate through addition of 15 mL isopropanol. After evaporation of the volatile components, the crude product was separated *via* column-chromatography using an eluent of chloroform/methanol/concentrated ammonia in a ratio of 100/10/1. The DAMA monomer was obtained after vacuum distillation as a clear colorless liquid in rather low yields (~ 20 %) and purity was proven with ¹H NMR spectroscopy (**Figure 6-S2**).

RAFT Polymerization of DAMA

In a typical reaction 1.00 g DAMA (4.67 mmol, 200 eq.), 5.20 mg 2-(2-cyanopropyl)dithio benzoate (CPDB, 2.35×10^{-2} mmol, 1 eq.), 1.00 mg AIBN (6.09×10^{-3} mmol, 0.25 eq.) and 4.00 mL anisole were placed in a round bottom flask sealed with a rubber septum and equipped with a stir bar. After purging the reaction mixture with argon for 30 min, the polymerization was started by placing the flask in an oil bath at 70 °C. Periodically, aliquots of 0.1 mL were removed with a gas-tight, argon flushed syringe for ^1H NMR analysis to monitor the conversion. The reaction was stopped after 5 h and 45 min at a conversion of 42 % by rapid cooling of the reaction mixture to room temperature and opening to air. Purification was achieved through dialysis to THF and subsequent freeze-drying from dioxane.

Quaternization of PDAMA

For the quaternization 0.0562 g of PDAMA (0.52 mmol of nitrogen atoms) was dissolved in 10 mL of deionized water and 0.25 mL methyl iodide (4.02 mmol, 7.7 fold excess compared to nitrogen atoms) was added. The solution was stirred for at least 48 h at room temperature. Excess quaternization agent was removed by dialysis against 20:80 and 50:50 water:dioxane mixtures for two days, respectively. Afterwards, the quaternized PDAMAq was freeze-dried and from ^1H NMR measurements a degree of quaternization of 100 % was determined, as indicated by the complete shift of the corresponding signals (Figure 6-2).

Characterization

Size Exclusion Chromatography (SEC). For the PB and BV precursor polymers and BVT triblock terpolymers, an instrument equipped with four PSS-SDVgel columns (5 μm , 8 \times 300 mm) with a porosity range from 10^2 to 10^5 Å (PSS Mainz, Germany) was used together with a differential refractometer and a UV detector at 260 nm. Measurements were performed in THF with a flow rate of 1 mL/min using toluene as internal standard at 40 °C. The system was calibrated with narrowly distributed 1,4-PB standards. SEC measurements of PDAMA were performed on a system equipped with a set of two columns (8 μm , 8 \times 300 mm), PL-aquagel-OH and PL-aquagel-OH-30 and a differential refractometer. A mixture of 60 % H_2O with 0.01 mol/L NaH_2PO_4 and 0.1 mol/L NaN_3 at

pH = 2.5 and 40 % methanol was used as eluent at an elution rate of 1 mL/min at 35 °C. PDMAEMA samples were used for calibration.

MALDI-ToF-MS. Measurements were performed on a Bruker Daltonics Reflex III instrument equipped with an N₂ Laser (337 nm) and an acceleration voltage of 20 kV in positive ion mode. Sample preparation was done according to the “dried-droplet” method. In detail, matrix (DCTB, conc. 20 mg / mL), analyte (conc. 10 mg / mL) and salt (AgTFA, conc. 10 mg / mL) were separately dissolved in THF, subsequently mixed in a ratio of 20/5/1 μ L. Approximately 1 μ L of the final mixture was applied to the target spot and left to dry under air.

¹H NMR. Spectra were recorded on a Bruker Ultrashield 300 machine with a 300 MHz operating frequency using either deuterated chloroform or deuterated water as solvents.

Dynamic Light Scattering (DLS). Measurements were performed on an ALV DLS/SLS-SP 5022F compact goniometer system with an ALV 5000/E cross correlator and a He–Ne laser ($\lambda = 632.8$ nm). The measurements were carried out in cylindrical scattering cells ($d = 10$ mm) at an angle of 90°. Angular-dependent light scattering experiments were performed at angles ranging from 30° to 120° with an interval of 10°. Prior to the measurements samples were passed through nylon filters (Magna, Roth) with a pore size of 5 μ m to remove impurities/dust particles. The CONTIN algorithm was applied to analyze the obtained correlation functions. Apparent hydrodynamic radii (harmonic z-average radius, $\langle R_h \rangle_{z,app.}$) were calculated according to the Stokes–Einstein equation and polydispersities were obtained *via* the cumulant analysis where applicable.

Zeta Potential. The zeta potential of micellar solutions was determined on a Malvern Zetasizer Nano ZS. The electrophoretic mobilities (u) were converted into zeta potentials *via* the Smoluchowski equation $\zeta = u\eta/\epsilon_0\epsilon$, where η denotes the viscosity and $\epsilon_0\epsilon$ the permittivity of the solvent (water). Values were determined in triplicate from the same sample.

Cryogenic Transmission Electron Microscopy (cryo-TEM). For cryo-TEM studies, a drop (~ 2 μ L) of the aqueous micellar solution ($c \sim 0.5$ g \times L⁻¹) was placed on a lacey carbon-coated copper TEM grid (200 mesh, Science Services), where most of the liquid was removed with filter paper, leaving a thin film spread between the carbon coating. The specimens were shock vitrified by rapid immersion into liquid ethane in a temperature-controlled freezing unit (Zeiss Cryobox, Zeiss NTS GmbH) and cooled to approximately

90 K. The temperature was monitored and kept constant in the chamber during all of the preparation steps. After freezing the specimens they were inserted into a cryo-transfer holder (CT3500, Gatan) and transferred to a Zeiss EM922 OMEGA EFTEM instrument. Measurements were carried out at temperatures around 90 K. The microscope was operated at an acceleration voltage of 200 kV. Zero-loss filtered images ($\Delta E = 0$ eV) were taken under reduced dose conditions. All images were recorded digitally by a bottom mounted CCD camera system (Ultrascan 1000, Gatan), and processed with a digital imaging processing system (Gatan Digital Micrograph 3.9 for GMS 1.4).

Results and Discussion

We have previously shown that polybutadiene-*block*-poly(1-methyl-2-vinylpyridinium)-*block*-poly(methacrylic acid) (BVqMAA) triblock terpolymers form multicompartment micelles in aqueous media with a polybutadiene core, an *im*-IPEC shell consisting of P2VPq and PMAA and a negatively charged corona of PMAA (when the degree of polymerization was higher for PMAA than for P2VPq). BVqMAA with different lengths of the PMAA segment were used and further complexation with VqEO or DqEO diblock copolymers or with quaternized PDMAEMAq led to multi-layered micellar IPECs, in case of DqEO even with a clearly distinguishable second IPEC shell.^{28,30} Herein, we investigate the complexation between BVqMAA with two different lengths of the corona segment (400 and 1350 repeating units) and poly(2-((2-(dimethylamino)ethyl)methylamino)ethyl methacrylate) (PDAMAq, **Scheme 6-1**), a polycation carrying two positive net charges per monomer unit and with a high structural similarity to PDMAEMAq. First, we shortly describe the structure of the BVqMAA before we focus on the preparation of PDAMAq using reversible addition fragmentation transfer (RAFT) polymerization, followed by subsequent quaternization. Afterwards, PDAMAq and BVqMAA are mixed at different ratios of positive to negative charges, $Z_{+/-}$, and the resulting structures are analyzed in detail with microscopic and light scattering techniques.

Characterization of the Precursor Micelles (BVqMAA₄₀₀ and BVqMAA₁₃₅₀)

The synthesis of the polybutadiene-*block*-poly(2-vinylpyridine)-*block*-poly(*tert*-butyl methacrylate) (BVT) triblock terpolymers has been described previously and was achieved through sequential living anionic polymerization in THF at low temperatures (see **Scheme 6-S1**).^{16,32} However, slight termination occurred upon addition of *t*BMA, shown in the SEC traces in **Figure 6-S1**. We expect traces of the BV diblock copolymer to be incorporated in the final micellar structures. The degrees of polymerization, DP, for each block and the characterization data of the two triblock terpolymers used for this study are given in **Table 6-1**. We describe materials with identical lengths of the first (PB) and second (P2VP) block, only differing in the length of the third segment, *Pt*BMA.

Table 6-1. Molecular characterization of BVT and BVqMAA triblock terpolymers.

Polymer ^{a)}	M _n [kg/mol]	PDI ^{d)}	Block weight fractions (PB; P2VP/P2VPq; PtBMA/PMAA)
B ₈₃₀ V ₁₈₀ T ₄₀₀	121 ^{b)}	1.04	0.37; 0.16; 0.47
B ₈₃₀ V ₁₈₀ T ₁₃₅₀	256 ^{b)}	1.08	0.18; 0.07; 0.75
B ₈₃₀ Vq ₁₈₀ MAA ₄₀₀	101 ^{c)}	-	0.45; 0.21; 0.34
B ₈₃₀ Vq ₁₈₀ MAA ₁₃₅₀	183 ^{c)}	-	0.24; 0.12; 0.64

a) Subscripts denote the degrees of polymerization of the respective blocks; b) calculated from a combination of MALDI-ToF-MS and ¹H NMR data; c) calculated from degrees of polymerization without taking the counterions of P2VPq into account; d) determined from SEC measurements with THF as eluent and linear polystyrene as calibration standard.

The transformation of BVT to BVqMAA was carried out according to procedures reported earlier.^{29,30} Briefly, the P2VP segment was quaternized using dimethyl sulfate, followed by hydrolysis of the PtBMA block to yield PMAA. The respective weight fractions of the constituting blocks before and after this modification route are also shown in **Table 6-1**. For BVqMAA₄₀₀, the PB has the largest weight fraction (45 %), followed by PMAA (34 %). On the other hand, for BVqMAA₁₃₅₀, the PMAA segment with 64 % has the largest weight fraction. Micelle formation was achieved through dialysis to aqueous buffer solution at pH 10 and the resulting MCMs were characterized with cryogenic transmission electron microscopy (cryo-TEM) and dynamic light scattering (DLS) (**Figure 6-1**).

Both BVqMAA₄₀₀ and BVqMAA₁₃₅₀ feature a PB core, a P2VPq/PMAA *im*-IPEC shell, and a PMAA corona, the latter being distinctly longer in case of BVqMAA₁₃₅₀. From DLS measurements, BVqMAA₄₀₀ micelles are slightly smaller with $\langle R_h \rangle_{z,app.} = 164$ nm (dispersity index, DI = 0.14) as compared to BVqMAA₁₃₅₀ with $\langle R_h \rangle_{z,app.} = 187$ nm (DI = 0.15). In case of BVqMAA₁₃₅₀, a minute fraction of aggregates at higher hydrodynamic radii can be seen. The size of the micellar core and corona was separately determined from the cryo-TEM micrographs by counting of at least 30 micelles (**Table 6-2**).

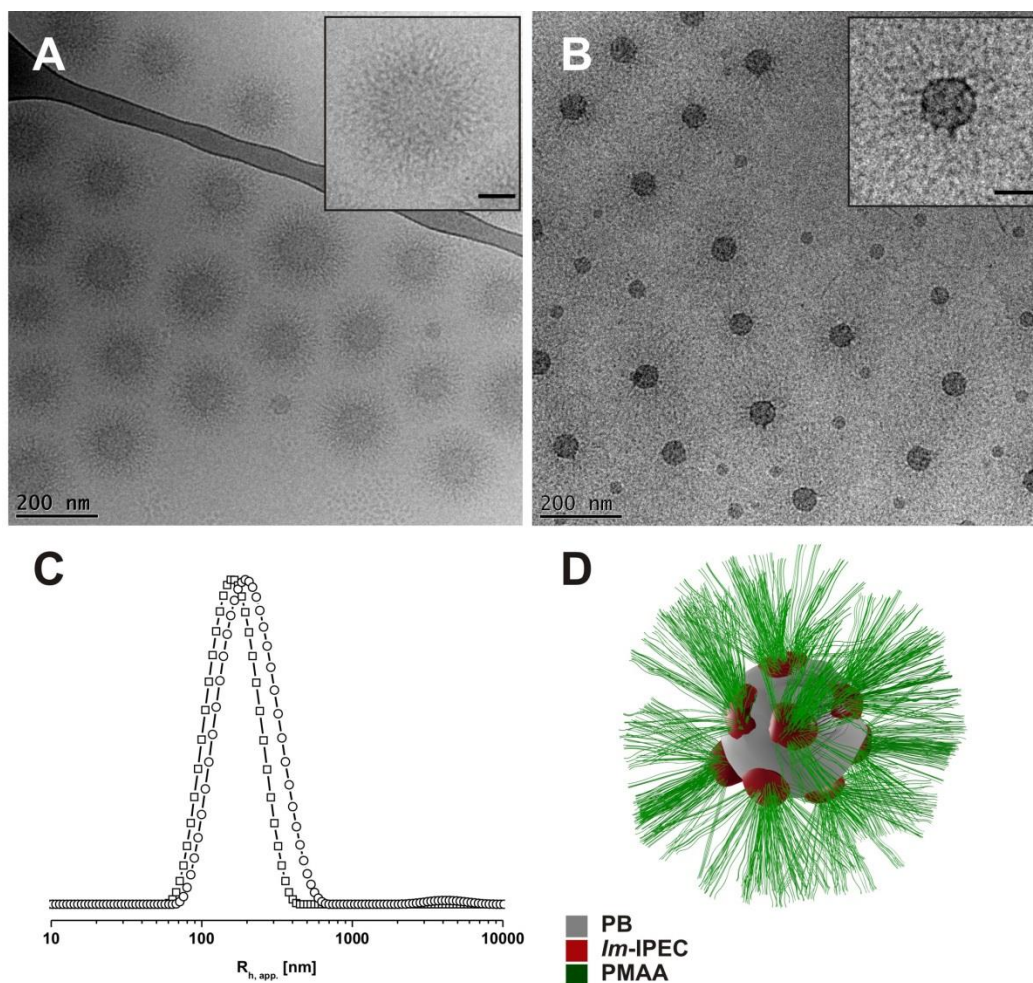


Figure 6-1. Cryo-TEM micrographs of BVqMAA₄₀₀ (A, conc. = 1.2 g/L) and BVqMAA₁₃₅₀ (B, conc. = 0.29 g/L) MCMs in pH 10 buffer with an ionic strength of ca. 0.05 M. Insets show enlargements of single micelles with the scalebar representing 50 nm. (C) Intensity weighted CONTIN plots of the same micellar solutions from DLS measurements, BVqMAA₄₀₀, \square , $\langle R_h \rangle_{z,app.} = 164$ nm, DI = 0.14; BVqMAA₁₃₅₀, \circ , $\langle R_h \rangle_{z,app.} = 187$ nm, DI = 0.15. (D) Schematic illustration of the proposed general MCM structure. The dimensions of individual compartments are not drawn according to scale.

Table 6-2. Number-average compartment sizes with standard deviation of the BVqMAA micelles as determined from cryo-TEM micrographs.

Compartment	BVqMAA ₄₀₀ [nm]	BVqMAA ₁₃₅₀ [nm]
$R_{micelle}$	114 ± 9	128 ± 16
R_{core}	46 ± 6	31 ± 3
D_{corona}	55 ± 7	-
$R_{micelle} - R_{core}$	68	97
$N_{agg.}$	5,500	1,700

We have used the half-distance between two micellar cores in **Figure 6-1** as an estimate of the micellar radius, R_{micelle} , confirming the trends from DLS measurements, although the overall sizes are smaller in cryo-TEM as compared to DLS data. This can be explained as the value from DLS represents a harmonic z-average radius, while cryo-TEM provides a number average. Furthermore, confinement of the micelles in the thin film during cryo-TEM measurements could lead to underestimation of the true micelle size in case of closely packed micelles. The core radii of BVqMAA₄₀₀ and BVqMAA₁₃₅₀ micelles differ significantly, even though the core-forming block is of the same length. BVqMAA₁₃₅₀ micelles have a core radius of 31 ± 3 nm, which is smaller than in case of BVqMAA₄₀₀ (46 ± 6 nm). From the core radius we roughly estimated the aggregation number, N_{agg} , according to **equation 6-1**, where we assumed the core to consist of pure PB. This assumption probably leads to an overestimation of the true N_{agg} since we did not take solvent molecules (e.g., dioxane) into account, which might be still trapped inside the core. Since we are mainly interested in the relative values of the two micelles the possible errors will cancel.

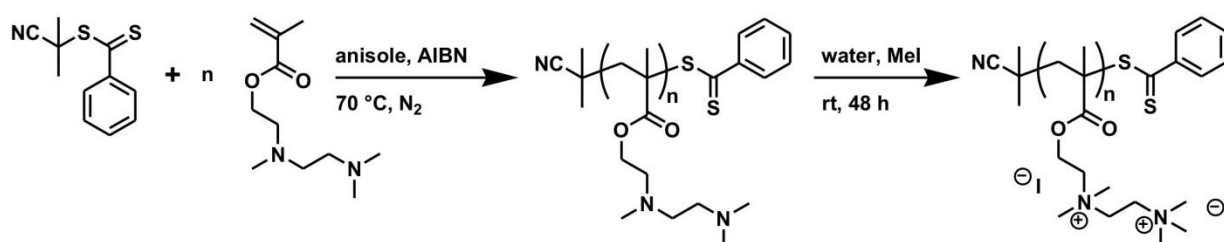
$$N_{\text{agg.}} = \frac{m_{\text{core}}}{m_{\text{PB}}^{\text{chain}}} = \frac{4 \cdot \pi \cdot N_A \cdot \rho_{\text{PB}} \cdot R_{\text{core}}^3}{3 \cdot M_{\text{PB}}^{\text{chain}}} \quad (6-1)$$

The calculated N_{agg} of BVqMAA₄₀₀ is approximately more than three times larger than that of BVqMAA₁₃₅₀. This is in accordance with theoretical prediction and our previous studies, where N_{agg} also decreased with increasing corona length.^{30,34} Due to the rather weak contrast, it was only possible to roughly determine the corona size of BVqMAA₄₀₀, but not that of BVqMAA₁₃₅₀. However, when subtracting R_{core} from the overall micelle radius, R_{micelle} , one can obtain an estimate of the corona size. Not surprisingly, this is considerably larger for BVqMAA₁₃₅₀ than for BVqMAA₄₀₀, by about 30 nm, highlighting the difference in hydrophilicity between the two triblock terpolymers presented here.

Synthesis of PDAMA

In comparison to our previous work using PDMAEMAq for further IPEC formation, here we were interested in polycations of similar structure, but with higher charge density. Poly(2-((2-(dimethylamino)ethyl)methylamino)-ethyl methacrylate) (PDAMA, **Scheme**

6-1) carries two amino groups per monomer unit. We were particularly interested in structural characteristics of micellar IPEC layers formed between PDAMAq and PMAA where we would expect a change in the IPEC compartment to a more dense structure due to the higher charge density in PDAMAq. The synthesis of PDAMA was first described by Sherrington et. *al.* by free radical polymerization and used as a chelating agent and polymeric support for copper complexes in the catalytic decomposition of the nerve agent Sarin.³⁵ Homo- and copolymers of PDAMA have already been used as non-viral gene transfection agents.³⁶⁻³⁸



Scheme 6-1. RAFT polymerization of DAMA and quaternization of PDAMA.

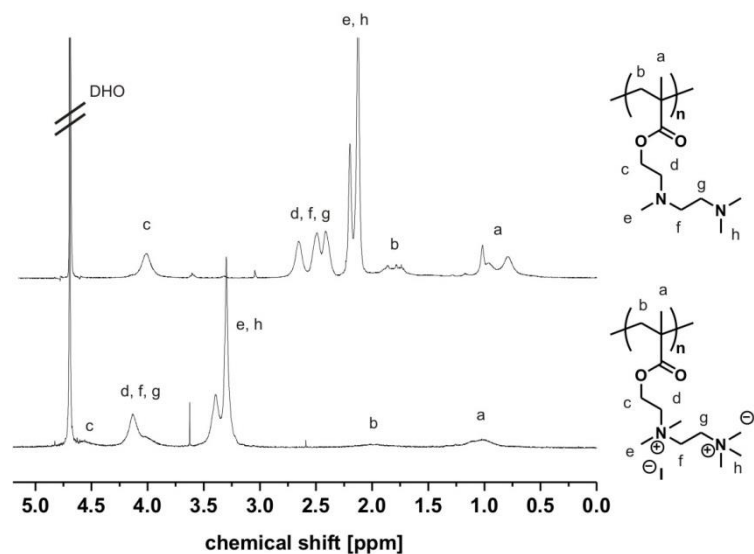


Figure 6-2. ¹H NMR spectra of PDAMA before (top) and after quaternization (bottom) in DHO.

We used RAFT polymerization to synthesize PDAMA of desired molecular weight. 2-(2-Cyanopropyl) dithiobenzoate (CPDB) was used as chain transfer agent (CTA) with AIBN as initiator in anisole as solvent, shown in **Scheme 6-1**. The DAMA/CTA/AIBN ratio was 200/1/0.25 the polymerization was conducted at 70 °C. After an induction period of about 50 min the polymerization started and the linearity of the first-order time-

conversion plot (**Figure 6-S3**) indicates a controlled polymerization. The reaction was quenched after 5.5 h, and a conversion of 42 % was determined from NMR measurements corresponding to a theoretical DP of 83 for PDAMA ($M_{n, \text{ theor.}} = 17,900 \text{ g/mol}$). SEC measurements of the resulting material proved to be rather difficult, presumably due to strong interaction of PDAMA with the column material in THF, DMF and DMAc as solvents. Even with a water/methanol mixture as eluent the interaction between column material and analyte was probably not fully suppressed and when using a PDMAEMA calibration a large deviation between theoretical and apparent molecular weight ($M_{n, \text{ app.}} = 65,500 \text{ g/mol}$; $M_{w, \text{ app.}} = 97,400 \text{ g/mol}$; PDI = 1.48) was observed. We therefore used the molecular weight of 17,900 g/mol calculated from conversion for the further description of PDAMA. Quaternization to PDAMAq was carried out by methylation of both tertiary nitrogens with methyl iodide. The ^1H NMR spectra before and after quaternization are given in **Figure 6-2**. Full quaternization was achieved, as can be seen from the complete shift of the $-\text{CH}_3$ signals e and h (9 protons at 2.0-2.3 ppm to 15 protons at 3.1-3.6 ppm) and $-\text{CH}_2-$ signals g, f and d (6 protons at 2.3-2.8 ppm to 6 protons at 3.8-4.3 ppm).

Micellar IPECs of BVqMAA₁₃₅₀ with PDAMAq

We first mixed PDAMAq with BVqMAA₁₃₅₀ micelles in pH 10 buffer solution, where PMAA is completely dissociated. The mixing ratio $Z_{+/-}$ is defined as the number of positive charges from the added polycation divided by the number of residual negative charges in the BVqMAA micelles (**equation 6-2**). The total amount of MAA units in the corona of the BVqMAA₁₃₅₀ micelles is reduced to 1170 by the *im*-IPEC formation with the 180 P2VPq units of the middle block. Therefore, $Z_{+/-} = 0$ refers to the pure BVqMAA₁₃₅₀ precursor micelles, while a ratio of 1 assumes that all MAA units are complexed.

$$Z_{+/-} = \frac{n_{\text{cationic}}}{n_{\text{anionic}}} = \frac{2 \cdot n_{\text{DAMAq}}}{n_{\text{MAA}} - N_{\text{Vq}}} \quad (6-2)$$

In the past, we observed remarkably slow kinetics for the IPEC formation when poly(1-methyl-2-vinylpyridinium methylsulfate)-*block*-poly(ethylene oxide) (VqEO) was used for complexation.²⁸ To ensure that complex formation was complete, here, the

micellar IPECs were stirred for at least one week after the addition of PDAMAq. Subsequently, the structures were analyzed using a combination of cryo-TEM and DLS (**Figure 6-3**). Stable micellar solutions were obtained for $Z_{+/-} \leq 0.75$, while macroscopic precipitation occurred at $Z_{+/-} = 0.9$, probably due to insufficient stabilization of the particles by PMAA. Zeta potential measurements of the micellar solutions in pH 10 buffer solution gave strongly negative values below -30 mV for all $Z_{+/-}$ values, ranging from 0 to 0.75 (see **Table 6-S1**) indicating that sufficient uncomplexed PMAA remains in the corona to stabilize the micelles. According to the cryo-TEM micrographs, low charge ratios ($Z_{+/-} = 0.1$) lead to a slight increase in the overall contrast within the corona, and the occurrence of small protrusions, attributed to IPEC compartments (**Figure 6-3A**, the inset shows a single object). More drastic structural changes can be seen at $Z_{+/-} = 0.25$, where newly formed IPEC patches can be clearly distinguished (**Figure 6-3B**). We expect these patches to consist of IPECs of PMAA and PDAMAq, collapsed due to charge neutralization, in analogy to earlier observations using PDMAEMAq.³⁰ However, instead of observing a rather homogeneous IPEC shell as before, distinct patches of a certain size are found. The proposed structure of such micellar IPECs with a patchy second IPEC shell is schematically illustrated in **Figure 6-3E**. With increasing $Z_{+/-}$, the patch size increases, as is expected for a further incorporation of PDAMAq chains. However, growth of the patches seems to proceed anisotropically along the *im*-IPEC/corona interface rather than radially outwards from the original patch. This is most prominent at $Z_{+/-} = 0.5$ (**Figure 6-3C**), where up to 3 patches per particle can be observed.

To better illustrate the growth of the patchy compartments with increasing $Z_{+/-}$ values, we counted the micelles from the available cryo-TEM images and sorted them into four categories (**Table 6-S2**) according to their compartment size. The four categories used are: no visible compartment, small compartment(s) enclosing less than half of the core, large compartment(s) enclosing more than half of the core and a complete shell. At low $Z_{+/-}$ values, only small compartments are formed, which grow in size with increasing amounts of added PDAMAq. When even more PDAMAq was added ($Z_{+/-} = 0.75$, **Figure 6-3D**), the majority of the structures features a complete second IPEC shell. In DLS experiments, Γ versus q^2 plots gave a linear relationship for all tested $Z_{+/-}$ values (**Figure 6-S4**) and the autocorrelation functions decreased monotonously (**Figure 6-S5**). The $\langle R_h \rangle_{z,app}$ at a scattering angle of 90° first decreases from 187 nm for $Z_{+/-} = 0$ (**Figure 6-1**) to 116 nm at $Z_{+/-} = 0.5$, while it again increases to 182 nm at $Z_{+/-} = 0.75$

(Figure 6-3F). The initial decrease is probably a result of corona contraction, while the increase of $\langle R_h \rangle_{z,app}$ and the dispersity index, DI, at higher $Z_{+/-}$ -ratios hints towards some aggregation.

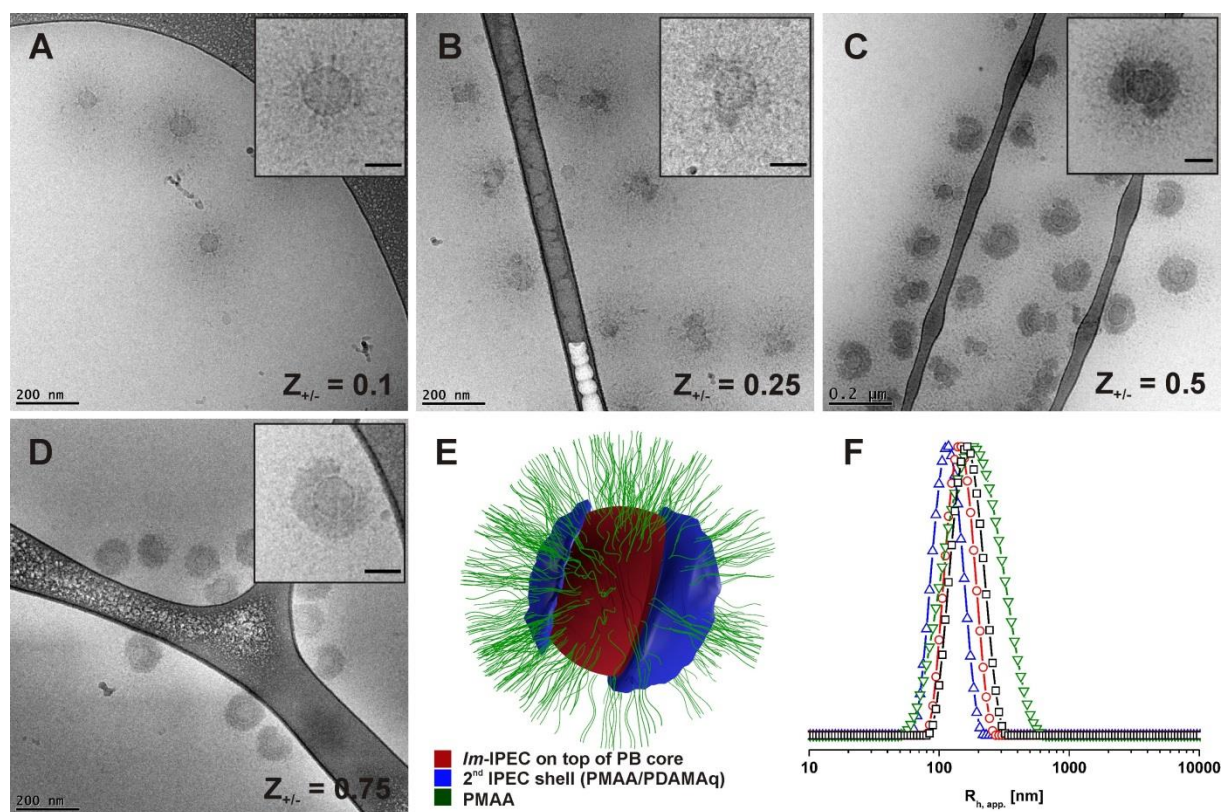


Figure 6-3. (A-D) Cryo-TEM micrographs of micellar IPECs of BVqMAA₁₃₅₀/PDAMAq with increasing charge ratios, $Z_{+/-} = 0.1, 0.25, 0.5$ and 0.75 in pH 10 buffer and an ionic strength of ca. 0.05 M; the scale bars represent 200 nm. The insets show single objects at higher magnification, the scale bars representing 50 nm. (E) Schematic representation of the proposed general structure of the micellar IPECs with two patches. (F) DLS CONTIN plots of micellar IPECs at different $Z_{+/-}$ (black \square : $Z_{+/-} = 0.1$, $\langle R_h \rangle_{z,app} = 166$ nm, DI = 0.07; red \circ : $Z_{+/-} = 0.25$, $\langle R_h \rangle_{z,app} = 145$ nm, DI = 0.05; blue \triangle : $Z_{+/-} = 0.5$, $\langle R_h \rangle_{z,app} = 116$ nm, DI = 0.06; green ∇ : $Z_{+/-} = 0.75$, $\langle R_h \rangle_{z,app} = 182$ nm, DI = 0.18) (F).

The spontaneous formation of anisotropic structures from a centrosymmetric precursor MCM through ionic interactions is rather unexpected. One possible explanation could be that the structures are kinetically trapped due to rapid initial IPEC formation as has been observed for BVqMAA micelles after the complexation with VqEO diblock copolymers.²⁸ As a result, insufficient chain mobility would prevent the relaxation to more energetically favorable structures, *i.e.* a homogeneous distribution of the IPEC around the core. To increase chain mobility, we increased the ionic strength of micellar IPECs from BVqMAA₁₃₅₀/PDAMAq with $Z_{+/-} = 0.5$ to approximately 0.55 M through the

addition of NaCl (pH 10 buffer with additional 500 mM NaCl). Under these conditions, the charges of the polyelectrolytes are screened and the IPEC shell is dissolved, resulting in a coexistence of BVqMAA₁₃₅₀ micelles and free PDAMAq chains. This is shown in **Figure 6-4A**, where the former patchy IPEC (PMAA/PDAMAq) has vanished and BVqMAA₁₃₅₀ micelles can be found. From these micrographs it is impossible to determine whether all PDAMAq chains are free in solution or if some PDAMAq still remains within the micellar corona. Even bare BVqMAA₁₃₅₀ micelles ($Z_{+/-} = 0$) show a certain corona contraction due to charge screening under these conditions (data not shown), resulting in similar structures in cryo-TEM. Subsequently, the same sample was dialyzed against pH 10 buffer without additional salt, allowing the IPEC shell to be slowly formed again. After dialysis we again observed micellar IPECs with a patchy IPEC shell (**Figure 6-4B**) similar to the structures observed before. Consequently, the patchy IPEC structure seems to be energetically favored and is not a result of kinetic trapping effects.

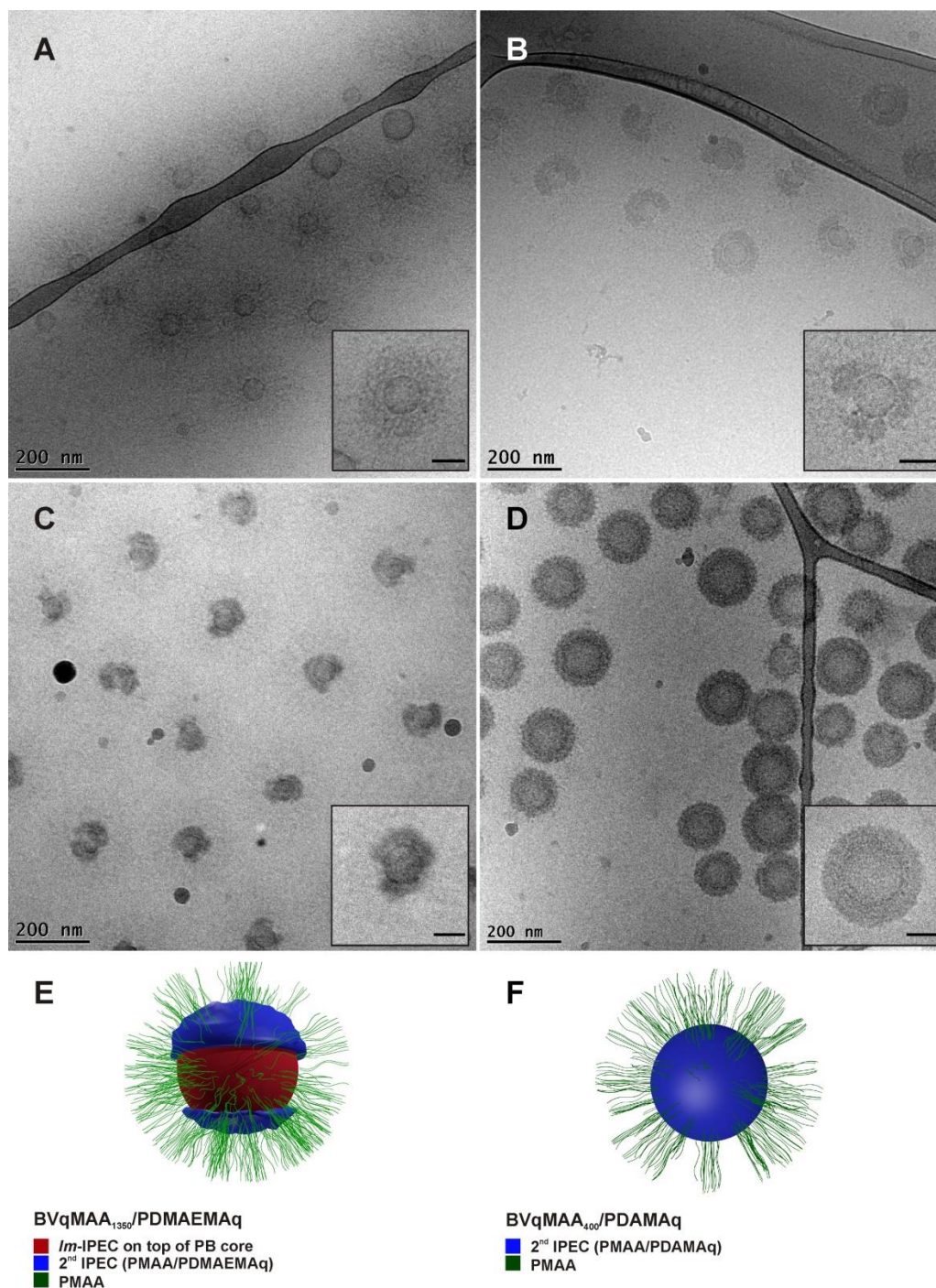


Figure 6-4. (A) Cryo-TEM micrographs of micellar IPECs of BVqMAA₁₃₅₀/PDAMAq in pH 10 buffer at $Z_{+/-} = 0.5$ with 500 mM NaCl and an ionic strength of ca. 0.55 M; (B) the same sample after dialysis to pH 10 buffer solution without additional salt (ionic strength = 0.05 M); (C) micrographs of BVqMAA₁₃₅₀/PDAMAq micelles in pH 10 buffer solution (ionic strength = 0.05 M) at $Z_{+/-} = 0.5$; (D) micrographs of BVqMAA₄₀₀/PDAMAq micelles in pH 10 buffer solution (ionic strength = 0.05 M) at $Z_{+/-} = 0.25$. The insets show single objects at higher magnification, the scale bars representing 50 nm. Schematic representation of the micellar IPECs of BVqMAA₁₃₅₀/PDAMAq (E) and BVqMAA₄₀₀/PDAMAq (F).

To check whether the patches originate from the increased charge density offered by PDAMAq, we also used PDMAEMAq₁₆₂³⁰ as a polycation. As can be seen in **Figure 6-4C**, comparable micellar IPECs were obtained, exhibiting several localized IPEC patches instead of a homogeneous IPEC shell.

Since neither kinetic trapping of the IPEC, nor the increased charge density of PDAMAq are responsible for the peculiar morphology of the micellar IPECs, we also investigated the influence of the PMAA corona length. The BVqMAA₁₃₅₀ used here has an exceptionally long corona compared to any of the previously used BVqMAA polymers. As compared to BVqMAA₁₃₅₀ with 1170 net negative charges BVqMAA₄₀₀ has only $400 - 180 = 220$ net negative charges per PMAA chain. When mixed with PDAMAq at $Z_{+/-} = 0.25$, stable micellar solutions were obtained and subsequently analyzed by cryo-TEM (**Figure 6-4D**). In this case, well-defined structures adopting a core-shell-shell-corona morphology with a continuous IPEC shell of PMAA/PDAMAq and a corona of excess PMAA were observed.

These structures are indeed very similar to those observed previously, where continuous IPEC layers were found for B₈₀₀Vq₁₉₀MAA₃₄₅, B₈₀₀Vq₁₉₀MAA₄₆₅ and B₈₀₀Vq₁₉₀MAA₅₅₀ MCMs upon complexation with PDMAEMAq.³⁰ Thus, the corona length seems to be the critical factor for the formation of the observed patchy IPEC shell. For an estimation of the hydrophilic-to-hydrophobic balance of the terpolymer micelles the weight fractions of the corona- and core-forming blocks are compared. Consequently, the *im*-IPEC of P2VPq/PMAA is included within the hydrophobic part while counterions are not taken into account for the calculation. According to this rough estimation, the materials used in our previous study (BVqMAA₃₄₅, BVqMAA₄₆₅, and BVqMAA₅₅₀) exhibit rather large hydrophobic weight fractions, w_h , between 0.73 and 0.86. In the case reported here, BVqMAA₄₀₀ is in the same range with $w_h = 0.81$, whereas BVqMAA₁₃₅₀ has a predominant hydrophilic weight fraction with $w_h = 0.45$. This seems to affect further IPEC formation, *i.e.* the formation of a patchy second IPEC shell. Since we already excluded that the structures are kinetically trapped or influenced by the nature of the polycation, it seems to be energetically favorable for the system to form isolated IPEC patches rather than a thin continuous layer. This effect is also supposed to play a role during the formation of localized IPEC patches within the *im*-IPEC shell of different BVqMAA MCMs.²⁹ A more detailed explanation can be given considering the respective interfaces: the newly formed IPEC shell has an interface with the micellar core consisting

of PB and the *im*-IPEC (IF-1, **Figure 6-5**, dashed yellow line), another one with the PMAA corona (IF-2, dashed red line), and at high $Z_{+/-}$ -ratios an additional interface with the surrounding medium (water) would be formed (IF-3, **Figure 6-5B**, dashed purple line).

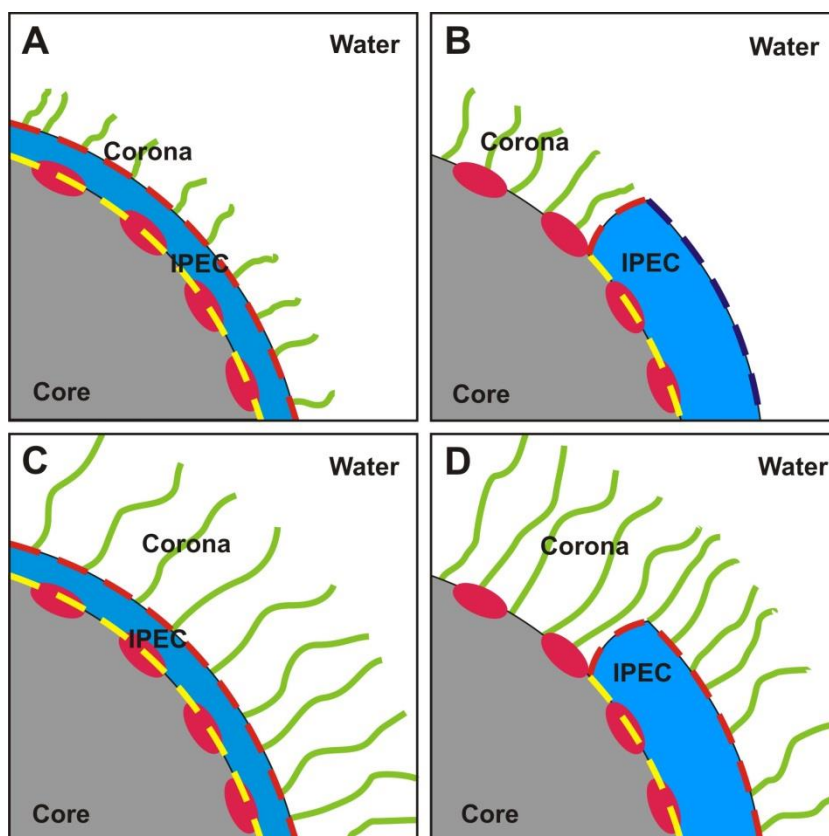


Figure 6-5. Schematic illustration of the potentially relevant interfaces in the formation of an additional IPEC shell in BVqMAA micelles with a short (A, B) or long (C, D) corona, leading to either continuous (A, C) or patchy (B, D) IPECs. The relevant interfaces of the newly formed IPEC are highlighted as dashed lines and are between the IPEC and the core (yellow), the corona (red), or water as the selective solvent (purple).

Four different cases of IPEC formation involving BVqMAA₄₀₀ (**Figure 6-5A** and **6-5B**) and BVqMAA₁₃₅₀ (**Figure 6-5C** and **6-5D**) micelles can now be considered. When micellar IPECs with a continuous shell are formed, the interfaces IF-1 and IF-2 are maximized, while IF-3 is absent (**Figure 6-5A, C**). On the other hand, when patches are formed, IF-1 is minimized. However, in case of a short PMAA segment this leads to the generation of a significant interface IF-3 (**Figure 6-5B**) and, potentially, a loss of colloidal stability, whereas long-corona micelles can minimize IF-1 without creating an additional IF-3 (**Figure 6-5D**). It therefore seems that micelles with a very long ionic

corona, as demonstrated for BVqMAA₁₃₅₀, preferentially form patchy IPEC compartments when complexed with oppositely charged polycations at low to intermediate $Z_{+/-}$ -ratios. We are aware that this explanation is solely based on simple considerations of the respective interfaces and does not include other effects like chain entropy or partial dissociation of the IPEC domains. However, our tentative model is supported by the results obtained for the systems BVqMAA₁₃₅₀/PDAMAq and BVqMAA₁₃₅₀/PDMAEMAq.

Conclusions

The formation of micellar IPECs between negatively charged BVqMAA precursor micelles and either PDAMAq or PDMAEMAq polycations leads to well-defined core-shell-shell-corona structures. We demonstrate that the formation of a compartmentalized additional IPEC shell in micellar IPECs can be favorable at low to intermediate $Z_{+/-}$ ratios when MCMs with a long corona-forming PMAA block are used. We propose an explanation for the structure formation based on the generated interfaces for different corona lengths of the underlying BVqMAA precursor micelles. In more general terms, this work represents a facile route for the formation of well-defined particles where the size can be adjusted by the underlying MCM system (e.g., molecular weight of BVqMAA) and compartmentalization of the shell is controlled by charge stoichiometry and corona length. Such structures represent very interesting models for pH-responsive soft and patchy colloids or multifunctional delivery vehicles. We are currently investigating the drug delivery properties of BVqMAA micelles. Furthermore, the presence of surface patches of unlike charge stoichiometry and hydrophilicity might turn out to be advantageous for the pH-dependent interaction with living matter, e.g. cell cultures when performing transfection or uptake studies.

Supporting Information

Molecular characterization data on BVT polymers and DAMA monomer, the kinetic plot of the DAMA polymerization, zeta potential and dynamic light scattering measurements of BVqMAA/PDAMAq micelles. These data are available free of charge via the Internet at <http://pubs.acs.org>.

Conflict of Interest Statement

The authors declare no conflict of interest.

Acknowledgements

C.V.S. acknowledges a scholarship from the State of Bavaria through the BayEFG program as well as ongoing support from the Elite Network of Bavaria (ENB). We thank Marietta Böhm for performing the SEC measurements. O. Borisov (Pau, France) and D.V. Pergushov (Moscow, Russia) are acknowledged for helpful discussions. F. H. S. is grateful for a starting independent researcher fellowship (Verband der Chemischen Industrie, VCI). Matthias Karg is acknowledged for help during manuscript preparation.

References

1. Bates, F. S.; Hillmyer, M. A.; Lodge, T. P.; Bates, C. M.; Delaney, K. T.; Fredrickson, G. H. *Science* **2012**, 336, 434.
2. Schacher, F. H.; Rupar, P. A.; Manners, I. *Angew. Chem., Int. Ed.* **2012**, 51, 7898.
3. Botiz, I.; Darling, S. B. *Mater. Today* **2010**, 13, 42.
4. Li, J.-G.; Lin, R.-B.; Kuo, S.-W. *Macromol. Rapid Commun.* **2012**, 33, 678.
5. Son, J. G.; Gwyther, J.; Chang, J.-B.; Berggren, K. K.; Manners, I.; Ross, C. A. *Nano Lett.* **2011**, 11, 2849.
6. Hamley, I. W. *Prog. Polym. Sci.* **2009**, 34, 1161.
7. Hawker, C. J.; Russell, T. P. *Mrs Bull.* **2005**, 30, 952.
8. Moffitt, M.; Khougaz, K.; Eisenberg, A. *Acc. Chem. Res.* **1996**, 29, 95.
9. Savic, R.; Eisenberg, A.; Maysinger, D. *J. Drug Targeting* **2006**, 14, 343.
10. Funhoff, A. M.; Monge, S.; Teeuwen, R.; Koning, G. A.; Schuurmans-Nieuwenbroek, N. M. E.; Crommelin, D. J. A.; Haddleton, D. M.; Hennink, W. E.; van Nostrum, C. F. *J. Control. Release* **2005**, 102, 711.
11. Harada-Shiba, M.; Yamauchi, K.; Harada, A.; Takamisawa, I.; Shimokado, K.; Kataoka, K. *Gene Ther.* **2002**, 9, 407.
12. Itaka, K.; Yamauchi, K.; Harada, A.; Nakamura, K.; Kawaguchi, H.; Kataoka, K. *Biomaterials* **2003**, 24, 4495.
13. Hinton, T. M.; Guerrero-Sanchez, C.; Graham, J. E.; Le, T.; Muir, B. W.; Shi, S.; Tizard, M. L. V.; Gunatillake, P. A.; McLean, K. M.; Thang, S. H. *Biomaterials* **2012**, 33, 7631..
14. Matsumoto, S.; Christie, R. J.; Nishiyama, N.; Miyata, K.; Ishii, A.; Oba, M.; Koyama, H.; Yamasaki, Y.; Kataoka, K. *Biomacromolecules* **2009**, 10, 119.
15. Nishiyama, N.; Jang, W.-D.; Kataoka, K. *New J. Chem.* **2007**, 31, 1074.
16. Schacher, F.; Yuan, J.; Schoberth, H. G.; Müller, A. H. E. *Polymer* **2010**, 51, 2021.
17. Stadler, R.; Auschra, C.; Beckmann, J.; Krappe, U.; Voight-Martin, I.; Leibler, L. *Macromolecules* **1995**, 28, 3080.
18. Li, Z. B.; Kesselman, E.; Talmon, Y.; Hillmyer, M. A.; Lodge, T. P. *Science* **2004**, 306, 98.
19. Marsat, J.-N. I.; Heydenreich, M.; Kleinpeter, E.; Berlepsch, H. v.; Böttcher, C.; Laschewsky, A. *Macromolecules* **2011**, 44, 2092.
20. Gröschel, A. H.; Walther, A.; Löbbling, T. I.; Schmelz, J.; Hanisch, A.; Schmalz, H.; Müller, A. H. E. *J. Am. Chem. Soc.* **2012**, 134, 13850.
21. Voets, I. K.; de Keizer, A.; de Waard, P.; Frederik, P. M.; Bomans, P. H. H.; Schmalz, H.; Walther, A.; King, S. M.; Leermakers, F. A. M.; Stuart, M. A. C. *Angew. Chem., Int. Ed.* **2006**, 45, 6673.
22. Walther, A.; Müller, A. H. E. *Soft Matter* **2008**, 4, 663.
23. Walther, A.; Müller, A. H. E. *Chem. Rev.* **2013**, ASAP, DOI: 10.1021/cr300089t.
24. Moughton, A. O.; Hillmyer, M. A.; Lodge, T. P. *Macromolecules* **2012**, 45, 2.
25. Gröschel, A. H.; Schacher, F. H.; Schmalz, H.; Borisov, O. V.; Zhulina, E. B.; Walther, A.; Müller, A. H. E. *Nat. Commun.* **2012**, 3.
26. Kabanov, V. A. *Russ. Chem. Rev.* **2005**, 74, 3.
27. Pergushov, D. V.; Müller, A. H. E.; Schacher, F. H. *Chem. Soc. Rev.* **2012**, 41, 6888.
28. Schacher, F.; Betthausen, E.; Walther, A.; Schmalz, H.; Pergushov, D. V.; Müller, A. H. E. *ACS Nano* **2009**, 3, 2095.
29. Schacher, F.; Walther, A.; Müller, A. H. E. *Langmuir* **2009**, 25, 10962.

30. Synatschke, C. V.; Schacher, F. H.; Förtsch, M.; Drechsler, M.; Müller, A. H. E. *Soft Matter* **2011**, 7, 1714.
31. Betthausen, E.; Drechsler, M.; Förtsch, M.; Pergushov, D. V.; Schacher, F. H.; Müller, A. H. E. *Soft Matter* **2012**, 8, 10167.
32. Sperschneider, A.; Schacher, F.; Gawenda, M.; Tsarkova, L.; Müller, A. H. E.; Ulbricht, M.; Krausch, G.; Köhler, J. *Small* **2007**, 3, 1056.
33. Auschra, C.; Stadler, R. *Polym. Bull.* **1993**, 30, 257.
34. Borisov, O. V.; Zhulina, E. B. *Macromolecules* **2002**, 35, 4472.
35. Blacker, N. C.; Findlay, P. H.; Sherrington, D. C. *Polym. Adv. Technol.* **2001**, 12, 183.
36. Bos, G. W.; Kanellos, T.; Crommelin, D. J. A.; Hennink, W. E.; Howard, C. R. *Vaccine* **2004**, 23, 460.
37. Cherng, J. Y. *J. Pharm. Pharmaceut. Sci.* **2009**, 12, 346.
38. Funhoff, A. M.; Van Nostrum, C. F.; Lok, M. C.; Kruijtzter, J. A. W.; Crommelin, D. J. A.; Hennink, W. E. *J. Control. Release* **2005**, 101, 233..

Supporting Information

Scheme 6-S1. Synthesis of BVT triblock terpolymers by sequential living anionic polymerization in THF at low temperatures and their conversion to BVqMAA triblock terpolymers through quaternization and subsequent acidic hydrolysis in dioxane.

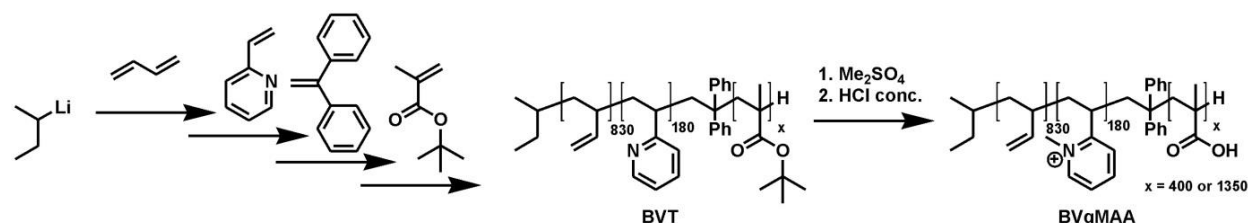
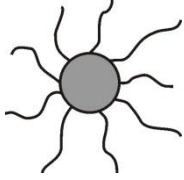
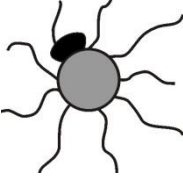
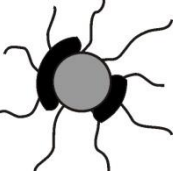
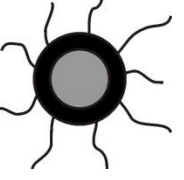


Table 6-S1. Zeta potential of BVqMAA₁₃₅₀/PDAMAq micelle solutions. Values represent mean \pm s. d.

	BVqMAA ₁₃₅₀ /PDAMAq				
Z _{+/-} value	0	0.1	0.25	0.5	0.75
Zeta Potential [mV]	-34.0 \pm 1.2	-33.2 \pm 2.6	-33.9 \pm 0.6	-31.8 \pm 1.5	-31.8 \pm 2.3

Table 6-S2: Distribution of micelle types (no compartment, small compartment(s), large compartment(s) and complete shell) in BVqMAA₁₃₅₀/PDAMAq samples at different Z_{+/-} values counted from cryo-TEM micrographs. At least 70 micelles were counted per sample.

BVqMAA ₁₃₅₀ / PDAMAq				
Z _{+/-} = 0	100 %	0 %	0 %	0 %
Z _{+/-} = 0.1	82 %	18 %	0 %	0 %
Z _{+/-} = 0.25	15 %	76 %	9 %	0 %
Z _{+/-} = 0.5	2 %	6 %	79 %	13 %
Z _{+/-} = 0.75	0 %	0 %	18 %	82 %

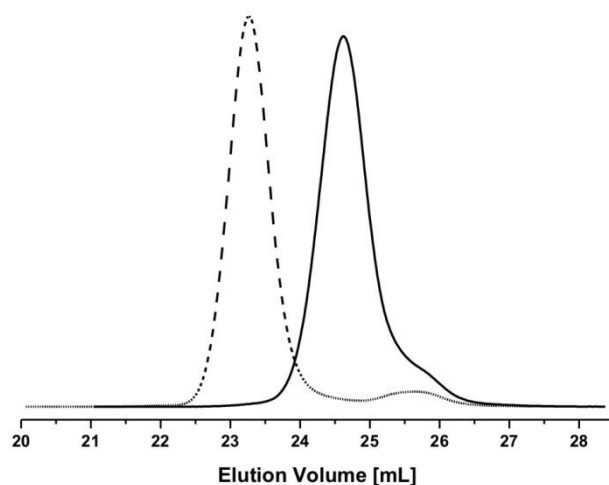


Figure 6-S1. SEC elution curves of B₈₃₀V₁₈₀T₄₀₀ (solid line) and B₈₃₀V₁₈₀T₁₃₅₀ (dotted line) triblock terpolymers in SEC with THF as solvent (RI signal).

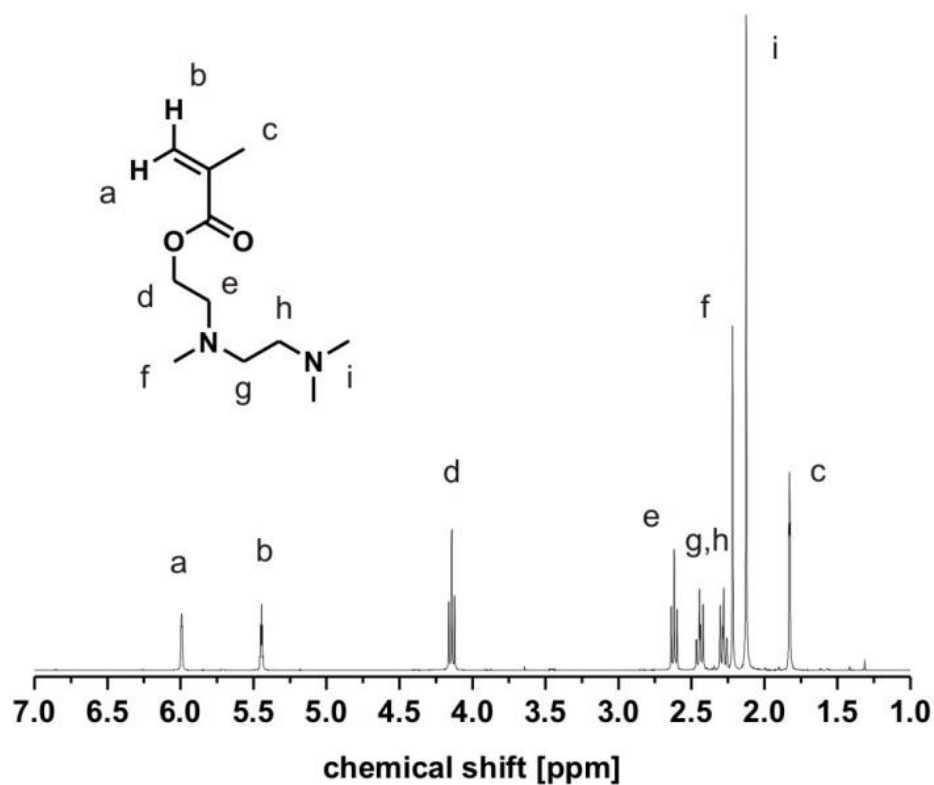


Figure 6-S2. ¹H NMR spectrum of DAMA in CDCl₃ after purification by column chromatography.

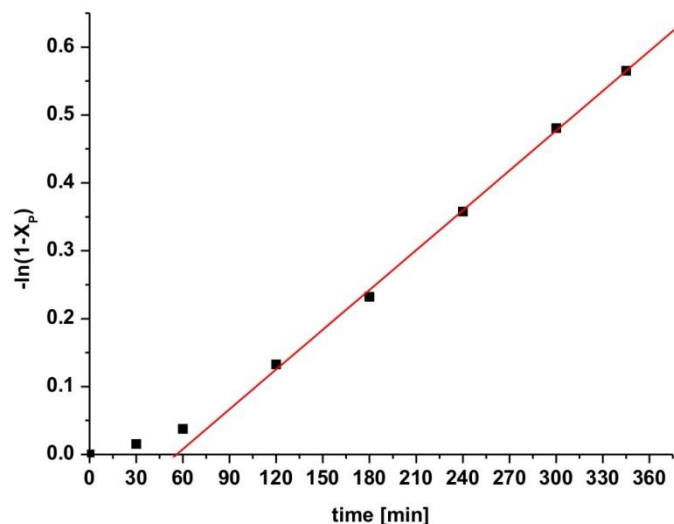


Figure 6-S3: First order kinetic plot for the RAFT polymerization of DAMA.

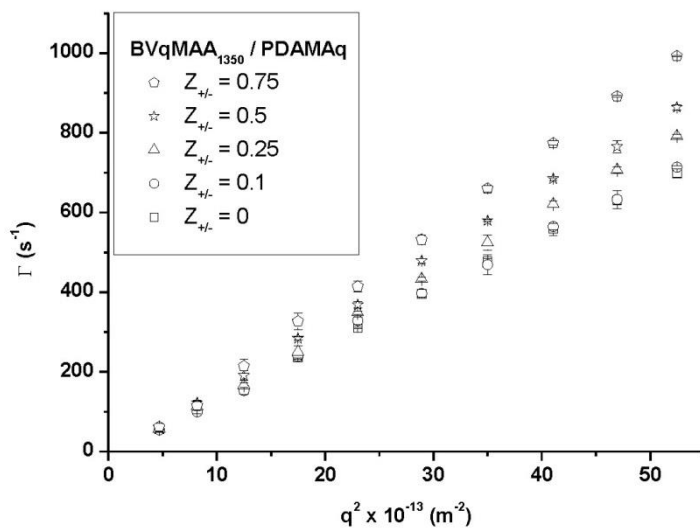


Figure 6-S4: Γ versus q^2 plots for BVqMAA₁₃₅₀/PDAMAq micelles at various $Z_{+/-}$ values.

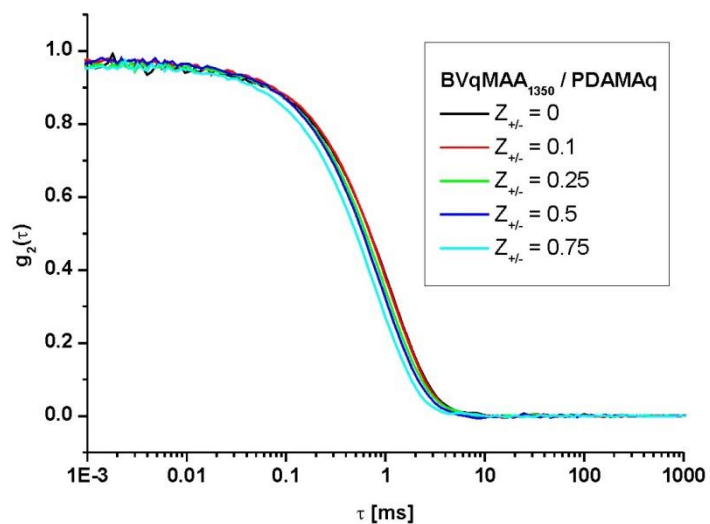
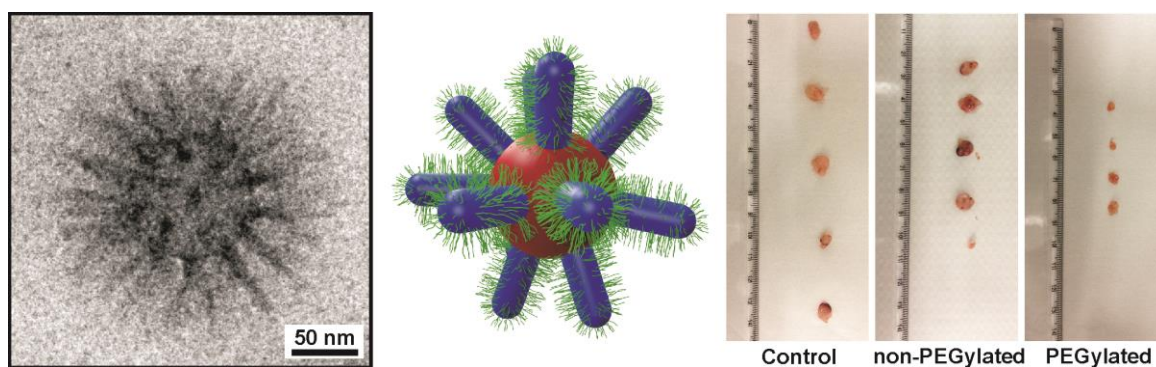


Figure 6-S5: Autocorrelation functions of BVqMAA₁₃₅₀/PDAMAq micelles at various $Z_{+/-}$ values from DLS measurements at a scattering angle of 90° .

Chapter 7

Multicompartment Micelles with Adjustable Poly(ethylene glycol) Shell for Efficient *in Vivo* Photodynamic Therapy



The work presented in this chapter has been published in *ACS Nano* as:

“Multicompartment Micelles with Adjustable Poly(ethylene glycol) Shell for Efficient *in Vivo* Photodynamic Therapy”

by Christopher V. Synatschke, Takahiro Nomoto, Horacio Cabral, Melanie Förtsch, Kazuko Toh, Yu Matsumoto, Kozo Miyazaki, Andreas Hanisch, Felix H. Schacher, Akihiro Kishimura, Nobuhiro Nishiyama, Axel H. E. Müller,* and Kazunori Kataoka* .

Abstract

We describe the preparation of well-defined multicompartiment micelles from polybutadiene-*block*-poly(1-methyl-2-vinyl pyridinium methyl sulfate)-*block*-poly(methacrylic acid) (BVqMAA) triblock terpolymers and their use as advanced drug delivery systems for photodynamic therapy (PDT). A porphyrazine derivative was incorporated into the hydrophobic core during self-assembly and served as a model drug and fluorescent probe at the same time. The initial micellar corona is formed by negatively charged PMAA and could be gradually changed to poly(ethylene glycol) (PEG) in a controlled fashion through interpolyelectrolyte complex formation of PMAA with positively charged poly(ethylene glycol)-*block*-poly(L-lysine) (PLL-*b*-PEG) diblock copolymers. At high degrees of PEGylation, a compartmentalized micellar corona was observed, with a stable bottlebrush-on-sphere morphology as demonstrated by cryo-TEM measurements. By *in vitro* cellular experiments, we confirmed that the porphyrazine-loaded micelles were PDT-active against A549 cells. The corona composition strongly influenced their *in vitro* PDT activity, which decreased with increasing PEGylation, correlating with the cellular uptake of the micelles. Also, a PEGylation-dependent influence on the *in vivo* blood circulation and tumor accumulation was found. Fully PEGylated micelles were detected for up to 24 h in the bloodstream and accumulated in solid subcutaneous A549 tumors, while non- or only partially PEGylated micelles were rapidly cleared and did not accumulate in tumor tissue. Efficient tumor growth suppression was shown for fully PEGylated micelles up to 20 days, demonstrating PDT efficacy *in vivo*.

Introduction

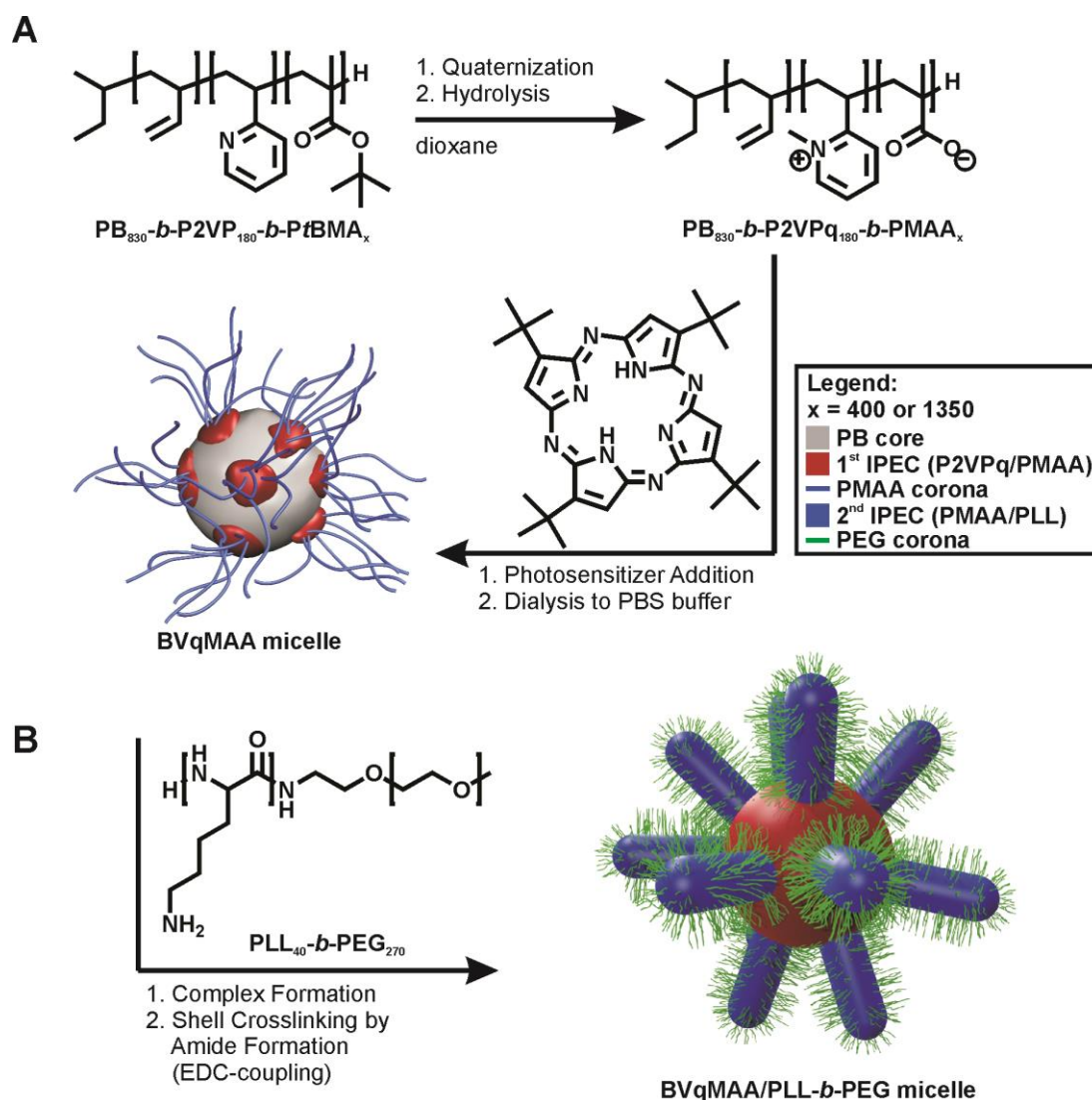
Nanostructured materials are gaining increasing interest for delivering bioactive agents.¹⁻⁵ Block copolymers are a highly versatile class of such materials and consequently have been explored for constructing efficient drug delivery systems (DDS) with increasing complexity.⁶ Thus, polymeric micelles, which self-assemble from amphiphilic block copolymers are being used for encapsulating drugs and genes in their core, thereby enhancing the availability of the drug in the organism and delivering the incorporated therapeutic molecules to specific tissues.⁷⁻⁹ Higher degree of sophistication can be provided to block copolymer-based DDS by supplying responsiveness to stimuli, such as pH, salt concentration, magnetic fields or light irradiation, and introducing ligand molecules for specific targeting of disease-related epitopes. Moreover, by combining imaging reporters with block copolymer systems, DDS can be made visible in biological conditions, facilitating the validation of their design. The dual therapeutic and diagnostic function within a single DDS platform, so called “theranostics”, also permits following the therapeutic response and the disease progression.¹⁰⁻¹² Accordingly, smart DDS capable of precisely engineering the loading of agents within their nanostructures may allow the optimization of both imaging sensitivity and therapeutic efficacy.¹³

In this regard, multicompartiment micelles (MCMs) grant the delivery of various active substances simultaneously, by chemically or physically incorporating them in different nanocompartments within the same particle. An elegant approach for the preparation of MCMs is the use of triblock terpolymers, *i.e.*, materials with at least 3 different polymer blocks. Proper choice of a selective solvent for one of the segments allows for the preparation of structures, which are further subdivided in the core or the shell.^{14, 15} Post-polymerization modification of active groups in MCMs further allows tailoring their properties, such as surface charge or targeting ligands, according to the desired application. For example, the negatively charged corona of core-shell-corona MCMs, prepared from triblock terpolymer polybutadiene-*block*-poly(1-methyl-2-vinyl pyridinium methyl sulfate)-*block*-poly(methacrylic acid) (PB-*b*-P2VPq-*b*-PMAA; BVqMAA), was modified through complexation with the positively charged block of poly(ethylene glycol)-*block*-poly(2-(dimethylamino)ethyl methacrylate) (PEG-*b*-PDMAEMAq), stabilizing the resulting complex MCMs in water.¹⁶ Despite the clear advantages of MCMs for delivering diagnostic and therapeutic molecules, few examples examining their biological applications can be found in the literature.¹⁷

In this contribution, we investigated the capability of MCMs prepared from BVqMAA triblock terpolymers as a novel drug delivery platform. BVqMAA micelles present three compartments, *i.e.* core, shell and corona, which can serve different functions in the drug delivery process. Thus, as efficient DDS should stably circulate in the bloodstream,^{18, 19} the properties of the corona of BVqMAA micelles will be important for stabilizing the micelles and avoiding aggregation in biological environments. Two BVqMAA triblock terpolymers, with a long and a short PMAA block, were used as starting material to evaluate the biological properties of the corresponding MCMs (**Scheme 7-1A**). Moreover, the effect of the corona composition was investigated by introducing increasing amounts of positively charged poly(ethylene glycol)-*block*-poly(L-lysine) (PLL-*b*-PEG) diblock copolymer to the PMAA corona, which lead to a gradual transition from the negatively charged corona of pure PMAA to the neutral corona of PEG from the same starting MCMs (**Scheme 7-1B**). In addition, the ability of BVqMAA micelles for delivering therapeutic molecules to tumor tissues was also considered. Thus, as the core of MCMs serves as a drug reservoir, we incorporated a hydrophobic porphyrazine derivative, which can serve both as a fluorescent probe and a photosensitizer (PS), *i.e.*, a drug that generates reactive oxygen species (ROS) upon light irradiation, for photodynamic therapy (PDT).²⁰⁻²³ Since the production of ROS in PDT is limited to the site of illumination, the light-induced cytotoxicity can be spatially controlled to the illuminated area. Nevertheless, because PS distributed to normal tissues, such as skin, causes photosensitivity, patients often have to avoid exposure to sunlight for several weeks. Therefore, promising MCM formulations for PDT treatment of cancer should successfully control the PS bioavailability and enhance the accumulation of the incorporated PS to tumor tissues. Accordingly, detailed studies on the biological properties of these particular MCMs were conducted both *in vitro* and *in vivo* with regard to their ability to function as DDS for PDT.

Results and Discussion

We prepared photosensitizer-carrying polymer micelles from polybutadiene-*block*-poly(2-vinylpyridine)-*block*-poly(*tert*-butyl methacrylate) (PB-*b*-P2VP-*b*-PtBMA; BVT, **Scheme 7-1a**, **Table 7-S1**) analogue to previously published procedures.¹⁶ After quaternization and hydrolysis to polybutadiene-*block*-poly(1-methyl-2-vinyl pyridinium methyl sulfate)-*block*-poly(methacrylic acid) (PB-*b*-P2VPq-*b*-PMAA; BVqMAA), MCMs of well-defined size and structure form spontaneously when the solvent is exchanged to water by dialysis.²⁴ The hydrophobic porphyrazine derivative, serving as photosensitizer (PS), is encapsulated in the PB core of the micelles, while the negatively charged corona from PMAA stabilizes the structures in solution. Two different examples of such micelles, differing in the length of the PMAA block, BVqMAA-1 with a short- ($DP_{\text{PMAA}} = 400$) and BVqMAA-2 with a long corona ($DP_{\text{PMAA}} = 1350$), were prepared in salt containing PBS buffer (10 mM + 140 mM NaCl at pH 7.4) to allow for *in vitro* and *in vivo* experiments. We used two different lengths of PMAA blocks for evaluating the effect of the length of the shell-forming block on the physicochemical and biological properties of the micelles. From potentiometric titration measurements, we determined more than 80 % of the MAA groups to be deprotonated at pH 7.4, rendering the BVqMAA micelles strongly negatively charged and thus highly stable under these conditions.



Scheme 7-1. (A) Preparative procedure to obtain PS carrying BVqMAA micelles in water. A BVT triblock terpolymer is quaternized and hydrolyzed in dioxane to give amphiphilic BVqMAA. After PS addition, self-assembly to micelles takes place through the exchange of solvent from dioxane to PBS buffer. (B) Complexation with PLL-*b*-PEG diblock copolymers and subsequent crosslinking of PMAA with PLL yields PEGylated micelles (BVqMAA/PLL-*b*-PEG).

Corona Modification of MCMs

Besides offering the possibility to conjugate functional molecules through esterification, the negatively charged carboxylic acid groups of the PMAA corona can be used for further functionalization through an interpolyelectrolyte complex (IPEC) formation with polycations.^{16, 25} Here, we integrated a poly(L-lysine)-*block*-poly(ethylene glycol) (PLL-*b*-PEG; **Table 7-S1**) diblock copolymer, as illustrated in **Scheme 7-1b**, simply by complexing PLL-*b*-PEG with long- and short corona BVqMAA micelles. The complexation ratio is given as $Z_{+/-}$ -value, which is defined as the ratio between cationic

lysine monomer units divided by the residual number of anionic MAA monomer units after taking the intra-micellar IPEC with Vq into account (see **equation 7-1**).

$$Z_{+/-} = \frac{n_{Lys}}{n_{MAA} - n_{Vq}} \quad (7-1)$$

This allows us to gradually change the corona composition from a pure PMAA corona for non-complexed micelles ($Z_{+/-} = 0$) to a complete PEG corona for micelles where all PMAA has been complexed with PLL to form an IPEC ($Z_{+/-} = 1$). Complexation ratios in between these two cases give partially PEGylated micelles. For each corona-length of the BVqMAA micelles, four ratios with PLL-*b*-PEG were prepared ($Z_{+/-} = 0; 0.25; 0.5$ and 1). To prevent any dissociation of the IPEC in biological surroundings, the lysine and MAA units were cross-linked with 1-ethyl-3-(3-dimethylaminopropyl) carbodiimide hydrochloride (EDC-coupling). The characterization of the resulting micelles by ζ -potential measurements and dynamic light scattering (DLS) as well as the determination of the corresponding mass and PS concentration is summarized in **Table 7-1**.

The mass loading of BVqMAA/PLL-*b*-PEG micelles with PS is between 6 and 12 %. The ζ -potential values of the non-PEGylated micelles were strongly negative, as was expected for the deprotonated PMAA corona at pH 7.4. With increasing complexation ratio, these values (after crosslinking) increased and reached almost zero at $Z_{+/-} = 1$, suggesting successful complex formation and surface coverage by PEG. The cumulant hydrodynamic diameter, D_h , of the micelles varied between 260 and 290 nm, but no significant correlation between complexation ratio and micellar size was observed. During IPEC formation, two opposing effects might simultaneously influence the size of the micelles. That is, through binding of the PMAA corona and its subsequent collapse to form the IPEC, the size of the micelles decreases, while the introduction of uncharged PEG into the corona increases micelle size. All the micelles show narrow D_h distributions with dispersities, D.I., between 0.026 and 0.073 and the core size of BVqMAA-1 and BVqMAA-2 remains essentially unchanged by PEGylation (**Table 7-S2**).

Table 7-1. Characterization of BVqMAA-1 and BVqMAA-2 micelles with increasing degree of PEGylation with regard to polymer and photosensitizer (PS) concentration, ζ -potential and cumulant hydrodynamic diameter with corresponding dispersity index (D.I.). All micelle solutions were in 10 mM PBS buffer solution at pH 7.4 with additional 140 mM NaCl.

Polymer	Z _{+/--} -value	Mass Conc. [g/L] ^a	PS Conc. [μ M] ^b	ζ -Potential [mV]	D _h [nm]	D.I.
BVqMAA-1	0	0.47	106	-28	259	0.043
	0.25	0.60	105	-7.5	262	0.043
	0.5	0.52	97	-4.0	264	0.049
	1	0.91	117	-0.2	286	0.059
BVqMAA-2	0	0.88	130	-31	287	0.052
	0.25	0.62	140	-13	280	0.073
	0.5	1.10	140	-6	255	0.026
	1	1.52	165	-2	280	0.028

a) Concentration of drug carrying polymer micelles determined by weight after freeze drying of aliquot dialyzed to MilliQ water to remove buffer salts; b) determined from absorbance at 552 nm and 620 nm of freeze-dried aliquot re-dissolved in DMAc.

The structure of BVqMAA/PLL-*b*-PEG micelles was investigated by cryogenic transmission electron microscopy (cryo-TEM) measurements, where the micellar structure can be imaged close to its native state in aqueous solution. The top row of **Figure 7-1** shows representative images from the BVqMAA-1/PLL-*b*-PEG micelles in PBS buffer solution with increasing amount of PLL-*b*-PEG used for complexation from left to right. In the bottom row, the corresponding structures from BVqMAA-2 are depicted. An overview of the sample is provided in each image, including the average D_h from light scattering measurements represented as a circle, while a single enlarged micelle is shown in the inset.

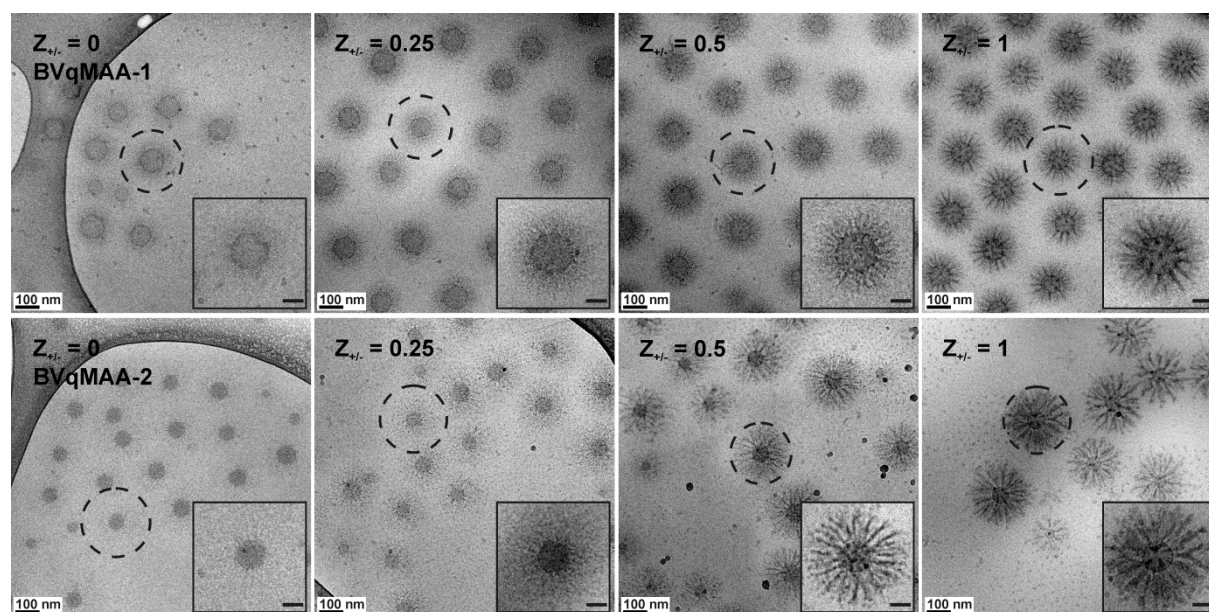


Figure 7-1. Cryo-TEM micrographs of BVqMAA micelles after complex formation with increasing amounts of PLL-*b*-PEG and subsequent crosslinking by EDC-coupling (scale bar = 100 nm). Top row: BVqMAA-1; bottom row: BVqMAA-2 micelles. The circle represents the average D_h of the respective sample determined by light scattering. The inset in each micrograph shows a single enlarged micelle from each batch with the scale bar representing 50 nm.

For the non-complexed BVqMAA-1 ($Z_{+/-} = 0$) micelles, a core-shell-corona structure was evident from the dark grey ring (intra-micellar IPEC between P2VPq and PMAA) surrounding the grey PB core. Water swells the PMAA corona of the micelles and consequently reduces the electron contrast, making it hard to distinguish from the surrounding water phase. As expected from theory,²⁶ the core-size of the BVqMAA-1/PLL-*b*-PEG micelles was larger than that of the corresponding BVqMAA-2/PLL-*b*-PEG micelles (**Table 7-S2**), due to a decreased aggregation number for longer PMAA chains in BVqMAA-2. Upon addition of PLL-*b*-PEG, the structure of the micelles gradually changed. At a low $Z_{+/-}$ -value of 0.25, the density of the corona increased and an enhanced contrast was observed in the cryo-TEM images, indicating a successful complex formation. However, when further PLL-*b*-PEG was added ($Z_{+/-} = 0.5$), the formation of a distinct IPEC structure occurred within the corona. Ray-like structures of high electron density appeared perpendicular to the micellar core, alternating with areas of lower electron density. At a $Z_{+/-}$ -value of 1, the segregation of the corona was most prominent for both micelles and the length of the individual rays slightly increased as compared to $Z_{+/-} = 0.5$. Interestingly, the length of the ray-like structures is considerably longer for BVqMAA-2, which is probably a result of its longer PMAA block as compared to BVqMAA-1. Generally, the cumulant hydrodynamic diameters measured for each

sample by DLS agree well with the size of the micelles found in cryo-TEM. Only for BVqMAA-2 samples at low complexation ratio, the micelles seem to pack closer than would be expected according to their size observed in light scattering experiments. However, this might originate from confinement effects during cryo-TEM sample preparation. Presumably, the dark rays consist of newly formed IPEC between PMAA and PLL, while the areas of low electron contrast can be attributed to water swollen PEG surrounding these IPEC domains; thus, this might be regarded as a “bottlebrush-on-sphere morphology”. Similar structures were previously observed exclusively as a transitional state within the first hours after mixing BVqMAA micelles with PEG-*b*-P2VPq diblock copolymers,²⁵ finally settling for a layered arrangement of the additional IPEC in an onion-type structure as was also found for PEG-*b*-PDMAEMAq as cationic block copolymer.¹⁶ However, in the current case, the observed structures remained unchanged for months. One possible reason for the peculiar morphology may be the secondary structure of PLL. Homopolymers of PLL are known to form intramolecular hydrogen bonds in their uncharged state, leading to the formation of α -helical secondary structures.²⁷ Indeed, CD-spectroscopy measurements as depicted in **Figure 7-S1** of the complex micelles confirmed the existence of α -helical structures, even after crosslinking, which were absent in solutions of non-complexed BVqMAA micelles in the same buffer, respectively. To clarify whether the secondary structure of PLL is indeed responsible for the peculiar morphology of the micellar corona, we synthesized a poly(D,L-lysine)-*block*-poly(ethylene glycol) (PDLL-*b*-PEG) diblock copolymer with similar block lengths, which cannot form α -helices (**Table 7-S1**). As expected, the CD-spectra indicated the absence of secondary structures (**Figure 7-S1**) for BVqMAA micelles after complex formation with PDLL-*b*-PEG. Nevertheless, comparable morphologies were found for BVqMAA/PDLL-*b*-PEG complexes (**Figure 7-S2**), leading to the assumption that the secondary structure formation of PLL is not responsible for the observed micellar morphology.

Another possible reason for the formation of the bottlebrush-on-sphere morphology is the block length ratio between PMAA and PLL. The positively charged lysine block has a rather short DP of 40 units (due to synthetic constraints on controlled block lengths of PLL), while the PMAA chain of the BVqMAA polymers even after intramolecular IPEC formation with P2VPq retains a length of 220 and 1170 theoretically accessible units for BVqMAA-1 and BVqMAA-2, respectively. Consequently, for full compensation of the

negative charges of a single PMAA chain 5.5 and 29 PLL-*b*-PEG chains are necessary on average for the short and long MAA blocks, respectively. To accommodate these large amounts of PLL-*b*-PEG diblock copolymer within the micelle corona, the system may adopt the observed bottlebrush morphology. With such a conformation, the PLL segments of PLL-*b*-PEG copolymers can reach the MAA units of the corona chains, forming interpolyelectrolyte complexes in the core of the bottlebrushes and segregating the PEG chains. In previous complexation experiments with polycation-*block*-PEG diblock copolymers,^{16, 25} the polycations were longer than in the current case and consequently a smaller amount of complexing polymer needed to be incorporated into the micelle corona eliminating the need for corona phase separation. The secondary structure and reduced chain flexibility of the PLL might further promote the formation of the observed structures.

Stability of Complex Micelles

IPEC formation is a reversible process and is driven by the gain in translational entropy upon release of low molecular weight counter-ions as well as electrostatic attraction between oppositely charged monomer units within the polyelectrolyte chains.²⁸ Therefore, an exchange of polyelectrolytes bound in the IPEC with competing polyions from the surrounding solution can occur under certain conditions, *i.e.*, when the polyelectrolyte chains within the complex are mobile. At high salt concentrations (typically 0.5 to 1 M) in the media, the charge attraction between polyelectrolytes is weakened and the IPEC is prone to even complete dissolution. Although such extreme salt concentrations do not occur in cell-culture medium or the blood, the presence of serum proteins combined with an increasing dilution of the BVqMAA/PLL-*b*-PEG micelles may lead to polyion exchange reactions, thereby changing the corona composition. To prevent any significant change after complex formation, lysine and methacrylic acid units were covalently crosslinked *via* amide bonds by EDC-coupling. The high stability of the resulting crosslinked micelles is shown in **Figure 7-2**, where the structures at original buffer conditions (10 mM PBS buffer at pH 7.4 with 140 mM NaCl) are compared to those at high ionic strength (10 mM PBS buffer at pH 7.4 with 990 mM NaCl), simulating highly challenging conditions in biological media.

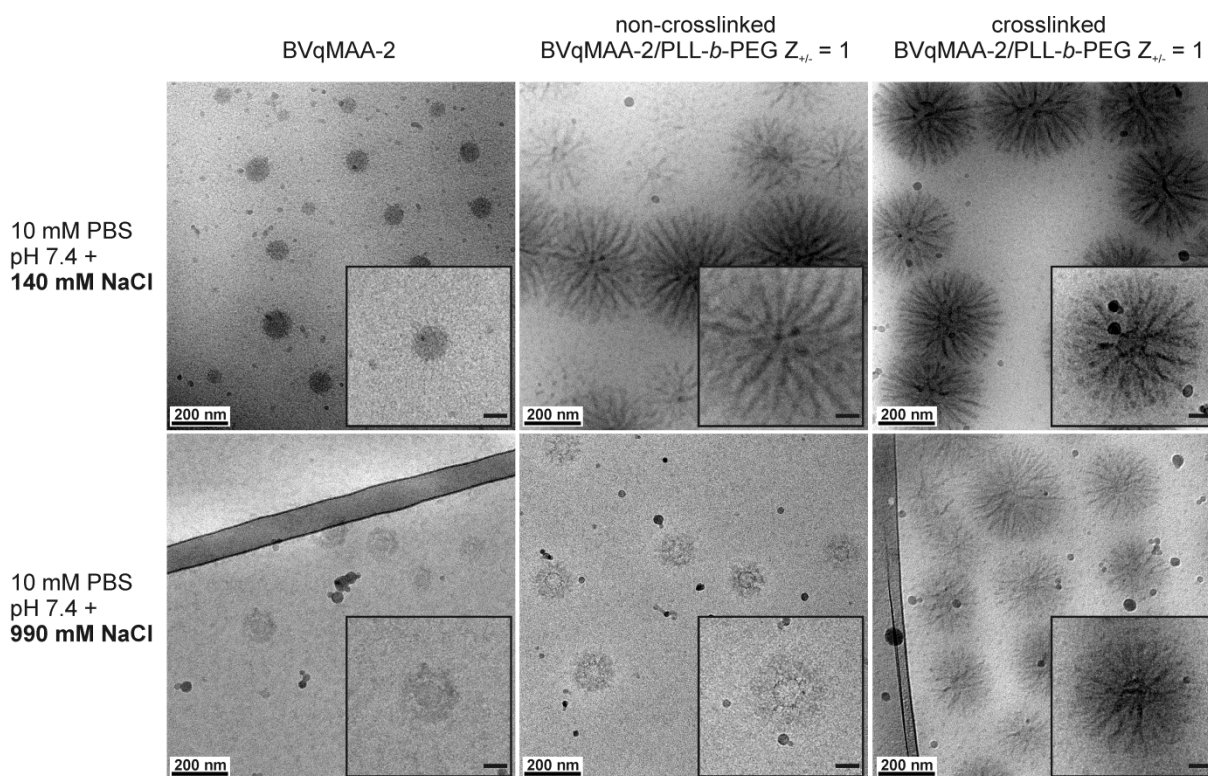


Figure 7-2. Micelle stability against challenging solvent conditions. Representative cryo-TEM micrographs of BVqMAA-2/PLL-*b*-PEG complex micelles in buffer solution at low (top row) and high (bottom row) ionic strength. Left column images show pure BVqMAA-2 micelles, while middle and right column images depict the complexes with PLL-*b*-PEG ($Z_{+/-} = 1$) before and after crosslinking, respectively. Scale bars in each micrograph represent 200 nm. The inset in each micrograph shows a single enlarged micelle in more detail with the scale bar representing 50 nm.

As can be seen from the top row images in **Figure 7-2**, at low salt concentration there is no significant structural difference between the BVqMAA-2/PLL-*b*-PEG micelles at a $Z_{+/-}$ -value of 1, before and after crosslinking, since both samples exhibit the previously discussed bottlebrush-on-sphere morphology. Upon increasing the salt concentration of the buffer from 140 mM to 990 mM NaCl, the corona of the original, non-complexed BVqMAA-2 micelles (bottom left image, **Figure 7-2**) collapsed due to charge screening. Also, the non-crosslinked and complexed micelles showed a collapse of the corona accompanied by a loss of the bottlebrush morphology, suggesting a partial dissolution of the IPEC domains. In contrast, the bottlebrush morphology is retained for crosslinked BVqMAA-2/PLL-*b*-PEG, even at high ionic strength of the solution. Since the crosslinked micelles showed a high tolerance against challenging solvent conditions, we expect the micelles to remain structurally intact and prevent polyion exchange reactions in biological surroundings.

Biological Characterization

Next, the biological properties of the BVqMAA micelles and their complexes with PLL-*b*-PEG were investigated. As a model drug, a hydrophobic porphyrazine derivative was incorporated into the micellar core during micelle formation. This general class of molecules has previously been used as photosensitizer (PS), creating reactive oxygen species (ROS) upon photoirradiation.²⁹ To test the capacity of the micelles for drug delivery, we evaluated the *in vitro* cytotoxicity and cellular uptake of the PS-loaded MCMs. Cellular toxicity was tested against A549 human lung cancer cells, which were treated with increasing concentrations of PS-carrying micelles followed by photoirradiation. From the relative viability data, we determined an inhibitory concentration for 50 % of the cells (IC₅₀), which is summarized in **Table 7-2** for different photoirradiation times, Z_{+/-}-values and both micelle types.

Table 7-2. *In vitro* PDT efficacy. IC₅₀ values (µg PS/mL medium) of BVqMAA/PLL-*b*-PEG micelles carrying PS against A549 cells in dependence of the degree of PEGylation and illumination time (0, 15 and 30 min) as determined by MTT assay.

Z _{+/-} -value	BVqMAA-1/PLL- <i>b</i> -PEG			BVqMAA-2/PLL- <i>b</i> -PEG		
	0min	15min	30min	0min	15min	30min
0	9.3	0.07	0.04	8	< 0.02	< 0.02
0.25	> 10	0.13	0.05	> 10	0.12	0.07
0.5	> 10	0.21	0.08	> 10	0.22	0.26
1	> 10	0.77	0.28	> 10	0.13	0.54

In the control samples without a photoirradiation step (0min), all the micelles had IC₅₀-values above or close to the maximum tested PS concentration of 10 µg/mL; IC₅₀-values drastically decreased upon illumination. Generally, a prolonged illumination resulted in an increased cytotoxicity (lower IC₅₀ values), as would be expected for a continuous ROS production leading to increasing cellular damage. Since PS-unloaded micelles (**Table 7-S3**) were not cytotoxic against these cells (**Table 7-S4**), the cytotoxicity observed for PS-carrying micelles upon irradiation should be a result of the ROS production from the PS. Interestingly, we found a strong influence of the PEGylation degree of the micelles on cytotoxicity, with illuminated non-PEGylated micelles exhibiting the lowest IC₅₀-values of all samples. The cytotoxicity of both micelle types (BVqMAA-1 and 2) decreased with increasing Z_{+/-}-value. The uptake behavior of the micelles could explain this observation (**Figure 7-3**). There, a strong dependence of the cellular uptake with the micelle corona composition was also found. Interestingly,

even though BVqMAA-1/PLL-*b*-PEG micelles exhibited high cell uptake of PS (especially for low $Z_{+/-}$ values), they failed to show strong photo-induced cytotoxicity, probably because ROS production from PS-loaded BVqMAA-1/PLL-*b*-PEG micelles was not as efficient as from PS-loaded BVqMAA-2/PLL-*b*-PEG micelles. The difference in the corona composition of the micelles may affect their interaction with both the surface of cells and the serum molecules in the medium. Thus, strongly charged colloidal objects, such as the micelles with a low degree of PEGylation, should strongly interact with proteins in the serum as well as the cell surface, resulting in enhanced cellular uptake. At the same time, micelles with near complete PEGylation have a nearly neutral ζ -potential in combination with a steric shielding effect from the PEG chains in the corona. Both effects should consequently decrease the interaction of the micelles with the cellular membrane, thereby decreasing cellular uptake.³⁰ In *in vitro* stability experiments, we found that the micelles remain stable in serum-containing cell culture media for at least 24 h, as only minor changes in the hydrodynamic radius of the micelles and the absence of large aggregates were observed (**Figure 7-S3**). In the measurement, protein adsorption could be masked to a certain extent through a simultaneous collapse of the corona. However, since most proteins in the cell culturing medium are also negatively charged we assume protein adsorption to occur only to a minor extent, at least *in vitro*.

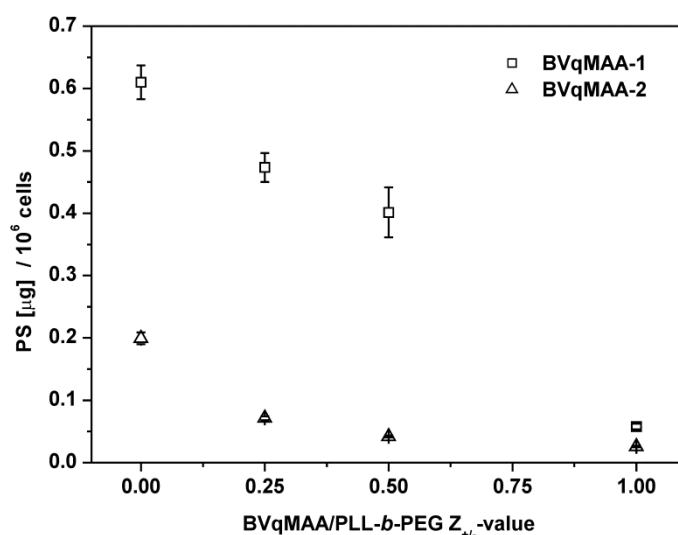


Figure 7-3. *In vitro* cellular uptake. Amount of PS per 10⁶ A549 cells in dependence of the $Z_{+/-}$ -value of BVqMAA/PLL-*b*-PEG micelles after an incubation time of 24 h (n = 3).

Since an increased blood circulation leads to an improved accumulation of nano-sized carriers in tumors due to highly permeable blood vessels and immature lymphatic systems, which is the so-called enhanced permeation and retention (EPR) effect,³¹ the surface modification of the micelles is expected to affect the blood circulation time and eventual accumulation in tumor tissue. We therefore evaluated the blood circulation of different BVqMAA/PLL-*b*-PEG micelles using intravital real-time confocal laser scanning microscopy (IVRTCLSM), which permits *in situ* monitoring and semi-quantitative analysis of fluorescence-labelled DDS.³² We intravenously injected both types of micelles (BVqMAA-1 and BVqMAA-2) with varying degrees of PEGylation to female Balb/c nu/nu mice, and observed the fluorescence of the PS in the earlobe vein to quantify the blood circulation (**Figure 7-4a and 7-4b**). Original fluorescence images shortly after injection and at 60 min circulation time are depicted in **Figure 7-S4**. As with the *in vitro* cellular uptake study, we found a strong dependence of the blood circulation time on the degree of PEGylation. Only fully PEGylated micelles had a prolonged plasma circulation of several hours: >20% for BVqMAA-1/PLL-*b*-PEG and >30% for BVqMAA-2/PLL-*b*-PEG at 2 h. All other micelles, which were partially or non-PEGylated, reached less than 10% in 15 min, indicating a fast clearance from the bloodstream. These results indicate an improvement of the circulation properties with increasing degree of PEGylation, as would be expected from the increased shielding effect of PEG and simultaneous reduction of charge density. Accordingly, long PEG chains and a high packing density are necessary to reduce protein adsorption on the surface of nanoparticles and extend their blood circulation, with the density being more significant than the length of the polymer. However, increasing density of PEG chains in the corona reduces chain mobility and flexibility, which in turn leads to less protein adsorption due to steric hindrance.^{30, 33} A correlation between better blood circulation and increased PEG density was recently shown for rod-like polymeric micelles from plasmid DNA complexed with different PLL-*b*-PEG diblock copolymers.³⁴ There, micelles with improved blood circulation properties had a “squeezed” PEG conformation, which impedes opsonization and subsequent clearance. Thus, when comparing the circulation times of the two fully PEGylated micelles, BVqMAA-2/PLL-*b*-PEG showed higher amounts in the plasma, with roughly 10 % of relative fluorescence intensity after 2 h, probably due to the larger amount of PLL-*b*-PEG necessary to reach complete compensation of the long MAA corona, *i.e.*, high PEG-density. Moreover, the circulation time observed for BVqMAA/PLL-*b*-PEG micelles is in between that reported for

different PEGylated polymersomes of similar size. While PICsomes with a size of 256 nm had a much longer circulation time ($T_{1/2} = 9.7$ h),³⁵ polymersomes from a PB-*b*-PEG diblock copolymer³⁶ were cleared more rapidly than BVqMAA/PLL-*b*-PEG micelles. Apart from the circulation time it is rather difficult to compare the herein demonstrated BVqMAA/PLL-*b*-PEG micelles with other systems as they are larger than most polymeric micelles and, while similar in size, the mechanical properties compared to polymersomes might differ significantly. Additionally, the surface topology resulting from the “bottlebrush-on-sphere” morphology might have an influence on the interaction with biological media.

To get more insight about the *in vivo* activity of the micelles, we evaluated the biodistribution of the micelles in mice bearing subcutaneous A549 tumors (**Figure 7-4c** and supporting **Figure 7-S5**). As can be seen in **Figure 7-4c**, the partially or non-PEGylated micelles could not deliver the PS to the tumor site and only fully PEGylated micelles showed high accumulation of the drug at approximately 4% of the injected dose in the tumors. These findings correlate with the prolonged circulation times of PEGylated micelles and indicate the tumor targeting of these micelles by EPR effect. Also, it is well known that nanoparticles larger than 200 nm are likely to be entrapped in liver and spleen.³⁵⁻³⁸ Indeed, the BVqMAA/PLL-*b*-PEG micelles were mainly cleared by spleen and liver (**Figure 7-S5**). The tumor targeting with the micelles might be further improved by decreasing their size below 200 nm.

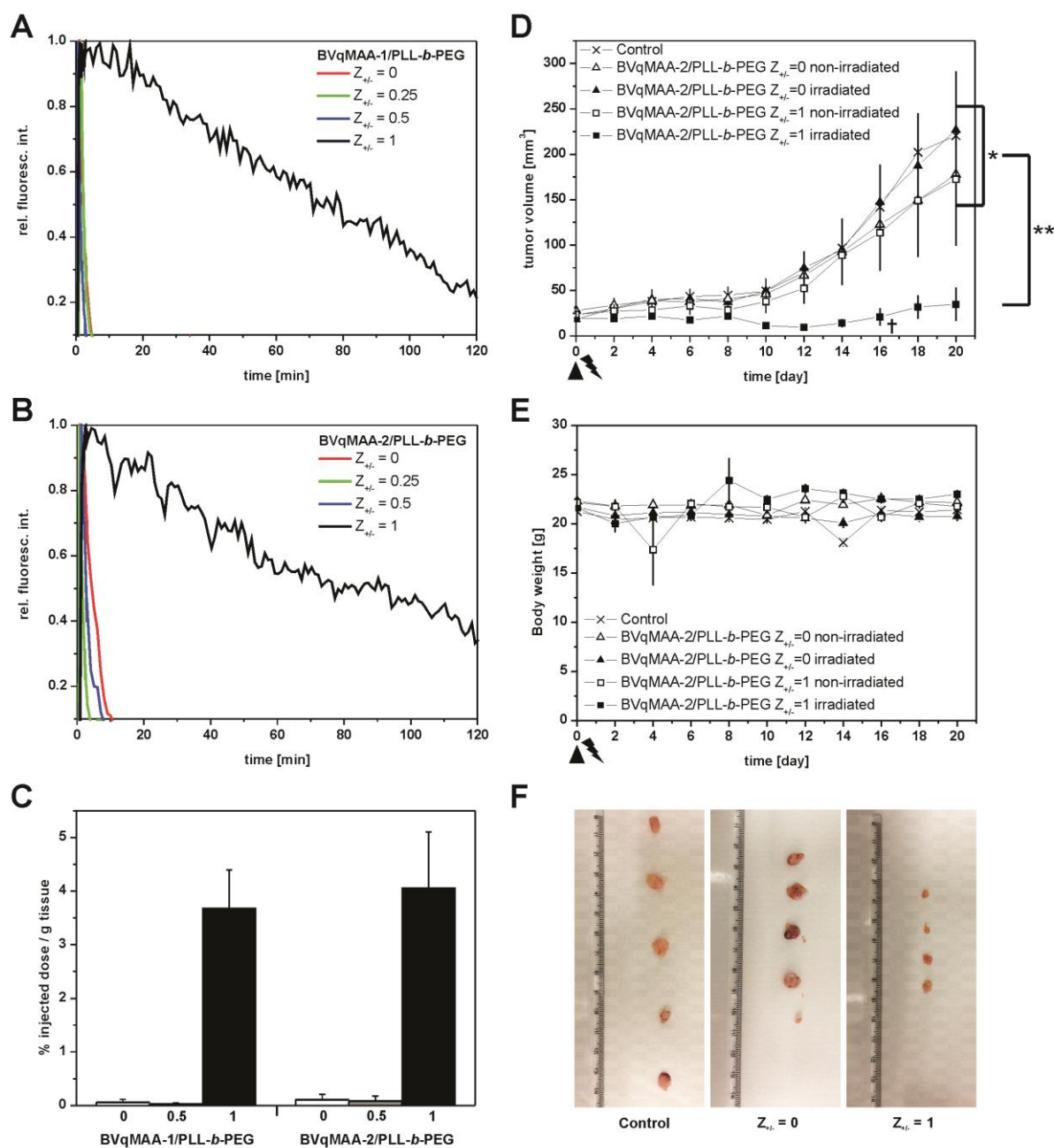


Figure 7-4. *In vivo* circulation time of PS-carrying BVqMAA-1 (A) and BVqMAA-2 (B) micelles with increasing degree of PEGylation in female Balb/c nu/nu mice. (C) Accumulation of PS in subcutaneous A549 tumor model 24 h after injection of BVqMAA/PLL-*b*-PEG $Z_{+/-} = 1$ micelles ($n = 4$). *In vivo* PDT efficacy study ($n = 5$). Evolution of the tumor volume (D) and body weight (E) with time. †: 1/5 tumor regression. * $p > 0.05$; ** $p < 0.001$. (F) Comparison of tumor sizes resected 21 days after BVqMAA-2/PLL-*b*-PEG injection and laser treatment.

The prolonged blood circulation and eventual enhanced tumor accumulation of fully PEGylated micelles led to efficient PDT treatment. We evaluated the PDT efficacy of BVqMAA-2/PLL-*b*-PEG micelles with $Z_{+/-} = 1$ against subcutaneous A549 tumors. Non-PEGylated BVqMAA-2 micelles and non-treated mice served as control. 24 h after

the injection, the mice were illuminated at the tumor site with a xenon lamp equipped with a 630 nm long-path filter to induce ROS production. The evolution of the tumor volume was monitored for 20 days as shown in **Figure 7-4d**. Only fully PEGylated micelles combined with photoirradiation significantly inhibited the tumor growth, even leading to complete tumor regression in one mouse, while the non-PEGylated micelles after irradiation exhibited a negligible antitumor activity (**Figure 7-4d** and **Figure 7-4f**). Also, we found no significant change in the body weight (**Figure 7-4e**) throughout the whole study, suggesting a negligible toxicity of the micelles. Intense necrosis was observed at the tumor site (**Figure 7-S6**) for fully PEGylated micelles after photoirradiation, indicating successful ROS production. The necrosis might have induced an activation of the immune system, further aiding in tumor regression in addition to cellular damage from ROS. These findings clearly demonstrate the effective treatment of A549 tumors by modifying the corona of the micelles and the overall capacity of the BVqMAA/PLL-*b*-PEG micelles to successfully act as DDS.

Conclusions

BVqMAA triblock terpolymer micelles were shown to be effective delivery vehicles for a hydrophobic model drug, which proved to be efficient in PDT treatment of A549 lung-cancer cells both *in vitro* and *in vivo*. By changing the corona composition from a highly negatively charged PMAA to neutral PEG in a simple and controlled manner, we demonstrated the strong influence of the micellar corona on the interaction with biological systems, as is evident by differences in cellular uptake, blood circulation properties and PDT efficacy. The PMAA length of the underlying BVqMAA micelles was of minor importance for the biological properties of the micelles. In principle, any water soluble block copolymer with a positively charged segment can be used for the corona modification, thereby offering a simple tool to produce micelles with versatile corona functionalities. Specific targeting molecules could be easily introduced through this mechanism. It remains to be seen whether the observed “bottlebrush-on-sphere” morphology can have a beneficial influence, for example in cellular recognition. Future work is being directed at exploring the full potential of the different compartments of this advanced carrier system.

Experimental Section

Materials

For anionic polymerization THF (Sigma-Aldrich, *p.a.* quality) was first distilled over CaH₂ followed by a distillation over potassium and stored under N₂ before use. Butadiene (Rießner-Gase, 2.5) was purified by passing through columns filled with molecular sieves (4 Å) and basic aluminum oxide, before condensation into a glass reactor and storage over dibutylmagnesium. 2-Vinylpyridine (97%, Aldrich) was de-inhibited by passing through a basic aluminium oxide column, subsequently stirred for 30 min with 2 mL of trioctylaluminium per 10 mL of 2-vinylpyridine and finally condensed to a sealable glass ampule under reduced pressure. *tert*-Butyl methacrylate (*t*BMA, 98%, Aldrich) was stirred with 0.5 mL of trioctylaluminium per 10 mL of *t*BMA for 30 min and then condensed to a sealable ampule under reduced pressure. 1,1-Diphenylethylene (DPE, Aldrich, 97%) was stirred with *sec*-butyllithium (*sec*-BuLi) under N₂ and then distilled. *sec*-BuLi (Aldrich, 1.4 M in cyclohexane), dibutylmagnesium (Aldrich, 1M in heptane) and trioctylaluminum (Aldrich, 25 wt.% in hexane) were used as received. Quaternization of 2-vinylpyridine was performed with dimethyl sulfate (Me₂SO₄, >99%, Aldrich) and used without further purification. For hydrolysis of *Pt*BMA to PMAA conc. HCl (32 %, 1.2 g/L, Sigma-Aldrich) was used as received. NCA-_L-Lys(TFA) and NCA-_DLys(TFA) monomers were prepared by the Fuchs-Farthing method using triphosgene.³⁹ α -Methoxy- ω -amino-PEG (PEG-NH₂, M_n = 12,000 g/mol, PDI = 1.03) was purchased from NOF Corporation (Tokyo, Japan). DMF (*p.a.* quality, TCI) was stored over molecular sieves (4 Å) and subsequently distilled under vacuum and was stored under argon atmosphere before use. Methanol, dioxane (*p.a.* quality, TCI), *N,N*-dimethylacetamide (DMAc, *p.a.* quality, TCI) DMSO-d₆ and D₂O (both Sigma-Aldrich) were used without further purification. The porphyrazine derivate 2,7,12,17-tetra-*tert*-butyl-5,10,15,20-tetraaza-21*H*,23*H*-porphine (dye content 85 %, Sigma-Aldrich) and *N*-(3-Dimethylaminopropyl)-*N'*-ethylcarbodiimide hydrochloride (EDC, Sigma-Aldrich) were used as received. Sterile Millex AA syringe filters (0.8 μ m, mixed cellulose esters) were delivered from Millipore. Milli-Q water purified with a Millipore filtering system was used in all cases. For dialysis, membranes made from regenerated cellulose (Spectrum Laboratories, Spectra/Por MWCO 1 kDa, 3.5 kDa, 6-8 kDa and 12-14 kDa) were used.

Synthesis of Polybutadiene-*block*-poly(2-vinylpyridine)-*block*-poly(*tert*-butyl methacrylate) (BVT) Triblock Terpolymers

Sequential living anionic polymerization with *sec*-BuLi as initiator and THF as solvent in a laboratory autoclave (2.5 L) at low temperatures was used for the synthesis of BVT triblock terpolymers. The procedure was carried out analogue to our previously published procedures.^{40, 41} During the polymerization of the *tert*-butyl methacrylate (*t*BMA) block, samples were withdrawn at different conversions, thereby creating triblock terpolymers varying only in the block length of their final block, while both previous blocks are of the same length. In detail, 1.6 L of dry THF were placed in a 2.5 L laboratory autoclave (Büchi) and titrated at -20 °C with 16 mL of *sec*-BuLi solution (1.4 M in hexane) to remove any protic species that may terminate the polymerization and left to warm to room temperature overnight. The so-formed alkoxides exhibit stabilizing effects on the living chain end and in the case of *t*BMA well-defined polymers are accessible without addition of LiCl.⁴² After cooling the reaction solution to -70 °C, 0.69 mL of *sec*-BuLi (1 eq., 9.66×10^{-4} mol) were added, followed by the addition of 63.5 mL of butadiene (41.91 g, 800 eq., 0.7748 mol) and polymerization for 8 h at -25 °C and further 2 h at -10 °C. 2-Vinylpyridine (21.68 g, 210 eq., 0.2062 mol) was added at -70 °C and stirred for 2 h, before 0.85 mL of DPE (5 eq., 4.815×10^{-3} mol) was injected and the solution stirred for 2.5 h at -50 °C. Then, at -70 °C, 167.9 g of *t*BMA (1200 eq., 1.181 mol) were added to the solution, which led to an immediate rise in the temperature to -60 °C. The reaction temperature was increased to -50 °C and approximately 1/3 of the reaction solution was withdrawn and quenched in degassed isopropanol (200 mL) after 40 min, 2 h and 8 h of reaction time, respectively. The final polymer was obtained after precipitation from THF solution containing butylated hydroxytoluene (BHT) as stabilizer into a 1/1 mixture of methanol and H₂O. The degrees of polymerization of each block were calculated from a combination of MALDI-ToF-MS of the polybutadiene block and ¹H-NMR of the final triblock terpolymer and determined to be B₈₃₀V₁₈₀T₄₀₀ and B₈₃₀V₁₈₀T₁₃₅₀ for the two polymers used in this work, respectively. Size exclusion chromatography of the two polymers showed bimodal distributions in the elution curves of both polymers, which come from a small amount of terminated PB-*b*-P2VP diblock copolymer during the injection of *t*BMA monomer. The polydispersity indices (PDI) of the full sample were determined to be 1.04 and 1.08 for B₈₃₀V₁₈₀T₄₀₀ and B₈₃₀V₁₈₀T₁₃₅₀, respectively.

Synthesis of Polylysine-*block*-poly(ethylene glycol) (PLL-*b*-PEG and PDLL-*b*-PEG)

For the synthesis of PLL-*b*-PEG 1.059 g of *N*-carboxy anhydride of the trifluoroacetyl protected *L*-lysine (NCA-*L*-Lys(TFA), 3.949 mmol, 45 eq.) were placed under argon atmosphere in a 50 mL round-bottom-flask equipped with a magnetic stirrer bar, which had previously been evacuated overnight and were dissolved in 7 mL of dry DMF (containing 1 M thiourea). To this solution, 1.053 g of α -methoxy- ω -amino PEG (PEG-NH₂, 8.775×10^{-2} mmol, 1 eq.) with a number average molecular weight of 12,000 g/mol (PDI = 1.03) and dissolved in 1 mL of dry DMF (1 M thiourea) were added under argon atmosphere to serve as macroinitiator. The mixture was allowed to polymerize at 25 °C for 72 h until all monomer had been consumed as observed by IR spectroscopy (signals at 1850, 1760 and 915 cm⁻¹ disappear). The block copolymer was purified by dialysis against methanol (Spectra/Por membrane from regenerated cellulose with MWCO = 3,500 Da) for 2 d with repeated exchange of dialysis solution. Methanol was evaporated and the pure polymer (1.84 g, 95 % yield) was obtained after freeze-drying from dioxane. ¹H-NMR gave a degree of polymerization of 40 for the TFA-protected *L*-Lysine and SEC with DMF as eluent and PEG as calibration standard an apparent molecular weight of $M_{n, app.} = 22,100$ g/mol with a PDI of 1.05. Deprotection was achieved by dissolving 1 g of PLL(TFA)-*b*-PEG in 100 mL of methanol mixed with 10 mL of 5 M NaOH solution and stirring in an open flask at 35 °C for 10 h. The deprotected PLL-*b*-PEG diblock copolymer was purified by dialysis against pH 4 aqueous solution (Spectra/Por membrane from regenerated cellulose with MWCO = 1,000 Da) and obtained as a white powder after freeze-drying (800 mg, 86 % yield). ¹H-NMR (**Figure 7-S7**) showed full deprotection and unchanged degree of polymerization for the lysine block, giving PLL₄₀-*b*-PEG₂₇₀, where the subscripts denote the respective degrees of polymerization.

The synthesis of PDLL-*b*-PEG was achieved analogue to the procedure for PLL-*b*-PEG, except for using a 1/1 mixture between NCA-*D*-Lys(TFA) and NCA-*L*-Lys(TFA) as monomers. 96 % yield was obtained for the trifluoroacetyl-protected diblock copolymer PDLL(TFA)-*b*-PEG after purification, where ¹H-NMR showed a DP of 38 for the PDLL(TFA) block and SEC measurements with DMF as eluent gave $M_{n, app.} = 24,800$ g/mol with the PDI = 1.03. The yield of PDLL₃₈-*b*-PEG₂₇₀ after complete deprotection and purification was 58 %.

Synthesis of Polybutadiene-*block*-poly(1-methyl-2-vinyl pyridinium methyl sulfate)-*block*-poly(methacrylic acid) (BVqMAA) Triblock Terpolymer Micelles

In a typical reaction, 50 mg of B₈₃₀V₁₈₀T₄₀₀ (4.14×10^{-7} mol) were dissolved in 15 mL of dioxane (*p.a.* quality) in a round-bottom-flask equipped with a magnetic stirrer bar. After adding 0.94 g Me₂SO₄ (0.71 mL, 7.45×10^{-3} mol, 100 eq. compared to 2-vinylpyridine units), the flask was sealed and stirred for 5 d at 40 °C. Subsequently, 1.89 g of conc. HCl solution (1.57 mL, 1.65×10^{-2} mol, 100 eq. compared to *t*BMA units) were added and the mixture was refluxed at 110 °C for 24 h. For the preparation of PS-containing micelles 5.39 mg of porphyrazine derivate (1×10^{-5} mol) were dissolved in the mixture at ambient temperature. Self-assembly to B₈₃₀V_{q180}MAA₄₀₀ micelles was achieved through dialysis of the mixture first to 0.1 N NaOH solution (3 d with regular exchange of the dialysis solution, MWCO = 6-8 kDa) and finally dialysis to 10 mM PBS solution at pH 7.4 containing 140 mM NaCl for another 3 d. After dialysis was completed, part of the micelle solution was directly used for complex formation with PLL-*b*-PEG as described below. In the case of B₈₃₀V_{q180}MAA₁₃₅₀ micelles the preparation procedure was analogue to the one described above, but with adjusted amounts of material (31.45 mg B₈₃₀V₁₈₀T₁₃₅₀ triblock terpolymer, 8 mL dioxane, 0.28 g Me₂SO₄, 1.89 g conc. HCl and 5.48 mg porphyrazine derivate). The micelle solutions which were not used for complex formation with PLL-*b*-PEG were filtered with 0.8 μm syringe filters and the polymer concentration was determined by weight from aliquots after dialysis to Milli-Q water and freeze-drying. PS concentration was determined from freeze-dried aliquots by re-dissolving the PS in DMAc and measuring the absorbance at 552 nm and 620 nm.

Preparation and Crosslinking of BVqMAA/PLL-*b*-PEG

To BVqMAA micellar solutions in PBS buffer, PLL-*b*-PEG (or PDLL-*b*-PEG) was added from a stock solution (10 g/L in 10 mM PBS adjusted to pH 7.4 with additional 140 mM NaCl) and the complexes were allowed to form by shaking at room temperature for 7 d. The amount of added diblock copolymer was adjusted, so that $Z_{+/-}$ values of 0.25; 0.50 and 1 (see **equation 7-1**) compared to the residual MAA units after intramicellar complex formation (MAA – V_q units) were reached, thereby creating complex micelles with increasing degree of PEGylation. Subsequently, a four-fold excess of EDC compared to the COOH groups of PMAA was directly dissolved in the mixture

and was stirred for 12 h at room temperature, before dialysis against PBS buffer (10 mM at pH 7.4 with 140 mM NaCl) with a 6-8 kDa MWCO dialysis membrane for several days. PEGylated micelle solutions were then filtered with a 0.8 μm syringe filter and polymer and PS concentration was determined as described for the non-PEGylated BVqMAA micelles.

Characterization

MALDI-ToF-MS. Measurements were performed on a Bruker Daltonics Reflex III instrument equipped with an N_2 Laser (337 nm) and an acceleration voltage of 20 kV in positive ion mode. Sample preparation was done according to the “dried-droplet” method. In detail, matrix (DCTB, conc. 20 mg/mL), analyte (conc. 10 mg/mL) and salt (AgTFA, conc. 10 mg/mL) were separately dissolved in THF, subsequently mixed in a ratio of 20/5/1 μL . Approximately 1 μL of the final mixture was applied to the target spot and left to dry under air.

$^1\text{H-NMR}$. Spectra of PB, PB-*b*-P2VP and PB-*b*-P2VP-*b*-PtBMA were recorded on a Bruker Ultrashield 300 machine with a 300 MHz operating frequency using deuterated as solvent. PLL(TFA)-*b*-PEG and PLL-*b*-PEG were measured using a 300 MHz spectrometer (EX 300, JEOL, Tokyo, Japan) with DMSO- d_8 and D_2O as solvents, respectively.

Potentiometric Titration. Micelle solutions (1 mL of 1 g/L in water containing 140 mM NaCl) were adjusted to low pH through addition of 0.5 M HCl before being titrated at ambient temperature and under stirring with 0.01 N NaOH solution, while monitoring the solution pH with a pH electrode.

Dynamic Light Scattering (DLS). The z-average hydrodynamic diameter, D_h , of the micelles was determined by cumulant analysis at ambient temperature using a Zetasizer Nano-ZS instrument (Malvern Instruments, Malvern, UK) equipped with a He-Ne ion laser $\lambda = 633$ nm and at a scattering angle of 173° . A low volume quartz cuvette (ZEN2112) was used for each measurement. For serum stability experiments an ALV DLS/SLS-SP 5022F compact goniometer system with an ALV 5000/E cross correlator and a He-Ne laser ($\lambda = 632.8$ nm). The measurements were carried out in cylindrical scattering cells ($d = 10$ mm) at an angle of 90° and 37°C in triplicate on the same sample. The CONTIN algorithm was applied to analyze the obtained correlation functions. Apparent hydrodynamic radii were calculated according to the Stokes-Einstein equation.

ζ-potential Measurements. Measurements were performed in triplicate on the same instrument used for DLS with disposable capillary cells (DTS1061), where approx. 800 μL of the micelle solution in PBS (10 mM PBS at pH 7.4 with additional 140 mM NaCl) were used per sample. The ζ-potential was calculated from the obtained electrophoretic mobility by applying the Smoluchowski equation.

Cryogenic Transmission Electron Microscopy (cryo-TEM). For cryo-TEM studies, a drop (~2 μL) of the aqueous micellar solution ($c \sim 0.5 \text{ g}\times\text{L}^{-1}$) was placed on a lacey carbon-coated copper TEM grid (200 mesh, Science Services), where most of the liquid was removed with filter paper, leaving a thin film spread between the carbon coating. The specimens were shock vitrified by rapid immersion into liquid ethane in a temperature-controlled freezing unit (Zeiss Cryobox, Zeiss NTS GmbH) and cooled to approximately 90 K. The temperature was monitored and kept constant in the chamber during all of the preparation steps. After freezing the specimens they were inserted into a cryo-transfer holder (CT3500, Gatan) and transferred to a Zeiss EM922 OMEGA EFTEM instrument. Measurements were carried out at temperatures around 90 K. The microscope was operated at an acceleration voltage of 200 kV. Zero-loss filtered images ($\Delta E = 0 \text{ eV}$) were taken under reduced dose conditions. All images were recorded digitally by a bottom mounted CCD camera system (Ultrascan 1000, Gatan), and processed with a digital imaging processing system (Gatan Digital Micrograph 3.9 for GMS 1.4).

Size Exclusion Chromatography (SEC). For the PB and PB-*b*-P2VP precursor polymers and BVT triblock terpolymers, a Waters instrument calibrated with narrowly distributed 1,4-PB standards at 40 °C and equipped with four PSS-SDV gel columns (5 μm particle size) with a porosity range from 10^2 to 10^5 \AA (PSS, Mainz, Germany) was used together with a differential refractometer and a UV detector at 260 nm. Measurements were performed in THF with a flow rate of 1 mL/min using toluene as internal standard. For PEG-NH₂, PLL(TFA)-*b*-PEG and PDLL(TFA)-*b*-PEG polymers a Tosoh instrument (Yamaguchi, Japan) calibrated with PEG standards and equipped with three TSK columns (TSKguardcolumn HHR-L; TSKgel G4000HHR; TSKgel G3000HHR) and a refractive index detector (RI) at 40 °C was used. DMF with 10 mM LiCl was used as eluent at a flow rate of 0.8 mL/min. Sample concentration was 1 mg/mL and 100 μL were injected per measurement.

Serum Stability Experiments. Micellar solutions (non-drug-carrying micelles **Table 7-S3**) were prepared in Dulbecco's modified eagle medium (GIBCO) containing

10 % fetal bovine serum (GIBCO) at a concentration of 0.2 mg/mL and incubated at 37 °C in a water bath. At the appropriate times an aliquot (1 mL) was removed from the respective solution for light scattering measurement.

In Vitro Study

Cell Culturing Conditions. A549 human lung adenocarcinoma cells were purchased from Riken cell bank (Tsukuba, Japan). A549 cells were cultured with Dulbecco's modified eagle medium (Sigma, Japan) containing 10% fetal bovine serum (GIBCO, Japan) and Penicillin/Streptomycin (Sigma, Japan) in a humidified atmosphere containing 5% CO₂ at 37 °C. The passage of the cells was trypsinized with Trypsin-EDTA solution (Sigma, Japan) after being washed with D-PBS (Wako, Japan).

Cytotoxicity. A549 cells were seeded in 96-well plates at a density of 5,000 cells/well in 50 µL of medium and incubated overnight. Then, 50 µL of medium containing the appropriate amount of polymer micelles were added to each well. The first row of 12 rows in each 96-well plate contained only medium but no cells and was used as a background, while the second row contained cells but was not treated with micelles to serve as reference for cell viability. Samples treated with micelles (n = 4) had a maximum concentration of 10 µg/mL with regard to the amount of PS, which decreased by a factor of 2 for each step in the concentration range. Non-PS-carrying-polymer micelles were tested at a maximum polymer concentration of 0.1 mg/mL. After incubating for 24 h, the plates were illuminated under a 300-W halogen lamp (fluence rate, 3.0 mW cm⁻²) equipped with a band-pass filter (400–700 nm) for 0, 15 and 30 min, while being placed on a frozen refrigerant-filled 6-well plate for cooling. The medium was replaced with 100 µL of fresh medium per well after further incubating for 24 h. Then, 20 µL of MTT solution (5 mg/mL in PBS) was added to each well and the samples were incubated for further 3 h. Subsequently, 100 µL of SDS solution (20 %wt.) were added to each well and the plates were incubated overnight, before the absorption at 570 nm was determined with a plate-reader. The mean absorption value of the background row was subtracted before further evaluation. Cell viability was determined relative to the control row of each plate.

Cellular Uptake. A549 cells were seeded in 6-well plates at a density of 1×10⁶ cells/well in 2 mL of medium and incubated overnight before the medium was replaced by fresh DMEM containing micelles at 1µg PS/mL (2 mL/well total volume). After 24 h incubation, the PS-containing medium was removed and each well was washed twice

with cold PBS solution before 900 μ L of SDS solution (20 %wt.) were added. PS concentration was determined from the fluorescence signal at 627 nm (excitation at 400 nm) with a fluorophotometer after incubation overnight directly from SDS solutions. From a control plate, which had not been treated with the micelles, the cell number per well was determined by detaching the cells with trypsin solution and subsequent cell counting with a NucleoCounter NC-100 (Eppendorf AG, Hamburg, Germany). Measurements were performed in triplicate for each sample.

In Vivo Study

Breeding Information. 5 weeks-old female nude mice (Balb/c nu/nu mice: CAnN.Cg-Foxn^{1nu}/CrjCrlj) were purchased from Charles River Laboratories (Yokohama, Japan) *via* Oriental Yeast Co. Ltd. (Tokyo, Japan) and maintained under the standard conditions (20 °C, relative humidity, light/dark cycles) at our animal facilities in the University of Tokyo.

Blood Circulation Study. Blood circulation of the micelles was evaluated using intravital real-time confocal laser scanning microscopy (IVRTCLSM) in live mice. All images were acquired using a Nikon A1R confocal laser scanning microscope system attached to an upright ECLIPSE FN1 (Nikon Corp., Tokyo, Japan) equipped with a 20x objective (numerical aperture: 0.75), 561 nm laser, and a band-pass emission filter of 570–620 nm. Balb/c nu/nu mice were anesthetized with 2.0–3.0% isoflurane (Abbott Japan Co., Ltd., Tokyo, Japan) using a Univentor 400 anaesthesia unit (Univentor Ltd., Zejtun, Malta). Mice were then subjected to lateral tail vein catheterization with a 30 gauge needle (Dentronics Co., Ltd., Tokyo, Japan) connected to a nontoxic, medical grade polyethylene tube (Natsume Seisakusho Co., Ltd., Tokyo, Japan). Anesthetized mice were placed onto a temperature-controlled pad (Thermoplate; Tokai Hit Co., Ltd., Shizuoka, Japan) integrated into the microscope stage and maintained in a sedated state throughout the measurement. Ear-lobe dermis was observed following fixation beneath a coverslip with a single drop of immersion oil. Data were acquired at 12 frames/min for 3 min, followed by snap-shots every 1 min thereafter. Micelles were injected (200 μ L of the respective BVqMAA/PLL-*b*-PEG solution) *via* the tail vein 10 s after the start of video capture. Video data were analyzed by selecting regions of interest (ROIs) within blood vessels and the average fluorescence intensity per pixel for each time point was determined using the Nikon NIS-Elements C software (Nikon Corp.). *Relative*

fluorescence intensity shown in **Figure 7-4a** and **Figure 7-4b** was obtained with the following equation:

$$\text{relative fluorescence intensity} = (\text{fluorescence intensity at indicated time point} - \text{initial fluorescence intensity}) / (\text{maximum fluorescence intensity} - \text{initial fluorescence intensity})$$

Biodistribution Study. Balb/c nu/nu mice (n = 24) were inoculated subcutaneously with A549 cells (100 μL of 1×10^8 cells/mL). Tumors were allowed to grow for one week before the mice were separated into groups of 4. Then, polymer micelles with long- and short PMAA block and varying degree of PEGylation ($Z_{+/-} = 0; 0.25; 0.50$ and 1) were injected into the tail vein at 10 $\mu\text{g}/\text{mouse}$ based on the PS (maximum injection volume was 190 μL). 24 h post micelle injection, mice were sacrificed and kidneys, liver, spleen, lung and tumor were collected for the biodistribution study. The PS concentration of each sample was determined by fluorescence intensity at 627 nm in DCM (excitation at 400 nm) in a fluorophotometer after being extracted as follows: 250 μL and 1 mL of SDS solution (20 %wt.) were added to 50 μL of the heavy blood components and for 200 mg of tissue, respectively, and the samples were sonicated until a homogeneous mixture was obtained. Then, the samples were shaken overnight at room temperature before 200 μL of DCM was added, followed by a short sonication step. Plasma samples of 40 μL were mixed with 200 μL DCM, shaken at room temperature overnight, before being shortly sonicated with a sonication finger. All samples were then centrifuged at 10,000 g for 30 min to induce phase separation before measurement of the DCM phase.

Tumor Suppression Study. Balb/c nu/nu mice (n = 25) were inoculated subcutaneously with A549 cells (100 μL of 1×10^8 cells/mL). Tumors were allowed to grow for 10 days until they reach approximately 25 mm^3 . Mice were separated in groups of 5. Then, non PEGylated micelles and PEGylated micelles at 30 $\mu\text{g}/\text{kg}$ based on PS were intravenously injected. Twenty-four hours later, mice were irradiated at the tumor position for 1000 seconds at 100 mW/cm^2 by using a Xenon lamp with a 630 nm long-path filter (Asahi Spectra, Tokyo, Japan). Mice in control groups were not irradiated. The antitumor activity was evaluated in terms of tumor size (V), as estimated by the following equation:

$$V = a \times b^2/2$$

where a and b are the major and minor axes of the tumor measured by a caliper, respectively. The body weight was measured simultaneously and was taken as a

parameter of systemic toxicity. The statistical analysis of animal data was carried out by the unpaired student's t-test. All animal experiments were performed following the guidelines of the ethical committee of the University of Tokyo.

Conflict of Interest

The authors declare no competing financial interest.

Acknowledgements

C.V.S. gratefully acknowledges financial support through the BayEFG program (The State of Bavaria, Germany) and a Center for Medical Systems Innovations scholarship (CMSI, University of Tokyo, Japan) as well as ongoing support from the Elite Network of Bavaria (ENB). The authors thank S. Chuanoi for help with synthesizing PLL-*b*-PEG and H. Kinoh for assistance with cell culturing. We also thank M. Böhm and D. Schaal for help with some of the SEC- and CD-spectroscopy measurements, respectively. S. Deshayes, P. Saint-Cricq Riviere, X. Ling and R. J. Christie (Tokyo, Japan) are acknowledged for helpful discussions. T. Löbling (Bayreuth, Germany) prepared some of the graphic illustrations of the complex micelles.

Supporting Information Available

Molecular characterization of the polymer samples as well as physical and biological characterization of BVqMAA/PLL-*b*-PEG and BVqMAA/PDLL-*b*-PEG micelles is provided. This material is available free of charge *via* Internet at <http://pubs.acs.org>.

References

1. Ariga, K.; Ji, Q.; McShane, M. J.; Lvov, Y. M.; Vinu, A.; Hill, J. P. Inorganic Nanoarchitectonics for Biological Applications. *Chem. Mater.* **2012**, *24*, 728-737.
2. Goldberg, M.; Langer, R.; Jia, X. Nanostructured Materials for Applications in Drug Delivery and Tissue Engineering. *J. Biomater. Sci. Polym. Ed.* **2007**, *18*, 241-268.
3. Petkar, K. C.; Chavhan, S. S.; Agatonovik-Kustrin, S.; Sawant, K. K. Nanostructured Materials in Drug and Gene Delivery: A Review of the State of the Art. *Crit. Rev. Ther. Drug Carrier Syst.* **2011**, *28*, 101-164.
4. Shanmugam, T.; Banerjee, R. Nanostructured Self Assembled Lipid Materials for Drug Delivery and Tissue Engineering. *Ther. Delivery* **2011**, *2*, 1485-1516.
5. Tang, Z.; Wang, Y.; Podsiadlo, P.; Kotov, N. A. Biomedical Applications of Layer-by-Layer Assembly: From Biomimetics to Tissue Engineering. *Adv. Mater.* **2006**, *18*, 3203-3224.
6. Cabral, H.; Kataoka, K. Multifunctional Nanoassemblies of Block Copolymers for Future Cancer Therapy. *Sci. Technol. Adv. Mater.* **2010**, *11*, 014109.
7. Kataoka, K.; Harada, A.; Nagasaki, Y. Block Copolymer Micelles for Drug Delivery: Design, Characterization and Biological Significance. *Adv. Drug Delivery Rev.* **2001**, *47*, 113-131.
8. Miyata, K.; Christie, R. J.; Kataoka, K. Polymeric Micelles for Nano-Scale Drug Delivery. *React. Funct. Polym.* **2011**, *71*, 227-234.
9. Savic, R.; Eisenberg, A.; Maysinger, D. Block Copolymer Micelles as Delivery Vehicles of Hydrophobic Drugs: Micelle-Cell Interactions. *J. Drug Targeting* **2006**, *14*, 343-355.
10. Kelkar, S. S.; Reineke, T. M. Theranostics: Combining Imaging and Therapy. *Bioconjugate Chem.* **2011**, *22*, 1879-1903.
11. Kim, J.; Piao, Y.; Hyeon, T. Multifunctional Nanostructured Materials for Multimodal Imaging, and Simultaneous Imaging and Therapy. *Chem. Soc. Rev.* **2009**, *38*, 372-390.
12. Nyström, A. M.; Wooley, K. L. The Importance of Chemistry in Creating Well-Defined Nanoscopic Embedded Therapeutics: Devices Capable of the Dual Functions of Imaging and Therapy. *Acc. Chem. Res.* **2011**, *44*, 969-978.
13. Cabral, H.; Nishiyama, N.; Kataoka, K. Supramolecular Nanodevices: From Design Validation to Theranostic Nanomedicine. *Acc. Chem. Res.* **2011**, *44*, 999-1008.
14. Elsabahy, M.; Wooley, K. L. Strategies Toward Well-Defined Polymer Nanoparticles Inspired by Nature: Chemistry Versus Versatility. *J. Polym. Sci., Part A: Polym. Chem.* **2012**, *50*, 1869-1880.
15. Moughton, A. O.; Hillmyer, M. A.; Lodge, T. P. Multicompartment Block Polymer Micelles. *Macromolecules* **2012**, *45*, 2-19.
16. Synatschke, C. V.; Schacher, F. H.; Förtsch, M.; Drechsler, M.; Müller, A. H. E. Double-Layered Micellar Interpolyelectrolyte Complexes - How Many Shells to a Core? *Soft Matter* **2011**, *7*, 1714-1725.
17. Bastakoti, B. P.; Wu, K. C. W.; Inoue, M.; Yusa, S.-I.; Nakashima, K.; Yamauchi, Y. Multifunctional Core-Shell-Corona-Type Polymeric Micelles for Anticancer Drug-Delivery and Imaging. *Chem. Eur. J.* **2013**, *19*, 4812-4817.
18. Koo, H.; Huh, M. S.; Sun, I.-C.; Yuk, S. H.; Choi, K.; Kim, K.; Kwon, I. C. *In Vivo* Targeted Delivery of Nanoparticles for Theragnosis. *Acc. Chem. Res.* **2011**, *44*, 1018-1028.
19. Petros, R. A.; DeSimone, J. M. Strategies in the Design of Nanoparticles for Therapeutic Applications. *Nat. Rev. Drug Discov.* **2010**, *9*, 615-627.

20. Dolmans, D.; Fukumura, D.; Jain, R. K. Photodynamic Therapy for Cancer. *Nat. Rev. Cancer* **2003**, *3*, 380-387.
21. Henderson, B. W.; Dougherty, T. J. How Does Photodynamic Therapy Work? *Photochem. Photobiol.* **1992**, *55*, 145-157.
22. O'Connor, A. E.; Gallagher, W. M.; Byrne, A. T. Porphyrin and Nonporphyrin Photosensitizers in Oncology: Preclinical and Clinical Advances in Photodynamic Therapy. *Photochem. Photobiol.* **2009**, *85*, 1053-1074.
23. Palumbo, G. Photodynamic Therapy and Cancer: A Brief Sightseeing Tour. *Expert Opin. Drug Delivery* **2007**, *4*, 131-148.
24. Schacher, F.; Walther, A.; Müller, A. H. E. Dynamic Multicompartment-Core Micelles in Aqueous Media. *Langmuir* **2009**, *25*, 10962-10969.
25. Schacher, F.; Betthausen, E.; Walther, A.; Schmalz, H.; Pergushov, D. V.; Müller, A. H. E. Interpolyelectrolyte Complexes of Dynamic Multicompartment Micelles. *ACS Nano* **2009**, *3*, 2095-2102.
26. Borisov, O.; Zhulina, E.; Leermakers, F.; Ballauff, M.; Müller, A. H. E. In *Self Organized Nanostructures of Amphiphilic Block Copolymers I*; Müller, A. H. E.; Borisov, O., Eds.; Springer: Berlin / Heidelberg, 2011; pp 1-55.
27. Townend, R.; Kumosinski, T. F.; Timasheff, S. N.; Fasman, G. D.; Davidson, B. The Circular Dichroism of the β Structure of Poly-L-Lysine. *Biochem. Biophys. Res. Commun.* **1966**, *23*, 163-169.
28. Pergushov, D. V.; Müller, A. H. E.; Schacher, F. H. Micellar Interpolyelectrolyte Complexes. *Chem. Soc. Rev.* **2012**, *41*, 6888-6901.
29. Morgan, A. R.; Petousis, N. H.; van Lier, J. E. Synthesis and Photodynamic Activity of Some Tetraazoporphyrin Derivatives. *Eur. J. Med. Chem.* **1997**, *32*, 21-26.
30. Tonga, G. Y.; Saha K.; Rotello V. M. 25th Anniversary Article: Interfacing Nanoparticles and Biology: New Strategies for Biomedicine. *Adv. Mater.* **2013**, DOI: 10.1002/adma.201303001
31. Maeda, H.; Wu, J.; Sawa, T.; Matsumura, Y.; Hori, K. Tumor Vascular Permeability and the EPR Effect in Macromolecular Therapeutics: A Review. *J. Controlled Release* **2000**, *65*, 271-284.
32. Matsumoto, Y.; Nomoto, T.; Cabral, H.; Matsumoto, Y.; Watanabe, S.; Christie, R. J.; Miyata, K.; Oba, M.; Ogura, T.; Yamasaki, Y.; *et al.* Direct and Instantaneous Observation of Intravenously Injected Substances Using Intravital Confocal Micro-Videography. *Biomed. Opt. Express* **2010**, *1*, 1209-1216.
33. Owens III, D.E.; Peppas, N.A. Opsonization, Biodistribution, and Pharmacokinetics of Polymeric Nanoparticles. *Int. J. Pharm.* **2006**, *307*, 93-102.
34. Tockary, T. A.; Osada, K.; Chen, Q.; Machitani, K.; Dirisala, A.; Uchida, S.; Nomoto, T.; Toh, K.; Matsumoto, Y.; Itaka, K.; *et al.* Tethered PEG Crowdedness Determining Shape and Blood Circulation Profile of Polyplex Micelle Gene Carriers. *Macromolecules* **2013**, *46*, 6585-6592.
35. Anraku, Y.; Kishimura, A.; Kobayashi, A.; Oba, M.; Kataoka, K. Size-Controlled Long-Circulating PICsome as a Ruler to Measure Critical Cut-Off Disposition Size into Normal and Tumor Tissues. *Chem. Commun.* **2011**, *47*, 6054-6056.
36. Brinkhuis, R. P.; Stojanov, K.; Laverman, P.; Eilander, J.; Zuhorn, I. S.; Rutjes, F. P. J. T.; van Hest, J. C. M. Size Dependent Biodistribution and SPECT Imaging of ¹¹¹In-Labeled Polymersomes. *Bioconjugate Chem.* **2012**, *23*, 958-965.
37. Cho, W.-S.; Cho, M.; Jeong, J.; Choi, M.; Han, B. S.; Shin, H.-S.; Hong, J.; Chung, B. H.; Jeong, J.; Cho, M.-H. Size-Dependent Tissue Kinetics of PEG-Coated Gold Nanoparticles. *Toxicol. Appl. Pharmacol.* **2010**, *245*, 116-123.

38. Johnston, A. P. R.; Such, G. K.; Ng, S. L.; Caruso, F. Challenges Facing Colloidal Delivery Systems: From Synthesis to the Clinic. *Curr. Opin. Colloid Interface Sci.* **2011**, *16*, 171-181.
39. Fasman, G. D.; Idelson, M.; Blout, E. R. Synthesis and Conformation of High Molecular Weight Poly-Epsilon-Carbobenzyloxy-L-Lysine and Poly-L-Lysine.HCl. *J. Am. Chem. Soc.* **1961**, *83*, 709-712.
40. Schacher, F.; Yuan, J.; Schoberth, H. G.; Müller, A. H. E. Synthesis, Characterization, and Bulk Crosslinking of Polybutadiene-*block*-Poly(2-vinyl pyridine)-*block*-Poly(*tert*-butyl methacrylate) Block Terpolymers. *Polymer* **2010**, *51*, 2021-2032.
41. Sperschneider, A.; Schacher, F.; Gawenda, M.; Tsarkova, L.; Müller, A. H. E.; Ulbricht, M.; Krausch, G.; Köhler, J. Towards Nanoporous Membranes Based on ABC Triblock Terpolymers. *Small* **2007**, *3*, 1056-1063.
42. Stadler, R.; Auschra, C.; Beckmann, J.; Krappe, U.; Voight-Martin, I.; Leibler, L. Morphology and Thermodynamics of Symmetric Poly(A-*block*-B-*block*-C) Triblock Copolymers. *Macromolecules* **1995**, *28*, 3080-3097.

Supporting Information

Table 7-S1. Molecular characterization of BVT, BVqMAA, PLL(TFA)-*b*-PEG and PLys-*b*-PEG polymers.

Name	Polymer ^{a)}	M _n [g/mol]	PDI
BVT-1	B ₈₃₀ V ₁₈₀ T ₄₀₀	121,000 ^{b)}	1.04 ^{c)}
BVT-2	B ₈₃₀ V ₁₈₀ T ₁₃₅₀	256,000 ^{b)}	1.08 ^{c)}
BVqMAA-1	B ₈₃₀ Vq ₁₈₀ MAA ₄₀₀	101,000 ^{d)}	-
BVqMAA-2	B ₈₃₀ Vq ₁₈₀ MAA ₁₃₅₀	183,000 ^{d)}	-
	PLL(TFA) ₄₀ - <i>b</i> -PEG ₂₇₀	21,400 ^{b)}	1.05 ^{e)}
	PDLL(TFA) ₃₈ - <i>b</i> -PEG ₂₇₀	20,900 ^{b)}	1.03 ^{e)}
PLL- <i>b</i> -PEG	PLL ₄₀ - <i>b</i> -PEG ₂₇₀	17,500 ^{b)}	-
PDLL- <i>b</i> -PEG	PDLL ₃₈ - <i>b</i> -PEG ₂₇₀	17,300 ^{b)}	-

a) Subscripts denote the degree of polymerization of the respective blocks; b) calculated from a combination of MALDI-ToF-MS and ¹H-NMR data; c) determined from SEC measurements with THF as eluent and linear polystyrene as calibration standard; d) calculated from the degrees of polymerization without taking the counterions of quaternized 2-vinylpyridine into account; e) determined from SEC measurements with DMF as eluent and linear poly(ethylene glycol) as calibration standard.

Table 7-S2. Average core diameter of PS carrying BVqMAA/PLL-*b*-PEG complex micelles determined from cryo-TEM micrographs by measuring at least 50 micelles per sample with standard deviation.

Polymer	Z _{+/-} -value			
	0	0.25	0.5	1
BVqMAA-1	90 ± 12 nm	93 ± 11 nm	89 ± 9 nm	93 ± 9 nm
BVqMAA-2	76 ± 12 nm	70 ± 14 nm	64 ± 12 nm	65 ± 14 nm

Table 7-S3. Characterization of BVqMAA-1 and BVqMAA-2 control micelles with increasing degree of PEGylation without drug in regard to polymer concentration and cumulant hydrodynamic diameter. All micelle solutions were in 10 mM PBS buffer solution at pH 7.4 with additional 140 mM NaCl.

Polymer	Z _{+/-} -value	Polymer Conc. [g/L] ^a	D _h [nm]	D.I.
BVqMAA-1	0	0.80	250	0.094
	0.25	0.89	266	0.136
	0.5	1.00	244	0.111
	1	1.42	250	0.074
BVqMAA-2	0	0.94	346	0.123
	0.25	0.91	361	0.050
	0.5	1.18	359	0.021
	1	1.65	359	0.068

a) determined by weight after freeze drying of aliquot dialyzed to MilliQ water to remove buffer salts.

Table 7-S4. *In vitro* PDT efficacy. IC₅₀ values (mg polymer/mL medium) of BVqMAA/PLL-*b*-PEG control micelles without drug in A549 cells in dependence of the degree of PEGylation and illumination time as determined by MTT assay.

Z _{+/-} -value Illumination time	BVqMAA-1/PLL- <i>b</i> -PEG			BVqMAA-2/PLL- <i>b</i> -PEG		
	0min	15min	30min	0min	15min	30min
0	> 0.1	> 0.1	> 0.1	> 0.1	> 0.1	> 0.1
0.25	> 0.1	> 0.1	> 0.1	> 0.1	> 0.1	> 0.1
0.5	> 0.1	> 0.1	> 0.1	> 0.1	> 0.1	> 0.1
1	> 0.1	> 0.1	> 0.1	> 0.1	> 0.1	> 0.1

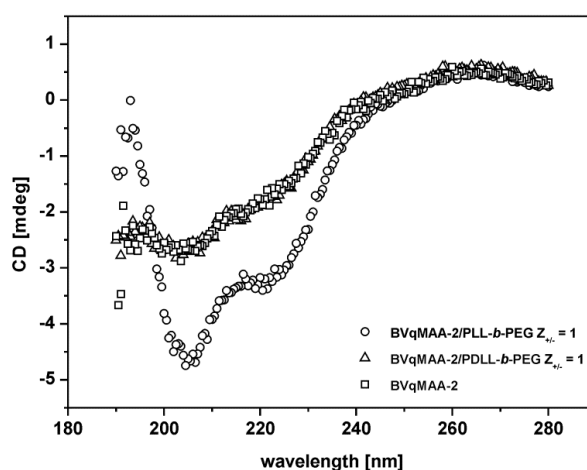


Figure 7-S1. CD-Spectra of BVqMAA-2 micelle solution (squares) and complexed micelles with PLL-*b*-PEG (circles), PDLL-*b*-PEG (triangles) at Z_{+/-} = 1.

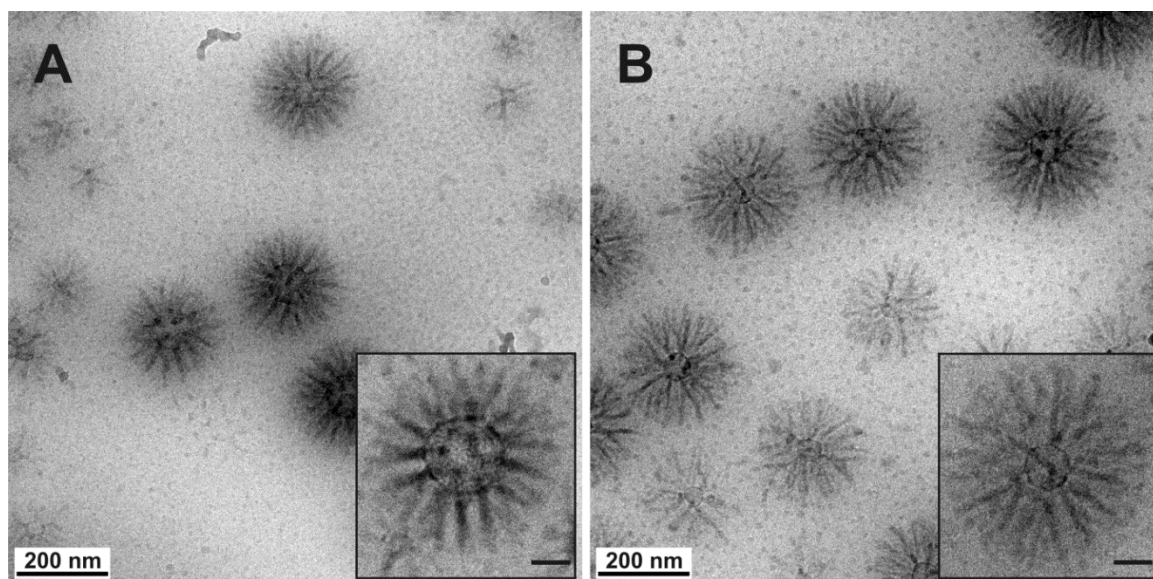


Figure 7-S2. Cryo-TEM micrographs of BVqMAA-1 (A) and BVqMAA-2 (B) micelles complexed with PDLL-*b*-PEG at $Z_{+/-} = 1$ in 10 mM PBS buffer at pH 7.4 with 140 mM NaCl after crosslinking. The insets show single enlarged micelles with the scale bar representing 50 nm.

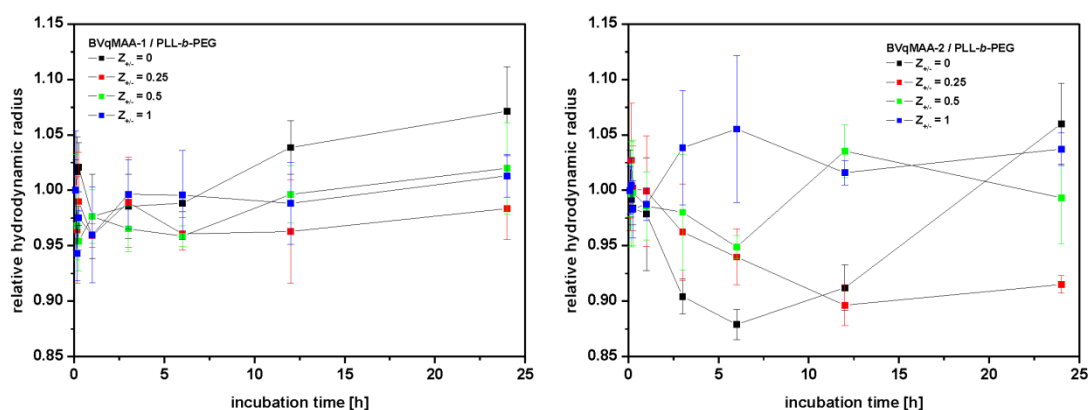


Figure 7-S3. Serum stability of BVqMAA/PLL-*b*-PEG micelles determined from light scattering measurements. Evolution of the relative hydrodynamic radius with incubation time. Measurements were performed at a micelle concentration of 0.2 mg/mL in DMEM medium containing 10 % fetal bovine serum and incubation temperature was 37 °C.

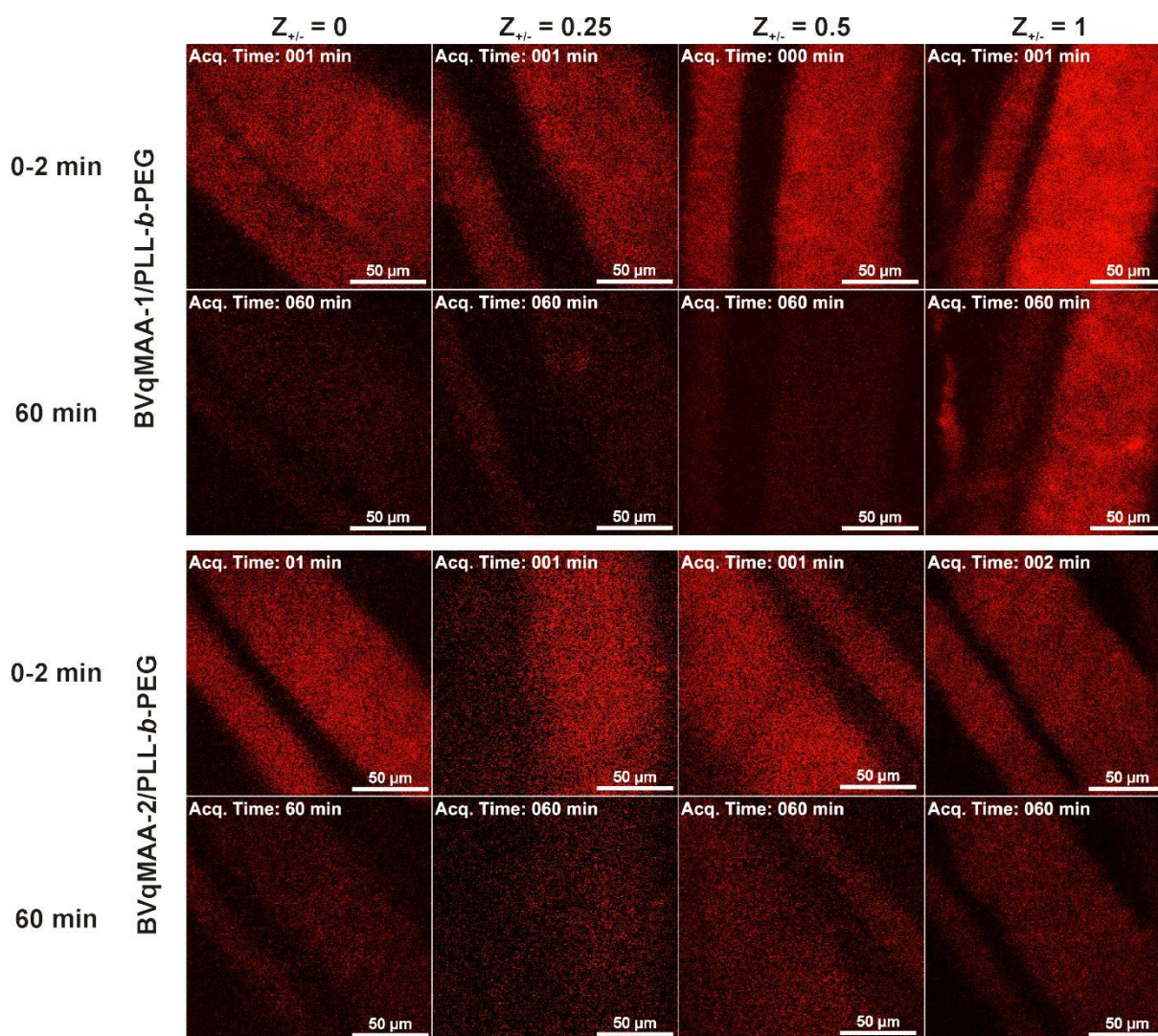


Figure 7-S4. Intravital real-time confocal laser scanning microscopy images of PS carrying BVqMAA/PLL-*b*-PEG micelles shortly after injection and 60 min post tail vein injection.

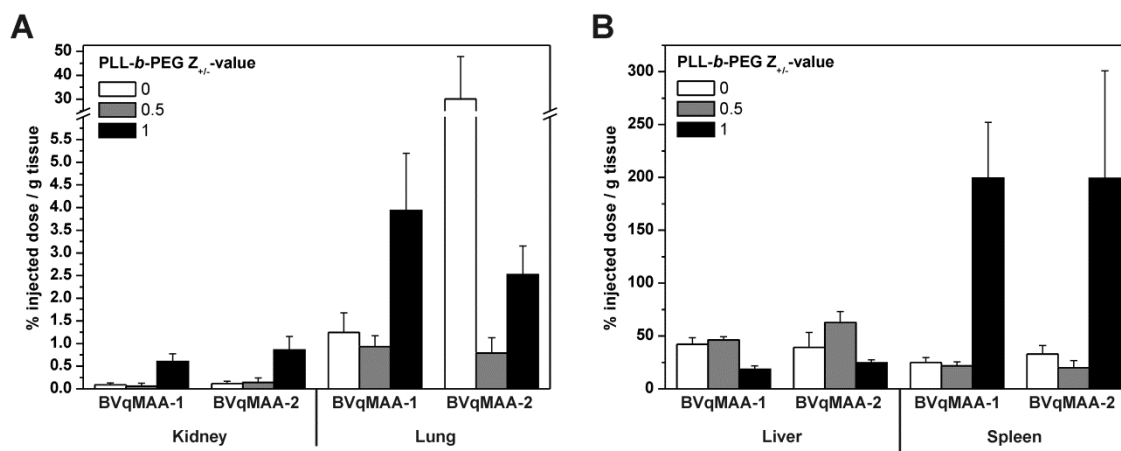


Figure 7-S5. Accumulation of PS in organs of Balb/c nu/nu mice ($n = 4$) 24 h after tail-vein injection in dependence of the degree of PEGylation of BVqMAA/PLL-*b*-PEG micelles. Injected dose is 10 μ g of PS per mouse.

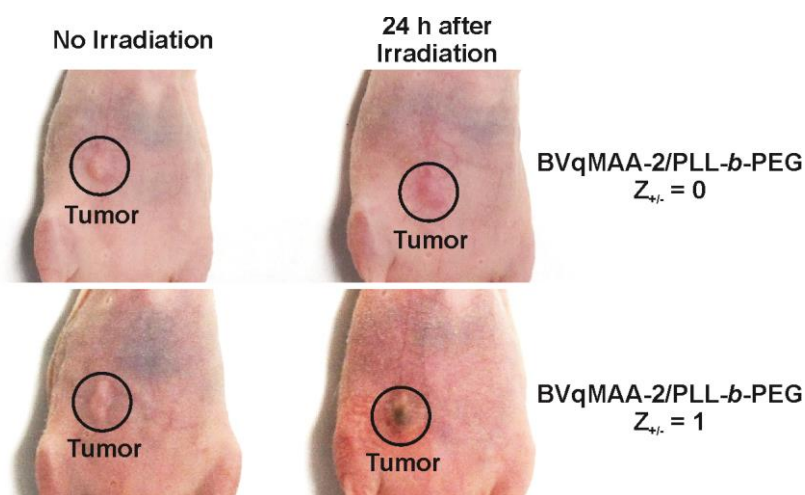


Figure 7-S6. Comparative images of the tumor site in mice with (right images) and without (left images) photoirradiation 24 h after injection of PS carrying BVqMAA-2/PLL-*b*-PEG micelles with $Z_{+/-} = 0$ (top) and $Z_{+/-} = 1$ (bottom).

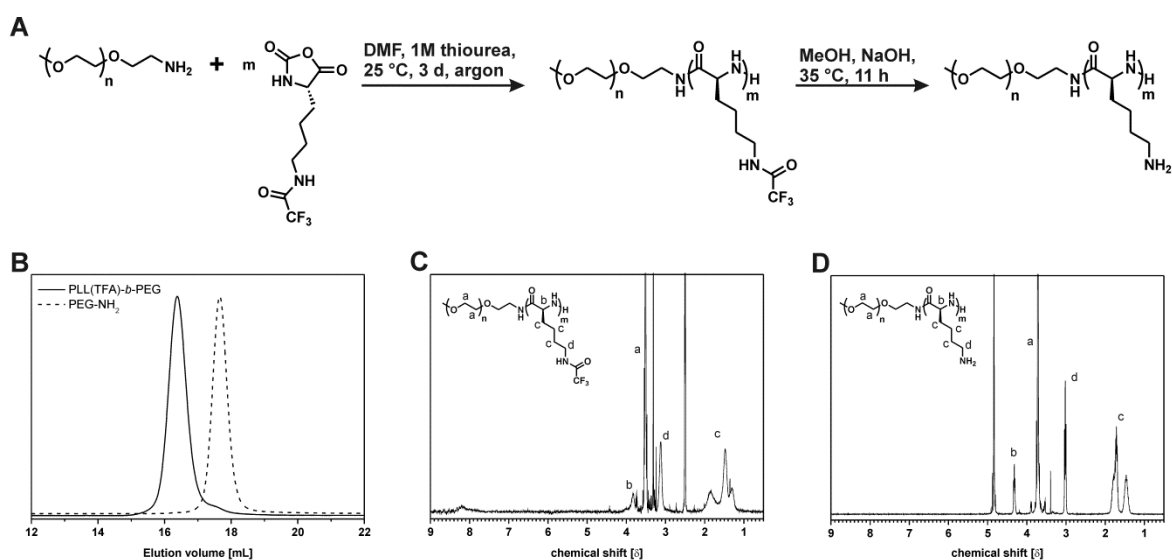


Figure 7-S7. Synthetic procedure for the preparation of PLL-*b*-PEG (A); Elution curves of PEG-NH₂ macroinitiator and PLL(TFA)-*b*-PEG using DMF as eluent and PEG as calibration standard (B); ¹H-NMR spectra of PLL(TFA)-*b*-PEG (C, recorded in DMSO-*d*₈) and PLL-*b*-PEG (D, recorded in D₂O).

List of Publications

Publications

- [13] **C.V. Synatschke**, T. Nomoto, H. Cabral, M. Förtsch, K. Tou, Y. Matsumoto, K. Miyazaki, A. Hanisch, F.H. Schacher, A. Kishimura, N. Nishiyama, A.H.E. Müller, K. Kataoka, “Multicompartment Micelles with Adjustable Poly(ethylene glycol) Shell for Efficient *in Vivo* Photodynamic Therapy”, *ACS Nano*, **2014**, DOI: 10.1021/nn4028294.
- [12] **C.V. Synatschke**, T. Löbbling, M. Förtsch, A. Hanisch, F.H. Schacher, A.H.E. Müller, “Micellar Interpolyelectrolyte Complexes with a Compartmentalized Shell”, *Macromolecules* **2013**, *46*, 6466-6474.
- [11] W. Xu, I. Choi, F.A. Plamper, **C.V. Synatschke**, A.H.E. Müller, V.V. Tsukruk, “Nondestructive Light-Initiated Tuning of Layer-by-Layer Microcapsule Permeability”, *ACS Nano* **2013**, *7*, 598-613.
- [10] L.V. Sigolaeva, D.V. Pergushov, **C.V. Synatschke**, A. Wolf, I. Dewald, I.N. Kurochkin, A. Fery, A.H.E. Müller, “Co-Assemblies of Micelle-Forming Diblock Copolymers and Enzymes on Graphite Substrate for an Improved Design of Biosensor Systems”, *Soft Matter* **2013**, *9*, 2858-2868.
- [9] A. Schallon, **C.V. Synatschke**, V. Jérôme, A.H.E. Müller, R. Freitag, “Nanoparticulate Nonviral Agent for the Effective Delivery of pDNA and siRNA to Differentiated Cells and Primary Human T Lymphocytes”, *Biomacromolecules* **2012**, *13*, 3463–3474.
- [8] **C.V. Synatschke**, T. Nomoto, A. Kishimura, A.H.E. Müller, K. Kataoka, “Towards Multi-Functional Drug Delivery Systems from Ionic Triblock Terpolymer Micelles”, *Polymer Preprints (American Chemical Society, Division Polymer Chemistry)* **2012**, *53*, 398-399.
- [7] **C.V. Synatschke**, A. Schallon, V. Jérôme, R. Freitag, A.H.E. Müller, “Influence of Polymer Architecture and Molecular Weight of Poly(2-(dimethylamino)ethyl methacrylate) Polycations on Transfection Efficiency and Cell Viability in Gene Delivery”, *Biomacromolecules* **2011**, *12*, 4247-4255.

- [6] A. Schallon, **C.V. Synatschke**, D.V. Pergushov, V. Jérôme, A.H.E. Müller, R. Freitag, “DNA Melting Temperature Assay for Assessing the Stability of DNA Polyplexes Intended for Nonviral Gene Delivery”, *Langmuir* **2011**, 27, 12042-12051.
- [5] I. Choi , R. Suntivich , F.A. Plamper , **C.V. Synatschke**, A.H.E. Müller, V.V. Tsukruk, “pH-Controlled Exponential and Linear Growing Modes of Layer-by-Layer Assemblies of Star Polyelectrolytes”, *Journal of the American Chemical Society* **2011**, 133, 24, 9592–9606.
- [4] **C.V. Synatschke**, F.H. Schacher, M. Förtsch, M. Drechsler, A.H.E. Müller, “Double-Layered Micellar Interpolyelectrolyte Complexes – How Many Shells to a Core?”, *Soft Matter* **2011**, 7, 1714-1725.
- [3] A.H.E. Müller, E. Betthausen, M. Müllner, F.H. Schacher, **C.V. Synatschke**, A. Walther, A. Wolf, “Self-Organized Nanostructures from New Block Co- and Terpolymers”, *Polymer Preprints (American Chemical Society, Division Polymer Chemistry)* **2010**, 51, 308-309.
- [2] A. Schallon, V. Jérôme, A. Walther, **C.V. Synatschke**, A.H.E. Müller, R. Freitag, “Performance of Three PDMAEMA-Based Polycation Architectures as Gene Delivery Agents in Comparison to Linear and Branched PEI”, *Functional and Reactive Polymers* **2010**, 70, 1-10.
- [1] S. Sinnwell, **C.V. Synatschke**, T. Junkers, M.H. Stenzel, C. Barner-Kowollik, “A Study into the Stability of 3,6-Dihydro-2H-thiopyran Rings: Key Linkages in the RAFT Hetero-Diels-Alder Click Concept”, *Macromolecules* **2008**, 41, 7904-7912.

Patent Applications

- [2] R. Freitag, V. Jérôme, A.H.E. Müller, H. Schmalz, A. Schallon, **C.V. Synatschke**, A. Majewski, “Utilization of Magnetic Nanoparticles as Intracellular Pull-Down System”, EP 11 166 113.8 (13.05.2011), to: Universität Bayreuth
- [1] R. Freitag, V. Jérôme, A.H.E. Müller, H. Schmalz, A. Schallon, **C.V. Synatschke**, A. Majewski, “Nonviral Transfection Systems “, EP 11 166 108.8 (13.05.2011), to: Universität Bayreuth

Acknowledgements

Even the greatest of times has to come to an end at some point. During the time I spent working on this thesis, I was fortunate to meet a great number of friendly, helpful and often inspiring people. Without them, I would not have come to where I am now and would not have had so much fun on the way to that destination. All of You, who helped me along the way, be it through professional advice, a helping hand or love and support, I give my deepest thanks!

First and foremost, I thank Prof. Axel H. E. Müller. He supervised my work and gave advice, even when the topic became more and more biomedical, which we maybe both did not anticipate in the beginning. His way of doing research - always in active and open collaboration with other researchers from all over the world - is the role-model I aspire to achieve in my future work as well. The group-spirit that made working in MC² special was due to his way of leading the group. His kindness towards me and confidence in me has been the greatest motivation. Prof. Müller enabled me to travel to a great number of conferences and meetings right from the beginning of my thesis, where I could present my work. There, I got to meet other researchers, discuss science and “grow” into the community. I thank him for all those opportunities he created and the responsibilities he trusted me with.

Prof. Felix H. Schacher has been a trusted advisor for any questions of a more practical nature, like experimental procedures and a good writing style for manuscripts, and I wish to thank him for all the involvement he had in my work. He was invaluable for extracting a good “story” out of the mass of data and I have learned a lot from him.

A special thanks goes to Anja Schallon. With her unending enthusiasm and energy, she really captivated me for the gene delivery topic, and finally made it a much larger part of this thesis than I initially expected. I will miss our discussions over a never-ending supply of coffee.

The MC²-Team deserves a very BIG thanks. Working in the group has been a wonderful experience, and I have never met a group that shared a similar spirit as we did in MC². Thanks for the everyday help in the laboratories, for many a coffee, cake, beer and Schnapps shared in the kitchen, the countless barbeques and all the fun we had on our trips to conferences.

The technicians kept the lab in good working condition. I want to thank Melanie Förtsch and Annika Pfaffenberger for taking care of all my TEM samples and together with Dane Blasser for forming my “MALDI-Team”. Together we kept the old lady in good shape. Marietta Böhm, I thank for always being there to measure the tricky samples I prepared for SEC. Further, Annette Krökel took care of much of the administrative work occurring in the lab, and could always tell me where to find the odd missing piece of equipment, glassware or consumable. Thank you for that.

I also thank the “good soul” of the MC², Gaby Oliver, who somehow always managed to get things done with the university administration even on very short notice. She worked her miracle ways to re-organize the group money and always found a follow-up contract from various sources for me.

Many people came and went in MC² during my time there. Thanks for the remarkable atmosphere you created (in no particular order): Markus Müllner, Andreas Hanisch, Thomas Ruhland, Alexander Majewski, André Gröschel, Tina Löbling, Eva Betthausen, Andrea Wolf, Stephan Weiß, Sandrine Tea, André Pfaff, Alexander Schmalz, Joachim Schmelz, Stefan Reinicke, Zhicheng Zheng, Francesca Bennet, Holger Schmalz, Markus Drechsler, Anja Goldmann, Jiayin Yuan, Andreas Walther, Jun Ling, Jie Kong, Weian Zhang, Marina Krekhova, Stefan Döhler, Shohei Ida, Tony Granville, Hülya Arslan, Ivan Babin, Meirav Ben-Lulu and Tomohiro Hirano. The “Russian Mafia” consisting of Dmitry (Dima) Pergushov, Larissa Siegolaeva, Alexander (Sasha) Yakimansky and Oleg Borisov, as well as the corresponding “Spanish Mafia”: Ramón Novoa-Carballal, Lourdes Pastor-Pérez and Ainhoa Tolentino Chivite. My students and “Hiwi’s” also deserve a big thank you for all the effort they put into their work: Annika Eckardt, Fabian Pooch, Irina Weber and Tobias Rudolph.

I would also like to thank Prof. Ruth Freitag for the good collaboration I had with her group and for the support, especially in the final part of my thesis.

From conferences, meetings and collaborations I thank those people who did influence my work, or discussed ideas. Steffen Weidner, Jana Falkenhagen, Volker Sauerland, Christo Tsvetanov, Darrin Pochan, Christopher Barner-Kowollik, Helmut Schlaad, Felix Plamper, Vladimir Tsukruk, Jürgen Senker, Andreas Fery, Takuzo Aida, Matthias Karg, Markus Retsch, Helmut Ringsdorf, Amir Fahmi, Harald Pasch, Ian Manners and Eugenia Kumacheva.

During my 6-months research stay at the University of Tokyo, I met many people who made my time there an exceptional experience. First among those people is Prof. Kazunori Kataoka, whom I deeply respect and who has impressed me as being a researcher of rare quality. Within his group or connected with the University of Tokyo I want to thank Horacio Cabral, Takahiro Nomoto, Stefanie Deshayes, Philippe Saint-Cricq Riviere, Tomeu (The Bastard) Soberats, Adrien Kaeser, Xiao Ling, Kazuko Toh, Yu Matsumoto, Sayan Chuanoi, Yuuki Mochida, Mitsuru Naito, Akihiro Kishimura, Nobuhiro Nishiyama, R. James (Jim) Christie and Yutaka Miura.

I am further grateful for financial support I received from various sources during my work, most importantly from the State of Bavaria, the German Academic Exchange Service, the Center for Medical Systems Innovation and the SFB 840.

Many friends have supported me throughout the PhD process and I cannot name you all. Let it suffice to say you are an important part of my life. Thank you Anja, for all the love and support you gave me during those wonderful 6 years that we shared. I wish you the best for your future and hope to remain a small part of that.

Most importantly, I want to thank my family. My mother Elisabeth I thank for supporting me unconditionally, always listening to my adventures, successes and in some rare cases my frustrations. Both my sisters Dagmar and Franziska have been an inspiration to me and have shown me choices I might not have known without them.

“There is a theory which states that if ever anyone discovers exactly what the Universe is for and why it is here, it will instantly disappear and be replaced by something even more bizarre and inexplicable.

There is another theory which states that this has already happened.”

— *Douglas Adams, The Restaurant at the End of the Universe*

Erklärung

Die vorliegende Arbeit wurde von mir selbständig verfasst und ich habe dabei keine anderen als die von mir angegebenen Hilfsmittel oder Quellen verwendet.

Ferner habe ich nicht versucht, anderweitig mit oder ohne Erfolg eine Dissertation einzureichen oder mich einer Doktorprüfung zu unterziehen.

Bayreuth, den 15. Januar 2014

Christopher Volker Synatschke